Investigation of the Production, Isolation and Bioactivity of the Rishirilide Natural Products including Crystallographic Studies

by

Lina Mardiana

A thesis submitted in partial fulfilment of the requirements for the degree of

Doctor of Philosophy

December 2020

Acknowledgements

On this occasion, first I would like to express my sincere gratitude to my supervisor Dr Michael Hall for his continuous guidance, support, and patience throughout my PhD study, as I have learnt so much under his supervision. Dr Hall has been an excellent supervisor and his guidance helped me in all the time of research and writing this thesis. I could not have imagined having a better supervisor and mentor for my PhD study. Thanks again Dr Hall, you are the best!

Furthermore, I would like to thank all of the past and present members of the MJH research group who have been a pleasure to work with. I would like to specifically thank Dr Kin Lok Ho for his support during my thesis writing. I would like to thank everyone in the MJH research group (Ronnie Ragbirsingh, Rafid Taj-Aldeen, Yanhua Zhong, Damon Wen, Felicity Frank, Aminah Almarshad, Dr Hadiza Aminu Isah, Dr Andrew Tyler and Dr Stephanie Morton), the Johnston lab, the Demuris lab (Dr Nick Allenby, Dr Richard Lewis, Dr Adam Hopkin and Jenileima Devi) and Biomolecular lab at Devonshire for creating a wonderful place to work and make friends. I would miss you all.

My sincere thanks also go to my colleagues at CBCB and Pinnacle, particularly Dr Bernhard Kepplinger, Dr Kaveh Emami and Dr Joe Gray for their assistance in microbiology work and their analysis during the course of my PhD research. I also wish to thank the staff at Newcastle University, particularly Dr Corrine Wills, Professor William McFarlane and Dr Casey Dixon for their excellent NMR work, also Dr Paul Waddell and Dr Michael Probert for their assistance in X-ray crystallography.

I also want to thank my sponsor, Indonesian Endowment Fund (LPDP) for giving me financial support and a lifetime experience to study my PhD in Newcastle University, UK.

Finally, I wish to thank my mother, my husband, my wonderful and beautiful daughters (Meisha, Natasha and Meirisha, I love you so much!) and my brothers for their endless support and encouragement to the successful completion of my PhD.

Thank you again to all of you.

Abstract

The emergence of antibiotic resistant pathogenic bacteria has created a growing demand for research into new antibiotics. Bacterial natural products, particularly from the genus *Streptomyces*, have historically provided the basis for many clinically used antibiotics. In this project we have examined a class of natural product polyketides from *Streptomyces* as potential new mode of action antibiotics.

We have focussed our investigation on two polyketides, (-)-rishirilide A and (+)-rishirilide B, originally isolated from *Streptomyces rishiriensis* OFR-1056. Following optimisation of fermentation and isolation protocols, milligram quantities of both (-)-rishirilide A and (+)-rishirilide B were obtained from *Streptomyces albus*::cos4. (-)-Rishirilide A displays antibiotic activity against Gram-positive bacteria (MICs: *S. aureus,* 1.56 µg/mL; *B. subtilis,* 3.125 µg/mL). Mode of action investigations showed that treatment with (-)-rishirilide A results in the depolarization of the bacterial cell membrane (*B. subtilis* 168CA). This may be due to (-)-rishirilide A acting as an irreversible inhibitor through Michael addition with a thiol containing enzyme. Further work will involve the synthesis of chemical probes based on (-)-rishirilide A to identify target enzymes.

Additionally, we have supported this work with a study into the high-throughput nanoscale crystallisation (ENaCt) of natural products for single crystal X-ray analysis. Using ENaCt we have examined the crystallisation of a range of natural products. Cannabidiol and rifampicin crystals were obtained, and single crystal X-ray diffraction analysis successfully performed.

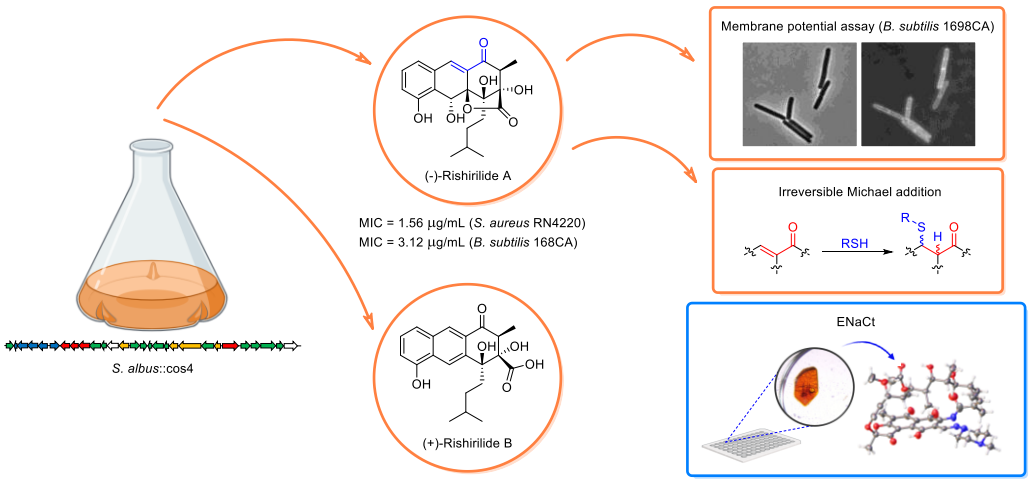

Graphical abstract of the investigation of the production, isolation, and bioactivityof the natural products rishirilides including crystallographic studies.

Abbreviations

ATP	Adenosine Triphosphate
B	Biological
BCG	Biosynthetic gene cluster
BPC	Base Peak Chromatogram
Calcd	calculated
CBD	Cannabidiol
CDC	Centre for Disease Control and Prevention
CD_3COCD_3	Deuterated acetone
CD_3OD	Deuterated methanol
COSY	Correlated spectroscopy
CSD	Cambridge Structural Database
CuAAC	Copper alkyne-azide cycloaddition
d	Doublet
DCM	Dichloromethane
DTT	Dithiothreitol
DHF	Dihydrofolate
DHFS	Dihydrofolate synthase
DHPS	Dihydropteroate synthase
DIPEA	Diisopropylethylamine
DMF	Dimethyl formamide
DMSO	Dimethylsulfoxide
DNA	Deoxyribonucleic acid
DO	Dissolved oxygen
EIC	Extracted Ion Chromatogram
ENaCt	Encapsulated Nanodroplet Crystallisation
ESBL	Extended spectrum of β-lactamase
ESI	Electron spray ionisation

ESKAPE	*Enterococcus faecium, Staphylococcus aureus, Klebsiella pneumoniae, Acinetobacter baumannii, Pseudomonas aeruginosa*, and *Enterobacter* spp.
EtOAc	Ethyl acetate
EU	European Union
FA	Formic acid
FC-40	Fluorinert 40
FDA	Food and Drugs Association
FY	Fomblin Y
g	gram
GYM	Glucose yeast extract maltose
h	hour
HMBC	Heteronuclear multiple bond coherence
HPLC	High performance liquid chromatography
HRMS	High resolution mass spectroscopy
HSQC	Heteronuclear single quantum coherence
IC	Inhibitory concentration
IR	Infrared
J	coupling constant
LCMS	Liquid chromatography mass spectroscopy
m	Multiplet
MDR	Multidrug resistant
MeCN	Acetonitrile
MeI	Methyl iodide
MeOH	Methanol
mg	milligram
MIC	Minimum inhibitory concentration
min	minutes
mM	millimolar concentration
mRNA	messenger RNA

MRSA	methicillin-resistant *Staphylococcus aureus* (MRSA)
NA	Nutrient agar
NAG	N-acetylglucosamine
NAM	N-acetylmuramic acid
NB	Nutrient broth
NMR	Nuclear magnetic resonance
NOESY	Nuclear overhauser effect spectroscopy
*p*ABA	*para*-amino benzoic acid
PBP	Penicillin binding protein
PDMSO	Polydimethylsiloxane
ppm	parts per million
p-TSA	*para*-Toluenesulfonic acid
q	Quartet
RNAP	RNA polymerase
RPM	rounds per minute
rRNA	ribosomal RNA
s	Singlet
SCXRD	Single crystal x-ray diffraction
SEC	Size exclusion chromatography
SFM	Soya flour mannitol
SPE	Solid phase extraction
t	triplet
TB	Tuberculosis
t-BuOH	*t*-butanol
$TMSCHN_2$	Trimethylsilyldiazomethane
TOCSY	Total correlated spectroscopy
tRNA	transferRNA
WHO	World Health Organization
XDR	Extensively drug-resistant

X-Gal	X-Galactopyranoside
ZOI	Zone of inhibition

Table of Contents

Chapter 1. Introduction

This PhD project will focus on the discovery of novel antibiotics from natural products that have the potential to tackle the rise of antibiotic resistance. Our research will involve the study of two polyketide natural products, (-)-rishirilide A and (+)-rishirilide B, from *S. albus*::cos4, which potentially possess antibiotic activity. Following the isolation of these natural products we will study their antibiotic mode of action. Due to the difficulties in structural elucidation of isolated natural products, alongside our main work on (-)-rishirilide A and B, we will also undertake research into a new crystallographic method for natural product structure elucidation and apply this approach to the crystallisation and X-ray analysis of our isolated natural products.

1.1 The golden era of antibiotic discovery

1.1.1 Impact of antibiotics on human health

Since penicillin was discovered in 1928, it is estimated to have been used in the treatment of over 200 million people.[1] This 'golden drug' has been used for the treatment a range of infectious diseases including staphylococcal, streptococcal, and pneumococcal infections.[2] Historically, tuberculosis (TB), an infectious disease caused by *Mycobacterium tuberculosis*, was a significant health problem which contributed about 25% of all deaths in England in 1815, until the discovery of the first effective anti-TB antibiotic, streptomycin, in 1946.[3,4] The Office of National Statistics subsequently reported an 80% decrease in the number of deaths from TB between 1944 and 1955.[5] In 1900, the three leading causes of deaths were pneumonia, TB, diarrhoea and enteritis, all caused by bacterial infection. By 1997, following the introduction of effective antibiotics, these diseases have almost disappeared (Figure **1.1**).[1]

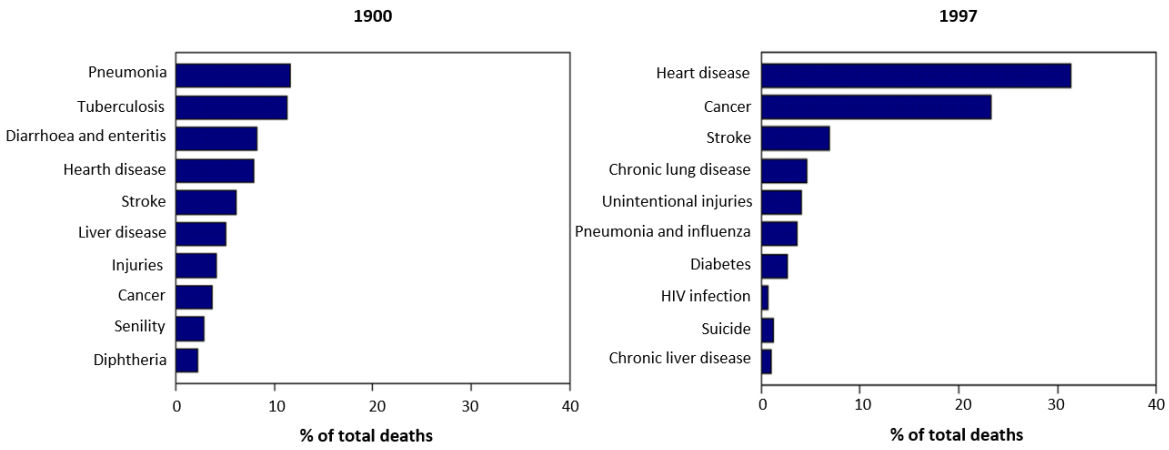

Figure 1.1: The leading causes of death in the United States by percentage between 1900 and 1997.[1]

1.1.2 Natural product antibiotics

Many clinically used antibiotics are derived from natural products, discovered from the genus actinomycetes.[6,7] Actinomycetes are a diverse group of Gram-positive actinobacteria which display filamentous, branching mycelium. Actinomycetes are typically found in soils and are a source of a wide range of natural products. Much of the early work in this field was carried out by the group of Waksman. The Waksman group screened many bacteria for their production of natural product antibiotics, leading to the discovery of many important natural product antibiotics including actinomycin D (dactinomycin) (**1**), neomycin B (**2**), streptomycin (**3**), streptothricin E (**4**) and candicidin (**5**) (Figure **1.2**).[8,9]

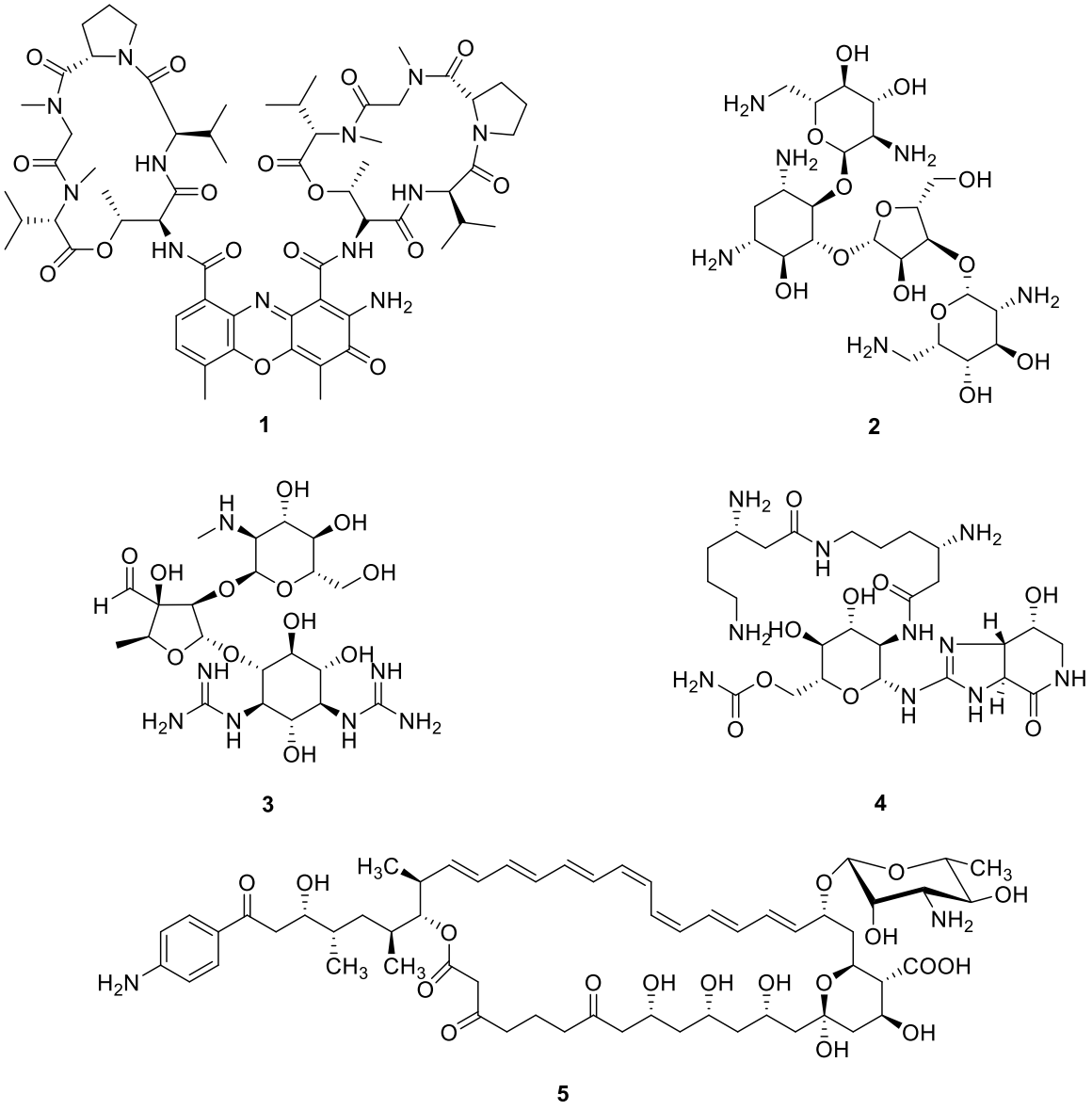

Figure 1.2: Natural product antibiotics isolated by the Waksman group: actinomycin D (dactinomycin) (**1**), neomycin B (**2**), streptomycin (**3**), streptothricin E (**4**), and candicidin (**5**).

1.1.3 Mode of action of antibiotics

Antibiotics have many different modes of action which inhibit (bacteriostatic) or kill (bactericidal) infectious bacteria. There are five main modes of action of clinically used antibiotics which interfere with key processes in bacterial metabolism (Figure **1.3**).

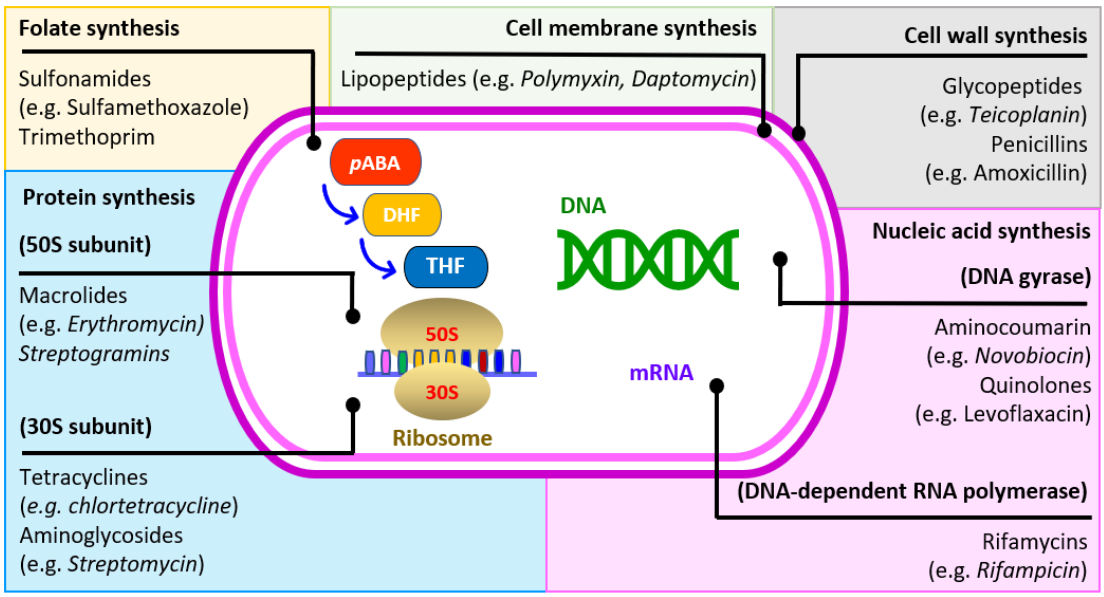

Figure 1.3: The five main modes of action of clinically antibiotics (antibiotics derived from natural products in italics).

A. Protein synthesis

Ribosomes are present in all living cells and are responsible for the synthesis of proteins. The bacterial ribosome consists of both RNA and proteins, known as a ribonucleoprotein complex. The ribosome consists of two components, the large subunit (50S) and the small subunit (30S). The small subunit of ribosome (30S) decodes the genetic information contained in the messenger RNA (mRNA), while the large subunit (50S) catalyses the biosynthesis of proteins.[10] The inhibition of either two subunits will interrupt the process of protein synthesis.

Natural product antibiotics that target the 30S subunit include the tetracyclines and the aminoglycosides. The tetracyclines (e.g. chlortetracycline (**6**)), inhibit the binding of aminoacyl-tRNA to the 30S subunit and prevent protein chain growth. The aminoglycosides (e.g. streptomycin (**3**)) bind to the small 16s rRNA component of the 30S subunit and interfere with the association of the 30S and 50S subunits. This results in errors in protein synthesis and ultimately cell death.[11]

Natural product antibiotics that target the 50S subunit include the macrolides (e.g. the natural product antibiotic, erythromycin (**7**)). Erythromycin (**7**) interferes with aminoacyl translocation, blocking the A site and preventing further protein chain growth (Figure **1.4**).[10]

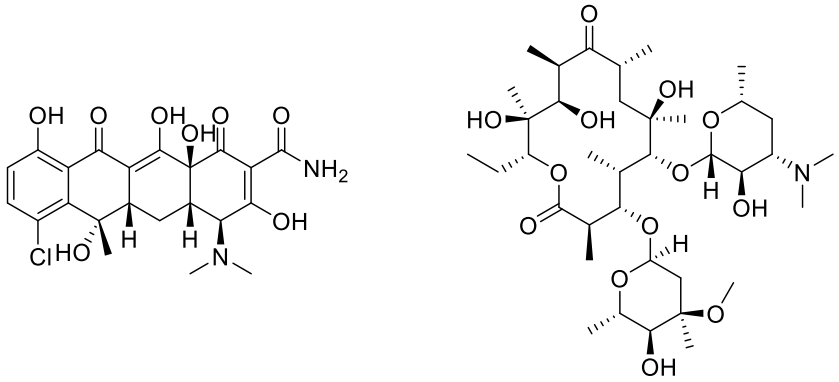

6 **7**

Figure 1.4: Natural product antibiotics that target protein synthesis: chlortetracycline (**6**) and erythromycin (**7**).

B. Folate synthesis

Folate, also known as vitamin B_9, is an essential dietary vitamin in humans. However, bacteria synthesise their own folate rather than obtaining it from their environment. All living organisms need folate for the biosynthesis of nucleotides and thus DNA. Without folate, bacterial cell growth is inhibited. As part of the biosynthesis of folate, bacteria use *para*-amino benzoic acid (*p*ABA) (**8**) as a biosynthetic precursor. During folate biosynthesis, *p*ABA (**8**) reacts with 7,8-dihydro-6-hydromethylpterin pyrophosphate (**9**) to make 7,8-dihydropteroate (**10**), mediated by dihydropteroate synthase (DHPS) (**11**). Subsequently, 7,8-dihydropteroate (**10**) reacts with L-glutamate acid (**12**) to make 7,8-dihydrofolate (DHF) (**13**), mediated by dihydrofolate synthase (DHFS) (**14**). Subsequently DHF (**13**) is reduced by dihydrofolate reductase (DHFR) (**15**) to give 5,6,7,8-tetrahydrofolate (THF) (**16**), the active form of folic acid. Antibiotics that inhibit the folate biosynthesis pathway include both the sulfonamides and the trimethoprims. Sulfonamides (e.g. sulfamethoxazole (**17**)) inhibit DHPS (**11**), whilst the trimethoprims (e.g. trimethoprim (**18**)) inhibit DHFR (**15**) and as such they are often used in combination synergistically to disrupt folate biosynthesis (Figure **1.5**).[12]

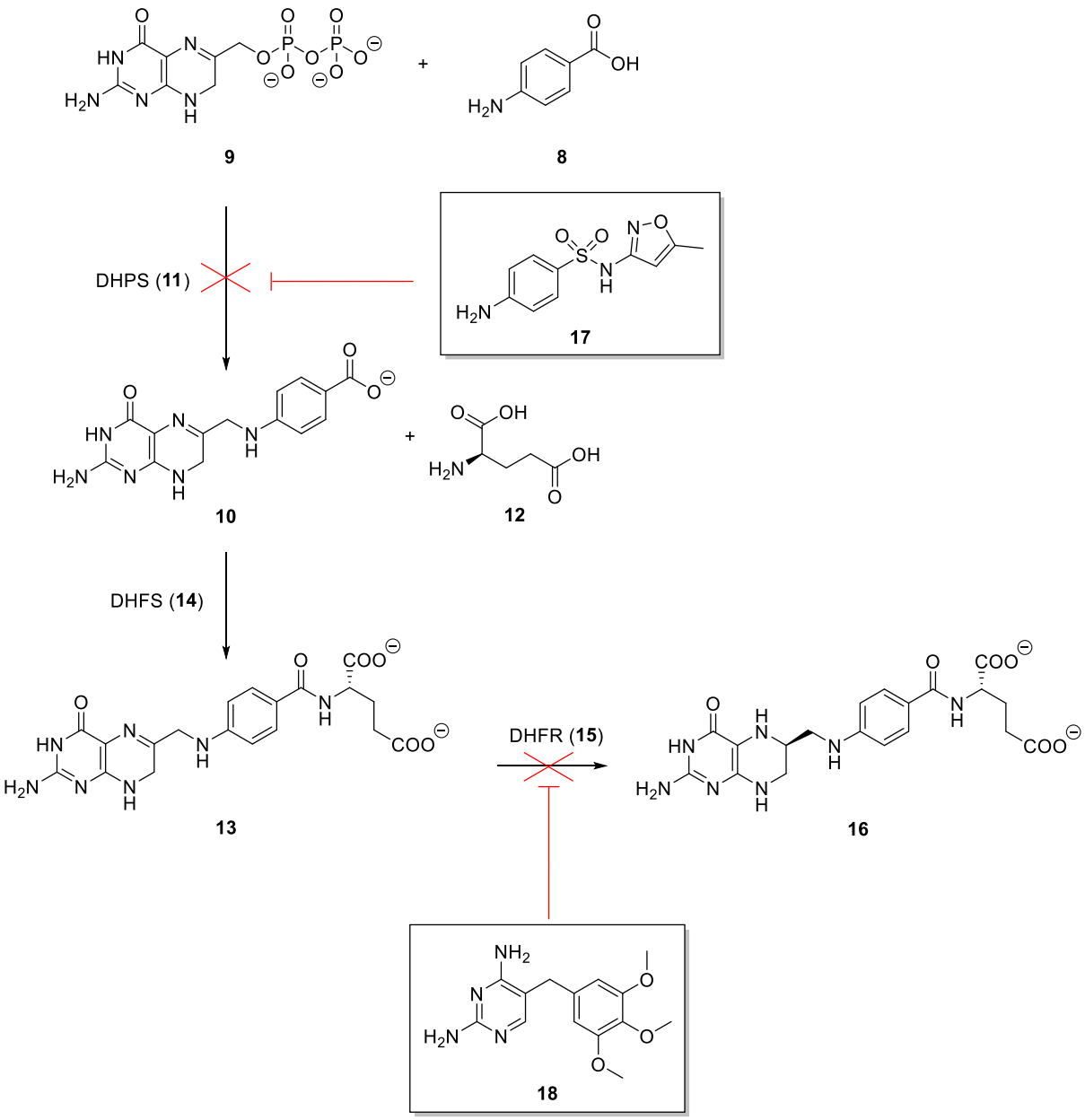

Figure 1.5: Bacterial tetrahydrofolate biosynthesis disrupted by sulfamethoxazole (**17**) and trimethoprim (**18**). (DHPS = Dihydropteroate synthase (**11**), DHFS = Dihydrofolate synthase (**14**), DHFR = Dihydrofolate reductase (**15**)).

C. Nucleic acid synthesis

DNA gyrase

Deoxyribonucleic acid (DNA) is a biopolymer that carries the genetic information required for a living organism. DNA consists a double helix of two strands of polynucleotides, which contain four bases, cytosine (C), guanine (G), adenine (A) and thymine (T). DNA replication is a biological process when one copy of DNA is transformed into two copies. In bacteria, DNA

replication occurs during cell division, therefore inhibition of DNA replication will prevent bacterial growth.

DNA replication starts the uncoiling of supercoiled DNA by DNA gyrase followed by the separation of the double helix into two single strands, mediated by a helicase. This forms an area known as the replication fork, the point at which the two strands of DNA separate. Each DNA single strand, known as the leading and lagging strands, is then used as a template to make a new DNA. This process involves a primase, an enzyme which catalyses the synthesis of a short RNA segment, called primer. This primer is complementary to the DNA single strand and used as a starting point by DNA polymerase to form the new DNA strand (Figure **1.6**). As the replication fork moves forward, the supercoiled DNA must be continually uncoiled by DNA gyrase to allow DNA replication.[13]

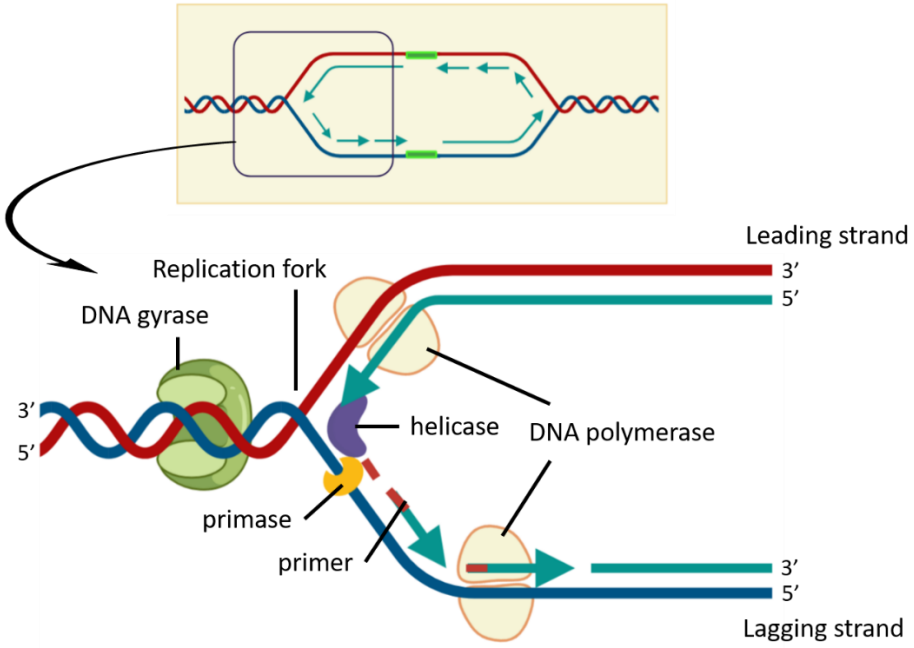

Figure 1.6: The mechanism of bacterial DNA replication.

The aminocoumarins (e.g. the natural product antibiotic novobiocin (**19**)) and quinolones (e.g. the synthetic antibiotic levofloxacin (**20**)), bind to DNA gyrase and inhibit the uncoiling of the DNA supercoils during DNA replication (Figure **1.7**). Inhibition of DNA gyrase prevents DNA replication and thus inhibits bacterial growth.

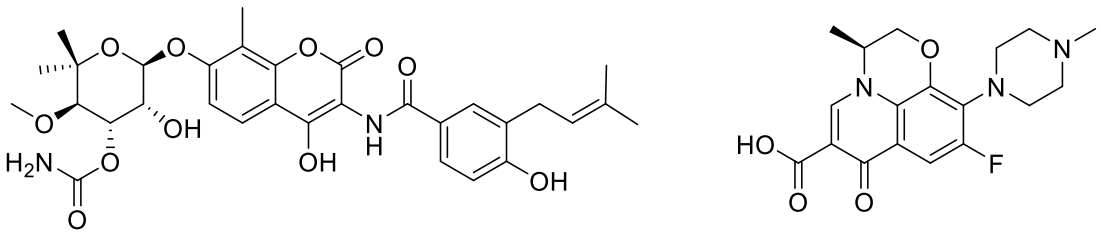

19 **20**

Figure 1.7: Antibiotics that target DNA gyrase in bacterial DNA replication: novobiocin (**19**) and levofloxacin (**20**).

DNA-dependent RNA polymerase

Ribonucleic acid (RNA) consists of a single strand of polynucleotides, which consists of four bases cytosine (C), guanine (G), adenine (A), and uracil (U). RNA plays important role in the synthesis of both DNA and proteins in all living cells. Protein production in bacteria involves two key steps, transcription and translation. Transcription is when a single strand of DNA is used as a template to make the corresponding single strand of messenger RNA (mRNA). Translation is when the mRNA is used to make the corresponding polypeptide. [14]

In bacteria, transcription is governed by DNA-dependent RNA polymerase (RNAP), a large enzyme made up of several subunits (α, β, β' and ω). RNAP synthesise RNA from a DNA template. RNA synthesis starts with opening of the double stranded DNA with a helicase. RNA is then synthesised by adding the complementary nucleotides to the template single strand DNA in the 3' to 5' direction (Figure **1.8**).

The rifamycins (e.g. rifampin (**21**), derived from the natural product rifamycin by semi-synthesis) binds to the β-subunit of RNAP and inhibits the transcription of mRNA. Thus, protein synthesis is inhibited, resulting bacterial cell death.[14]

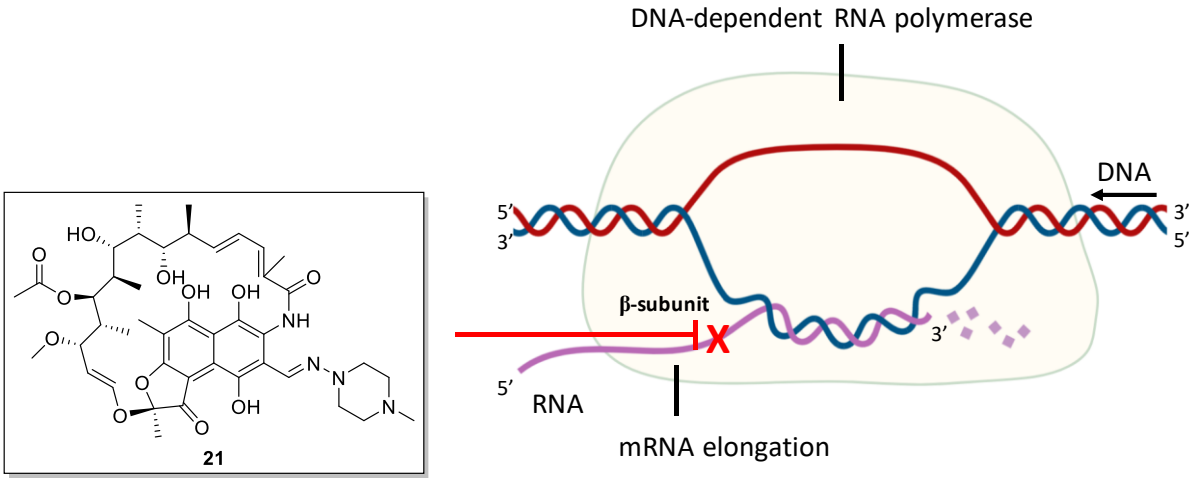

Figure 1.8: Mechanism of the inhibition of RNA synthesis by rifampin (**21**).

D. Bacterial cell membrane

The bacterial cell membrane is made up of a permeable phospholipid bilayer, which regulates many important processes such as the transport of nutrients (e.g. sugar and amino acids) and ions (e.g. Na^+, K^+, Ca^{2+} and Cl^-) into the cell as well as the elimination of waste out of the cell (e.g. CO_2).

There are two kinds of transport that occur via the bacterial cell membrane, passive transport and active transport. Passive transport is a process that allows small molecules and ions to pass across the cell membrane by diffusion. Whilst, in active transport, energy is used to move molecules and ions into the cell. The energy for this active transport is obtained from adenosine triphosphate (ATP). The sodium-potassium pump (Na^+/K^+ pump) is an example of an active transport system where sodium ions are pumped out of a cell and potassium ions are pumped into a cell. The difference in Na^+ and K^+ ion concentrations across the membrane results in a charge between outside and inside of the bacterial cell membrane, known as the membrane potential. To maintain the membrane potential, bacteria use energy from ATP to pump three Na^+ ions out for every two K^+ ions in, through ion channels in the cell membrane (Figure **1.9**).[15]

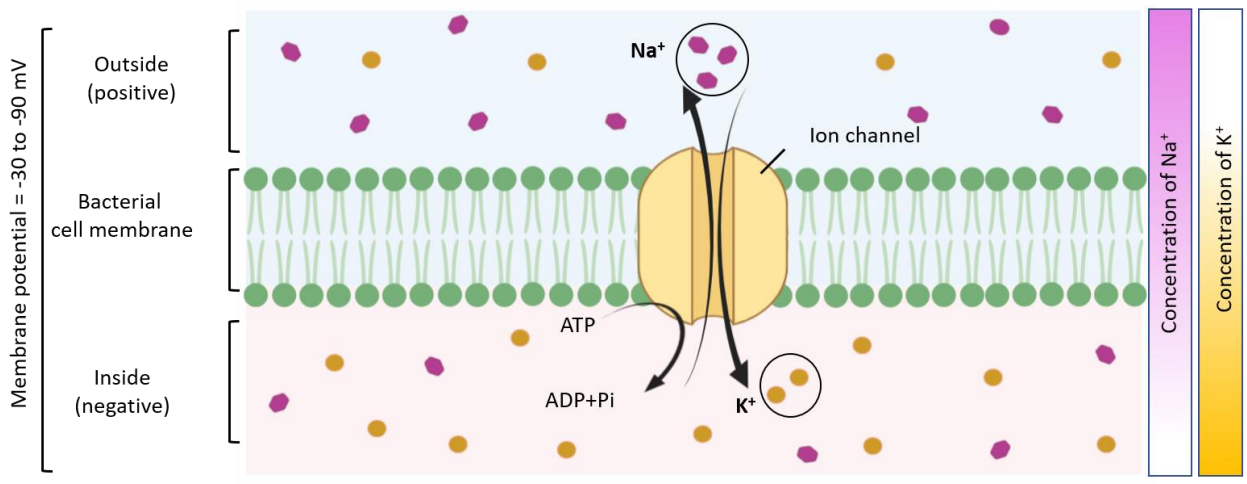

Figure 1.9: Mechanism of bacterial active transport membrane.

When a cell membrane is disrupted, sodium ions will pass into the cell and potassium ions will leave the cell, because of their relative concentrations inside and outside the cell membrane. This causes a subsequent decrease in membrane potential, leading to depolarization of the cell membrane, resulting in cell death.[16]

The lipopeptides (e.g. the natural product antibiotic daptomycin (**22**)) target the bacterial cell membrane. In solution, daptomycin (**22**) forms a supramolecular complex with several other daptomycin (**22**) molecules, held together by ionic interactions with calcium ions (Ca^{2+}). The supramolecular daptomycin-Ca^{2+} complex then inserts into the bacterial cell membrane and creates a pore, a hole in the cell membrane which is large enough to allow passage of ions. The resulting pore causes depolarization of the membrane by allowing sodium ions in and potassium ions out of the cell. As more pores are formed, the loss of membrane potential results in bacterial cell death (Figure **1.10**).[17,18]

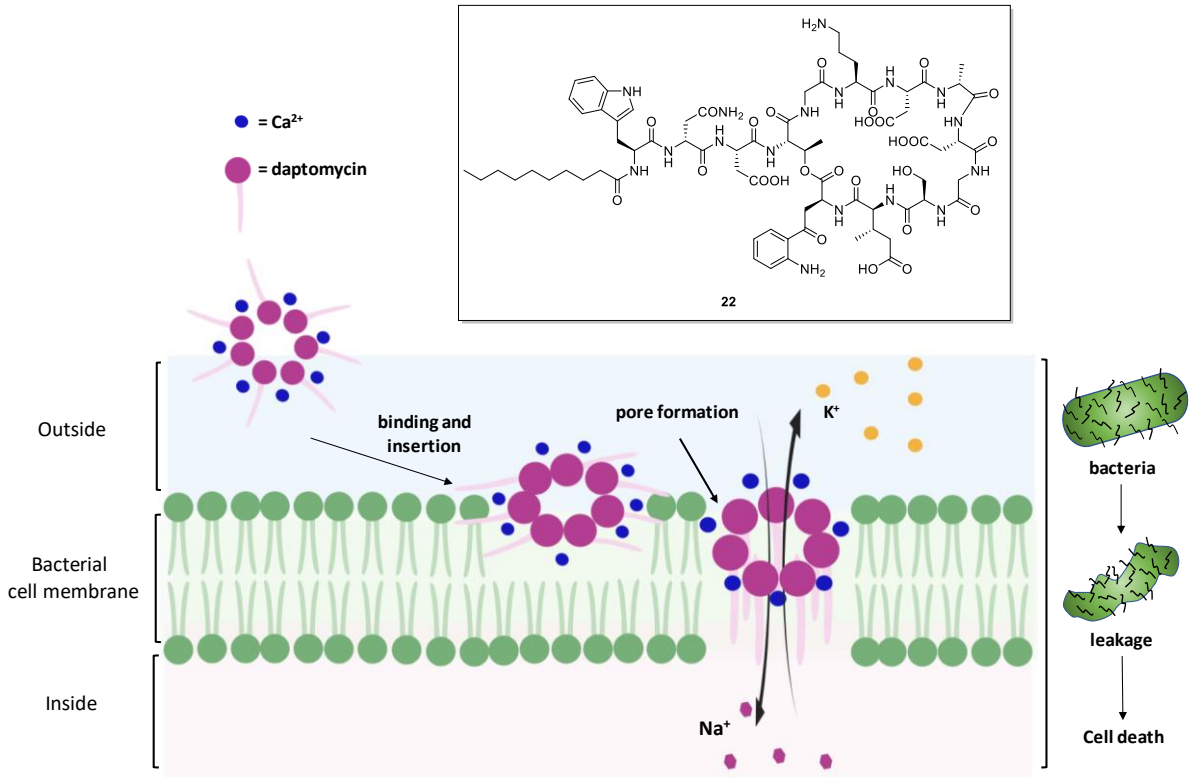

Figure 1.10: Mode of action of the natural product antibiotic, daptomycin (**22**).[15]

E. Bacterial cell wall

The bacterial cell wall is an important part of a bacteria which maintains bacterial structure integrity as well as protecting the bacteria from environmental stress.[19] The bacterial cell wall contains peptidoglycan, which consists of a linear polysaccharide, containing strands of *N*-acetylglucosamine (NAG) and *N*-acetylmuramic acid (NAM) linked in the β-(1→4) direction. The polysaccharide of NAG and NAM, also known as glycan, are crosslinked by short peptides between the NAM residues. The peptide crosslinks typically consist of four amino acids on each NAM, which are crosslinked via the L-lysine and D-alanine residues. The process of peptidoglycan crosslinking is known as transpeptidation and is mediated by a transpeptidase such as penicillin binding protein (PBP).

In bacteria, the peptidoglycan layer is different depending on the species, including differences in both constituent monomers and cross-linking patterns. For example, Gram positive bacteria have a thick peptidoglycan layer, whilst Gram-negative bacteria have a much thinner peptidoglycan layer sandwiched between two phospholipid bilayers (Figure **1.11**). Antibiotics therefore tend to be more active against Gram-positive, over Gram-negative

bacteria due to increased in penetration of the Gram-negative cell envelope. When the synthesis of peptidoglycan is inhibited, the bacteria can lose structural integrity, leading to cell death.[20]

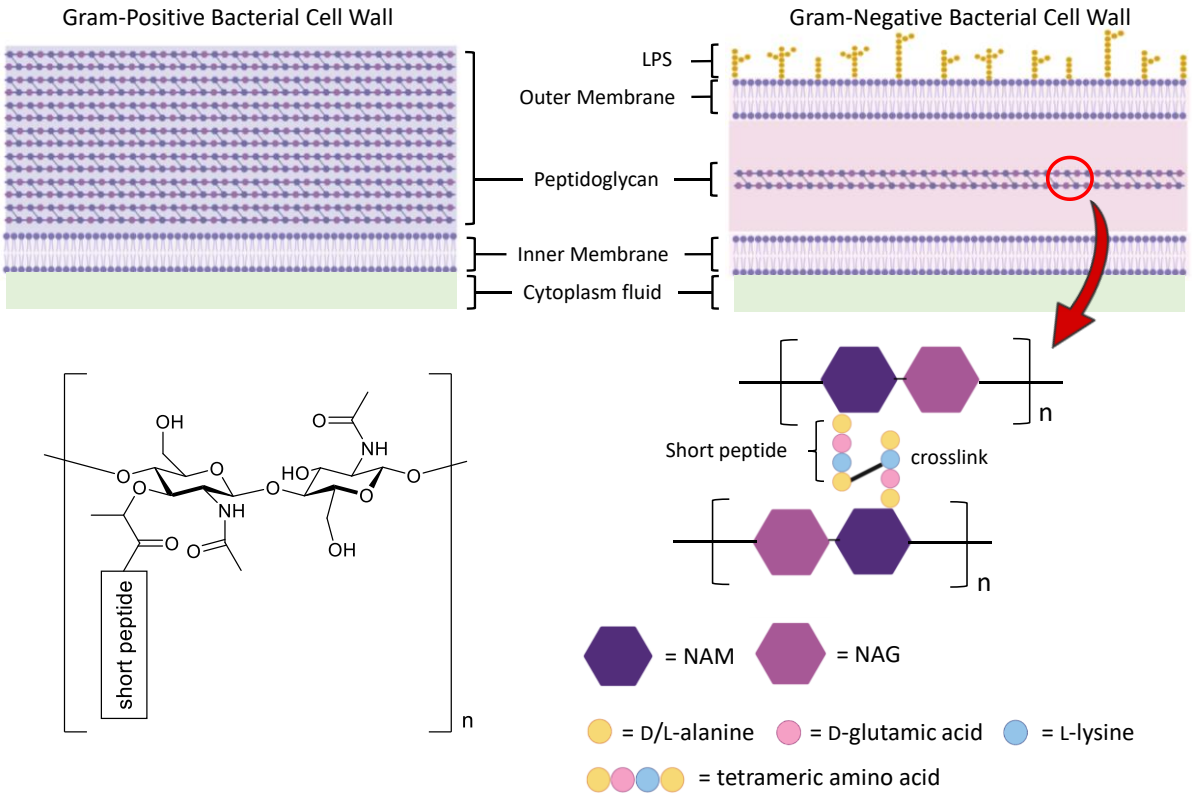

Figure 1.11: Gram-positive and Gram-negative bacterial cell walls and transpeptidation cross-link in peptidoglycan.[21]

Antibiotics that inhibit the transpeptidation step in the synthesis of bacterial peptidoglycan include both the glycopeptides and the penicillins. The glycopeptides (e.g. the natural product antibiotic vancomycin (**23**)) binds to the terminal D-alanine-D-alanine amino acids of the crosslinking precursor peptide via hydrogen bonding interactions and prevents the binding of the transpeptidase to the end of amino acid chain, thus inhibiting the peptidoglycan crosslink.[22]

The penicillins (e.g. the semi-synthetic natural product antibiotic amoxicillin (**24**)) are an important class of antibiotics, which have been clinically used since the 1940's. The penicillins bind to penicillin binding proteins (PBPs). The binding of penicillins to PBPs results in covalent modification of PBP. Both vancomycin (**23**) and amoxicillin (**24**) inhibit the synthesis of

bacterial cell wall preventing cell growth and ultimately results in cell death for dividing cells (Figure **1.12**).[23]

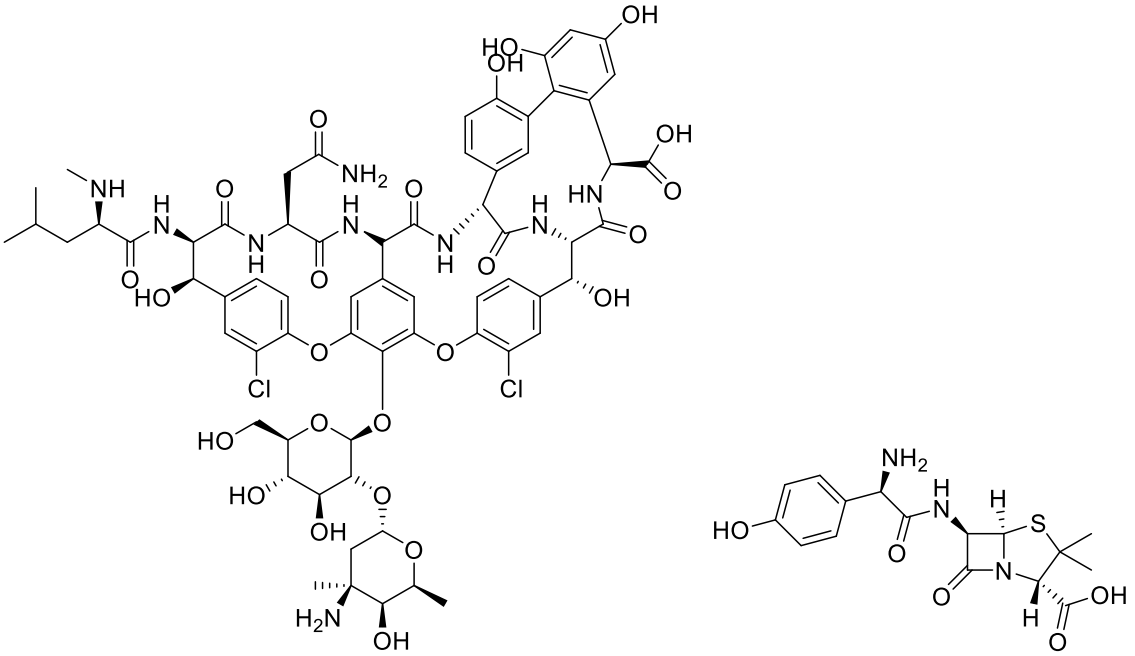

23 **24**

Figure 1.12: Natural products antibiotics that inhibit the synthesis of the bacterial cell wall: vancomycin (**23**) and amoxicillin (**24**).

1.2 Antibiotic resistance

Bacteria have ability to continually evolve and adapt to their environment. When a population of bacteria are exposured to an antibiotic, some individual bacteria show a natural resistance to that antibiotic. These bacteria survive and pass their resistance traits to their offspring. Repeated exposure to the same antibiotic results in repeated selection of the most resistant mutants leading to an antibiotic resistant strain of bacteria. Once a bacterial strain becomes immune to an antibiotic, it is known as antibiotic resistant strain. Antibiotic resistant pathogenic bacteria can be very dangerous as any infection becomes hard to treat.[24]

1.2.1 Antibiotic resistance in pathogenic resistance

The concept of antibiotic resistance in pathogenic bacteria was highlighted by Fleming as far back as 1945. In his Nobel Prize lecture, he gave the following hypothetical scenario: “Mr. X has a sore throat. He buys some penicillin and gives himself, not enough to kill the

Streptococci but enough to educate them to resist penicillin. He then infects his wife. Mrs. X gets pneumonia and is treated with penicillin. As the *Streptococci* are now resistant to penicillin the treatment fails. Mrs. X dies. Who is primarily responsible for Mrs. X's death? Why Mr. X whose negligent use of penicillin changes the nature of the microbe".[4] In fact strains of *Staphylococcus* resistant to penicillin were known in 1940, two years before the first commercial use of penicillin in 1942, with penicillin resistance in *Pneumococcus* being observed a few years later in 1965 (Figure **1.13**).[24]

The appearance of resistant pathogenic bacteria has been observed for all of the currently known antibiotic classes, often soon after their introduction. In the case of levofloxacin (**20**), which was discovered in 1996 and used to treat *Pneumococcus* infections, resistance was observed in the same year. Similarly, in the cases of linezolid and ceftaroline, antibiotic resistance first appeared in *Staphylococcus* just a year after the introduction of these antibiotics (Figure **1.13**).

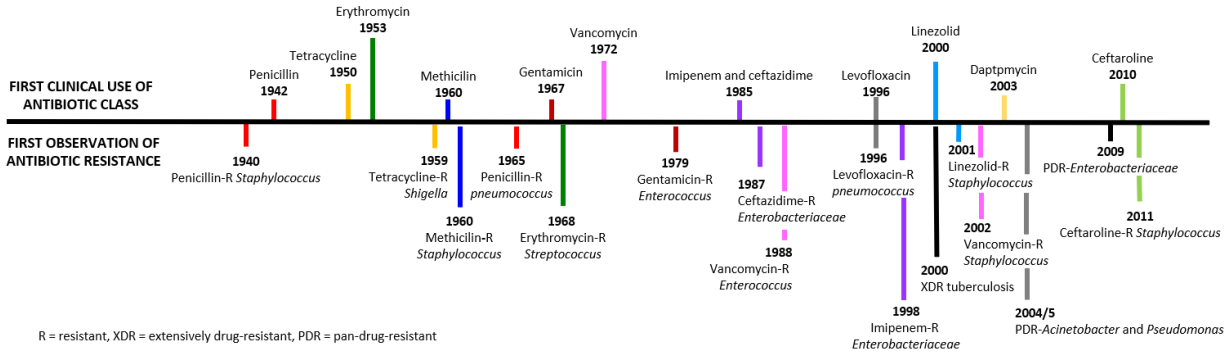

Figure 1.13: Timeline of the first clinical use of an antibiotic verses the first observation of antibiotic resistance in a pathogenic bacterium.

1.2.2 Disease burden as a consequence of antibiotic resistance

As highlighted in the World Health Organization (WHO) report (2014), the rise of antibiotic resistance in pathogenic bacteria is a significant threat to global human health.[25] Antibiotic resistance is on the increase in all parts of the world. For example, in the United States of America (USA) in 2013, approximately 2 million cases of infection with antibiotic resistant bacteria were recorded and more than 23,000 people died as a result of these infections.[26,27] Meanwhile in 2017 in the European Union (EU), approximately 25,000 people died because of infections from antibiotic resistant bacteria. Due to a predicted continuance rise in

antibiotic resistance infections, it is predicted that in EU in 2050, there may be up to 390,000 deaths per year from antibiotic resistant infectious diseases.[28]

Tuberculosis (TB) is infectious disease caused by *Mycobacterium tuberculosis* and is a major concern with respect to antibiotic resistance. In 2018 the WHO reported that there were approximately 10 million people infected with TB worldwide. There were 30 countries with particularly high TB rates, accounting for 87% of all new TB cases, with eight countries (India, China, Indonesia, Philippines, Pakistan, Nigeria, Bangladesh and South Africa) accounting for two thirds of the total number of cases. Of the reported new TB cases in 2018, there were 484,000 cases of rifampicin-resistant TB (RR-TB) along with 377,500 new cases of multidrug-resistant TB (MDR-TB) and extensively drug-resistant TB (XDR-TB). MDR-TB is resistant to the first line anti-TB drugs (isoniazid and rifampicin), whilst XDR-TB is also resistant to the fluoroquinolones and at least one of the three injectable second-line drugs (amikacin, kanamycin, or capreomycin).[29]

Antibiotic resistance is also common in many other diseases caused by pathogenic bacteria. In 2019, the Centers for Disease Control (CDC) highlighted several key pathogenic bacteria of specific concern with respect to antibiotic resistance, namely *Enterococcus faecium, Staphylococcus aureus, Klebsiella pneumoniae, Acinetobacter baumannii, Pseudomonas aeruginosa*, and *Enterobacter* spp. Known collectively as the ESKAPE pathogens, these bacteria are a major cause of antibiotic resistant infections. For example, in USA in 2017, there were 197,000 cases and approximately 9,100 deaths reported caused by the extended spectrum of β-lactamase resistant (ESBL) *Enterobacteriaceae.* In the USA in 2017, there were 323,700 cases and approximately 10,600 deaths reported caused by multi-drug resistant (MDR) *Staphylococcus aureus.* MDR *S. aureus* is classed as resistant to penicillin, methicillin, linezolid, vancomycin (**23**) and ceftaroline.[30]

Therefore, in order to overcome the continued rise in resistant pathogenic bacteria in a number of strategies are being attempted. Many countries are attempting to implement antibiotic stewardship approaches, to reduce the use of antibiotics in both humans and animals to slow down the rate of appreacrance of new strains of resisntant pathogenic bacteria. In addition, new antibiotics are often held in reserve and only used in critical cases, slowing the appearance of resistance. However, despite these measures, new strains of

pathogenic bacteria continue to arise, and as such there remains a pressing need to discover new antibiotics that are active against resistant pathogenic bacteria.

1.3 Microbes as a source of antibiotics

In this thesis, we will define natural products as secondary metabolites which are produced by a living organism. Natural products have been a focus of research for many years due to their interesting and diverse bioactivities. In fact, many of the clinically used antibiotic drugs are derived from microbial natural products either as unchanged natural products (e.g. vancomycin (**23**)), semi-synthetic natural products (e.g. rifampin (**21**)) or as totally synthetic molecules but based on a natural product (e.g. brodimoprin).[31]

An example of a class of clinically used antibiotic derived from a natural product are the penicillins. Penicillin G, also known as benzylpenicillin, was first isolated from the fungus *Penicillium chrysogenum* in 1928 by Fleming *et al*. and was first used in the clinic in 1942 to treat bacterial infections caused by *Staphylococcus* and *Streptococcus.*[2,32] Subsequently, many semi-synthetic penicillins have been developed for clinical use. Starting 1960, methicillin was introduced to the clinic as the first semi-synthetic penicillin, followed by oxacillin (1960), cloxacillin (1960), flucloxacillin (1961), dicloxacillin (1961), ampicillin (1961), carbenicilllin (1967), pivampicillin (1971), amoxicillin (1972), metampicillin (1972), talampicillin (1974), ticarcillin (1975), bacampicillin (1975), mezlocillin (1977), azlocillin (1977), epicillin (1979), piperacillin (1980), clavulanic acid (1981), temocillin (1984), sulbactam (1986), and tazobactam (1992).

Newman and Cragg reviewed the drugs approved for clinical use between 1981 and 2019. They showed that of the 1394 small molecules approved for clinical use, 32.6% were either unaltered natural products (N, 5.1%) or natural product derivatives (ND, 27.5%).[28] Unaltered natural products (N) are secondary metabolites, isolated directly from living organism (e.g. bacteria, fungi or plants), whilst natural product derivatives (ND) are natural products modified by semi-synthesis.[31] Of the small molecules approved for clinical use, 68.5% have arisen from natural product research. This includes, synthetic drugs based on a NP pharmacophore (S*,4.8%), synthetic drugs which act as natural product mimics (S/NM, 15.7%) and synthetic drugs based on a natural product pharmacophore which act as natural

product mimics (S*/NM, 14.8%). Therefore, in total of all the small molecules approved for clinical use, 35.3% were inspired by natural products (Figure **1.14**).[31]

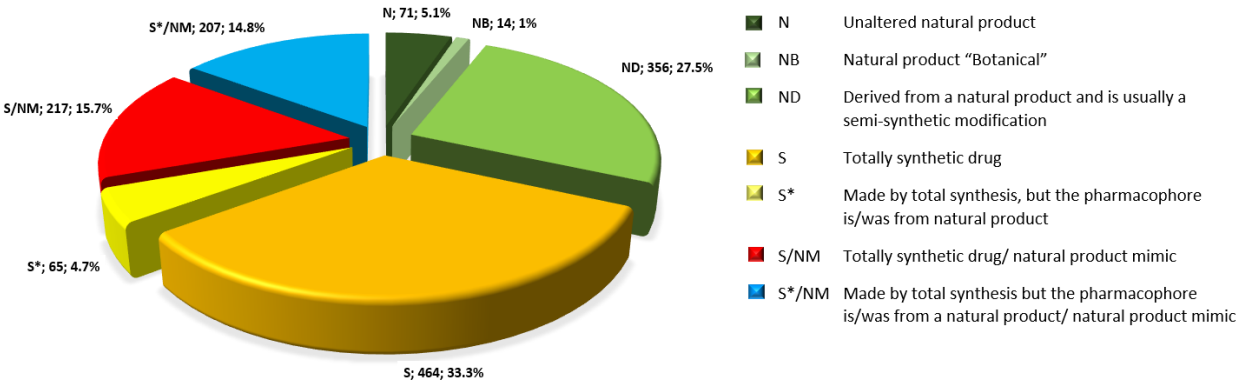

Figure 1.14: All small molecules approved drugs between 1981 and 2019.

In the specific case of antibiotics, 162 new chemical entities were approved for use between 1981 and 2019, of which 36 were large peptides, 4 were proteins (B, 2%), 32 were vaccines (V, 20%) and 126 were small molecules (78%). Of the 126 small molecule approved for clinical use as antibiotics, 11 were natural products (N, 7%), 78 were semi-synthetic natural products (ND, 48%) and 1 was a synthetic drug based on a natural product pharmacophore, which acts as a natural product mimic (S*/NM, 1%) (Figure **1.15**).[31]

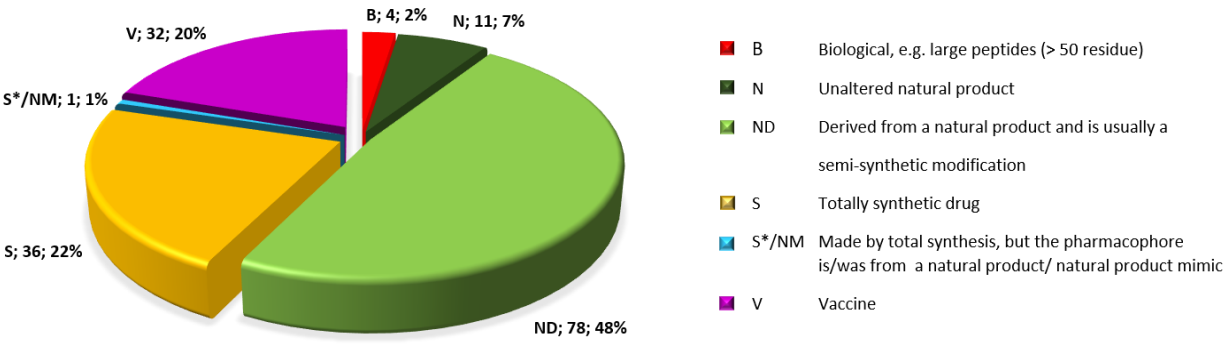

Figure 1.15: Clinically used antibiotics discovered between 1981 and 2019.

Interestingly, of the 89 clinically used antibiotics approved between 1981 and 2019 derived from natural products, 44 were natural products or natural product derivatives arising from Actinobacteria (49%). Actinobacteria are well known for their biosynthesis of complex

secondary metabolites, especially the genus *Streptomyces.* One of the first ever antibiotics, streptomycin, was isolated from *Streptomyces griseus* by the Waksman's group in 1943.[33] Since then, many antibiotics have been isolated from *Streptomyces* bacteria including the cephalosporins (*S. clavuligerus*, 1945), chloramphenicol (*S. venezuelae,* 1949), neomycin (*S. fradie*, 1949), the tetracyclines (*S. aureofaciens,* 1950), nystatin (*S. noursei,* 1950), viomycin (*S. puniceus*/*S. vinaceus*, 1951), virginiamycin (*S. virginiae,* 1952), lincomycin (*S. lincolnensis,* 1952), cycloserine (*S. garyphalus,* 1955), vancomycin (*S. orientalis,* 1956), novobiocin (*S. niveus*, 1956), kanamycin (*S. kanamyceticus,* 1957), fosfomycin (*S. fradiae,* 1969), ribostamycin (*S. ribosidificus,* 1970), miokamycin (*S. mycarofaciensis,* 1985), imipenem (*S. cattleya,* 1985), rokitamycin (*S. kitasatoensis,* 1986), dalfopristin (*S. pristinaespiralis,* 1999), daptomycin (*S. roseosporus,* 2003) and platensimycin (*S. platensis,* 2006).[34]

1.4 Modern natural product isolation approaches

The majority of the known antibiotic natural products were previously isolated from bacteria using a "classical" bioassay guided fractionation approach in which bacterial fermentation broth is fractionated via a number of chromatography steps, with the most bioactive fraction selected at each stage, leading to a final isolated natural product. However, this approach has failed to continue to discover new compounds and often leads to rediscovery of known natural products. The failure to discover new compounds has been attributed to a number of reasons including: (a) lack of diversity in the bacteria examined, (b) reliance on a limited range of bioassays and (c) the use of similar growth conditions for bacteria.

To overcome these issues a number of modern natural product isolation approaches have been developed, which we will review herein.

1.4.1 Novel antibiotic natural products from extremophiles

Extremophiles are understudied microorganisms which live in extreme conditions such as very low or high pHs, very cold or hot temperatures, high pressures, high salinities or are exposured to ionising radiation.[35] In order to survive in these extreme conditions, the extremophiles have evolved unique metabolic pathways, including those that are based on the metabolisms of molecules such as methane or elemental sulphur. Due to their unique

metabolism and their understudied nature it has been proposed that they may be important sources of undiscovered natural products.[36] For example, abyssomicin C (**25**), is a novel antibiotic polyketide produced by *Verrucosispora* AB-18-032, an Actinobacteria isolated from a depth of over 280 meters in the Sea of Japan (Figure **1.16**).[37,38]

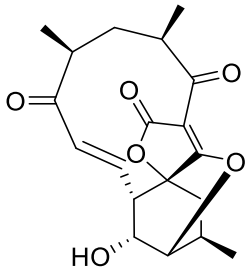

25

Figure 1.16: The natural product antibiotic abyssomicin C (**25**).

1.4.2 Novel antibiotic natural products from "unculturable bacteria"

Only 1% of the total known microbial species can be cultured under normal laboratory growth conditions, the other 99% being defined as "unculturable bacteria".[39] Since "unculturable bacteria" have not been previously investigated as sources of natural products, if they could be grown, they could be an important source of new molecules.

For example, Epstein *et al.* have devised an iCHIP (isolation CHIP) approach for the isolation and culturing of previously unculturable bacteria. This iCHIP technology was used to isolate a new species of β-proteobacteria, *Eleftheria terrae*, which produced teixobactin (**26**). Teixobactin (**26**) is a novel natural product antibiotic which has activity against Gram-positive pathogens including methicillin-resistant *Staphylococcus aureus* (MRSA) with minimum inhibition concentration (MIC) of 0.25 μg/mL (Figure **1.17**).[40,41]

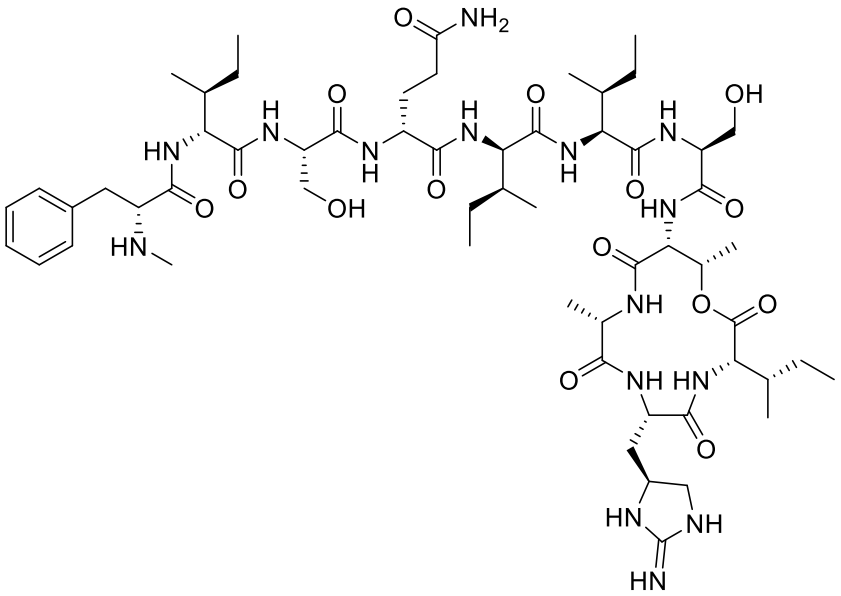

26

Figure 1.17: The natural product antibiotic teixobactin (**26**).

1.4.3 Novel antibiotic natural products through heterologous expression of 'silent' biosynthetic gene clusters

A biosynthetic gene cluster (BGC) encodes for the proteins responsible for the biosynthesis of a secondary metabolite.[42,43] However, when bacteria are cultured under normal laboratory conditions, many BGCs are not expressed (described as "silent") and the corresponding natural products are not produced.[44,45] To solve this problem, the "silent" gene cluster can be introduced into a heterologous host (an engineered bacterium from different species) and the host modified to "turn on" the expression of the BGC followed by the isolation and characterisation of the natural product thus produced.[46,47] For example, the genome of the marine actinomycete *Saccharomonospora sp*. CNQ-490 contains 19 BGCs, one of which has a high degree of similarity with the BGC known to encode for the production of the clinically approved natural product antibiotic daptomycin (**22**). However, no daptomycin like molecules could be detected from fermentations of *Saccharomonospora sp*. CNQ-490. Therefore this "silent" gene cluster was introduced into a heterologous host, *Streptomyces coelicolor*. Following fermentation of the heterologous host, a novel antibiotic lipopeptide, taromycin A (**27**) was isolated, which shows activity against MRSA (MIC = 12.5 μg/mL).[48] Taromycin A (**27**)

differs from daptomycin (**22**) through two aryl chlorinations and modified lipophilic side chain (Figure **1.18**).[49]

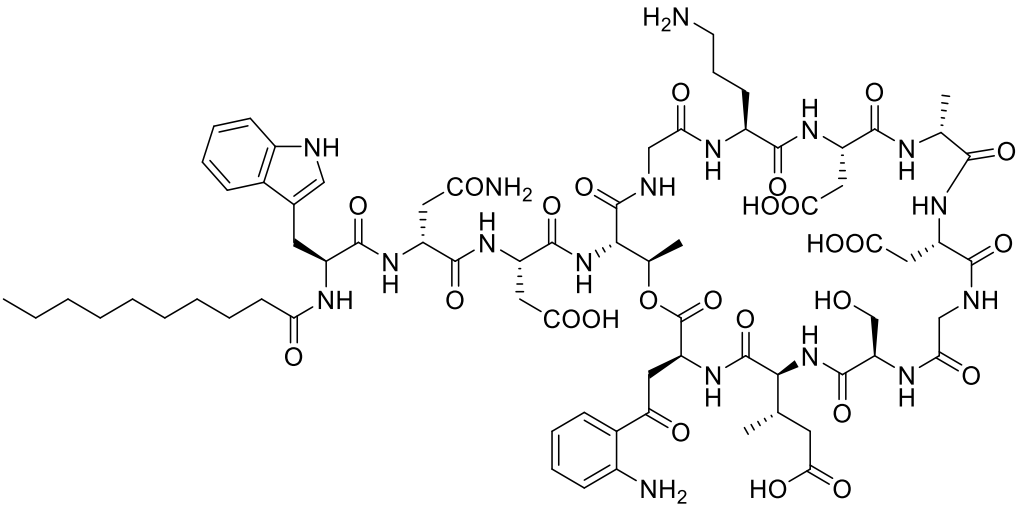

22

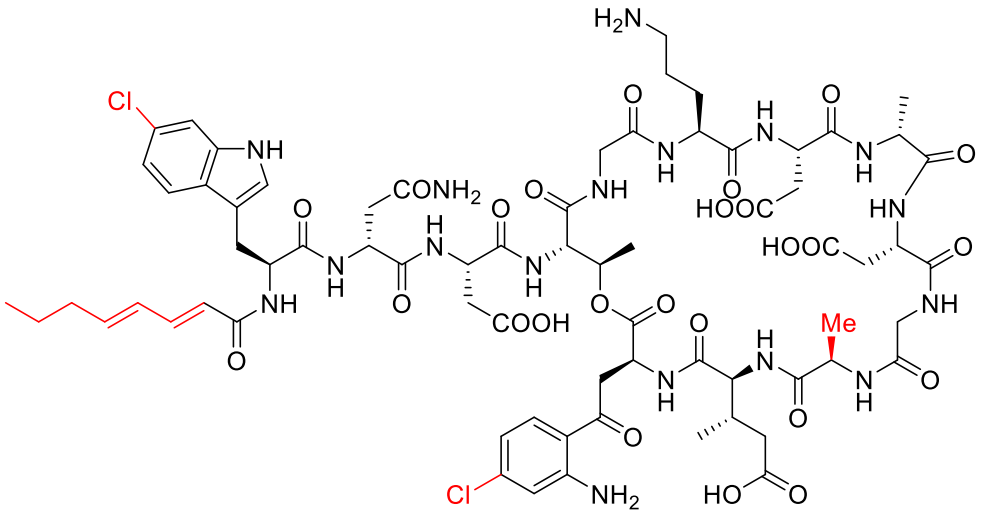

27

Figure 1.18: The different functional groups of daptomycin (**22**) vs taromycin A (**27**) (highlighted in red).

1.5 New natural product polyketide antibiotics from Actinobacteria

The natural product DEM30355/A (**28**) was isolated from an extremeophilic Actinobacteria (*Amycolaptosis sp.* DEM30355) by our collaborator, Dr Kepplinger. DEM30355/A (**28**) is a polyketide natural product with a highly oxygenated fused tricyclic structure, containing five contiguous stereocentres and three quaternary centres. The absolute configuration of DEM30355/A (**28**) has been previously determined using X-ray diffraction analysis to be

(2*S*,3*S*,4*R*,4a*R*,10*R*)-DEM30355/A (**28**) (Table **1.1**). In preliminary testing, DEM30355/A (**28**) showed inhibition against a range of Gram-positive bacteria (Table **1.1**).[50]

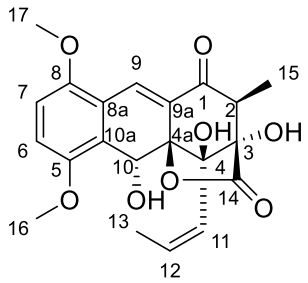

(2*S*,3*S*,4*R*,4a*R*,10*R*)-DEM30355/A

28

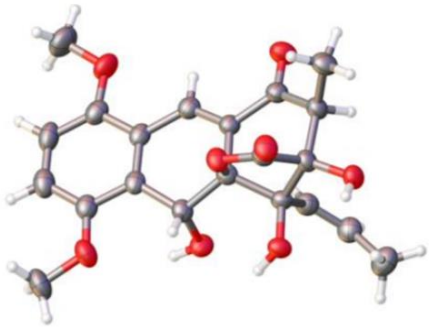

Bacteria	MIC (μg/mL)	Bacteria	MIC (μg/mL)
Bacillus subtilis	16	*Streptococcus pyogenes*	8
Enterococcus faecalis	16	*Staphylococcus aureus*	4
Enterococcus faecium	64	*Staphylococcus aureus (MRSA)*	8
Listeria monocytogenes	16	*Staphylococcus epidemidis*	8

Table 1.1: Molecular structure (**left**) and X-ray crystal structure (**right**) of DEM30355/A (**28**). Table of minimum inhibitory concentration (MIC) of DEM30355/A (**28**) against a range of Gram-positive bacteria.[50]

Interestingly, the molecular structure of DEM30355/A (**28**) is similar to that of (-)-rishirilide A (**29**), a polyketide natural product isolated from *S. rishiriensis* OFR-1056. Both DEM30355/A (**28**) and (-)-rishirilide A (**29**) have a fused tricyclic structure with a lactone bridge between the central ring and the right-hand ring. DEM30355/A (**28**) has two methoxy groups on the aromatic ring (C-5 and C-8) and a *cis*-alkene attached at C-4, whilst (-)-rishirilide A (**29**) contains a single hydroxyl group at the C-5 position of the aromatic ring and an isopentyl group at the C-4 position (Figure **1.19**).

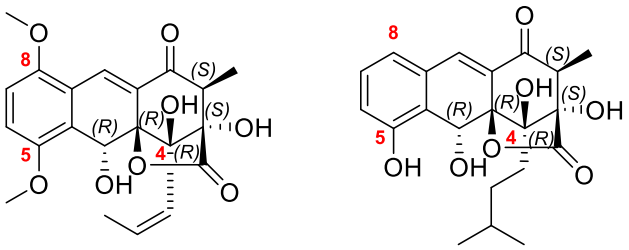

28 **29**

Figure 1.19: DEM30355/A (**28**) and (-)-rishirilide A (**29**).

Although (-)-rishirilide A (**29**) has been shown to be a weak inhibitor of α-2-macroglobulin (IC_{50} 100 µg/mL), nothing is known about its potential as an antibiotic.[51]

1.6 Project aim

Therefore, the aim of this PhD project is to determine if (-)-rishirilide A (**29**) has antibiotic activity, based on its structural similarity to DEM30355/A (**28**). To achieve this, we will examine methods for the production and isolation of (-)-rishirilide A (**29**) via optimised bacterial fermentation. We will then examine the antibiotic activity and mode of action of this understudied natural product.

Chapter 2. Production and Isolation of (-)-Rishirilide A and (+)-Rishirilide B

Based on the structural similarity between (-)-rishirilide A (**29**) and DEM30355/A (**28**), we proposed that (-)-rishirilide A (**29**) might show similar antibiotic activity to the known antibiotic DEM30355/A (**28**). In this chapter, we aim to examine the production of (-)-rishirilide A (**29**) and isolate sufficient quantities of it to show if it has antibiotic activity as we have speculated (Figure **2.1**).

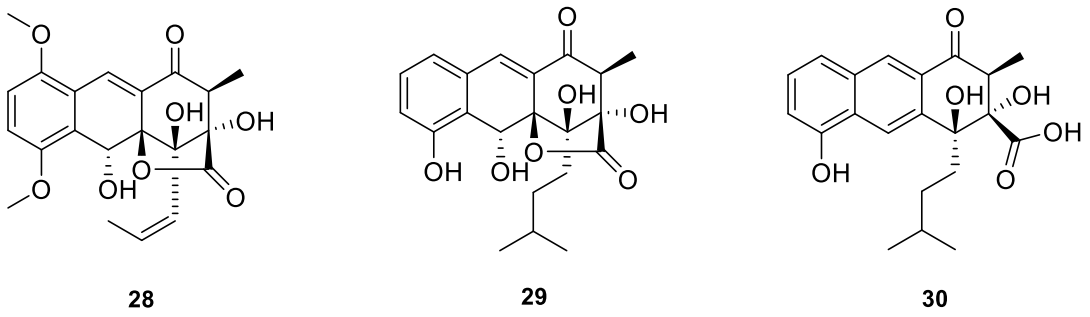

Figure 2.1: The natural products DEM30355/A (**28**), (-)-rishirilide A (**29**), and (+)-rishirilide B (**30**).

(-)-Rishirilide A (**29**) along with a related polyketide (+)-rishirilide B (**30**), were originally isolated from *Streptomyces rishiriensis* OFR-1056 by Iwaki *et al*. in 1984.[51] Although, (-)-rishirilide A (**29**) and (+)-rishirilide B (**30**) are known as inhibitors of *α*-2-macroglobulin (α2M) with an IC_{50} of 100 μg/mL for (-)-rishirilide A (**29**) and 35 μg/mL for (+)-rishirilide B (**30**), nothing is known about their antibiotic activities.[51]

Following this work, in 2012 the Bechthold group from Freiburg, Germany, reported the reisolation of both (-)-rishirilide A (**29**) and (+)-rishirilide B (**30**) from *S. bottropensis*. As part of this work, Bechthold *et al.* also identified threebiosynthetic gene clusters (BGCs) of type II polyketide synthases (PKSs) which encode for the production of the mensacarcin (*msn* cluster), the rishirilide (*rsl* cluster), and a putative spore pigment (*mec* cluster) in *S. bottropensis.* To study the biosynthesis of rishirilides, Bechthold *et al.* introduced the *rsl* cluster (known as cosmid 4 or cos4) into a general heterologous host, *Streptomyces albus* J1074, by intergeneric conjugation. Therefore, *S. albus*::cos4 makes both (-)-rishirilide A and (+)-rishirilide B.[52]

To support our studies, we chose to employ *S. bottropensis* as a source of the rishirilides due to the availability of the strain. The *S. bottropensis* used herein was supplied by the group of Bechthold.

2.1 Examination of the production of (-)-rishirilide A and (+)-rishirilide B from *S. bottropensis*

Our first challenge was to determine whether *S. bottropensis* could be used to produce sufficient quantities of both (-)-rishirilide A (**29**) and (+)-rishirilide B (**30**) for further study. To determine this, we decided to evaluate the production of secondary metabolites by *S. bottropensis* in liquid medium containing glucose yeast extract and maltose (GYM), based on a modified protocol by Yan.[52]

2.1.1 Fermentation of *S. bottropensis* in liquid medium (GYM)

To test the production of (-)-rishirilide A (**29**) and (+)-rishirilide B (**30**) from *S. bottropensis*, we carried out a 2 x 500 mL liquid fermentation of *S. bottropensis* in GYM medium. We used GYM medium because GYM is a simple and good medium for many *Streptomyces spp*. Therefore, to begin with, *S. bottropensis* was grown on solid soya flour mannitol (SFM) agar and one eighth of the area of the agar plate containing *S. bottropensis* colonies was inoculated into 50 mL of tryptic soy broth (TSB) in a 250 mL baffled flask. The culture was incubated at 28 °C in a shaking incubator (140 rpm) overnight. Subsequently, the inoculant was transferred into two 2 L baffled flasks, each containing 500 mL of GYM, and incubated at 28 °C (140 rpm) for five days with pH monitoring.

During the fermentation of *S. bottropensis*, we carried out a Kirby-Bauer disk diffusion assay to examine the antibiotic activity of the fermentation broth as a rapid test for the production of secondary metabolites. In this Kirby-Bauer disk diffusion assay, *Escherichia coli* K12-ATCC25404, KanR (*E. coli*^{kanR}) was used as the pathogenic Gram-negative bacterium, in which kanamycin used as a selective agent to isolate *E. coli* containing gene for kanamycin resistance. For the Gram-positive bacterium, *Bacillus subtilis*, *YvqI* strain with erythromycin resistance (*B. subtilis*^{eryR})[53], was used as a selective agent to isolate *B. subtilis* containing erythromycin resistance. A positive Kirby-Bauer disk diffusion assay will not give direct evidence for the production of the rishirilides (as the antibiotic activity is unknown and may be masked by the presence of other secondary metabolites) but should indicate when

secondary metabolite production occurs. Besides producing the rishirilides, *S. bottropensis* is known to produce bottromycin, mensacarcin, dunaimycin, and scabichelin which have numerous bioactivities including antibacterial, antifungal, and anticancer activity.[54,55]

The Kirby-Bauer disk diffusion assays of the fermentation broth of *S. bottropensis* showed no activity against Gram-negative *E. coli*^{kanR} (Table **2.1**, day 0 and 1). However, from the second day of fermentation the Kirby-Bauer disk diffusion assays shows activity against Gram-positive *B. subtilis*^{eryR}. Gram-positive bacteria are more susceptible to antibiotics than Gram-negative bacteria and therefore are more likely to show a positive result, even at low concentrations of antibiotic. Thus, the observed activity against *B. subtilis*^{eryR} supports the production of secondary metabolites in both test fermentations (Table **2.1**).

Day	pH		ZOI (against *E. coli*^{kanR})		ZOI (against *B. subtilis*^{eryR})	
	Flask 1	Flask 2	Flask 1	Flask 2	Flask 1	Flask 2
0	7	7	-	-	-	-
1	8	8	0	0	0	0
2	8	8	0	0	11	9
3	8	8	0	0	10	6
4	8	8	0	0	10	6
5	8	8	0	0	7	7

Table 2.1: The pH and antibiotic activity of the fermentation broth of *S. bottropensis* against *E. coli*^{kanR} and *B. subtilis*^{eryR}, ZOI = radius of the zone of inhibition in mm.

Now that we have confirmed the production of secondary metabolites from *S. bottropensis*, in the next step we decided to harvest the fermentation broth to test for the presence of the target molecules (-)-rishirilide A (**29**) and (+)-rishirilide B (**30**).

2.1.2 Extraction of the fermentation broth of *S. bottropensis*

In order to isolate the secondary metabolites, Amberlite XAD-16N was added into the fermentation broth of *S. bottropensis* and the broth was placed on a shaker overnight. The Amberlite XAD-16N was separated by filtration, washed with water, and soaked in methanol overnight. The Amberlite XAD-16N was removed by filtration and the methanol extract was concentrated under reduced pressure. Water was added to the methanol extract and the resulting mixture of methanol-water was washed with petroleum ether to remove lipids, acidified with $HCl_{(aq)}$ 1M (pH4), and extracted with ethyl acetate. The resulting ethyl acetate extract was evaporated under reduced pressure to give dark brown gum (16.5 mg) which then analysed using analytical HPLC.

2.1.3 HPLC analysis of the ethyl acetate extract of the fermentation broth of *S. bottropensis*

To prepare a sample for HPLC analysis, the ethyl acetate extract of *S. bottropensis* was dissolved in methanol and then diluted with water to give a 20:80, methanol:water solution. The sample was filtered with a 0.22 µm Millipore syringe filter to remove any remaining particles and analysed by reversed phase C-18 HPLC with UV/Vis monitoring at 254 nm.

The HPLC chromatogram showed the presence of (+)-rishirilide B (**30**) as a small peak at retention time of 17.7 minutes, confirmed by the analysis of the UV/Vis spectra (λ_{max} = 220,

275, 315 and 390 nm). This data is consistent with the UV/Vis spectra of (+)-rishirilide B (**30**) reported by Iwaki.[51] However, HPLC analysis of the ethyl acetate extract of *S. bottropensis* did not show the presence of (-)-rishirilide A (**29**) (Figure **2.2**).[56,57]

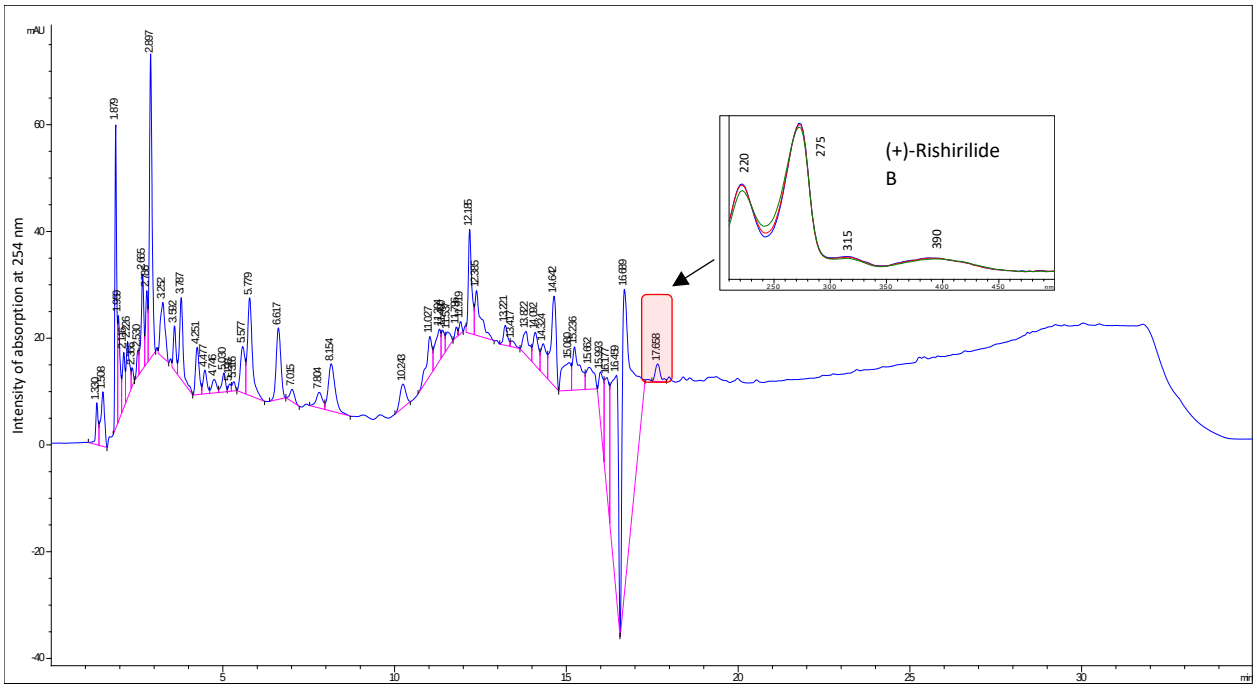

Figure 2.2: HPLC chromatogram of the ethyl acetate extract of *S. bottropensis* at 254 nm. Peak at retention time of 17.7 minutes shows (+)-rishirilide B (**30**), UV/Vis spectrum shown as insert.

In conclusion, we have successfully carried out a liquid fermentation of *S. bottropensis* in GYM medium to produce secondary metabolites and confirmed the presence of the (+)-rishirilide B (**30**). Unfortunately, the corresponding (-)-rishirilide A (**29**) was not observed, suggesting that *S. bottropensis* is not a good production source of (-)-rishirilide A (**29**).

2.2 Examination of the production of (-)-rishirilide A and (+)-rishirilide B from *Streptomyces albus*::cos4

Due to the poor production of (-)-rishirilide A (**29**) by *S. bottropensis*, we decided to examine an alternative bacteria, *S. albus*::cos4, as a potential producer of (-)-rishirilide A (**29**). *S. albus*::cos4 is a heterologous host bacterium in which the 28 genes of the BGC of rishirilide B from S. bottropensis was inserted into S. albus J1074, to encode the production of the both (-)-rishirilide A (**29**) and (+)-rishirilide B (**30**) (Table **2.2**).[58]

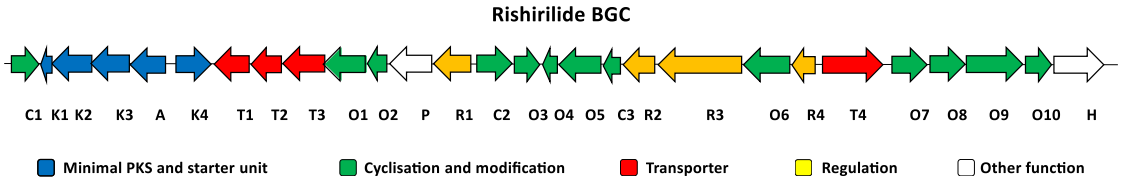

Genes	Product
rslC1	Putative cyclase/aromatase
rslK1	Acyl carrier protein
rslK2	Ketosynthase
rslK3	Ketosynthase
rslA	Acyltransferase
rslK4	Ketosynthase
rslT1	ABc transporter protein
rslT2	ABc transporter protein
rslT3	ABc transporter protein
rslO1	Luciferase-like monooxygenase
rslO2	Flavin reductase
rslP	Putative phospotransferase
rslR1	SARP regulatory protein
rslC2	Putative cyclase
rslO3	Ketoreductase
rslO4	Monooxygenase/ putative anthronoxygenase
rslO5	Oxidoreductase
rslC3	Putative cyclase/ aromatase
rslR2	SARP regulatory protein
rslR3	SARP regulatory protein
rslO6	Luciferase-like monooxygenase
rslR4	Putative transcriptional regulator
rslT4	Transporter protein
rslO7	Oxidoreductase
rslO8	Oxidoreductase
rslO9	FAD dependant monooxygenase

rslO10	Ketoreductase
rslH	Putative amidohydrolase

Table 2.2: Biosynthetic gene cluster of the rishirilides, including a list of the individual genes and their products.[58]

Bechthold *et al.* have proposed that both (-)-rishirilide A and (+)-rishirilide B are type II polyketides, biosynthesised from an isobutyrate-CoA starter unit and eight malonyl-CoA extender units. Following the construction of the carbon backbone through a standard polyketide biosynthesis, decarboxylation and epoxidation of the quinone ring, the epoxide is reductively ring opened by rslO5 with reduced Flavin mononucleotide ($FMNH_2$). Then the right-hand ring is expanded via an enzyme mediated Baeyer-Villiger oxidation (rslO9, $FADH_2$), the molecule undergoes an intramolecular aldol reaction (rslO9) and finally reduction (rslO8, NADPH) to give (-)-rishirilide A. It is then proposed that (+)-rishirilide B is formed through opening of the lactone and subsequent dehydration (rslO9) (Figure **2.3**).[59]

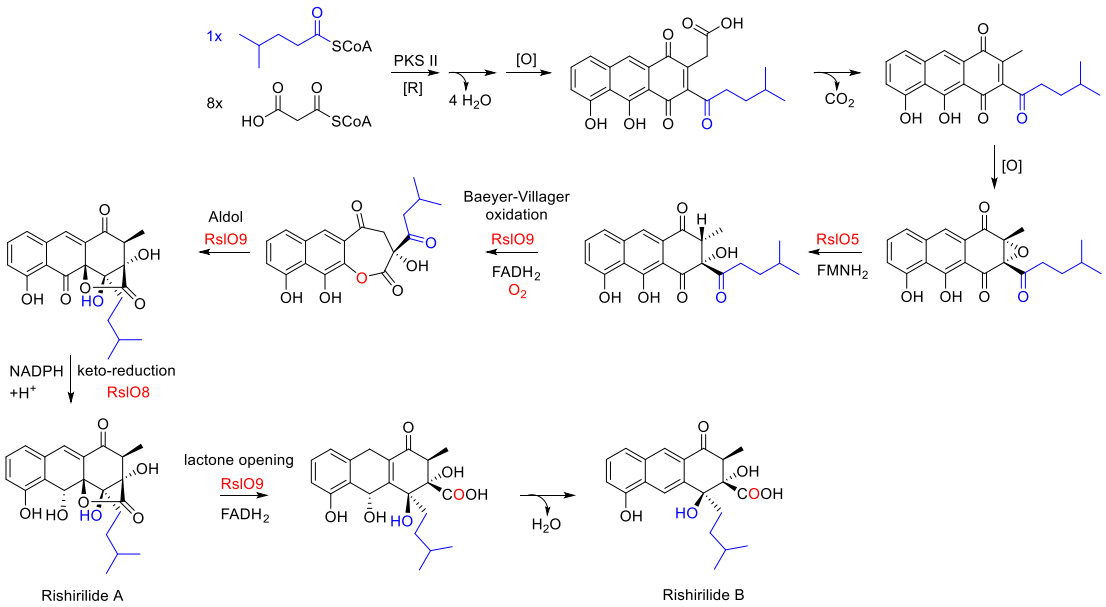

Figure 2.3: Proposed biosynthetic pathway of the rishirilides.[59]

S. albus::cos4 was created and supplied by the group of Bechthold, who have previously shown that it is capable of the production of both (-)-rishirilide A (**29**) and (+)-rishirilide B (**30**) from *S. albus*::cos4 on a small scale. Thus, we decided to examine the large scale fermentation of *S. albus*::cos4 as a potential source of (-)-rishirilide A (**29**).[52]

2.2.1 Fermentation of *S. albus*::cos4 in liquid medium (GYM)

Therefore we examined the fermentation of *S. albus*::cos4, following a similar method to that used of *S. bottropensis*, to test the production of (-)-rishirilide A (**29**) and (+)-rishirilide B (**30**).

As part of the construction of *S. albus*::cos4, a gene for apramycin resistance was included.[51] Therefore, apramycin (50 µg/mL) was added to all liquid medium for the fermentation of *S. albus*::cos4 to maintain a selection pressure for the retention of the rishirilde BGC. Following our previous fermentation of *S. bottropensis*, *S. albus::cos4* was grown on SFM agar, inoculated into TSB medium and incubated at 28 °C overnight. Subsequently the inoculant was transferred into two 2 L baffled flasks each containing 500 mL of GYM and incubated at 28 °C (140 rpm) for 5 days as before.

After 5 days, isolation of secondary metabolites from *S. albus*::cos4 was carried out as previously via liquid-solid extraction with Amberlite XAD-16N, elution with methanol and concentration under reduced pressure to give a methanol extract of *S. albus*::cos4. Subsequently, water was added, and the methanol-water mixture was washed with petroleum ether, acidified with $HCl_{(aq)}$ 1 M (pH4) and extracted with ethyl acetate. The resulting ethyl acetate extract was evaporated under reduced pressure to give a 56 mg of dark brown gum which then was analysed using analytical HPLC (Figure **2.4**).

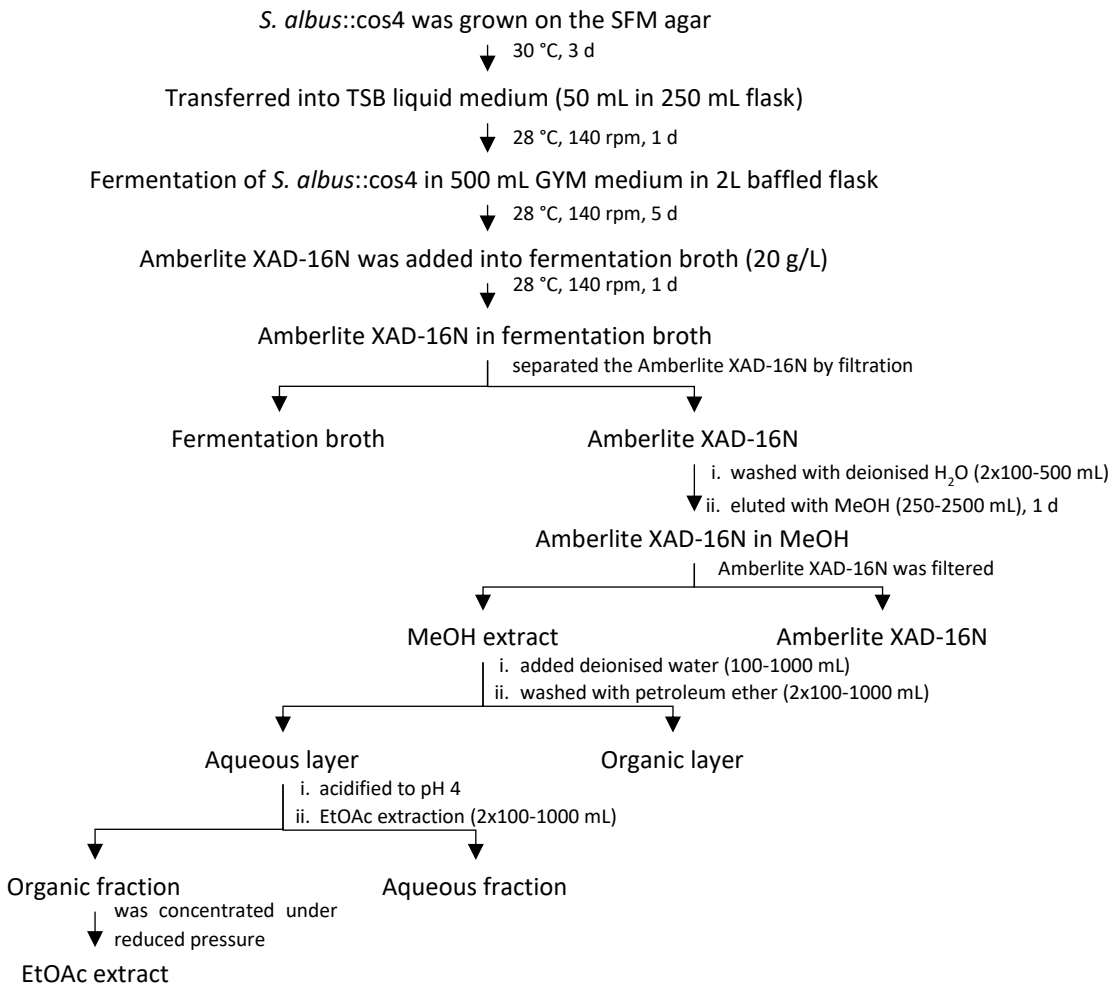

Figure 2.4: Flow diagram for the fermentation of *S. albus*::cos4 followed by extraction of secondary metabolites.

2.2.2 HPLC analysis of the ethyl acetate extract of the fermentation broth of *S. albus*::cos4

Following the same sample preparation method as for the *S. bottropensis* extract, the ethyl acetate extract was dissolved in 20:80, methanol:water, filtered (0.22 µm Millipore syringe filter) to give a yellow solution which was then analysed by HPLC. The analytical HPLC was performed using Agilent Eclipse Plus C-18 column (4.6 x 150 mm, 3.5 µm) a gradient method from 20:80 to 95:5, acetonitrile (0.1% by v/v FA):water (0.1% by v/v FA) over 35 minutes with a flowrate of 0.5 mL/min.

The HPLC chromatogram showed a key peak major at 22.294 minutes, confirmed by UV/Vis analysis to be (+)-rishirilide B (**30**) (Figure **2.5**). Unfortunately, we did not observe any peaks that clearly corresponded to (-)-rishirilide A (**29**) by HPLC.

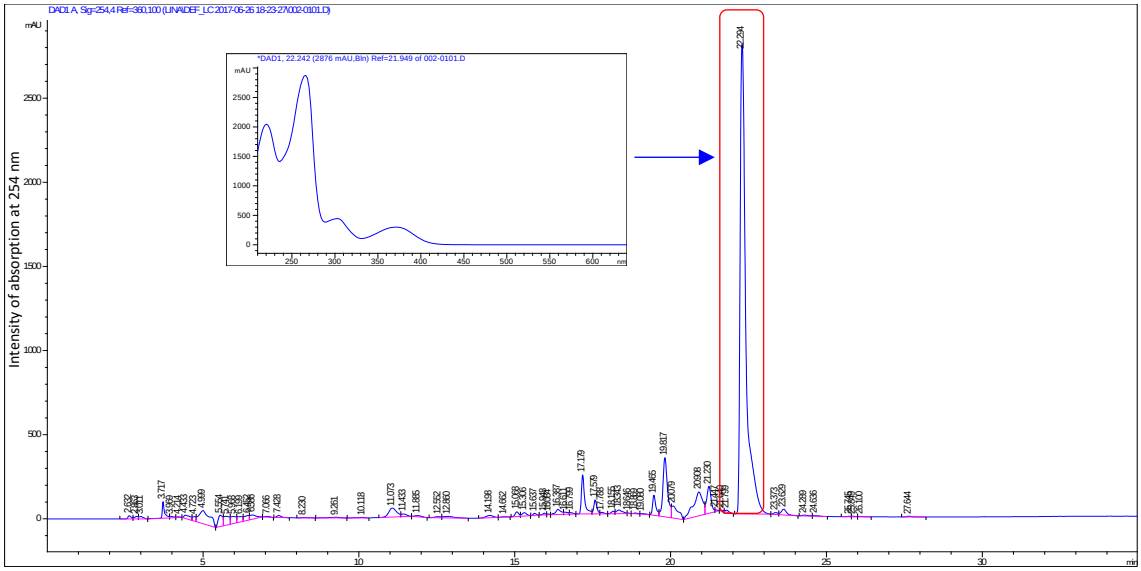

Figure 2.5: HPLC chromatogram of ethyl acetate extract of *S. albus*::cos4.

At this stage the ethyl acetate extract (*S. albus*::cos4) appeared to be predominately (+)-rishirilide B (**30**) by HPLC. Therefore, we decided to confirm this assignment by NMR. In order to further clean-up the ethyl acetate extract (*S. albus*::cos4) for NMR experiments, we carried out a solid phase extraction. The ethyl acetate extract (*S. albus*::cos4) was dissolved in water, loaded on to a HyperSEP C-18 (100 mg/3 mL) SPE cartridge, eluted with methanol, and evaporated under reduced pressure to give an ethyl acetate/SPE (*S. albus*::cos4) extract as a solid residue (27.5 mg).

2.2.3 ^{1}H TOCSY analysis of the ethyl acetate/SPE extract of *S. albus*::cos4

To provide confirmation of the production of (+)-rishirilide B (**30**) by *S. albus*::cos4, we decided to examine the ethyl acetate/SPE extract for by ^{1}H NMR.

Therefore, the ethyl acetate/SPE extract of *S. albus*::cos4 was dried overnight by high vacuum to remove any remaining solvent, dissolved with deuterated methanol (CD_3OD) and analysed by ^{1}H NMR (Dr Wills, Newcastle University).

The ^{1}H NMR spectrum was complex showing many signals across the whole spectra, likely due to the presence of many different secondary metabolites, making the assignment of any (+)-rishirilide B (**30**) present difficult. Due to the presence of several peaks in the aromatic region in the literature spectra of (+)-rishirilide B (**30**), we decided to focus on this region to look for

the presence of the natural product. Examination of the aromatic region showed ^{1}H NMR signals which looked similar to those reported for (+)-rishirilide B (**30**).

To further simplify analysis, we decided to carry out a total correlation spectroscopy (TOCSY) experiment. ^{1}H TOCSY shows correlations between all the protons within a particular spin system, in the case of (+)-rishirilide B (**30**) the aromatic protons.

The ^{1}H TOCSY spectrum showed that the proton signals at 6.93 (H-6), 7.32 (H-7), 7.47 (H-8) and 8.47 ppm (H-9) were part of a single spin system, and therefore part of the same molecule. These four signals correlated well with the reported spectra of (+)-rishirilide B (**30**), confirming the presence of the natural product (Figure **2.6**).

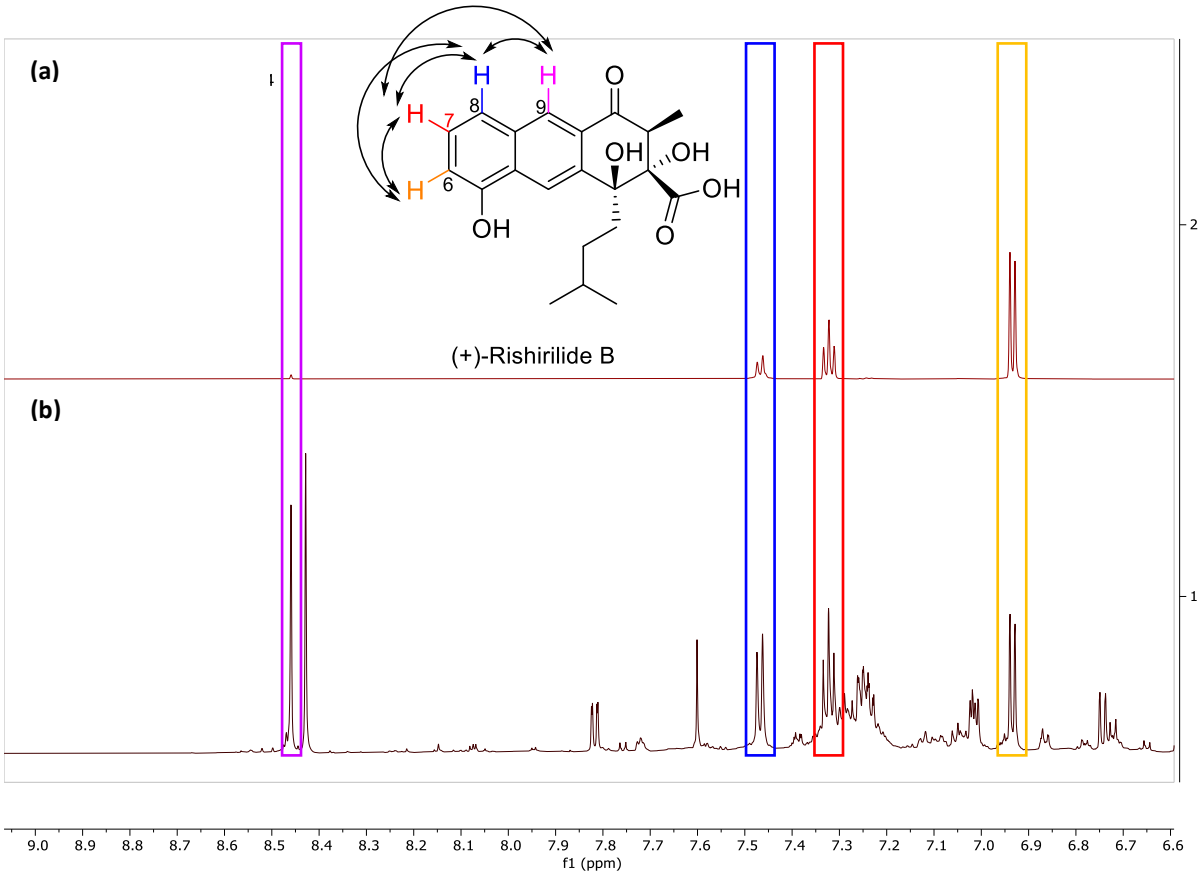

Figure 2.6: The aromatic region of the ^{1}H NMR spectra of the ethyl acetate/SPE extract of *S. albus*::cos4 with signals corresponding to the aromatic CHs of (+)-rishirilide B (**30**)highlighted; (**a**) ^{1}H TOCSY; (**b**) ^{1}H NMR spectra.

2.2.4 LCMS analysis of the ethyl acetate/SPE extract of *S. albus*::cos4

Due to the relative poor sensitivity of HPLC as an analytical method, we decided to further examine the ethyl acetate/SPE extract of *S.albus*::cos4 using LCMS, a more sensitive analytical tool, to look for trace production of (-)-rishirilide A (**29**).

Following the preparation of a sample for LCMS and subsequent analysis, the LCMS chromatogram showed a key peak at 30.2 minutes with *m/z* signals of 395.1483 and 767.3084, corresponding to $[M+Na]^+$ and $[2M+Na]^+$ ions of (+)-rishirilide B (**30**) respectively. Excitingly (-)-rishirilide A (**29**) could also be observed in the LCMS chromatogram with a peak at 20.7 minutes, with *m/z* signals of 411.1420 and 799.2973, corresponding to the $[M+Na]^+$ and $[2M+Na]^+$ ions of (-)-rishirilide A (**29**) (Figure **2.7**).

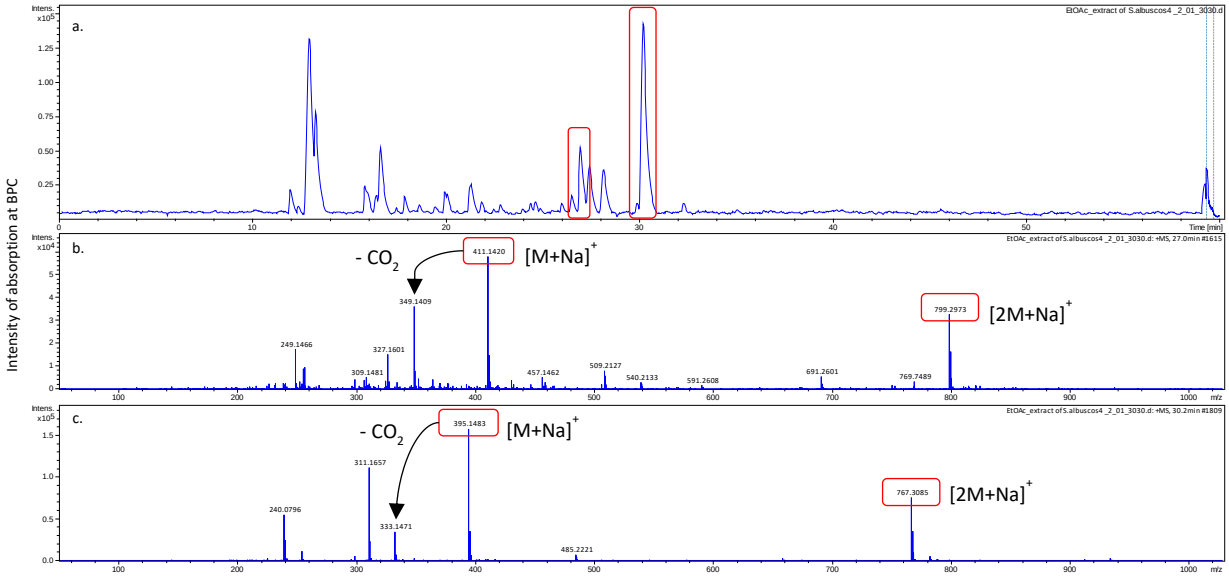

Figure 2.7: (**a**) LCMS chromatogram of the ethyl acetate/SPE extract of *S. albus*::cos4; (**b**) MS spectrum of the peak at 27.0 minutes corresponding to (-)-rishirilide A (**29**); (**c**) Mass spectrum of peak at 30.2 minutes corresponding to (+)-rishirilide B (**30**).

In conclusion, we have successfully shown that both (-)-rishirilide A (**29**) and (+)-rishirilide B (**30**) can be produced from *S. albus*::cos4 in liquid (GYM) medium. Under our conditions (+)-rishirilide B (**30**) is the major secondary metabolite, with (-)-rishirilide A (**29**) only formed in very small quantities. Therefore our next task was to scale up the fermentation of *S. albus*::cos4, to provide sufficient quantities of (-)-rishirilide A (**29**) for biological evaluation.

2.3 The isolation of (-)-rishirilide A and (+)-rishirilide B from *S. albus*::cos4

2.3.1 Large scale fermentation of *S. albus*::cos4 in liquid medium (GYM)

Therefore, to isolate a sufficient amount of (-)-rishirilide A (**29**) and (+)-rishirilide B (**30**) we decided to carry out a fermentation of *S. albus*::cos4 in liquid media on a 6 L scale with the aim of providing milligram quantities of (-)-rishirilide A (**29**).

Following the results of our previous small scale fermentation, *S. albus*::cos4 was grown on SFM agar, inoculated into two 250 mL baffled flasks each containing 50 mL TSB medium and incubated at 28 °C overnight. Subsequently the inoculant was transferred into three 1 L baffled flasks each containing 200 mL of GYM medium and incubated at 28 °C overnight. Next the inoculant was split between twelve 2 L baffled flasks each containing 500 mL of GYM medium. Altogether resulting 6 L of inoculated GYM medium was incubated at 28 °C (140 rpm) for 5 days (Figure **2.8**).

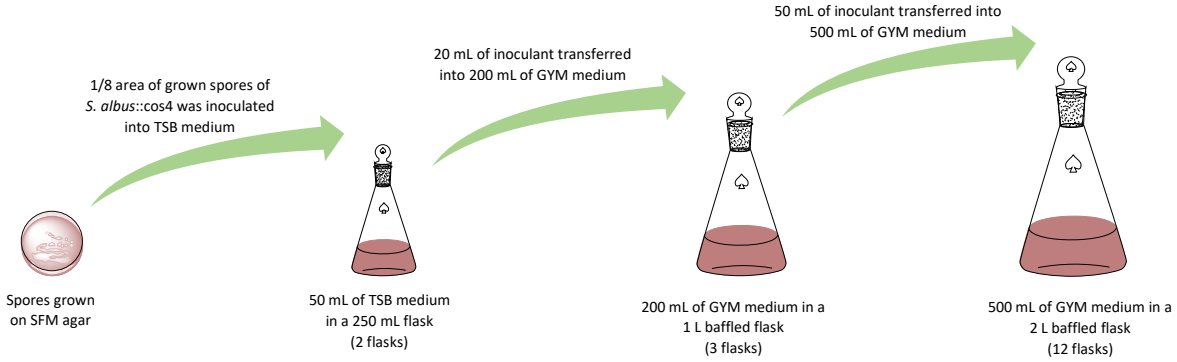

Figure 2.8: Flow diagram for the scale up fermentation of *S. albus*::cos4.

After 5 days, isolation of secondary metabolites including both (-)-rishirilide A (**29**) and (+)-rishirilide B (**30**) was carried out as previously through liquid-solid extraction with Amberlite XAD-16N, followed elution with methanol and concentration under reduced pressure. Following addition of water, the extract was washed petroleum ether, acidified to pH4 and extracted with ethyl acetate. The resulting ethyl acetate extract was evaporated under reduced pressure to give a 340 mg of dark brown gum.

During the course of the fermentation, the fermentation broth was tested on a daily basis for any contamination by other bacteria species. To test for contamination, a loopful of

fermentation broth was streaked onto a nutrient agar (NA) plate and the plate was incubated at 30 °C overnight. The next day, we examined the agar plate for any bacteria contamination by looking for the appearance of colonies with different morphologies to *S. albus*::cos4. Our 6 L fermentation of *S. albus*::cos4 did not show any contamination throughout the growth period (Figure **2.9**).

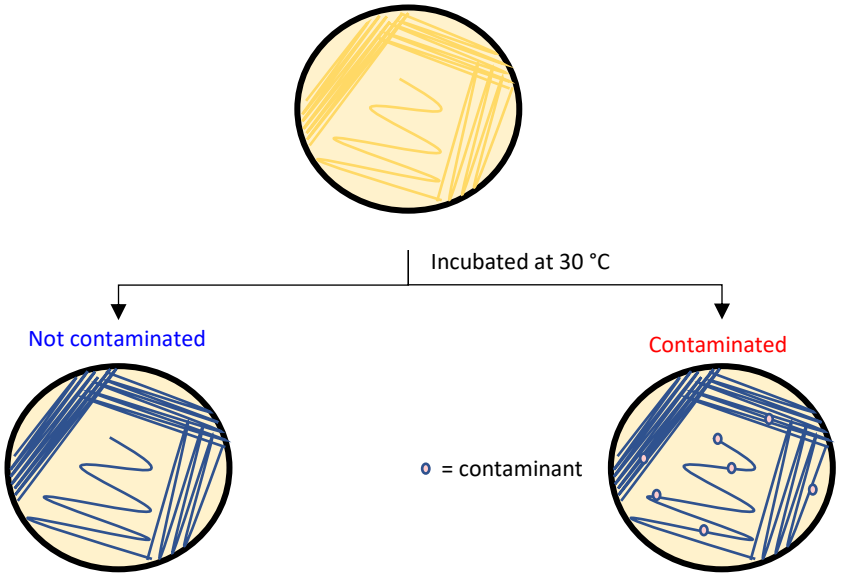

Figure 2.9: Test for bacterial contamination, (**left**) example of a non-contaminated fermentation, (**right**) example of a contaminated fermentation.

Having the ethyl acetate extract of *S. albus*::cos4 in hand, our next step was to test for the presence of (-)-rishirilide A (**29**) and (+)-rishirilide B (**30**) by HPLC.

2.3.2 HPLC and LCMS analysis of the ethyl acetate extract of the 6 L scale fermentation of *S. albus*::cos4

Therefore, we prepared a sample of the ethyl acetate extract for HPLC as previously in 20:80, methanol:water. Analytical HPLC was performed using a gradient elution from 20:80 to 95:5, acetonitrile (0.1% by v/v FA):water (0.1% by v/v FA) over 35 minutes with a flowrate of 0.5 mL/min, monitoring UV/Vis absorbance at 254 nm.

As previously, the HPLC chromatogram showed a peak at 22.148 minutes corresponding to (+)-rishirilide B (**30**), further confirmed by UV/Vis analysis. Examination of the UV/Vis spectra corresponding to the minor peaks in the HPLC chromatogram suggested that these were not (-)-rishirilide A (**29**). Interesting a large negative peak was observed at a retention time of 20.4

minutes and we envisaged that this negative peak could correspond to (-)-rishirilide A (**29**) due to the reported long wavelength absorption maxima of the natural product (λ_{max} = 319 nm). Thus, we repeated the HPLC analysis using the same sample, but monitoring UV/Vis absorbance at 320 nm. The HPLC chromatogram at 320 nm now showed a large positive peak at 20.4 minutes with a UV/Vis spectrum which matched the literature (Figure **2.10**).

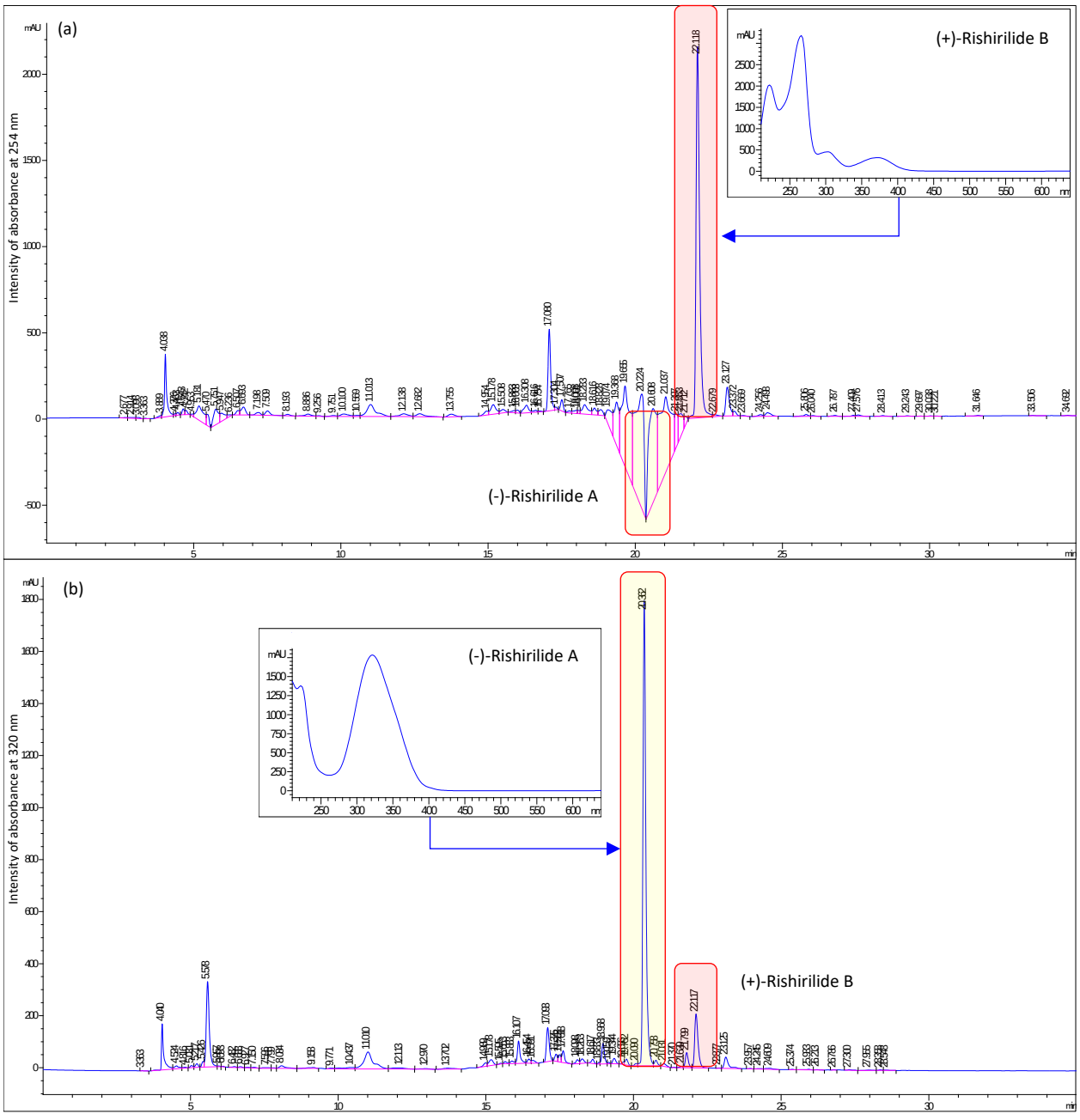

Figure 2.10: HPLC chromatograms of the ethyl acetate extract of *S. albus*::cos4; (**a**) with UV/Vis absorbance monitoring at 254 nm (**b**) with UV/Vis absorbance monitoring at 320 nm.

To further validate that the peaks at 20.4 and 22.1 minutes were (-)-rishirilide A (**29**) and (+)-rishirilide B (**30**) respectively, we then analysed these peaks by LCMS.

Therefore, to collect the two peaks at 20.4 and 22.1 minutes, we carried out a preparative HPLC experiment. For preparative HPLC, we used the same solvent gradient method as previously and collected our target peaks by automatic fraction collector. The two collected fractions were evaporated using a centrifugal evaporator.

Samples for LCMS were prepared in 20:80, methanol:water solution and the same solvent gradient method was used in LCMS analysis. The LCMS chromatogram of the 20.359 minute peak showed *m/z* signals of 411.1422 and 799.2946, corresponding to the $[M+Na]^+$ and $[2M+Na]^+$ ions of (-)-rishirilide A (**29**) respectively. The LCMS chromatogram of the 22.148 minute peak showed *m/z* signals at 395.1451, 417.1269 and 767.3020, corresponding to the $[M+Na]^+$, $[M+K]^+$ and $[2M+Na]^+$ ions of (+)-rishirilide B (**30**) respectively, confirming the presence of both (-)-rishirilide A (**29**) and (+)-rishirilide B (**30**).

In conclusion, we have successfully shown that fermentation (GYM) of *S. albus*::cos4 on a 6 L scale can produce both (-)-rishirilide A (**29**) and (+)-rishirilide B (**30**). Our next step was to isolate sufficient quantities of both (-)-rishirilide A (**29**) and (+)-rishirilide B (**30**) for further structural confirmation and bioactivity testing.

2.4 Purification of (-)-rishirilide A and (+)-rishirilide B from the ethyl acetate extract of 6L fermentation *S. albus*::cos4

2.4.1 Isolation of (-)-rishirilide A and (+)-rishirilide B through preparative HPLC

Since we initially required 10-20 milligrams of both (-)-rishirilide A (**29**) and (+)-rishirilide B (**30**) for further studies, we decided to use preparative HPLC, equipped with an autosampler and automated fraction collector, in order to gain rapid access to isolated material.

Therefore, we prepared samples for preparative HPLC in 20:80, methanol:water. Preparative HPLC was performed using a gradient elution (20:80 to 95:5, acetonitrile (0.1% by v/v FA):water (0.1% by v/v FA), 35 min, 1 mL/min)) with separation via a C-18 HPLC column (250 x 10.0 mm, 5 µm). Each preparative HPLC run involved the injection of 800 µL of sample, therefore separation of the total extract required more than 50 injections. The two peaks at

20.4 and 22.1 minutes were collected via automated fraction collector from each injection and pooled together.

The two pooled fractions were dried using a centrifugal evaporator and further purified by SPE to remove any residual formic acid. This gave two fractions containing (-)-rishirilide A (**29**) (white solid, 2.0 mg) and (+)-rishirilide B (**30**) (yellow solid, 2.2 mg).

2.4.2 Structural characterization of isolated (-)-rishirilide A and (+)-rishirilide B using ^{1}H NMR

The next step was to obtain ^{1}H NMR data for both fractions, to confirm the presence of (-)-rishirilide A (**29**) and (+)-rishirilide B (**30**) through comparison with the literature. Iwaki *et al.* had reported the ^{1}H NMR of (-)-rishirilide A (**29**) in CD_3OCD_3, and the ^{1}H NMR of (+)-rishirilide B (**30**) in CD_3OD. Thus, we prepared our ^{1}H NMR samples in the same deuterated solvents for easy comparison.

A. ^{1}H NMR of (-)-rishirilide A

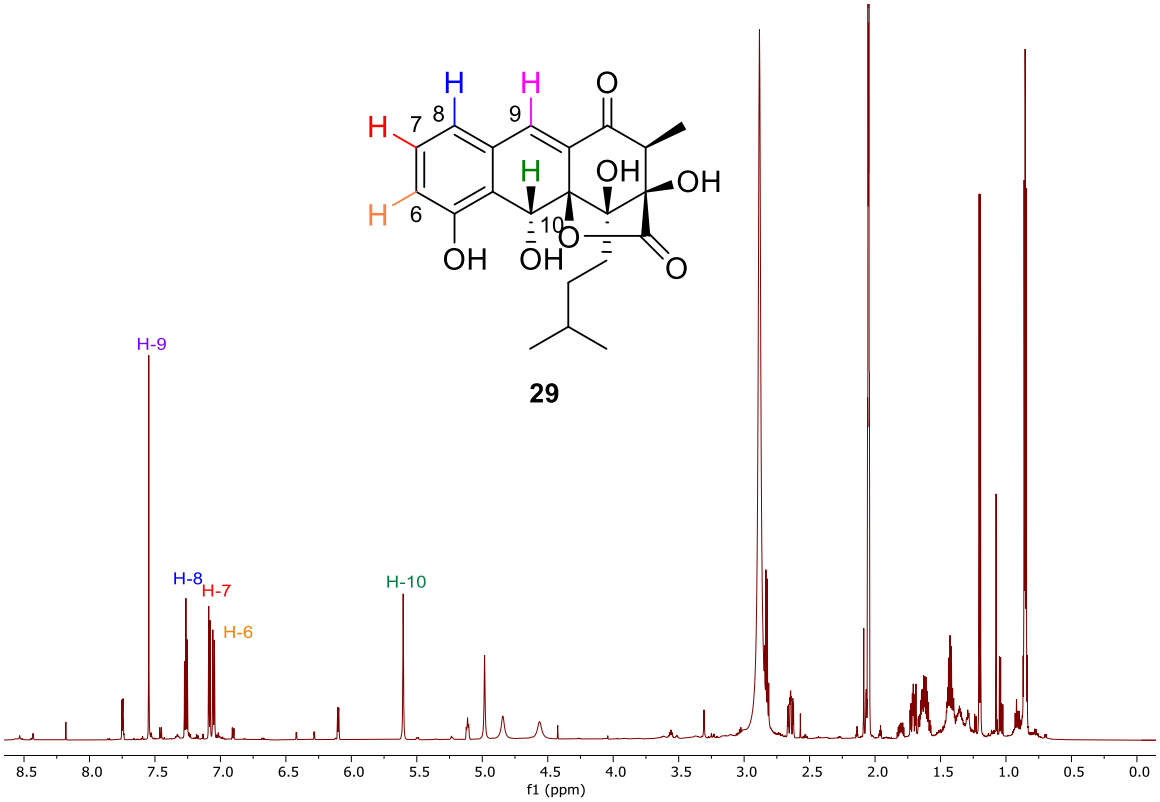

29

Figure 2.11: ^{1}H NMR spectrum of the fraction containing (-)-rishirilide A (**29**).

The ^{1}H NMR spectrum of the fraction containing (-)-rishirilide A (**29**) was compared to that previously published by the group of Iwaki. Our ^{1}H NMR data showed key signals corresponding to the H-6, H-7, H-8, H-9 and H-10 protons of (-)-rishirilide A (**29**) showing the presence of the natural product. It should be noted that a minor difference exists between the ^{1}H NMR of Iwaki *et al*. and that observed by ourselves, in the case of a potential 4-bond coupling between H-8 and H-9. Although we did not observe this coupling, likely due to the small coupling constant (J = 0.4 Hz) and differences in the NMR conditions, the NMR spctra are a sufficiently good match to show the presence of (-)-rishirilide A (**29**) (Figure **2.11**, Table **2.3**).

Position	Experiment, δ_H (J [Hz])[a]	Iwaki, δ_H (J [Hz])[b]
H-6	7.05 (dd, 8.2, 1.1)	7.06 (dd, 7.9, 1.4)
H-7	7.26 (t, 7.8)	7.26 (dd, 7.9, 8.0)
H-8	7.08 (dd, 7.5, 0.8)	7.08 (ddd, 8.0, 1.4, 0.4)
H-9	7.55 (s)	7.56 (d, 0.4)
H-10	5.60 (s)	5.61 (s)

[a] in CD_3OCD_3, 700MHz, [b] in CD_3OCD_3, 400 MHz

Table 2.3: The comparison of ^{1}H NMR spectral data of the (-)-rishirilide A (**29**) containing fraction and the literature.[51]

However, the ^{1}H NMR spectra of the fraction containing (-)-rishirilide A (**29**) showed a number of unassignable peaks, especially in the alkane region, suggesting the presence of a number of impurities.

When we repeated the ^{1}H NMR experiment on the next day, we observed that the ^{1}H NMR spectrum had become more complicated suggesting that (-)-rishirilide A (**29**) had degraded. The observed degradation of (-)-rishirilide A (**29**) may have occurred due to exposure to air (oxygen) whilst being stored at room temperature in solution (acetone) overnight (Figure **2.12**).

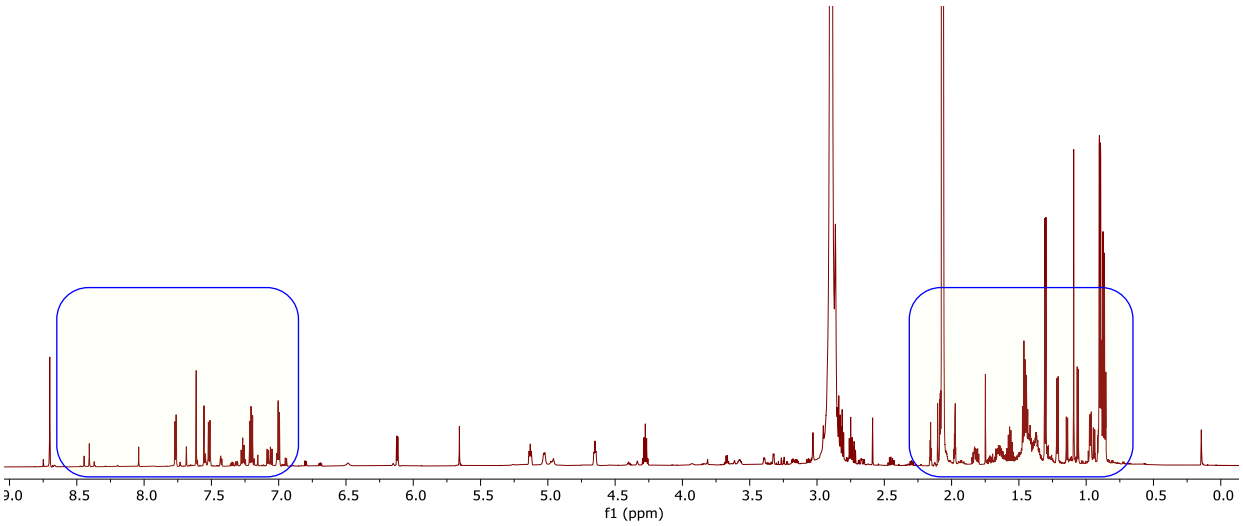

Figure 2.12: The ^{1}H NMR spectrum of the (-)-rishirilide A (**29**) fraction, following 24 hours at r.t. in CD_3COCD_3.

In order to identify the degradation products of the (-)-rishirilide A (**29**), we then carried out mass spectroscopy analysis to examine the molecular masses of this sample using LCMS/MS (Dr Gray, Pinnacle Laboratory, Newcastle University).

The LCMS/MS chromatogram showed three main peaks at 12.93, 18.94, and 22.03 minutes. The peak at 12.93 minutes showed a *m/z* signal of 389.1595, corresponding to the $[M+H]^+$ ion of (-)-rishirilide A (**29**), showing that some the natural product remained. The peak at 22.03 minutes showed a *m/z* signal of 345.1697, a molecular mass loss of 44 Da compared to the $[M+H]^+$ ion of (-)-rishirilide A (**29**). Thus, we proposed that the 22.03 minutes peak corresponded to a decarboxylation product ($-CO_2$) of (-)-rishirilide A (**29**). Meanwhile, the peak at 18.94 minutes showed a *m/z* signal of 343.1540, a molecular mass loss of 46 Da compared to the $[M+H]^+$ ion of (-)-rishirilide A (**29**). Thus, we proposed that this 18.94-minute peak corresponded to was a decarboxylation and oxidation of (-)-rishirilide A (**29**) (Figure **2.13**).

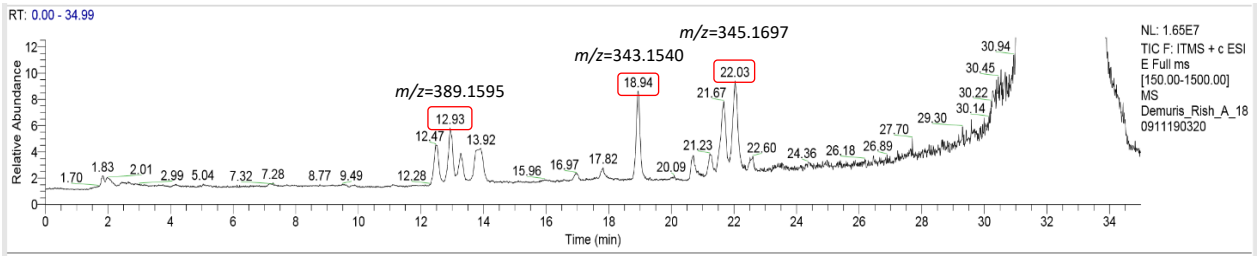

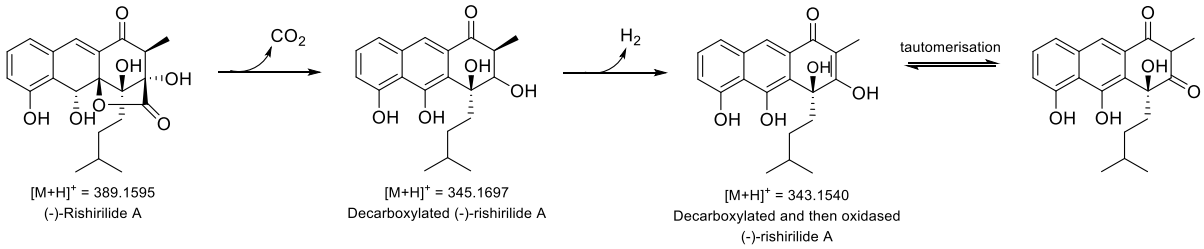

Figure 2.13: (**top**) LCMS/MS chromatogram of the (-)-rishirilide A (**29**) fraction, following 24 hours at r.t. in CD_3COCD_3; (**bottom**) the proposed structures of the observed degradation products of (-)-rishirilide A (**29**).

B. ^{1}H NMR of (+)-rishirilide B

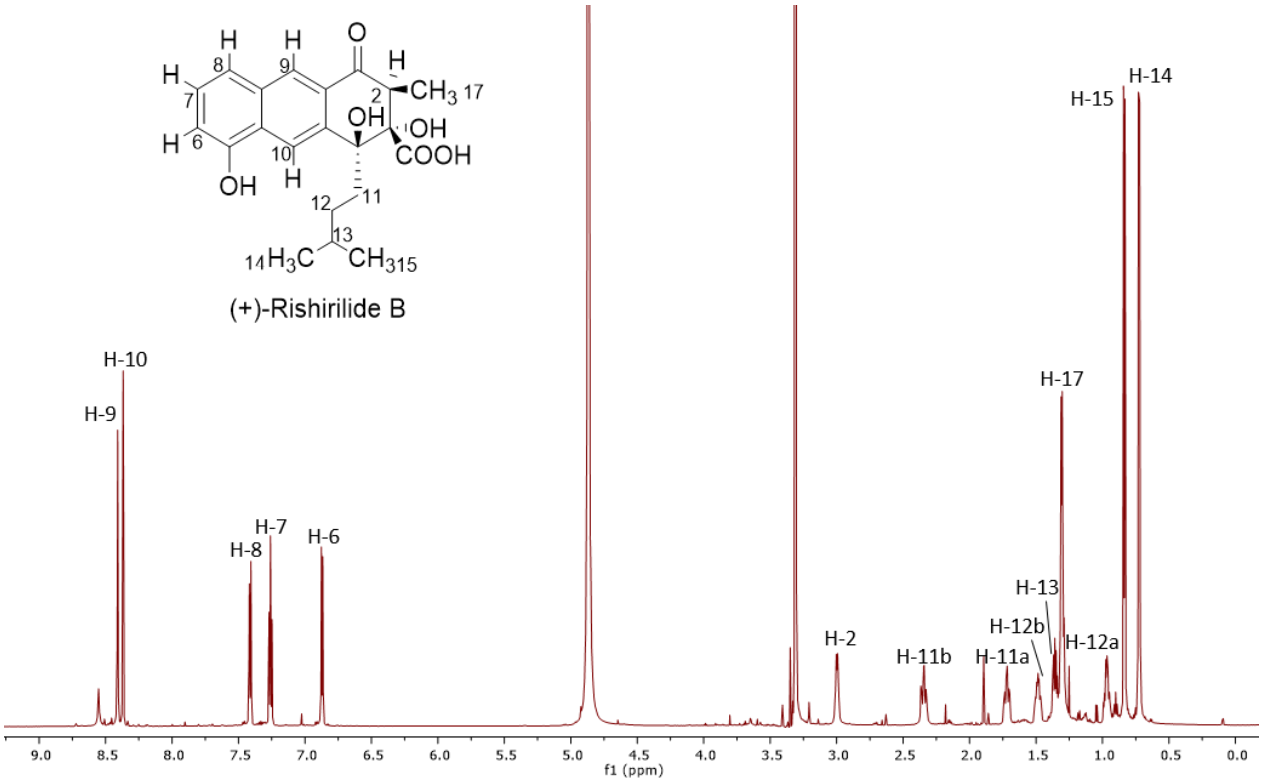

Figure 2.14: ^{1}H NMR spectrum of the fraction containing (+)-rishirilide B (**30**).

The ^{1}H NMR spectrum of the fraction containing (+)-rishirilide B (**30**) corresponded well with that reported by Iwaki, confirming the presence of the natural product along with some minor impurities (Figure **2.14**, Table **2.4**).

Position	Experiment, δ_H (J [Hz]) [a]	Iwaki, δ_H (J [Hz]) [b]
H-2	3.08 (q, 6.7)	3.06 (m)
H-6	6.87 (d, 7.5)	6.89 (d, 7.4)
H-7	7.26 (t, 7.8)	7.24 (dd, 7.4, 7.4)
H-8	7.45 (d, 8.2)	7.41 (d, 7.4)
H-9	8.41 (s)	8.41 (s)
H-10	8.37 (s)	8.37 (s)
H-11a	0.91 (ddd, 13.3, 6.8, 4.3)	1.45 – 1.73 (m)
H-11b	1.43 – 1.49 (m)	
H-12a	1.72 (ddd, 13.8, 12.2, 4.8)	2.34 (m)
H-12b	2.37 (ddd, 13.8, 12.4, 4.8)	
H-13	1.36 (m)	1.38 (m)
H-14	0.72 (d, 6.6)	0.70 (d, 6.6)
H-15	0.83 (d, 6.6)	0.81 (d, 6.6)
H-17	1.32 (d, 6.7)	1.31 (br d)

[a] in CD_3OD, 700MHz, [b] in CD_3OD, 400 MHz

Table 2.3: The comparison of ^1H NMR spectral data of the (+)-rishirilide B (**30**) containing fraction and the literature.[51]

In conclusion, we have successfully obtained samples of both (-)-rishirilide A (**29**) and (+)-rishirilide B (**30**) from our large scale (6 L) fermentation. 2.2 mg of (+)-rishirilide B (**30**) was obtained in reasonable purity, however the 2.0 mg of (-)-rishirilide A (**29**) was less pure and was found to degrade in solution. Unfortunately, the quantities and purities of the rishirilides produced by this method were insufficient for our planned biological evaluation of (-)-rishirilide A (**29**). We postulated that low yields and purities observed may be due to the stability of the rishirilides during the preparative HPLC purification, which involved over 2 weeks of purification time and exposed the rishirilides to acidic conditions (e.g. formic acid).

Thus, next we decided to re-examine our purification method in an attempt to isolate high purity (-)-rishirilide A (**29**) and (+)-rishirilide B (**30**).

2.4.3 Modified isolation method to obtain (-)-rishirilide A and (+)-rishirilide B from 6 L fermentation of *S. albus::cos4*

Therefore, next we decided to re-ferment *S. albus*::cos4 on a 6 L scale and isolate the rishirilides through a new method.

Following the previous method *S. albus*::cos4 was fermented in 6 L of GYM medium for 5 days. Initial isolation steps involved, solid-liquid extraction with Amberlite XAD-16N, washing with petroleum ether, and pH4 extraction with ethyl acetate, to give 401.3 mg of crude extract.

We then decided to carry out an initial purification of the crude ethyl acetate extract using normal-phase (NP) flash chromatography. The ethyl acetate extract was dry loaded onto silica using dichloromethane/methanol and then separated on a Biotage® SNAP ULTRA 50 g cartridge, using a gradient method of 100% dichloromethane to 100% methanol with a flowrate of 50 mL/min (Figure **2.15**).

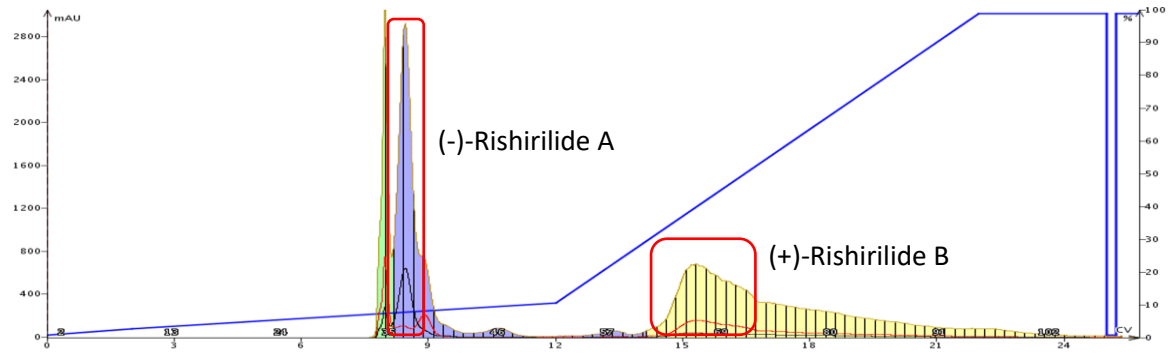

Figure 2.15: Chromatogram of NP flash chromatography of the ethyl acetate extract of *S. albus*::cos4.

Fractions obtained were analysed by thin layer chromatography (TLC, dichloromethane : methanol, 95:5) and based on the chromatogram and the TLC results were combined to give eight fractions. Subsequently, each fraction was evaporated and analysed by HPLC to look for the presence of (-)-rishirilide A (**29**) and (+)-rishirilide B (**30**). HPLC analysis (Agilent Eclipse Plus C-18 column (4.6 x 250 mm, 5 µm) with a similar gradient elution used previously)

showed that fraction 3 (45.5 mg) contained (-)-rishirilide A (**29**) and fraction 7 (114 mg) contained (+)-rishirilide B (**30**) (Figure **2.16**).

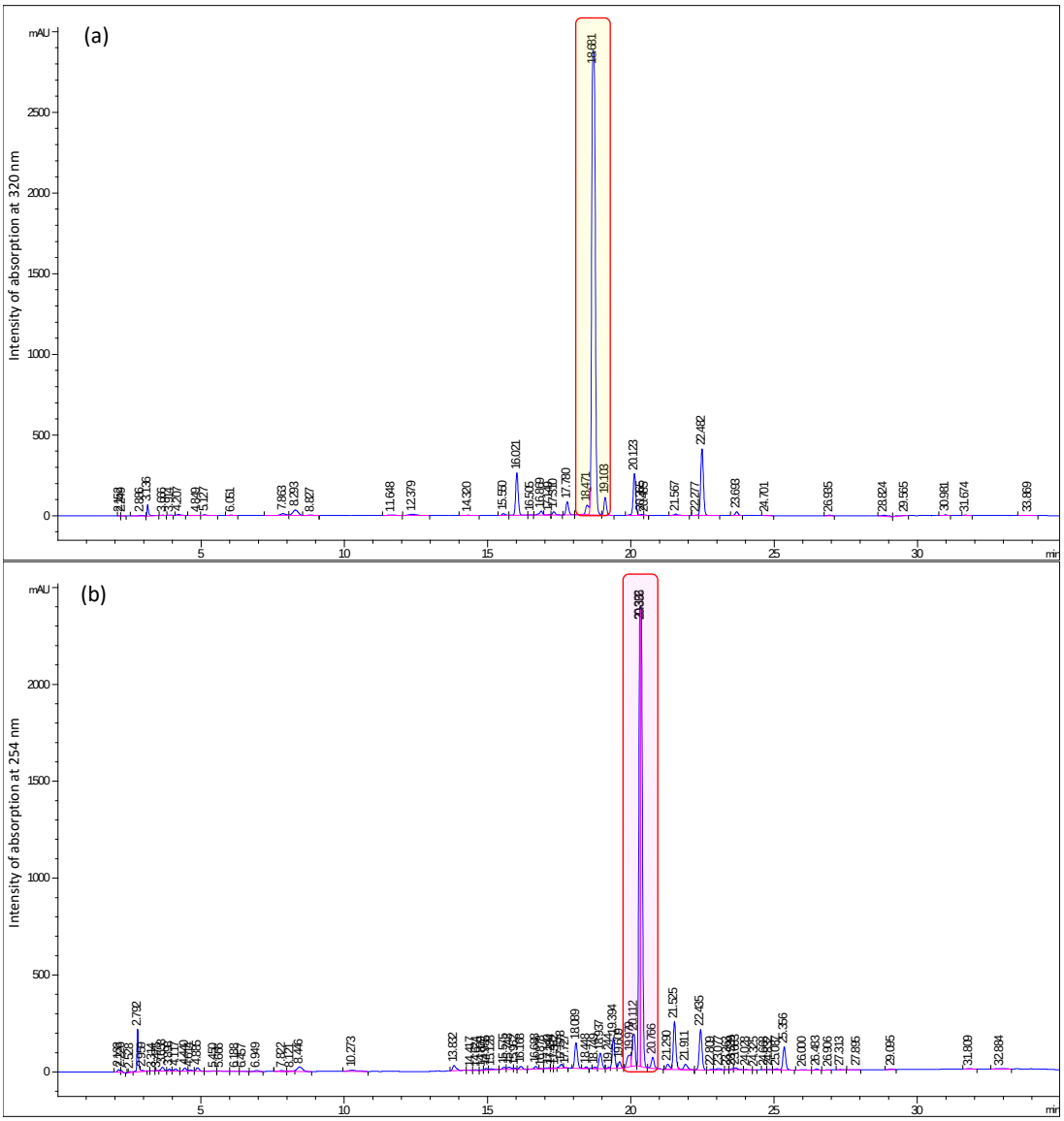

Figure 2.16: HPLC chromatograms of the ethyl acetate extract after NP flash chromatography; (**a**) fraction 3 containing (-)-rishirilide A (**29**); (**b**) fraction 7 containing (+)-rishirilide B (**30**).

Following this result, we then decided to undertake a second purification step (size exclusion (SE) chromatography) to improve the purity of the fractions containing (-)-rishirilide A (**20**) and (+)-rishirilide B (**30**). Both fraction 3 ((-)-rishirilide A (**29**)) and fraction 7 ((+)-rishirilide B (**30**)) were separated independently by SE chromatography (Sephadex LH-20 gel, length 40 cm and 5 cm diameter, methanol, 1 mL/min). The corresponding SE fractions containing (-)-rishirilide A (**29**) and (+)-rishirilide B (**30**) were collected based on their UV/vis absorption and

evaporated under reduced pressure to give 25.3 mg of (-)-rishirilide A (**29**) as a white solid, and 55.9 mg of (+)-rishirilide B (**30**) as a bright yellow solid. This gave an overall isolated production titre of 4.3 mg/L of (-)-rishirilide A (**29**) and 9.3 mg/L of (+)-rishirilide B (**30**). The presence of (-)-rishirilide A (**29**) and (+)-rishirilide B (**30**), was confirmed by analytical HPLC.

2.4.4 Structural characterization of isolated (-)-rishirilide A and (+)-rishirilide B using NMR.

To further confirm the purity of isolated (-)-rishirilide A (**29**) and (+)-rishirilide B (**30**), we decided to obtain NMR data for literature comparison.

In our previous NMR work we had employed CD_3COCD_3 as the NMR solvent for the examination of (-)-rishirilide A (**29**), however that appeared to result in sample degradation. Therefore, in the following analysis we will use deuterated methanol, CD_3OD, for the NMR of (-)-rishirilide A (**29**), which will also allow for direct comparison with work of Bechthold.[57]

A. NMR spectra of (-)-rishirilide A

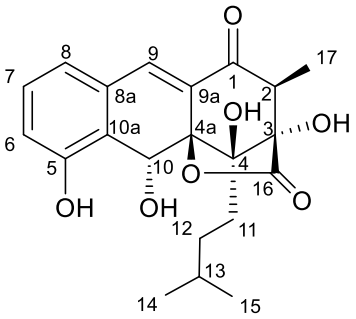

29

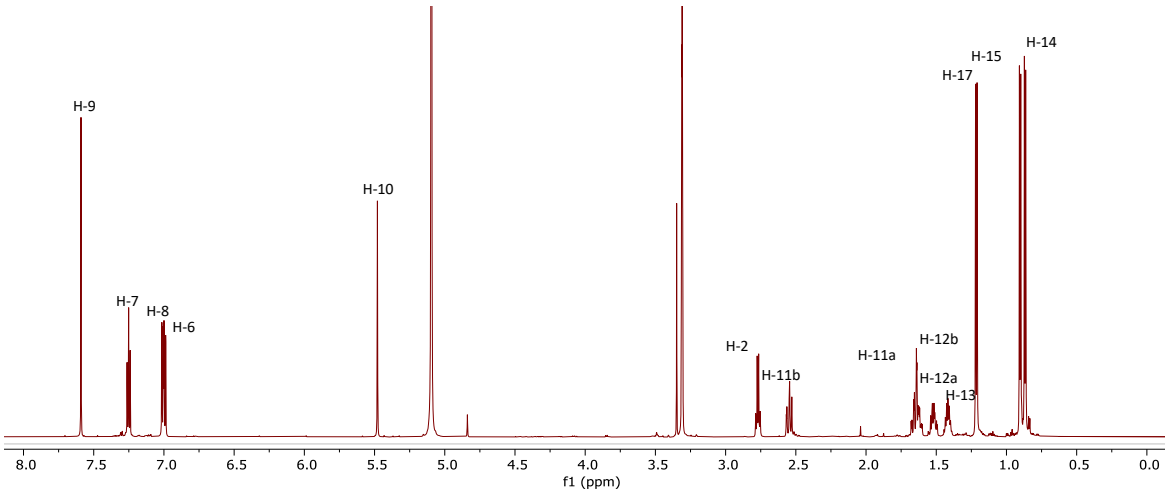

Figure 2.16: 700 MHz ^{1}H NMR spectrum of isolated (-)-rishirilide A (**29**) in CD_3OD.

The ^{1}H NMR spectrum of (-)-rishirilide A (**29**) corresponded well with that reported by Bechthold, demonstrating excellent purity for (-)-rishirilide A (**29**) (Figure **2.17**, Table **2.5**).[57]

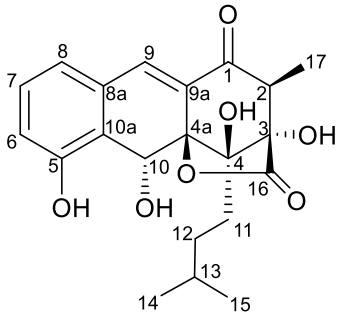

29

Position (P)	Spectra data from experiment In CD_3OD		Spectra data from literature[55] In CD_3OD	
	δ_c ppm [a]	δ_H ppm [b] (multiplicity, *J* in Hz)	δ_c ppm [c]	δ_H ppm [d] (multiplicity, *J* in Hz)
1	199.4		199.4	
2	50.7	2.77 (q, 7.5)	50.7	2.77 (q, 7.0)
3	81.8		81.8	
4	82.0		82.1	
4a	85.4		85.4	
5	156.8		156.8	
6	120.6	6.99 (dd, 8.2, 1.0)	120.7	6.89 (d)
7	131.1	7.25 (t, 7.8)	131.0	7.24 (dd, 8.0)
8	123.7	7.01 (d, 7.4)	123.8	6.89 (d)
8a	123.2		131.9	
9	139.7	7.59 (s)	139.6	7.57 (s)
9a	131.8		131.9	
10	64.3	5.48 (s)	64.6	5.49 (s)
10a	131.9		132.2	
11a	31.0	1.63-1.68 (m)	32.6	1.49 – 1.70 (m)
11b		2.52-2.57 (m)		2.52 (m)
12a	32.6	1.52 (dddd, 12.9, 11.4, 9.9, 4.2)	31.0	1.49 – 1.70 (m)
12b		1.62 (ddd, 12.7, 5.6, 3.0)		
13	30.1	1.42 (m)	30.0	1.41 (m)
14	22.7	0.87 (d, 6.6)	22.7	0.86 (d, 6.0)

15	23.3	0.90 (d, 6.6)	23.1	0.89 (d, 6.0)
16	177.6		177.5	
17	12.6	1.21 (d, 7.5)	12.6	1.21 (d, 8.0)

[a] 176 MHz; [b] 700 MHz; [c] 76 MHz; [d] 300 MHz

Table 2.5: Comparison of the ^{1}H and ^{13}C NMR spectral data for isolated (-)-rishirilide A (**29**) verse the literature.

In the original ^{1}H NMR assignment the two diastereotopic methylenes at C-11 and C-12 were reported as a two-complex overlapped multiplets. Our use of high field (700 MHz) ^{1}H NMR has allowed us to separate these signals and observe them in more detail.

Following 700 MHz ^{1}H NMR and 176 MHz ^{13}C NMR experiments, HSQC was used to assign the proton and carbon signals associated to the two diastereotopic methylenes at C-11 and C-12. HSQC shows proton – carbon single bond correlations, allowing the assignment of the diastereotopic methylene protons H-11a and H-11b, and the diastereotopic methylene protons H-12a and H-12b (Figure **2.18**).

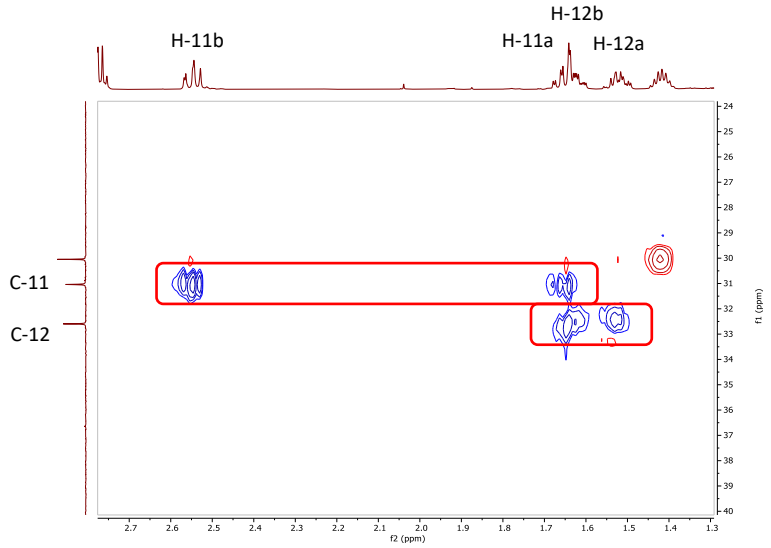

Figure 2.18: HSQC spectrum of (-)-rishirilide A (**29**) showing the correlation between the diastereotopic protons (Ha and Hb) and the adjacent carbons at C-11 and C-12.

Although the two diastereotopic proton signals at C-11 were still observed as multiplets, the coupling constants of the two diastereotopic proton signals at C-12 could be determined. Both diastereotopic proton signals at C-12 (1.52 and 1.62 ppm) showed a key coupling constant ($^{2}J_{H\text{-}H}$) of approximately 12.8 Hz, confirming a geminal coupling between them and thus a diastereotopic arrangement.

B. NMR spectra of (+)-rishirilide B.

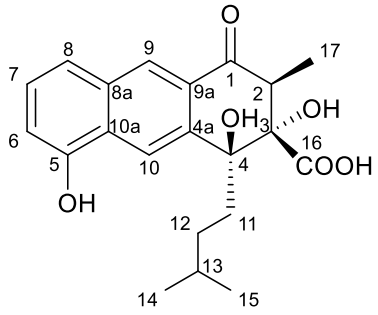

30

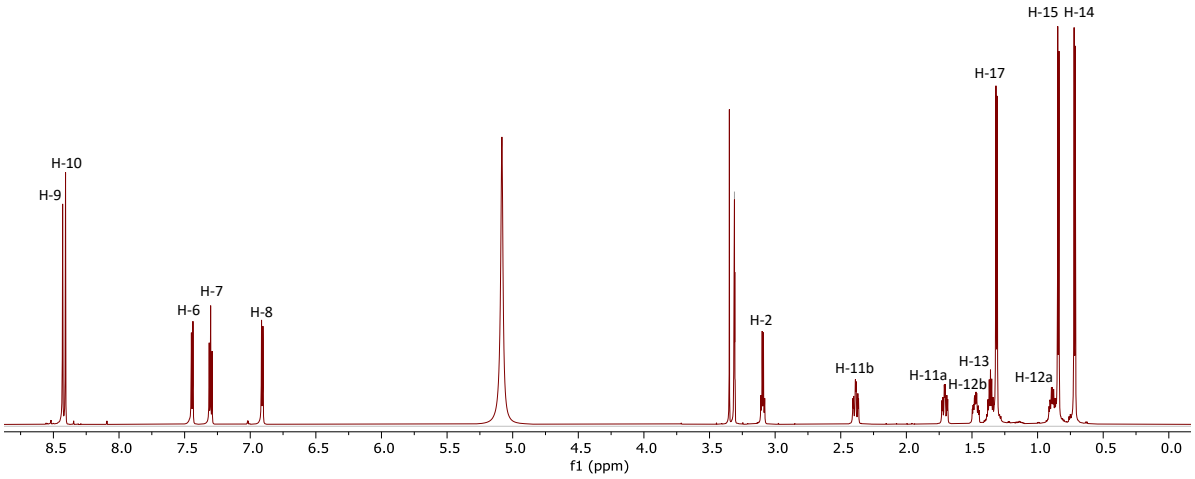

Figure 2.19: 700 MHz ^{1}H NMR spectrum of isolated (+)-rishirilide B (**30**) in CD_3OD.

The ^{1}H NMR and ^{13}C NMR spectrum our isolated (+)-rishirilide B (**30**) in CD_3OD closely matched that reported by Bechthold (d_6-DMSO) and Iwaki (CD_3OD/ d_6-DMSO) (Figure **2.19**, Table **2.6**).[51,57]

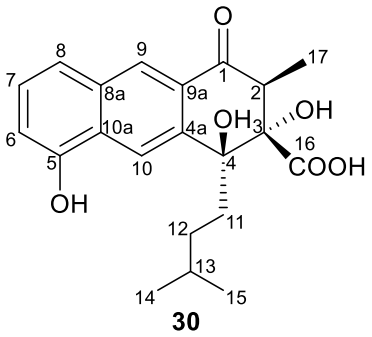

30

Position (P)	Spectra data from experiment In CD_3OD		Spectra data from literature[55] In d_6-DMSO	
	δ_C ppm [a]	δ_H ppm [b] (multiplicity, *J* in Hz)	δ_C ppm [c]	δ_H ppm [d] (multiplicity, *J* in Hz)
1	199.6		197.3	
2	49.6	3.09 (q, 6.7)	35.1	2.95 (q, 6.7)
3	85.7		77.0	
4	78.8		83.5	
4a	140.3		140.6	
5	154.7		153.2	
6	111.1	6.91 (dd, 7.5, 1.0)	111.6	6.92 (d, 7.4)
7	127.8	7.30 (t, 7.8)	125.6	7.28 (dd, 7.4)
8	121.4	7.44 (d, 8.2)	119.8	7.45 (d,7.4)
8a	134.4		132.4	
9	127.8	8.43 (s)	126.4	8.27 (s)
10	121.3	8.41 (s)	109.8	8.25 (s)
9a	131.0		126.1	
10a	128.1		131.0	
11a	36.5	1.71 (ddd, 13.8, 12.3, 4.7)	49.7	1.49 – 1.63 (m)
11b		2.39 (ddd, 13.8, 12.3, 4.0)		
12a	32.7	0.89 (tdd, 12.6, 6.7, 4.5)	32.7	2.15 – 2.30 (m)
12b		1.47 (tdd, 12.6, 6.6, 3.9)		
13	29.7	1.36 (dt, 13.3, 6.6)	29.7	1.21-1.33 (m)
14	22.9	0.84 (d, 6.6)	22.9	0.76 (d, 6.6)
15	23.2	0.72 (d, 6.6)	23.2	0.65 (d, 6.6)
16	175.8		175.8	
17	10.5	1.31 (d, 6.7)	10.5	1.17 (d, 6.6)

[a] 176 MHz; [b] 700 MHz; [c] 100 MHz; [d] 400 MHz

Table 2.6: The ^1H and ^{13}C NMR spectral data of (+)-rishirilide B (**30**).[55]

As with (-)-rishirilide A (**29**), in the ^{1}H NMR work of Bechthold, the proton signals associated with the two diastereotopic methylenes at C-11 and C-12 were reported as two complex multiplets. However, our 700 MHz ^{1}H NMR spectrum allowed the observation of distinct proton signals for each of the diastereotopic methylenes at C-11 and C-12.

The signals corresponding to the diastereotopic methylene protons, H-11a/H-11b and H-12a/H-12b, were assigned using HSQC (Figure **2.20**).

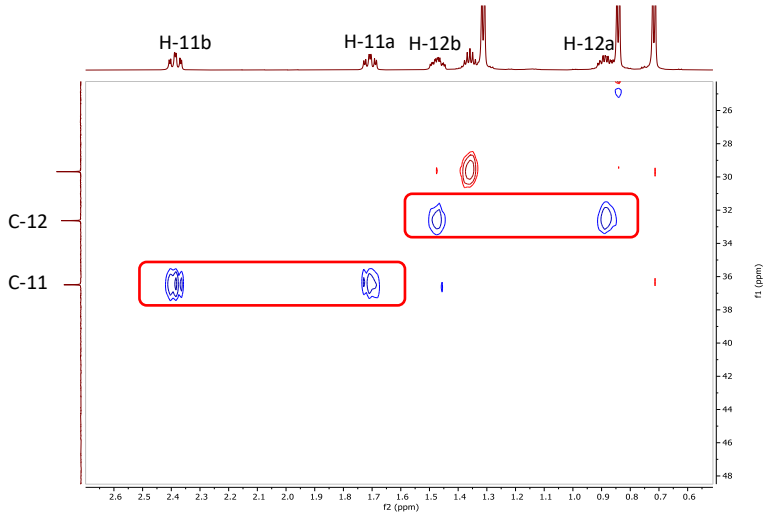

Figure 2.20: HSQC spectrum of (+)-rishirilide B (**30**) showing the correlation between the diastereotopic protons (Ha and Hb) and the adjacent carbons at C-11 and C-12.

The diastereotopic proton signals for C-11 (1.71 and 2.39 ppm) and C-12 (0.89 and 1.47 ppm) showed key coupling constants ($^{2}J_{H\text{-}H}$) of 13.8 Hz and 12.6 Hz respectively, confirming geminal couplings between each carbon-protons correlation.

In conclusion, we have fully assigned the NMR spectra of both natural products, (-)-rishirilide A (**29**) and (+)-rishirilide B (**30**), and thus successfully confirmed their structure and purity. With this success, next we attempted to carry out a further scale-up of the fermentation of *S. albus*::cos4.

2.5 Large scale fermentation of *S. albus*::cos4 in liquid medium (GYM) using a 20 L bioreactor

Bacterial fermentation in shake flasks limits the total volume of fermentation broth possible to a few litres, larger scale fermentation requires the use of different technology such as a stirred tank bioreactor. However bacterial growth in shake flasks and in bioreactors can be

very different, therefore next we decided to test the fermentation of *S. albus*::cos4 in a 20 L bioreactor. This would then allow us to understand the rishirilide production of *S. albus*::cos4 in a bioreactor allowing us to scale-up the future production of both (-)-rishirilide A (**29**) and (+)-rishirilide B (**30**).

Therefore, a stirred 20 L EZ-Control bioreactor was used for the fermentation of *S. albus*::cos4 (GYM), equipped with a dissolved oxygen sensor (DO), a temperature sensor, and a heating blanket.

Following the previous fermentation method on a 6 L scale, *S. albus*::cos4 was grown on SFM agar, inoculated into a 250 mL baffled flask containing 50 mL TSB medium and incubated at 28 °C overnight. Subsequently the inoculant was transferred into a 1 L baffled flasks containing 500 mL of GYM medium and incubated at 28 °C overnight. Next, 100 mL of the inoculant was transferred into a 5 L baffled flask containing 800 mL GYM medium and incubated at 28 °C overnight. This 800 mL inoculant was then transferred into a 20 L bioreactor containing 16 L GYM medium, incubated at 30 °C, at pH 7, and stirred at 250 rpm for 5 days (Figure **2.21**).

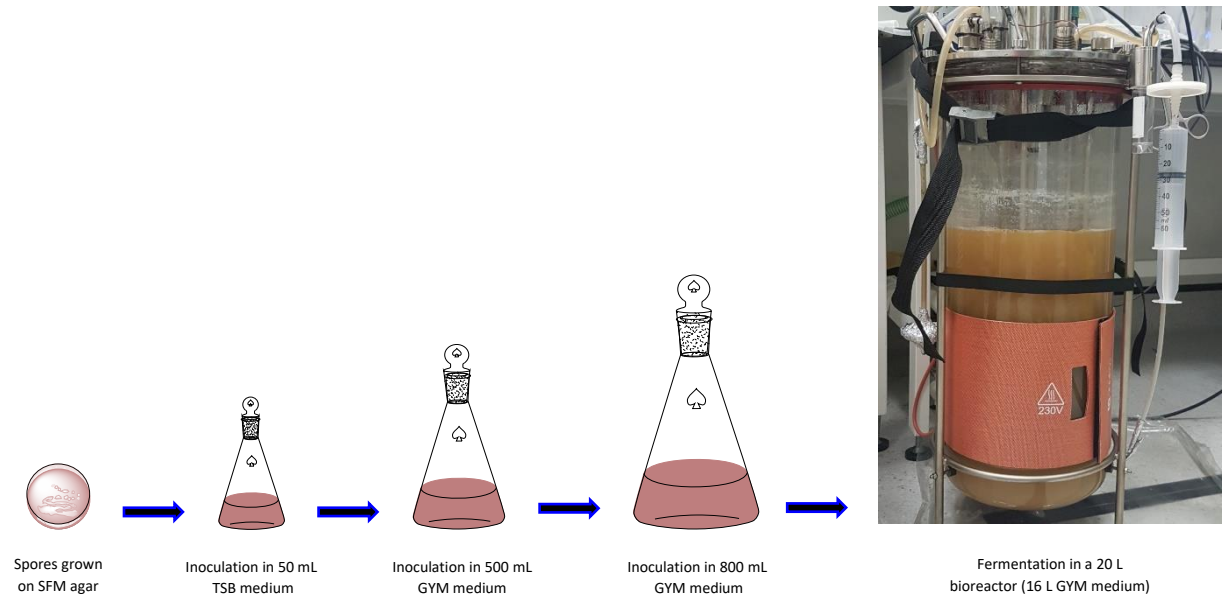

Figure 2.21: Flow diagram of liquid fermentation of *S. albus*::cos4 using a 20 L bioreactor.

During the 5 day 16 L fermentation of *S. albus*::cos4, the fermentation broth was tested on a daily basis for any contamination by other bacteria. No contamination was observed throughout the fermentation process.

Based on our previous successful isolation methods, after 5 days, we carried out initial isolation involving solid-liquid extraction with Amberlite XAD-16N, washing with petroleum ether, and pH4 extraction with ethyl acetate, to give 3.67 g of crude extract of *S. albus*::cos4.

Then, we carried out a similar purification approach as the 6 L scale fermentation. The fractions containing the rishirilides were first isolated from the crude extract by normal-phase flash chromatography (Biotage® SNAP ULTRA 100g cartridge, gradient: 100% dichloromethane to 100% methanol). This initial purification step resulted in eight fractions, which were then analysed by HPLC (Agilent Eclipse Plus C-18 (250 x 4.6 mm, 5µm) using a gradient elution (5:95 to 95:5, acetonitrile (0.1% by v/v FA) and water (0.1% by v/v FA)) over 35 minutes at a flow rate of 0.5 mL/min, to look for the presence of (-)-rishirilide A (**29**) and (+)-rishirilide B (**30**). Fraction 2 was shown to contain (-)-rishirilide A (**29**) whilst fraction 4 contained (+)-rishirilide B (**30**) (Figure **2.22**).

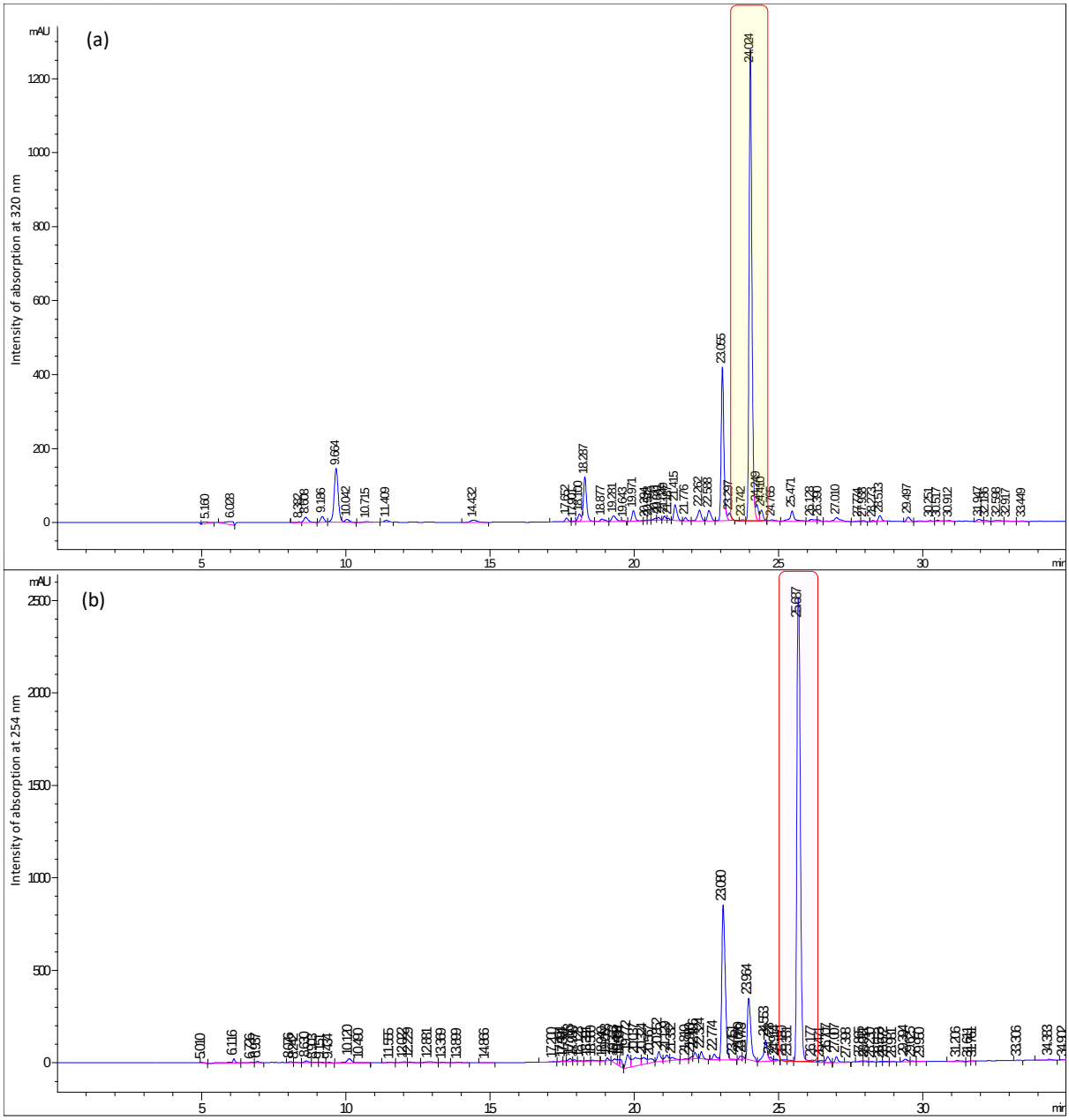

Figure 2.22: HPLC chromatogram of the ethyl acetate after flash chromatography; (**a**) fraction 2 containing (-)-rishirilide A (**29**); (**b**) fraction 4 containing (+)-rishirilide B (**30**).

Since we already had significant quantities of (+)-rishirilide B (**30**) in hand, and the main target of our fermentation efforts was (-)-rishirilide A (**29**), we decided to focus on the purification of (-)-rishirilide A (**29**).

Therefore, we carried out a second isolation step, using SE chromatography, to further purify (-)-rishirilide A (**29**). Fraction 2, which contained (-)-rishirilide A (**29**), was separated by SE chromatography (Sephadex LH-20 gel, length 40 cm, 5 cm diameter, methanol, 1 mL/min). The corresponding SE fractions containing (-)-rishirilide A (**29**) were collected (based on their

UV/Vis absorption) and evaporated under reduced pressure to give 13.2 mg of (-)-rishirilide A (**29**) as a white solid. The purity of (-)-rishirilide A (**29**) was confirmed by analytical HPLC (Figure **2.23**).

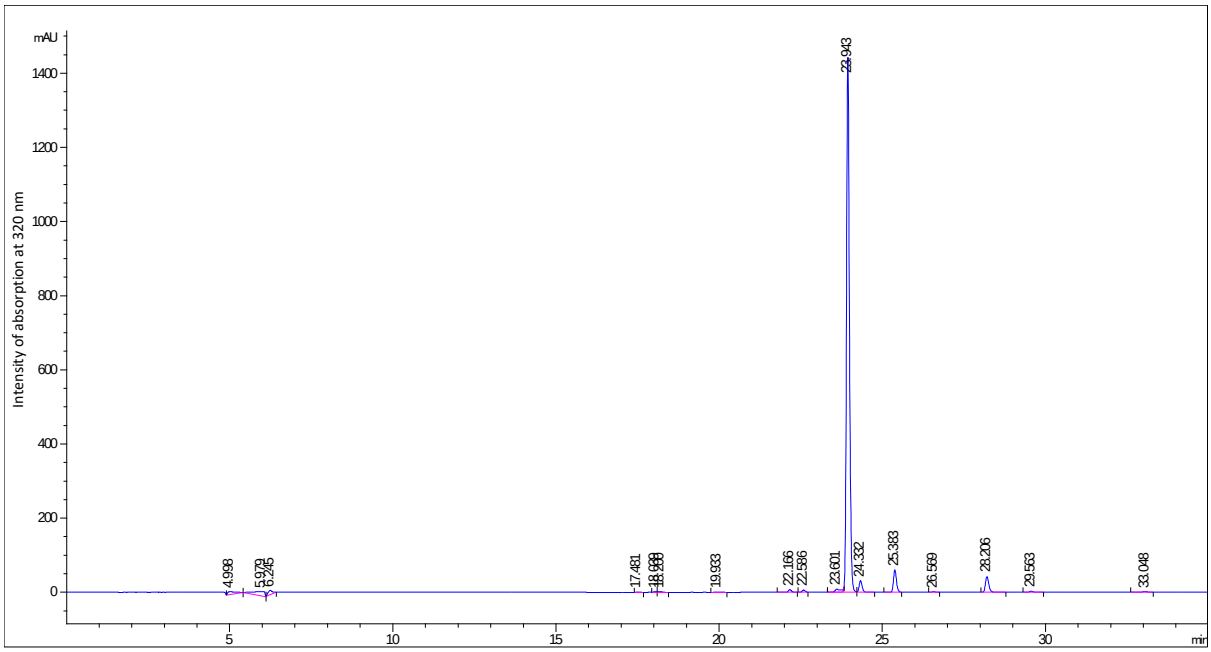

Figure 2.23: HPLC chromatogram of fraction 2 containing (-)-rishirilide A (**29**) after purified by SE chromatography.

In conclusion, we have successfully demonstrated the production of both natural products, (-)-rishirilide A (**29**) and (+)-rishirilide B (**30**), through the fermentation of *S. albus*::cos4 in a 20 L bioreactor. However, the production titre of (-)-rishirilide A (**29**) in the 20 L bioreactor was 0.8 mg/L, significantly lower than the 4.3 mg/L observed in previous 6 L scale fermentation in shake flasks. The low yield production titre of (-)-rishirilide A (**29**) in the 20 L bioreactor verses shake flask is likely due to the differences in the fermentation conditions. Future work would involve optimisation of the bioreactor fermentation of *S. albus*::cos4 to allow the large scale future production of both (-)-rishirilide A (**29**) and (+)-rishirilide B (**30**).

2.6 Conclusion

The aim of this chapter was to isolate sufficient quantities of (-)-rishirilide A (**29**) and (+)-rishirilide B (**30**) to allow for the future investigation of the hypothesised antibiotic activity of (-)-rishirilide A (**29**).

To obtain both (-)-rishirilide A (**29**) and (+)-rishirilide B (**30**) we examined a number of fermentation approaches for both the wild type producer *S. bottropensis* and the heterologous host *S. albus*::cos4.

Liquid fermentation of as the wild type producer *S. bottropensis* showed only the production of small quantities of (+)-rishirilide B (**30**). Whilst fermentation of the heterologous host, *S. albus*::cos4, in shake flask produced both (-)-rishirilide A (**29**) and (+)-rishirilide B (**30**). Following optimisation of the isolation procedure, 25.3 mg of (-)-rishirilide A (**29**) and 55.9 mg of (+)-rishirilide B (**30**) were isolated from 6 L of fermentation broth. The structures and purity of both (-)-rishirilide A (**29**) and (+)-rishirilide B (**30**) were confirmed by HPLC, LCMS and NMR studies. Furthermore, initial trial fermentation of *S. albus*::cos4 in a 20 L bioreactor, showed production of both (-)-rishirilide A (**29**) and (+)-rishirilide B (**30**), although future optimisation will be required to increase the production titres.

Thus with >25 mg of (-)-rishirilide A (**29**) and >55 mg of (+)-rishirilide B (**30**) in hand, we will proceed in the next chapter, to examine the antibiotic activity of both (-)-rishirilide A (**29**) and (+)-rishirilide B (**30**) against both Gram-positive and Gram-negative bacteria.

Chapter 3. Investigation of the Potential Antibiotic Activity and Mode of Action of (-)-Rishirilide A and (+)-Rishirilide B

In the previous chapter, we have demonstrated the production and isolation two natural product polyketides, (-)-rishirilide A (**29**) (>25 mg) and (+)-rishirilide B (**30**) (>55 mg) through the fermentation of *S. albus*::cos4 in liquid medium (GYM). In this chapter, we aim to examine both (-)-rishirilide A (**29**) and (+)-rishirilide B (**30**) for their potential antibiotic activity, and if active, we will carry out an investigation into their mode of action.

3.1 Preliminary antibiotic activity testing of (-)-rishirilide A and (+)-rishirilide B

To examine the potential antibiotic activity of both (-)-rishirilide A (**29**) and (+)-rishirilide B (**30**), we initially decided to carry out a Kirby-Bauer disc diffusion test against two bacterial strains commonly used by our collaborator in the search for novel antibiotics, Gram-positive bacteria, *B. subtilis*^{eryR} and Gram-negative bacteria, *E. coli* K12 ATCC25404 (*E. coli*^{kanR}).[53]

The Kirby-Bauer disc diffusion assay was carried out as follows. Samples of both (-)-rishirilide A (**29**) and (+)-rishirilide B (**30**) were prepared in methanol (1 mg/mL) and 10 µL of each solution was transferred onto small discs of sterile filter paper and allowed to dry. Paper discs containing (-)-rishirilide A (**29**) and (+)-rishirilide B (**30**) was placed onto agar plates containing either *B. subtilis*^{eryR} or *E. coli*^{kanR}. The resulting agar plates were then incubated at 30 °C overnight and then checked for the presence of zones of inhibition (ZOI), which would indicate antibiotic activity (Figure **3.1**).

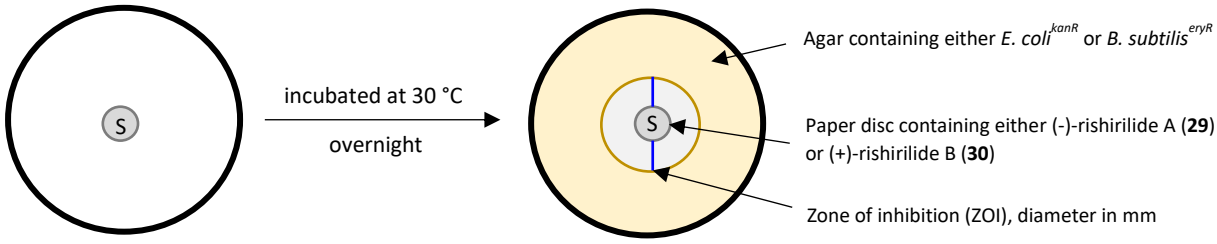

Figure 3.1: Illustration of the key steps involved in a Kirby-Bauer disc diffusion assay

In our Kirby-Bauer disc diffusion assay, (+)-rishirilide B (**30**) showed no ZOIs verses for both *E. coli*^{kanR} and *B. subtilis*^{eryR}, suggesting that (+)-rishirilide B (**30**) does not show significant antibiotic activity against either Gram-negative or Gram-positive bacteria. (-)-Rishirilide A (**29**)

showed no ZOI against *E. coli*^{kanR}, however a ZOI (13 mm) was observed verses *B. subtilis*^{eryR}. This data suggests that (-)-rishirilide A (**29**) does not show significant antibiotic activity against Gram-negative but does show antibiotic activity against Gram-positive bacteria.

Following our Kirby-Bauer disc diffusion assays, to gain further insight into the antibiotic activity of (-)-rishirilide A (**29**), we next decided to determine the minimum inhibitory concentrations (MICs) against two Gram-positive bacteria, *S. aureus* RN4220 and *B. subtilis* 168CA. For comparison the MICs of DEM30355/A (**28**), a related natural product, against *S. aureus* and *B. subtilis* were also determined at the same time. MIC assays were carried out by our collaborator Dr B. Kepplinger (Table **3.1**).

	(-)-Rishirilide A (μg/mL)	DEM 30355/A (μg/mL)
S. aureus RN4220	1.56	3.125
B. subtilis 168CA	3.125	12.5

Table 3.1: Comparison of MICs between (-)-rishirilide A (**29**) and DEM 30355/A (**28**).

The MIC assays confirmed that (-)-rishirilide A (**29**) has antibiotic against two Gram-position bacteria, *S. aureus* RN4220 (1.56 μg/mL) and *B. subtilis* 168CA (3.125 μg/mL). Interestingly, (-)-rishirilide A (**29**) also showed slightly better antibiotic activity verses the closely related natural product DEM30355/A (**28**).

In conclusion, we have successfully demonstrated that (+)-rishirilide B (**30**) does not appear to have antibiotic activity against either the Gram-negative or Gram-positive bacteria tested. However (-)-rishirilide A (**29**) does show antibiotic activity against Gram-positive bacteria, with MICs of 1.56 μg/mL and 3.125 μg/mL against *S. aureus* RN4220 and *B. subtilis* 168CA respectively, is slightly more potent than DEM30355/A (**28**) and has an MIC in the range typically observed for clinically used antibiotics.[60]

3.2 Investigation of mode of action of (-)-rishirilide A

3.2.1 Mode of action investigation of (-)-rishirilide A using a panel of *B. subtilis* reporter strains

Now that we knew that (-)-rishirilide A (**29**) shows antibiotic activity against Gram-positive bacteria, in the next step we decided to investigate the antibiotic mode of action of (-)-rishirilide A (**29**).

Therefore, we carried out a further Kirby-Bauer disc diffusion assay of (-)-rishirilide A (**29**) against a panel of *B. subtilis* reporter strains, which can be used to indicate common antibacterial modes of action, alongside (+)-rishirilide B (**30**) as a negative control.[61] We selected five reporter strains of *B. subtilis,* each of which can report a different antibiotic mode of action, namely *YvqI*^{eryR} (Lipid II (cell envelope))[53], *YvqS*^{eryR} (RNA synthesis)[62], *YpuA*^{eryR} (cell wall synthesis)[63], *YjaX*^{eryR} (protein synthesis)[62], and *YheH*^{eryR} (fatty acid synthesis)[62].

These *B. subtilis* reporter strains are bioengineered with selected marker genes which are upregulated within the reporter strains when certain modes of action are detected from the bioactive natural product being tested. For example, a reporter strain such as *B. subtilis YvqI*, a cell envelope reporter can detect a bioactive natural product that kills bacteria through inhibition of cell envelope synthesis.

The *B. subtilis* reporter strains are grown in the presence of X-Gal (5-bromo-4-chloro-3-indoyl-β-D-galactopyranoside) (**31**). When the reporter strain is exposed to an antibiotic with a specific mode of action, it upregulates the LacZ gene which encodes for the production of β-D-galactosidase, an enzyme that cleaves the X-Gal (**31**) indicator to produce galactose (**32**) and 5-bromo-4-chloro-3-hydroxyindole (**33**). The 5-bromo-4-chloro-3-hydroxyindole (**33**) then undergoes oxidative dimerisation to give 5,5'-dibromo-4,4'-dicholoroindigo (**34**), a blue dye that can be seen as a blue halo typically on the edge of the around the ZOI in a Kirby-Bauer disc diffusion assay (Scheme **3.1**).

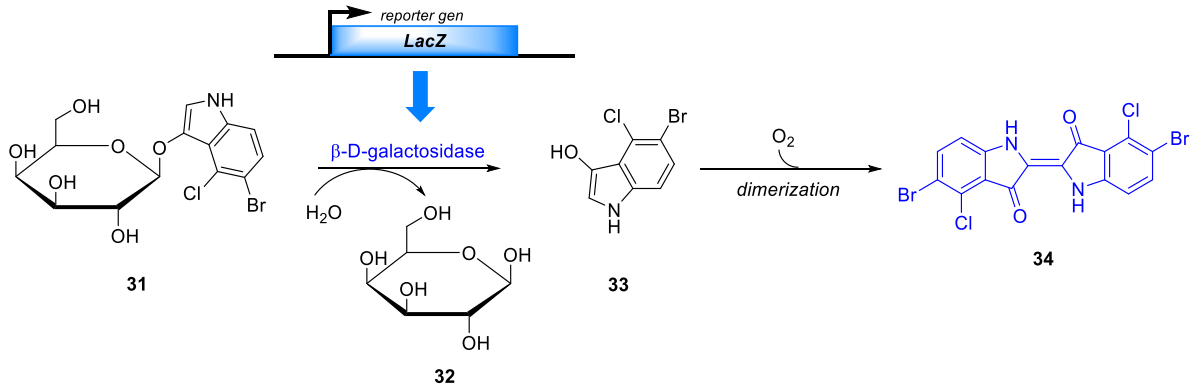

Scheme 3.1: Enzyme mediated production of 5,5'-dibromo-4,4'-dicholoroindigo (**34**) from X-Gal (**31**) by *B. subtilis* reporter strains.

Therefore both (-)-rishirilide A (**29**) and (+)-rishirilide B (**30**) were dissolved in methanol (1 mg/mL) and impregnated (10 µL) into discs of sterile filter paper. The (-)-rishirilide A (**29**) and (+)-rishirilide B (**30**) containing discs were transferred onto a five agar plates containing the five different reporter strains of erythromycin resistant *B. subtilis* (*YvqI*^{eryR}, *YvqS*^{eryR}, *YpuA*^{eryR}, *YjaX*^{eryR} and *YheH*^{eryR}). The agar plates were then incubated at 30 °C overnight and then checked for the presence of both zones of inhibition (ZOI) and blue halos which would indicate an antibiotic mode of action (Figure **3.2**, table **3.2**).

Reporter strains	Mode of action	Positive control	Negative control	ZOI of (-)-rishirilide A/ mm
YvqI^{eryR}	Lipid II (cell envelope)	Bacitracin	(+)-Rishirilide B	13
YvqS^{eryR}	RNA synthesis	Rifampicin	(+)-Rishirilide B	13
YupA^{eryR}	Cell wall synthesis	Cefotaxime	(+)-Rishirilide B	13
YheH^{eryR}	Protein synthesis	Chloramphenicol	(+)-Rishirilide B	13
YjaX^{eryR}	Fatty acid synthesis	Triclosan	(+)-Rishirilide B	13

Table 3.2: Antibiotic activity testing of (-)-rishirilide A (29) against a panel of reporter strains of erythromycin-resistant *B. subtilis*.

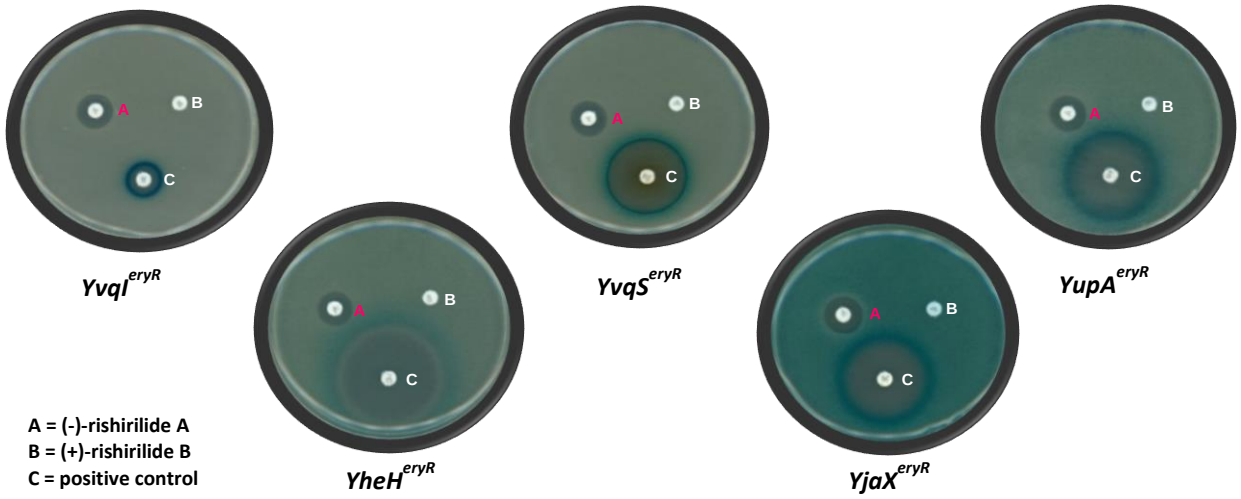

Figure 3.2: Antibiotic activity testing of (-)-rishirilide A (**29**) against a panel of reporter strains of erythromycin-resistant *B. subtilis*, showing ZOIs and blue halos.

As expected, no ZOIs were observed for (+)-rishirilide B (**30**). We did observe ZOIs for (-)-rishirilide A (**29**) against all five reporter strains of *B. subtilis* (*YvqI*^{eryR}, *YvqS*^{eryR}, *YpuA*^{eryR}, *YjaX*^{eryR} and *YheH*^{eryR}), confirmed that (-)-rishirilide A (**29**) was active against these strains. However, no blue halos were observed for (-)-rishirilide A (**29**) in presence of all five *B. subtilis* reporter strains (*YvqI*^{eryR}, *YvqS*^{eryR}, *YpuA*^{eryR}, *YjaX*^{eryR} and *YheH*^{eryR}). This suggests that the mode of action of (-)-rishirilide A (**29**) is not one of the following known modes of action tested, namely inhibition of Lipid II synthesis (*YvqI*^{eryR}), inhibition of RNA synthesis (*YvqS*^{eryR}), inhibition of cell wall synthesis (*YpuA*^{eryR}), inhibition of protein synthesis (*YjaX*^{eryR}), and inhibition of fatty acid synthesis (*YheH*^{eryR}).

In conclusion, we have successfully shown that (-)-rishirilide A (**29**) was active against a panel of erythromycin-resistant *B. subtilis*. However, the use of these reporter strains has failed to provide a clear mode of action.

3.2.2 Mode of action investigation of (-)-rishirilide A through a membrane depolarization assay

Parallel work by Dr B. Kepplinger on the related natural product DEM30355/A (**28**) indicated a possible mode of action involving the depolarisation of the cell membrane. Therefore, we decided to carry out a similar study on (-)-rishirilide A (**29**) to gain more insight into mode of action. As discussed in chapter 1, the maintenance of membrane potential is essential for bacterial function, disruption of membrane potential can therefore lead to cell death.[58]

Therefore, a membrane depolarisation assay was used to test if the presence of (-)-rishirilide A (**29**) could lead to the depolarization of the bacterial cell membrane and the loss of membrane potential. We employed a single cell-based fluorescence microscopy-based assay to measure membrane depolarisation involving the use of a voltage-sensitive dye.[58] The Gram-positive bacteria *B. subtilis* 168CA was used as the test bacterium, gramicidin (**35**) was used as the positive control and the voltage-sensitive dye of 3,3-dipropylthiadicarbocyanine iodide, $DiSC_3(5)$ (**36**), was used to probe the polarisation state of the membrane.

Gramicidin (**35**) is a mixture of three related short peptides (gramicidin A, B, and C). Two molecules of gramicidin (**35**) come together to form an ion channel in the bacterial cell membrane, resulting in the loss of membrane potential and ultimately cell death (Figure **3.3**).

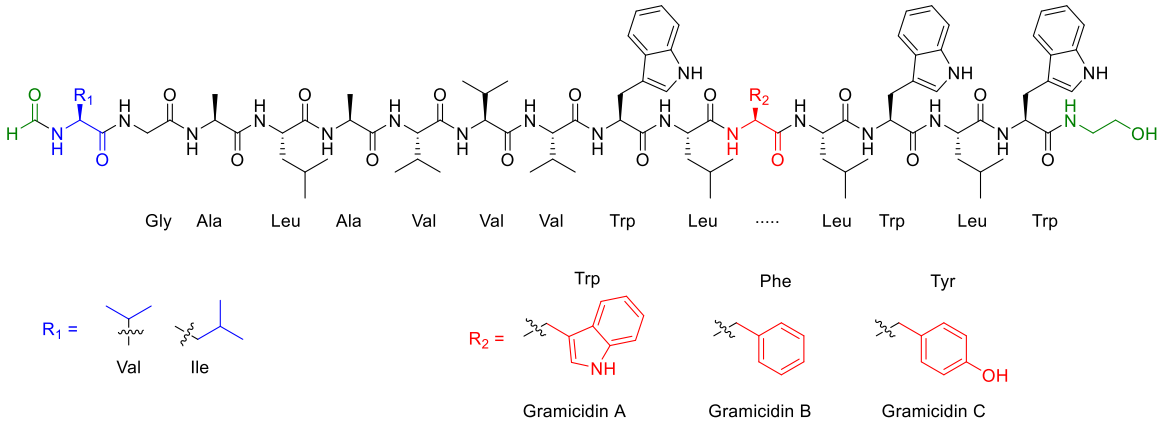

Figure 3.3: The gramicidin (**35**) contains of Val and Ile at R_1; Gramicidin A (R_2 = Trp), B (R_2 = Phe) and C (R_2 = Tyr)

$DiSC_3(5)$ (**36**) is a cationic membrane-permeable fluorescence dye based on a carbocyanine scaffold. It is used as a fluorescence probe to monitor membrane potential of bacterial cells. Due to the cationic nature of $DiSC_3(5)$ (**36**) it accumulates inside the bacterial cell, because of the negative polarisation of the interior of the bacteria. Thus, bacteria with a polarised membrane become fluorescent (Figure **3.4**).

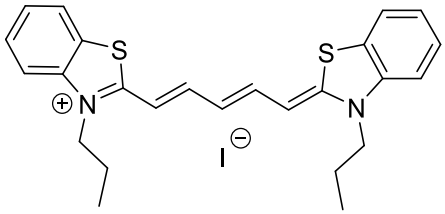

Figure 3.4: 3,3'-Dipropylthiadicarbocyanine iodide, $DiSC_3(5)$ (**36**).

Therefore, our collaborator Dr B. Kepplinger treated a suspension of *B. subtilis* 168CA cells with $DiSC_3(5)$ (**36**) followed by the test compounds, gramicidin (**35**) or (-)-rishirilide A (**29**). The *B. subtilis* 168CA cells were incubated and then imaged by both phase contrast and fluorescence microscopy (Figure **3.5**).[65,66]

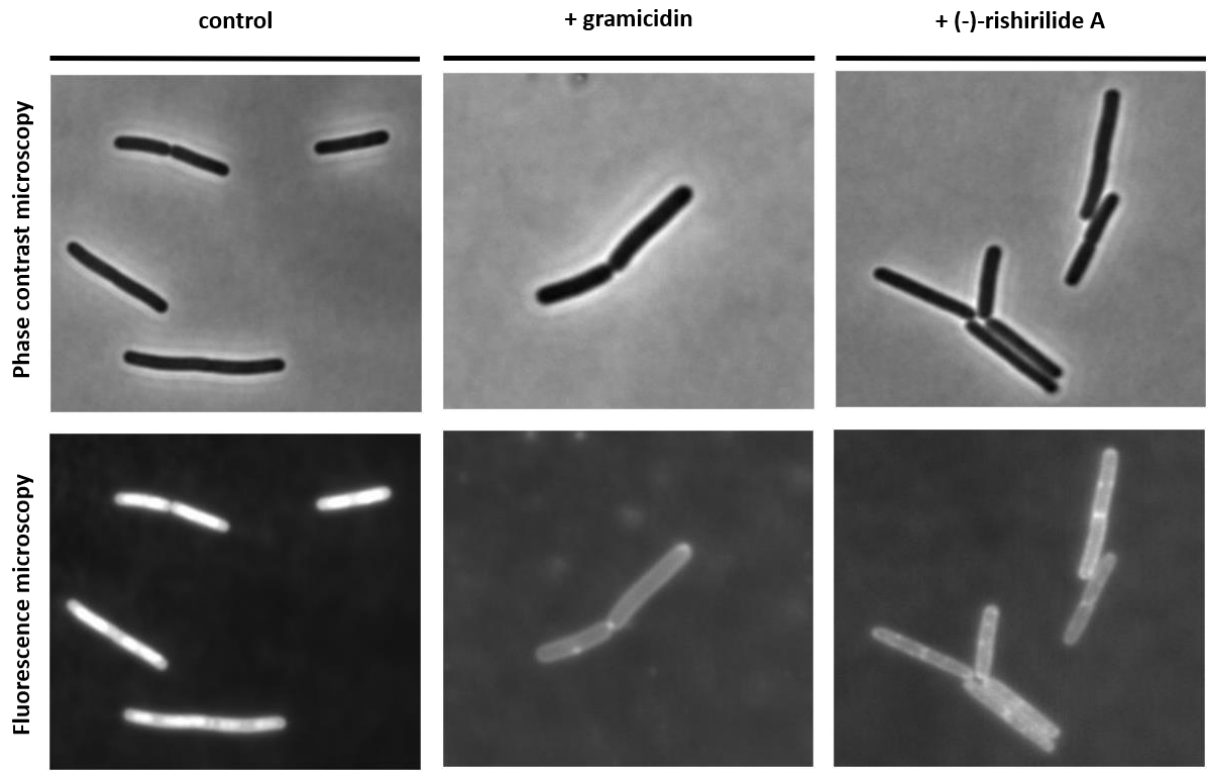

Figure 3.5: Microscopy of *B. subtilis* 168CA with $DiSC_3(5)$ (**36**); (**top**) phase contrast images; (**bottom**) fluorescence images with(**left**) control, (**middle**) gramicidin (**35**), (**right**) (-)-rishirilide A (**29**).

Fluorescence microscopy of the control experiment of *B. subtilis* 168CA with $DiSC_3(5)$ (**36**) showed significant fluorescence from within the cells due to the accumulation of $DiSC_3(5)$ (**36**), suggesting a well-energized cell membrane.

In the experiment containing *B. subtilis* 168CA, $DiSC_3(5)$ (**36**) and gramicidin (**35**), the bacterial cells showed much reduced fluorescence, indicating a depolarisation of the membrane caused by the formation of ion channels by the gramicidin (**35**).

Finally, in the experiment containing *B. subtilis* 168CA, $DiSC_3(5)$ (**36**) and (-)-rishirilide A (**29**), a similar result to gramicidin (**35**) was observed. This suggest that the loss of fluorescence is due to the loss of membrane potential on treatment with (-)-rishirilide A (**29**). However, based on the structural differences between gramicidin (**35**) and (-)-rishirilide A (**29**), it is unlikely

that (-)-rishirilide A (**29**) acts as an ionophore through the formation of an ion channel a pore forming agent. However (-)-rishirilide A (**29**) maybe inhibiting an enzyme mediated mechanism responsible for the maintenance of the membrane potential.

In conclusion, we have shown that (-)-rishirilide A (**29**) can cause the membrane depolarisation in *B. subtilis* 168CA, suggesting a possible mode of action involving maintenance of membrane potential.

3.3 Conclusion

The aim of this chapter was to examine both (-)-rishirilide A (**29**) and (+)-rishirilide B (**30**) for potential antibiotic activity and investigate their potential modes of action.

(+)-Rishirilide B (**30**) did not show any antibiotic activity against either Gram-positive or Gram-negative bacteria, whilst (-)-rishirilide A (**29**) did show antibiotic activity against the Gram-positive bacteria *S. aureus* RN4220 and *B. subtilis* 168CA, with MICs of 1.56 µg/mL and 3.125 µg/mL respectively.

The use of *B. subtilis* reporter strains (*YvqI*^{eryR}, *YvqS*^{eryR}, *YpuA*^{eryR}, *YjaX*^{eryR} and *YheH*^{eryR}) did not clearly indicate a mode of action. A membrane depolarisation assay using $DiSC_3(5)$ (**36**), showed that (-)-rishirilide A (**29**) did cause the loss of membrane potential in *B. subtilis* 168CA. However, the exact mechanism by which (-)-rishirilide A (**29**) causes membrane depolarisation is still unclear. Therefore, in the next chapter, we will continue to examine the potential mode of action of (-)-rishirilide A (**29**) as an enzyme inhibitor.

Chapter 4. (-)-Rishirilide A as a Potential Michael Acceptor

As discussed previously, in this chapter we intend to further investigate the mode of action of (-)-rishirilide A (**29**). It is interesting to note that (-)-rishirilide A (**29**) shows antibiotic activity, whilst (+)-rishirilide B (**30**) does not. This is likely to be due to the structural differences between the two molecules. One of the main differences of (-)-rishirilide A (**29**) verses (+)-rishirilide B (**30**) is the presence of an α,β-unsaturated ketone moiety (Figure **4.1**).

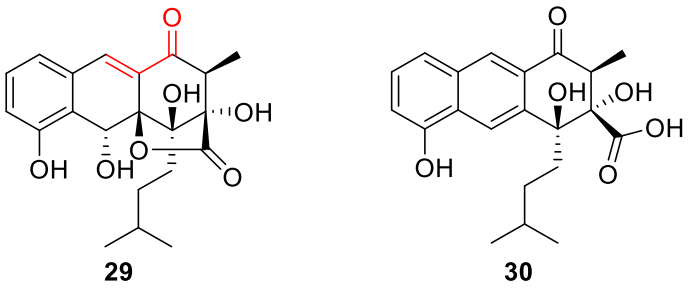

Figure 4.1: (-)-Rishirilide A (**29**) and (+)-rishirilide B (**30**), α,β-unsaturated ketone moiety highlighted in red.

α,β-Unsaturated ketones readily undergo 1,4-conjugate additions, also known as Michael additions, with soft nucleophiles such as thiols. Therefore α,β-unsaturated ketones are known as Michael acceptors. Many enzymes contain reactive thiols and α,β-unsaturated ketones can react with these thiols, acting as irreversible enzyme inhibitors through covalent bond formation. Unselective inhibition of thiol containing enzymes results in poisoning of the host organism. However, a number of drugs containing α,β-unsaturated ketones have been developed which can selectively and irreversibly inhibit a target enzyme leading to a therapeutic effect.

A number of α,β-unsaturated ketone containing natural products have been investigated as potential drugs (e.g. helenalin (**37**) and hypothemycin (**38**)).[67] Furthermore a number of selective irreversible enzyme inhibitors, containing acrylamide groups, have been approved for clinical use in the treatment of cancer (e.g. afatinib (**39**) and ibrutinib (**40**)) (Figure **4.2**).

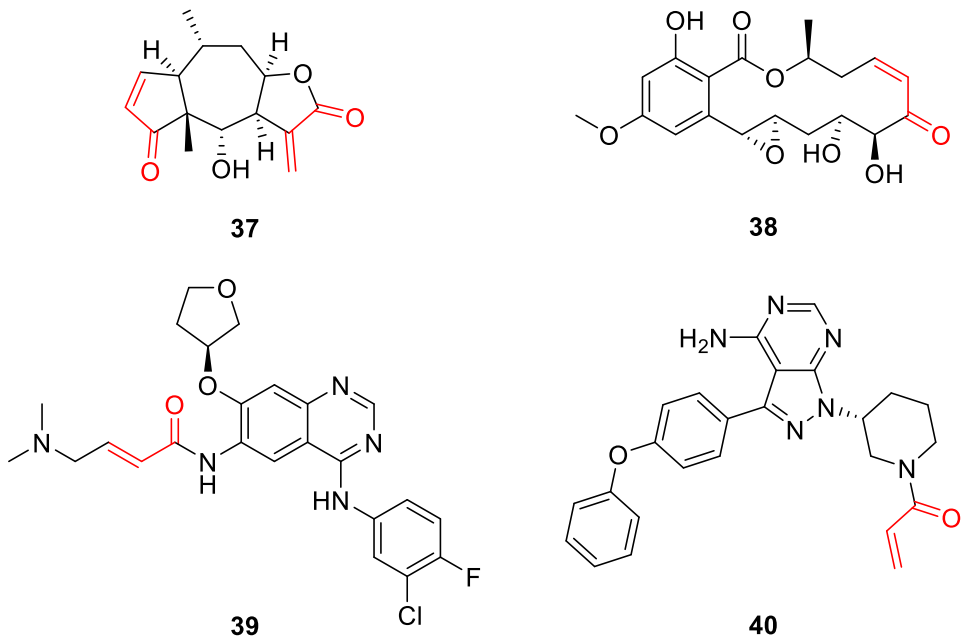

Figure 4.2: Examples of natural product and modern drugs containing α,β-unsaturated ketone: helenalin (**37**) andhypothemycin (**38**); acrylamide: afatinib (**39**) and ibrutinib (**40**).

Therefore, we proposed that the mode of action of (-)-rishirilide A (**29**) may involve a Michael addition of a thiol group of a target enzyme, resulting in irreversible inhibition (Scheme **4.1**).

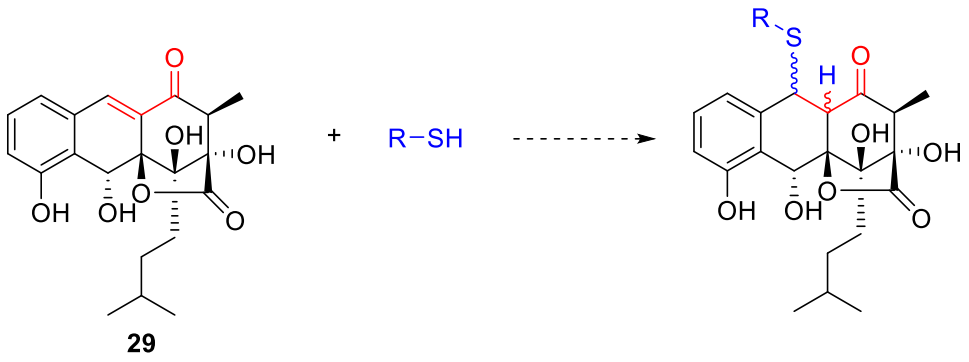

Scheme 4.1: Michael addition of (-)-rishirilide A (**29**) with thiols.

Based on this propose we decided to examine the addition of biologically relevant thiol containing molecules to (-)-rishirilide A (**29**), to determine (-)-rishirilide A (**29**) can act as a Michael acceptor.

4.1 Michael addition chemistry of (-)-rishirilide A

4.1.1 Michael addition with L-cysteine

In our initial work we started with the investigation of the Michael addition chemistry of (-)-rishirilide A (**29**) with a simple biological thiol, namely the amino acid L-cysteine (**41**).

We wished to carry out our test Michael additions close to the physiological conditions found within a bacterial cell. Therefore, we decided to use water as the reaction solvent at pH 7 and room temperature. Since we only had access to a few milligrams of (-)-rishirilide A (**29**), we chose to follow the reactions by LCMS. Due to the sensitivity of LCMS this allowed us to conduct our experiments on small scale, reducing the amounts of (-)-rishirilide A (**29**) required.

Thus, to 654 µL of water, was added 96 µL of a 0.01 M solution of L-cysteine hydrochloride (**41**) in water and 250 µL of a 2.57 mM solution of (-)-rishirilide A (**29**) in methanol, to give a 1 mL solution with final concentrations of 0.96 mM (1.5 eq.) and 0.64 mM (1 eq.) for L-cysteine hydrochloride (**41**) and (-)-rishirilide A (**29**) respectively. The resulting mixture was stirred in a small pear-shaped flask for 150 minutes at room temperature. At 30, 60, 90, 120 and 150 minutes a 50 µL aliquot of the reaction mixture was taken, diluted into 250 µL of water in order to stop the reaction, and then analysed by LCMS. The LCMS was performed using a gradient method from 5:95 to 95:5, acetonitrile (0.1% by v/v FA) : water (0.1% by v/v FA) with a flowrate of 0.2 mL/min over 40 minutes (Scheme **4.2**).

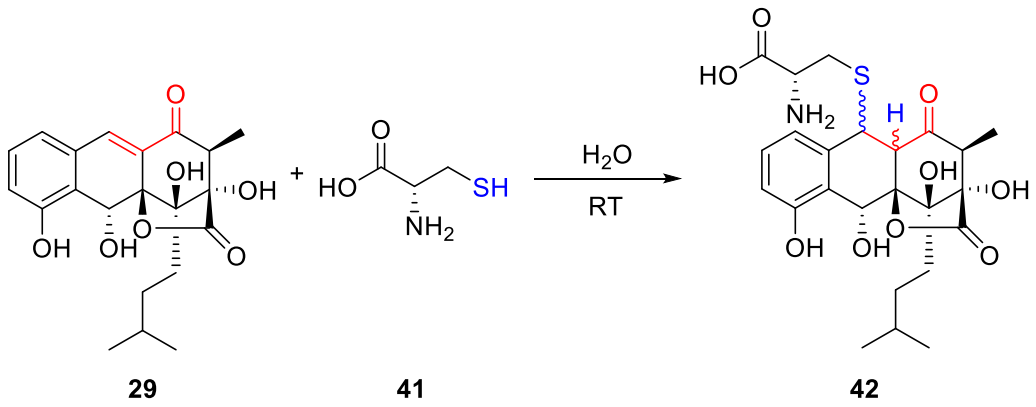

Scheme 4.2: Michael addition of (-)-rishirilide A (**29**) with L-cysteine (**41**).

After 30 minutes, LCMS analysis of the resulting reaction mixture showed that all of the starting (-)-rishirilide A (**29**) was consumed. The (-)-rishirilide A-cysteine Michael addition product (**42**) was observed in the LCMS chromatogram with a peak at 13.3 minutes (*m/z* = 492.1729 $[M\text{-}H_2O+H]^+$, 510.1821 $[M+H]^+$ and 1019.3533 $[2M+H]^+$). In addition a further small peak was observed at 13.7 minutes (*m/z* = 492.1705 $[M\text{-}H_2O+H]^+$ and 510.1829 $[M+H]^+$), which we believe corresponds to the $[M+H]^+$ ion of a related diasteromeric (-)-rishirilide A-cysteine (**42**) minor product. No significant changes to the LCMS was observed after 60, 90, 120 and 150 minutes of reaction time (Figure **4.3**).

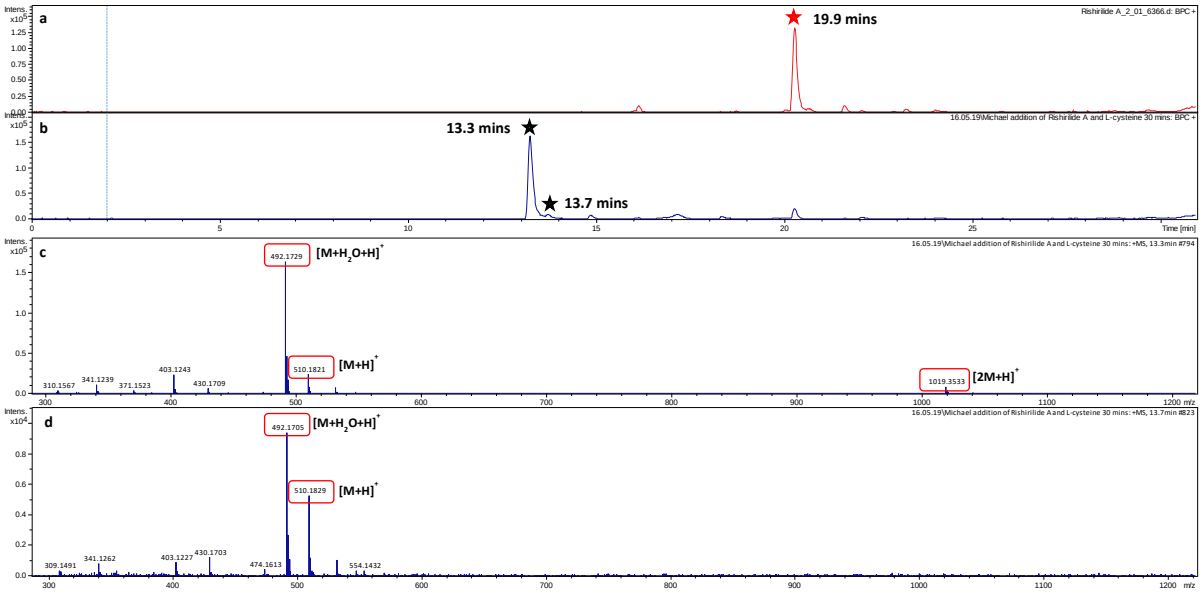

Figure 4.3: LCMS analysis of the Michael addition reaction of (-)-rishirilide A (**29**) with L-cysteine (**41**). (**a**) Base peak chromatogram (BPC) of (-)-rishirilide A (**29**) for comparison (peak indicated with a red star); (**b**) BPC of the Michael addition of (-)-rishirilide A (**29**) with L-cysteine (**41**) after 30 mins: Michael addition (-)-rishirilide A-cysteine products (**42**) (black stars); Mass spectrum of (-)-rishirilide A-cysteine (**42**): (**c**) at 13.3 mins; (**d**) at 13.7 mins.

In conclusion, we successfully shown that (-)-rishirilide A (**29**) does react with L-cysteine hydrochloride (**41**) in a Michael addition to give (-)-rishirilide A-cysteine (**42**), showing that (-)-rishirilide A (**29**) can act as a Michael acceptor.

4.1.2 Michael addition of (-)-rishirilide A with L-cysteine methyl ester

Next, we wished to expand the range of thiols examined in the Michael addition chemistry of (-)-rishirilide A (**29**). Thus, following a similar method to that used in the previous Michael addition with L-cysteine hydrochloride (**41**), to 654 µL of water was added 96 µL of a 0.01 M solution of L-cysteine methyl ester hydrochloride (**43**) in water and 250 µL of a 2.57 mM

solution of (-)-rishirilide A (**29**) in methanol, to give a 1 mL solution with final concentrations of 0.96 mM (1.5 eq.) and 0.64 mM (1 eq.) for L-cysteine methyl ester hydrochloride (**43**) and (-)-rishirilide A (**29**) respectively. Again, the reaction mixture was stirred for 180 minutes at room temperature, and after 30, 60, 90, 120, 150 and 180 minutes 50 µL aliquots of the reaction mixture were taken out, diluted into 250 µL of water and analysed by LCMS using the same solvent gradient method as previously (Scheme **4.3**).

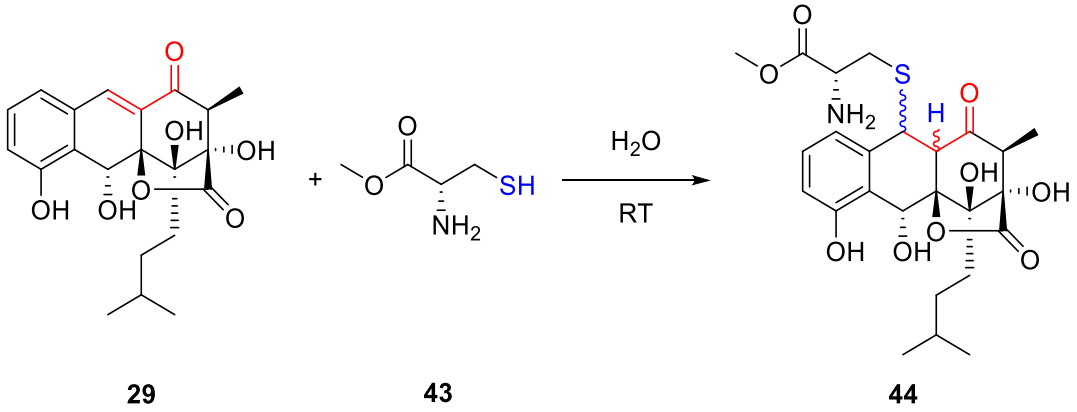

29 **43** **44**

Scheme 4.3: Michael addition of (-)-rishirilide A (**29**) with L-cysteine methyl ester (**43**).

The LCMS chromatogram of the resulting reaction mixture after 30 minutes showed four major peaks at 15.1, 17.8, 19.3 and 20.3 minutes. The peak at 20.3 minutes was identified as that corresponding to unreacted (-)-rishirilide A (**29**), suggesting a slightly slower reaction with L-cysteine methyl ester hydrochloride (**43**) in comparison with L-cysteine hydrochloride (**41**). Based on the their expect masses, (-)-rishirilide A-cysteine methyl ester Michael addition products (**44**) were observed on the LCMS chromatogram at 15.1 minutes (*m/z* = 506.1878 $[M\text{-}H_2O+H]^+$, 524.1981 $[M+H]^+$, 546.1800 $[M+Na]^+$) and at 19.3 minutes (*m/z* = 506.1870 $[M\text{-}H_2O+H]^+$, 524.1988 $[M+H]^+$, 546.1805 $[M+Na]^+$). The confirming the presence of two diastereomeric (-)-rishirilide A-cysteine methyl ester Michael addition products (**44a** and **44b**). Interestingly, a peak observed at 17.8 minutes showed an *m/z* signal of 506.1867, corresponding to a postulated $[M\text{-}H_2O+H]^+$ ion of Michael addition product (**44**), however no $[M+H]^+$ or $[M+Na]^+$ ions could be observed. This suggested that the peak at 17.8 minutes may correspond to a dehydrated form of (-)-rishirilide A-cysteine methyl ester Michael addition products (**44**), formed under the Michael addition reaction conditions. Again, no significant

changes in the LCMS chromatograms were observed for sample taken after 60, 90, 120, 150 and 180 minutes (Figure **4.4**).

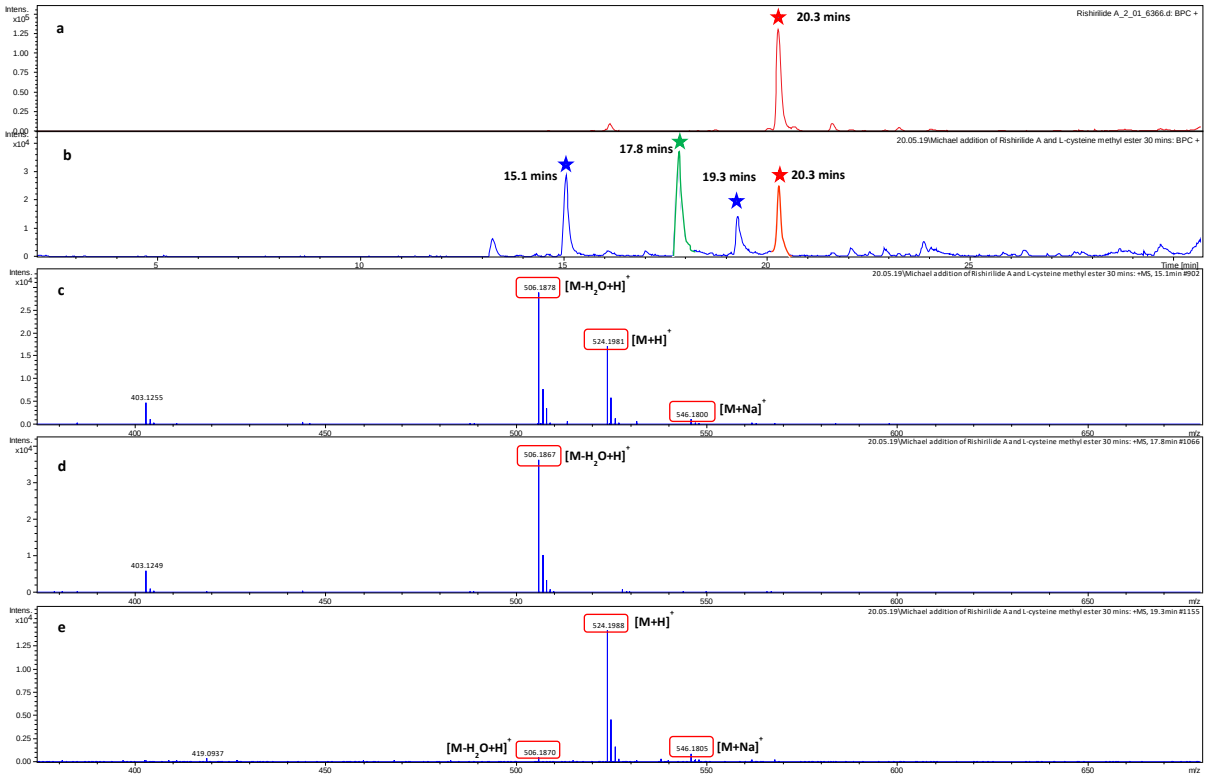

Figure 4.4: LCMS analysis of the Michael addition of (-)-rishirilide A (**29**) with L-cysteine methyl ester (**43**) after 30 minutes. (**a**) Base peak chromatogram (BPC) of (-)-rishirilide A (**29**) (peak indicated with a red star); (**b**) BPC of the Michael addition of (-)-rishirilide A (**29**) with L-cysteine methyl ester (**43**) after 30 mins: Michael addition products (**44**) (blue stars), dehydrated Michael addition product (green star), unreacted (-)-rishirilide A (**29**) (red star); (**c**) Mass spectrum of Michael addition product (**44**) at 15.1 mins; (**d**) Mass spectrum of dehydrated Michael addition product at 17.8 mins; (**e**) Mass spectrum of Michael addition product (**44**) at 19.3 mins.

In conclusion, we have successfully shown that Michael addition of (-)-rishirilide A (**29**) with L-cysteine methyl ester hydrochloride (**43**) does occur, albeit more slowly than with L-cysteine hydrochloride (**41**), with the presence of unreacted (-)-rishirilide A after 30 mins reaction time.Two diastereomers of the Michael addition products were observed (**44a** and **44b**) along with a postulated Michael addition-dehydration product. Next step, we decided to examine the Michael addition of (-)-rishirilide A (**29**) with short peptides containing cysteine.

4.1.3 Michael addition of (-)-rishirilide A with a cysteine containing short peptide

Encouraged with the previous results of the Michael addition reactions of (-)-rishirilide A (**29**), with both L-cysteine (**41**) and L-cysteine methyl ester (**43**), next we decided to examine the

Michael addition of (-)-rishirilide A (**29**) with a short peptide containing a cysteine (Scheme **4.4**).

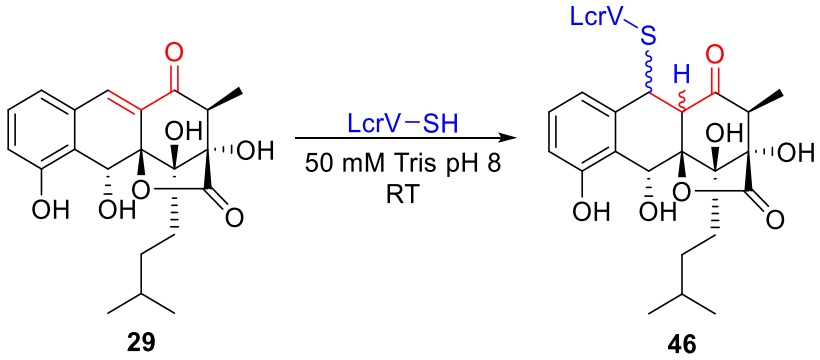

Scheme 4.4: Michael addition of (-)-rishirilide A (**29**) with LcrV (272 – 291) (**45**) to give (-)-rishirilide A-LcrV (272 – 291) adduct (**46**).

The short peptide, LcrV (272 – 291) (**45**) was chosen to better represent the Michael addition chemistry of an enzyme, as any target enzyme cysteine would be surrounded with additional amino acid residues, sterically shielding the thiol from reaction. LcrV (272 – 291) (**45**) is a peptide derived from the LcrV protein, a bacterial virulence factor produced by *Yersinia pestis.*[68] LcrV (272 – 291) (**45**) is a 20-mer polypeptide covering the 272 – 291 amino acids of the LcrV protein, containing a cysteine at residue 273 (Figure **4.5**).

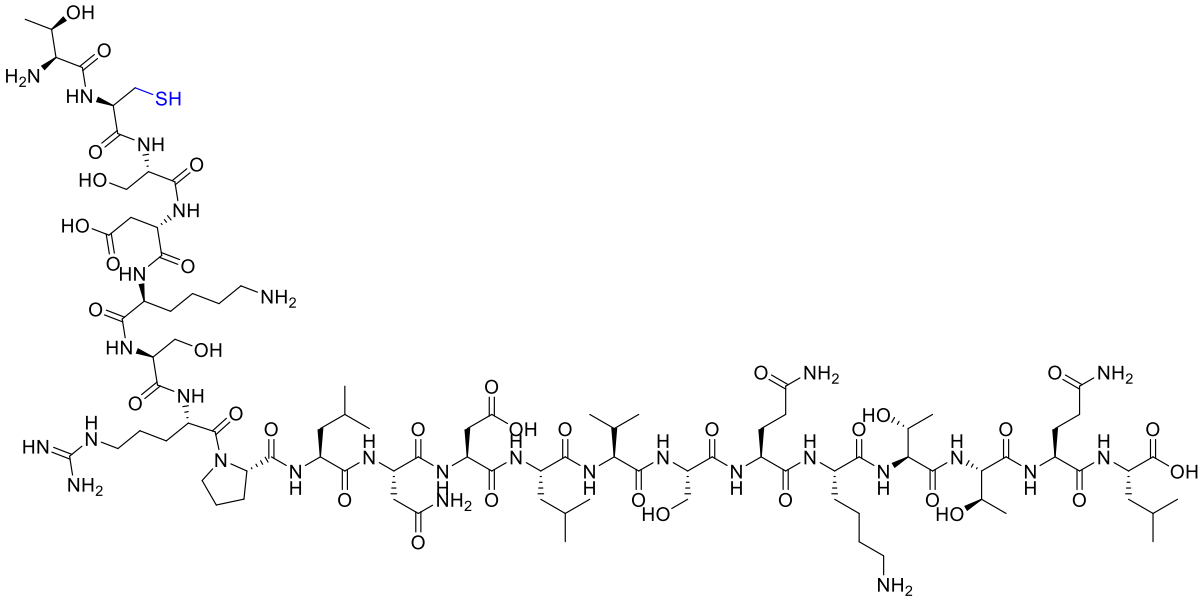

Figure 4.5: LcrV (272 – 291) peptide (**45**).

Before we used LcrV (272 – 291) (**45**) to test the Michael addition to (-)-rishirilide A (**29**), we decided to confirm structure by LCMS. Thus, to 1 µL of a 4.5 mM LcrV (272 – 291) (**45**) solution in 20 mM dithiothreitol (DTT) was added 1 µL of water, and 0.25 µL of a 0.5 M Tris buffer pH 8. It should be noted that dithiothreitol (DTT) was included in these experiments as a mild reducing agent, to prevent the oxidative dimerization of LcrV (272 – 291) (**45**) through disulphide bond formation. The resulting mixture was mixed in a 0.2 mL Eppendorf tube for 5 seconds (vortex) and then analysed by LCMS. Just prior to LCMS analysis, formic acid was added to the sample to a final concentration of 0.1% by v/v, to equilibrate the sample with the mobile phase pH before analysis. The LCMS was performed using a gradient method from 5:95 to 95:5, acetonitrile (0.1% by v/v FA) : water (0.1% by v/v FA) with a flowrate of 0.2 mL/min over 60 minutes.

The LCMS chromatogram showed a key peak at 15.1 minutes with *m/z* signals of 1118.0842, 745.7317, 559.5537, corresponding to the $[M+2H]^{2+}$, $[M+3H]^{3+}$, and $[M+4H]^{4+}$ ions, confirming the molecular weight and thus amino acid composition of LcrV (272 – 291) (**45**) (Figure **4.6**).

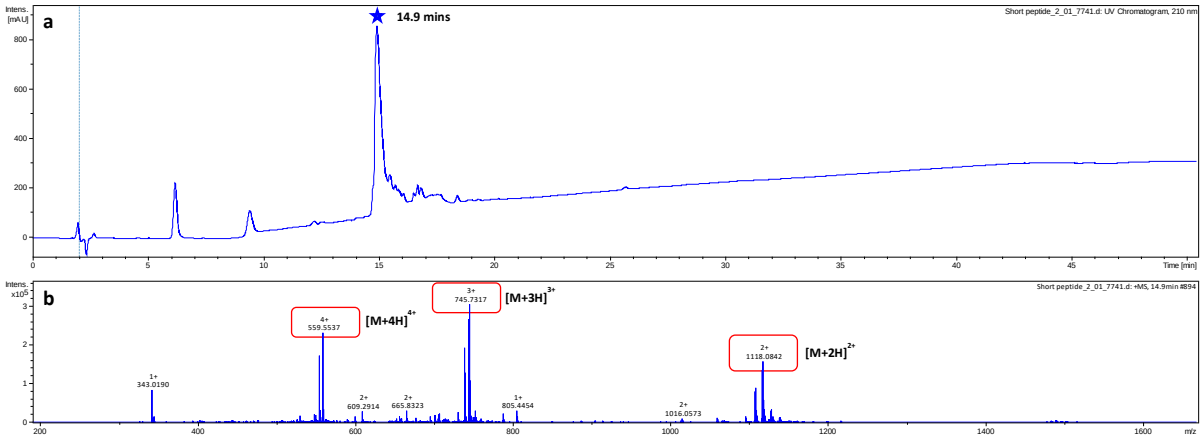

Figure 4.6: (**a**) LCMS chromatogram of LcrV (272 – 291) (**45**) (indicated with blue star); (**b**) Mass spectrum of LcrV (272 – 291) (**45**) at 14.9 minutes.

Next, we carried out the Michael addition of (-)-rishirilide A (**29**) with LcrV (272 – 291) (**45**). Due to the limited mass of LcrV (272 – 291) (**45**) available, we decided to use a modified method of Simon *et al.* to minimise the mass of LcrV (272 – 291) (**45**) required for the experiment, whilst maintaining the same ratio of (-)-rishirilide A (**29**) to thiol. Thus, to 1.9 µL of water, was added 4.4 µL of a 4.5 mM solution of LcrV (272 – 291) (**45**) in 20 mM DTT, 5 µL of a 200 mM solution of Tris buffer (pH 8 in water) and 8.7 µL of a 23 mM solution of (-)-

rishirilide A (**29**) in methanol, to give a 20 µL solution with final concentrations of 1 mM (0.1 eq.) LcrV (272 – 291) (**54**) with 4.4 mM DTT, 50 mM Tris buffer, and 10 mM (1 eq.) for, (-)-rishirilide A (**29**).[63] Note that a sub-stoichiometric quantity of LcrV (272 – 291) (**45**) was employed due to the limited mass available. Furthermore, DTT is also present in the reaction mixture as a reducing agent to maintain the free thiol of LcrV (272 – 291) (**45**). However, due to the high relative concentration of DTT, it may also compete with LcrV (272 – 291) (**45**) in the Michael addition reactions of (-)-rishirilide A (**29**). The resulting mixture was mixed in a 0.2 mL Eppendorf tube for 5 seconds (vortex). After 0, 15, 30, 45, and 60 minutes at room temperature 2 µL aliquots of the reaction mixture were taken, diluted into 10 µL of water to stop the reaction, and then analysed by LCMS using the same solvent gradient method as previously. Reference samples were also prepared containing only LcrV (272 – 291) (**45**) or (-)-rishirilide A (**29**) to aid in the identification of these molecules. Prior to each analysis formic acid was added to each sample to a final concentration of 0.1 % as before, the LCMS chromatogram of the reaction mixture after 0 minutes showed seven key peaks. A small peak was observed at 15.1 minutes (*m/z* = 559.5776 $[LcrV+4H]^{4+}$, 745.7641 $[LcrV+3H]^{3+}$ and 1118.1315 $[LcrV+2H]^{2+}$), corresponding to unreacted LcrV (272 – 291) (**45**) (Figure **4.7**).

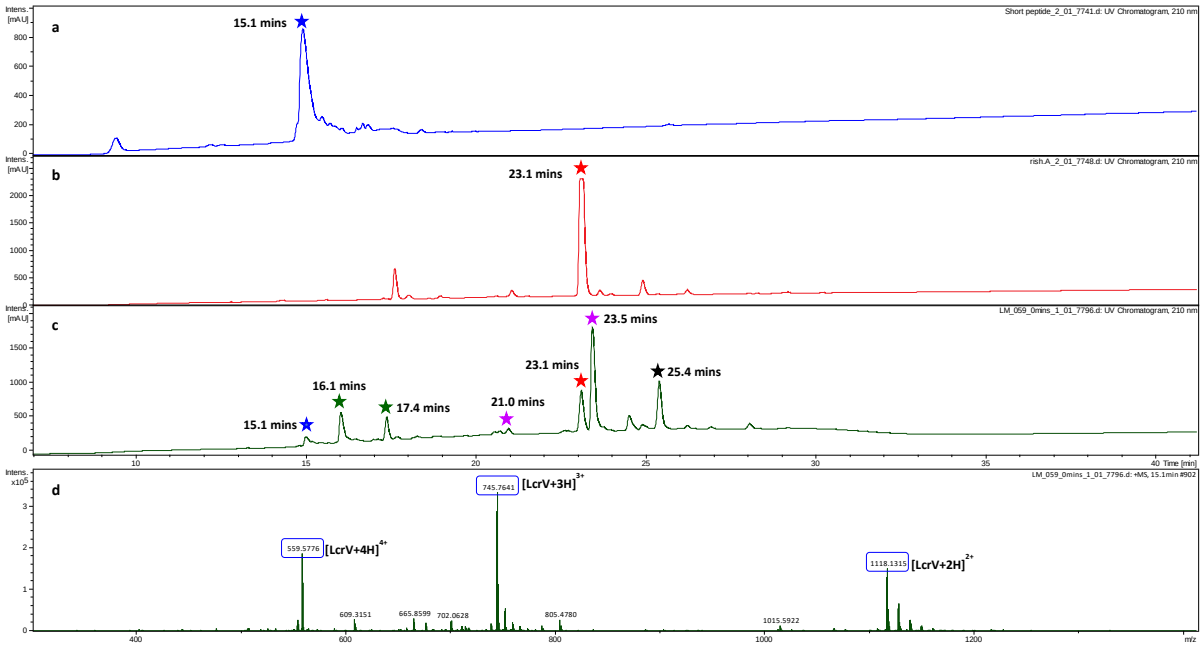

Figure 4.7: LCMS analysis of the Michael addition of (-)-rishirilide A (**29**) with LcrV (271-291) (**45**). (**a**) LCMS chromatogram of LcrV (271-291) (**45**) (peak indicated with a blue star); (**b**) LCMS chromatogram of (-)-rishirilide A (**29**) (red star); (**c**) LCMS chromatogram of the Michael addition reaction after 0 mins: the Michael addition product (green stars), unreacted (-)-rishirilide A (**29**) (red star), (-)-rishirilide A and DTT adducts (purple stars), (+)-rishirilide B (**30**) (black star); (**d**) Mass spectrum of unreacted LcrV (272-291) (**45**) at 15.1 mins.

Furthermore, two peaks observed at 16.1 and 17.4 mins (*m/z* = 875.1551 $[Rish.A+LcrV+3H]^{3+}$ and 1312.2145 $[Rish.A+LcrV+2H]^{2+}$) corresponded to the expected (-)-rishirilide A-LcrV (272 – 291) Michael adduct (**46**). This shows that the Michael addition of (-)-rishirilide A (**29**) with LcrV (272-291) (**45**) did occur, to give two diastereomeric Michael addition adducts (**46a** and **46b**). We also observed *m/z* signals corresponding to LcrV (272-291) (**45**) (*m/z* = 559.5776 $[LcrV+4H]^{4+}$, 745.7641 $[LcrV+3H]^{3+}$ and 1118.1315 $[LcrV+2H]^{2+}$) which may arise due to *in situ* fragmentation of (-)-rishirilide A-LcrV (272 – 291) Michael adduct (**46**) via a retro-Michael like reaction (Figure **4.8**).

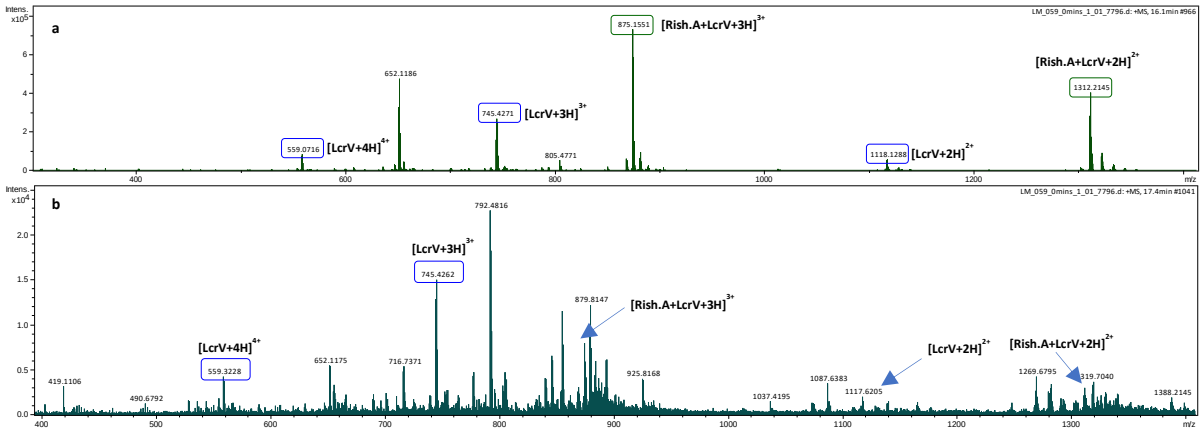

Figure 4.8: Mass spectrum of the Michael addition products (**46**) of (-)-rishirilide A (**29**) and LcrV (272-291) (**45**): (**a**) at 16.1 mins; (**b**) at 17.2 mins.

A small peak observed at 21.0 mins (*m/z* = 565.1833 $[Rish.A+DTT+Na]^{+}$) corresponded to a one to one Michael addition product of (-)-rishirilide A and DTT (**47**), a by-product arising through reaction with the reducing agent present in the LcrV (272 – 291) (**45**) sample. Furthermore, another peak observed at 23.5 mins (*m/z* = 953.3498 $[(2xRish.A)+DTT+Na]^{+}$) corresponded to the two to one Michael addition product of two molecules of (-)-rishirilide A with one molecule of DTT (**48**) (Figure **4.9,** Scheme **4.5**).

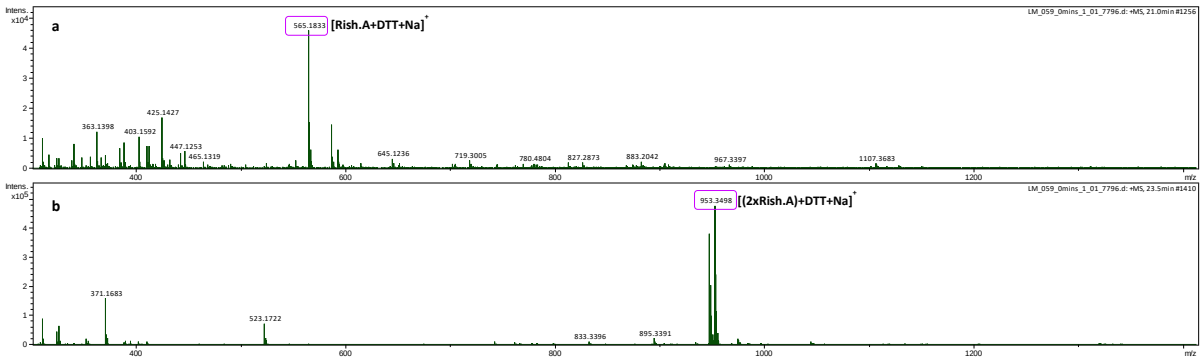

Figure 4.9: Mass spectrum of the Michael addition products (**47** and **48**) of (-)-rishirilide A (**29**) and DTT: (**a**) at 21.0 mins; (**b**) at 23.5 mins.

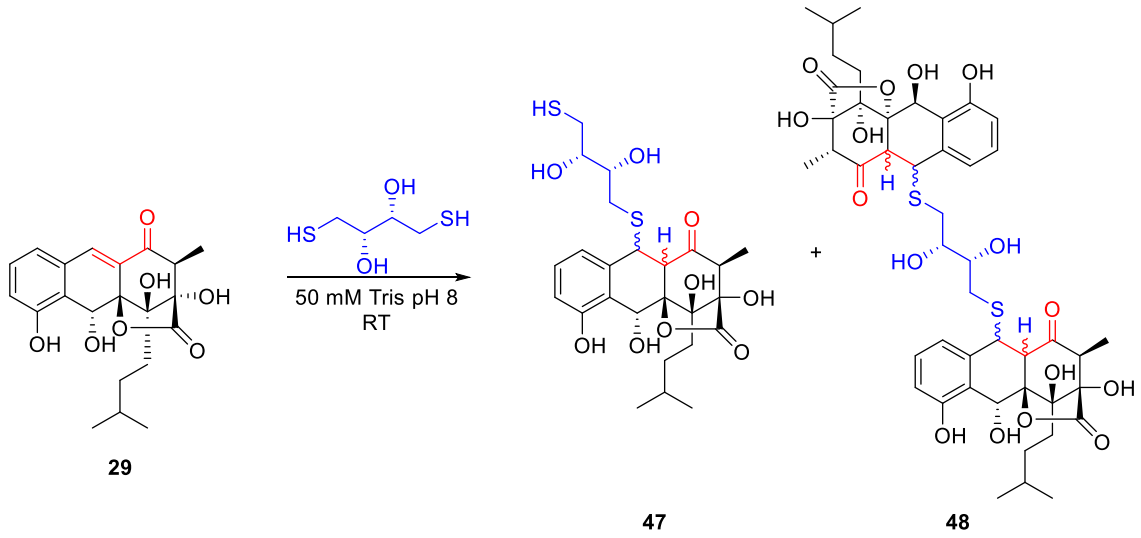

Scheme 4.5: Michael addition products (**47** and **48**) of (-)-rishirilide A (**29**) with DTT.

A peak observed at 23.1 mins (*m/z* = 411.1624 $[Rish.A+Na]^+$, 799.3327 $[(2xRish.A)+Na]^+$, and 1118.4915 $[(3xRish.A)+Na]^+$) corresponded to the unreacted of (-)-rishirilide A (**29**). Interestingly a further minor peak at 25.4 minutes was assigned as (+)-rishirilide B (**30**) (*m/z* = 395.1661 $[Rish.B+Na]^+$, 767.3404 $[(2xRish.B)+Na]^+$). This peak may arise due to the presence of (+)-rishirilide B (**30**) as a minor contaminant in the original sample or be due to the formation of (+)-rishirilide B (**30**) or a related isomeric molecule under the reducing reactions conditions (Figure **4.10**).

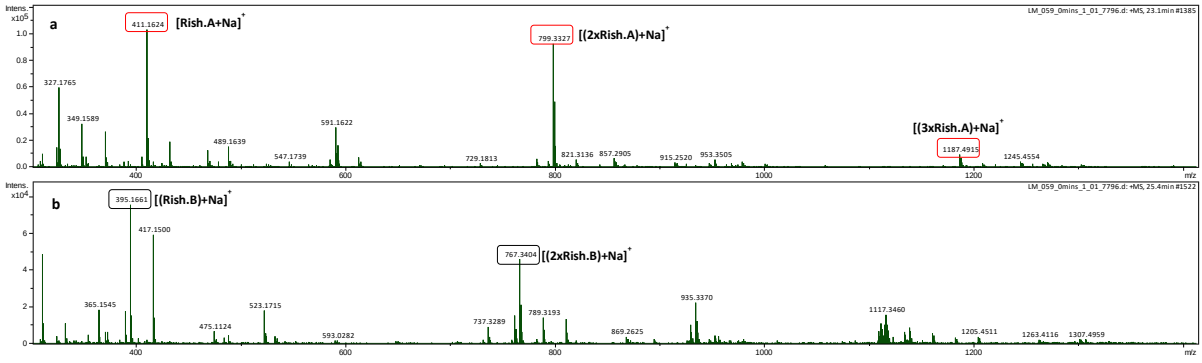

Figure 4.10: (**a**) Mass spectrum of unreacted (-)-rishirilide A (**29**) at 23.1 mins; (**b**) Mass spectrum of (+)-rishirilide B (**30**) at 25.4 mins.

The LCMS chromatograms taken at 15, 30, 45, 60 and 120 minutes showed no significant changes in the reaction mixture. This suggests that the Michael addition reaction between (-)-rishirilide A (**29**) and LcrV (272 – 291) (**45**) had gone to completion prior to the sample analysis of our first time point.

In conclusion we have shown that the Michael addition of (-)-rishirilide A (**29**) can occur with the short thiol containing peptide LcrV (272 – 291) (**45**) as a model for the Michael addition to a possible target enzyme. It should also be noted that the Michael addition reactions were very fast under our reaction conditions, further studies would be required to probe the rate of these reaction further. These reactions were also complicated by the Michael addition reactions of (-)-rishirilide A (**29**) with the DTT present in the samples.

4.2 Michael addition chemistry of (+)-rishirilide B

To help to validate the mode of action of (-)-rishirilide A (**29**), we next decided to carry out a series of comparative experiments with the non-bioactive (+)-rishirilide B (**30**) as a negative control. (-)-Rishirilide A (**29**) shows antibiotic activity against Gram-positive bacteria, whilst (+)-rishirilide B (**30**) does not, despite the two molecules having very similar structures. Interestingly in (+)-rishirilide B (**30**) the α,β-unsaturated ketone moiety is contained within an aromatic ring and as such is likely to be much less reactive towards Michael addition chemistry. Therefore, we hypothesised that the antibiotic activity of the rishirilides is positively correlated to their reactivity as Michael acceptors. To examine this postulate, we decided to examine the Michael addition chemistry of (+)-rishirilide B (**30**) with the same thiol containing small molecules and short polypeptide as used previously (Scheme **4.6**).

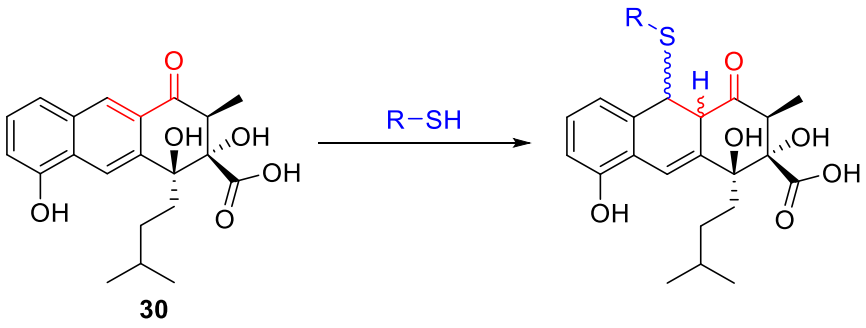

Scheme 4.6: Michael addition of (+)-rishirilide B (**30**) with thiol containing molecules.

4.2.1 Michael addition of (+)-rishirilide B with L-cysteine and L-cysteine methyl ester

In order to provide direct comparison with the Michael addition chemistry of (-)-rishirilide A (**29**), we initially examined the reaction of (+)-rishirilide B (**30**) with both L-cysteine (**41**) and L-cysteine methyl ester (**43**).

Following the Michael addition procedures as used for (-)-rishirilide A (**29**), (+)-rishirilide B (**30**) was reacted in two separate experiments with both L-cysteine hydrochloride (**41**) and L-cysteine methyl ester hydrochloride (**43**).

The following procedure was used for the Michael additions of (+)-rishirilide B (**30**) with L-cysteine hydrochloride (**41**) or L-cysteine methyl ester hydrochloride (**43**). To 649 µL of water was added 101 µL of a 0.01 M solution of L-cysteine hydrochloride (**41**) or L-cysteine methyl ester hydrochloride (**43**) in water and 250 µL of a 2.69 mM solution of (+)-rishirilide B (**30**) in methanol, to give a 1 mL solution with final concentrations of 1.01 mM (1.5 eq.) and 0.67 mM (1 eq.) for L-cysteine hydrochloride (**41**)/L-cysteine methyl ester hydrochloride (**43**) and (+)-rishirilide B (**30**) respectively. The resulting mixtures were reacted for 180 minutes at room temperature. After 30, 60, 90, 120, 150 and 180 minutes 50 µL aliquots of each reaction mixture were taken, diluted into 250 µL of water to stop the reaction, and subsequently analysed by LCMS (Scheme **4.7**).

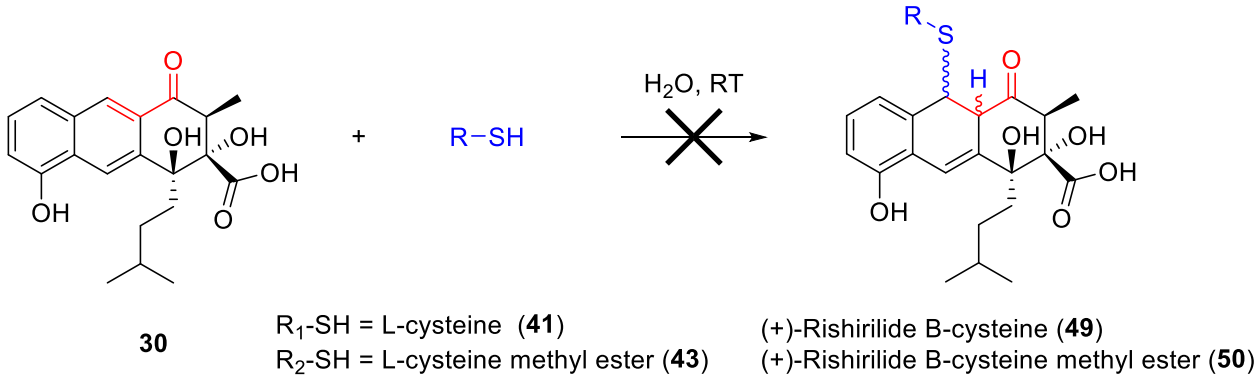

Scheme 4.7: Attempted Michael addition of (+)-rishirilide B (**30**) with L-cysteine (**41**) or L-cysteine methyl ester (**43**).

The LCMS chromatograms of the two Michael addition reactions of (+)-rishirilide B (**30**) and small molecule thiol (L-cysteine (**41**) or L-cysteine methyl ester (**43**)) after 180 minutes, did not show any peaks that corresponded to the potential Michael addition products. For comparison we have shown the LCMS after 30 minutes, which only showed a single peak at 22.1 minutes with *m/z* signals of 373.1701 and 395.1543, corresponding to the $[M+H]^+$ and $[M+Na]^+$ ions of (+)-rishirilide B (**30**) respectively. LCMS analysis of later reaction time points showed the same results. These results confirmed that the Michael addition reaction of (+)-rishirilide B (**30**) with either L-cysteine hydrochloride (**41**) or L-cysteine methyl ester hydrochloride (**43**) did not occur under these conditions even after 180 minutes, suggesting that (+)-rishirilide B (**30**) is a poor Michael acceptor (Figure **4.11**).

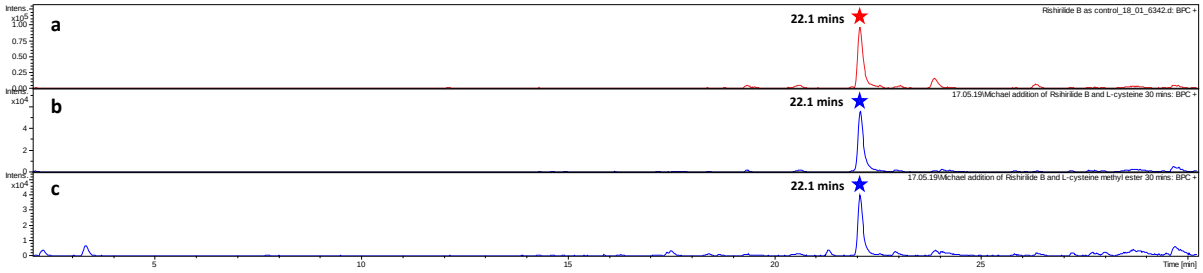

Figure 4.11: LCMS analysis of the Michael addition reactions of (+)-rishirilide B (**30**) with both L-cysteine (**41**) and L-cysteine methyl ester (**43**) after 30 minutes. (**a**) BPC of (+)-rishirilide B (**30**) for comparison (peak indicated with a red star); (**b**) BPC of Michael addition reaction with L-cysteine (**41**) (unreacted (+)-rishirilide B (**30**) indicated with a blue star); (**c**) BPC of Michael addition with L-cysteine methyl ester (**43**) (unreacted (+)-rishirilide B (**30**) indicated with a blue star).

4.2.2 Michael addition of (+)-rishirilide B with LcrV (271-291)

To further examine the Michael addition chemistry of (+)-rishirilide B (**30**), and to provide comparison with the chemistry of with (-)-rishirilide A (**29**), next we tested the reaction with LcrV (271-291) (**45**).

Thus, as before, to 4.6 µL of water, was added 4.4 µL of a 4.5 mM solution of LcrV (271-291) (**45**) in 20 mM DTT, 5 µL of a 200 mM Tris buffer (pH 8 in water) and 6 µL of a 33.3 mM solution of (+)-rishirilide B (**30**) in methanol, to give a 20 µL solution with final concentrations of 1 mM, 50 mM, and 10 mM for LcrV (271-291) (**45**), Tris buffer pH 8 and (+)-rishirilide B (**30**), respectively. The resulting mixture was mixed for 5 seconds (vortex). To monitor the progress of the reaction, 2 µL aliquots were taken after 0, 30 and 60 minutes at room temperature, diluted into 10 µL of water to stop the reaction, and then analysed by LCMS using the same solvent gradient method as previously. Prior to each LCMS analysis, formic acid was added to each sample to give a final concentration of 0.1 % (v/v) as previously (Scheme **4.8**).

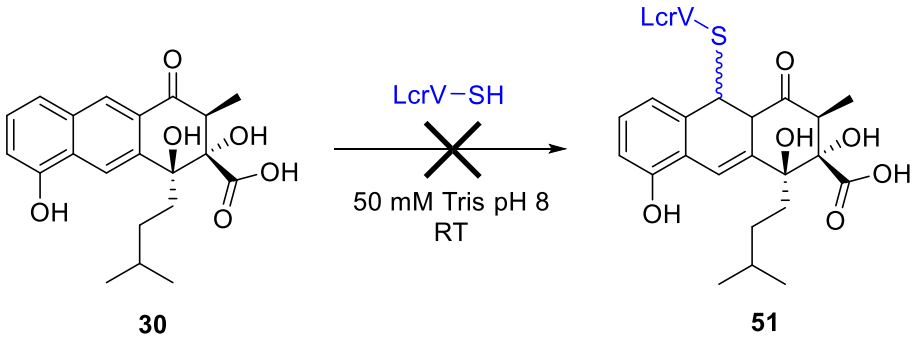

30 **51**

Scheme 4.8: Michael addition of (+)-rishirilide B (**30**) with LcrV (271-292) (**45**).

The LCMS chromatogram of the resulting reaction mixture after 30 minutes showed two peaks. The first peak at 14.9 minutes (*m/z* = 559.5741 $[LcrV+4H]^{4+}$, 745.7587 $[LcrV+3H]^{3+}$ and 1118.1217 $[LcrV+2H]^{2+}$) corresponded to the short peptide LcrV (271-291) (**45**), whilst the second peak at 25.4 minutes (*m/z* = 395.1656 $[Rish.B+Na]^{+}$ and 767.3363 $[(2xRish.B)+Na]^{+}$) corresponded to unreacted (+)-rishirilide B (**30**). No significant changes were observed by LCMS analysis after 30 and 60 minutes of reaction. These experiments showed no reaction of (+)-rishirilide B (**30**) with LcrV (271-291) (**45**) under these conditions (Figure **4.12**).

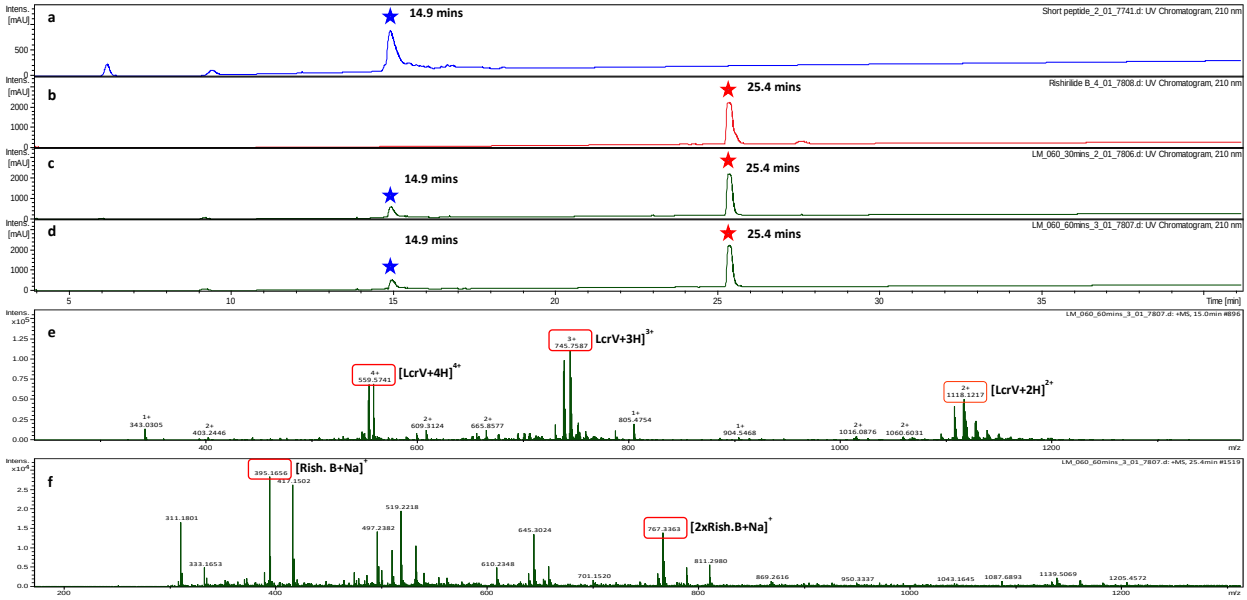

Figure 4.12: LCMS analysis of the Michael addition of (+)-rishirilide B (**30**) with LcrV (271-292) (**45**). (**a**) LCMS chromatogram of LcrV (271-292) (**45**) for comparison (peak indicated with a blue star); (**b**) LCMS chromatogram of (+)-rishirilide B (**30**) for comparison (red star); LCMS chromatogram of Michael addition of LcrV (271-292) to (+)-rishirilide B (**30**): unreacted LcrV (271-292) (**45**) (blue star), unreacted (+)-rishirilide B (**30**) (red star) after (**c**) 30 mins; (**d**) after 60 mins; Mass spectra of Michael addition reaction mixture after 60 mins: (**e**) at 14.9 mins (unreacted LcrV (271-292) (**45**)); (**f**) at 25.4 mins (unreacted (+)-rishirilide B (**30**)).

In conclusion, we have shown that (+)-rishirilide B (**30**) does not undergo Michael addition with short peptide LcrV (271-291) (**45**) even after 60 mins under our standard reaction conditions, reinforcing the idea that (+)-rishirilide B (**30**) is a poor Michael acceptor.

4.3 Michael addition chemistry of DEM30355/A

To further validate our hypothesis that the antibiotic activity of (-)-rishirilide A (**29**) is correlated to its reactivity as a Michael acceptor, we decided to examine the Michael addition chemistry of DEM30355/A (**28**). DEM30355/A (**28**) has a similar structure to (-)-rishirilide A (**29**), especially with respect to the α,β-unsaturated carbonyl, and also displays similar antibiotic activity against Gram-positive bacteria. Thus, if we can show that DEM30355/A (**28**) is a Michael acceptor, then Michael acceptor ability would positively correlate with antibiotic activity, and we could conclude that the mode of action of these natural products is likely due to irreversible enzyme inhibition (Figure **4.13**).

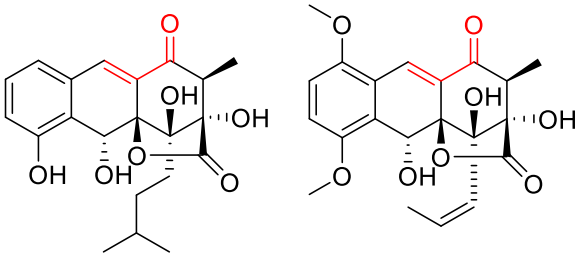

Figure 4.13: α,β-Unsaturated ketone moiety in (-)-rishirilide A (**29**) and DEM30355/A (**28**), highlighted red.

Thus, we decided to test the Michael addition chemistry of DEM30355/A (**28**) with the same thiol containing small molecules and short polypeptide (L-cysteine hydrochloride (**41**), L-cysteine methyl ester hydrochloride (**43**) and LcrV (271-291) (**45**) as used previously with (-)-rishirilide A (**29**) and (+)-rishirilide B (**30**) (Scheme **4.9**).

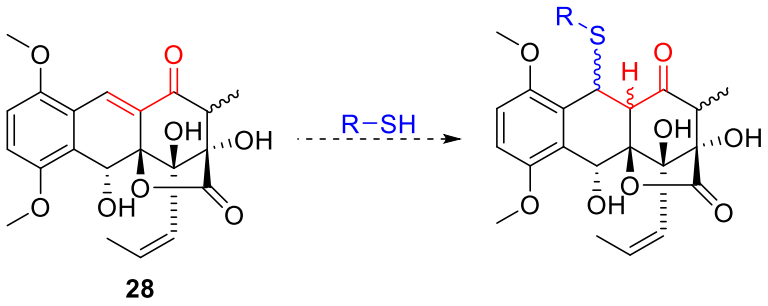

Scheme 4.9: Michael addition of DEM30355/A (**28**) with thiols.

4.3.1 Michael addition of DEM30355/A with L-cysteine and L-cysteine methyl ester

First, we examined the Michael addition reaction of DEM30355/A (**28**) with L-cysteine hydrochloride (**41**) and L-cysteine methyl ester hydrochloride (**43**).

The following protocols were used for the Michael addition of DEM30355/A (**28**) with L-cysteine hydrochloride (**41**) and L-cysteine methyl ester hydrochloride (**43**). To 725 µL of water, was added 75 µL of a 0.01 M solution of L-cysteine hydrochloride (**41**) or L-cysteine methyl ester hydrochloride (**43**) in water and 200 µL of a 2.50 mM solution of DEM30355/A (**28**) in DMSO, to give a 1 mL solution with final concentrations of 0.75 mM (1.5 eq.) and 0.5 mM (1 eq.) for L-cysteine hydrochloride (**41**)/L-cysteine methyl ester hydrochloride (**43**) and DEM30355/A (**28**) respectively. The resulting mixtures were reacted for 180 minutes at room

temperature. After 30, 60, 90, 120, 150 and 180 minutes 50 µL aliquots were diluted in 250 µL water and then analysed by LCMS (Scheme **4.10**).

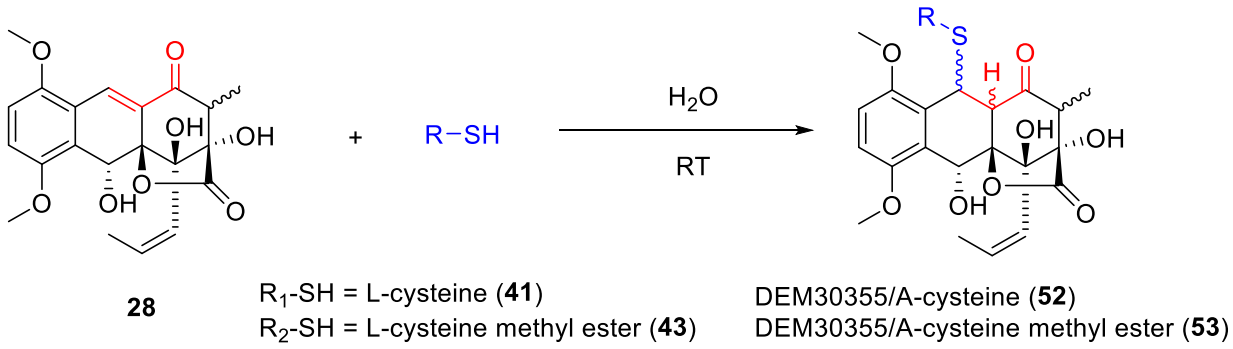

Scheme 4.10: Michael addition of DEM 30355/A (**28**) with L-cysteine (**41**) or L-cysteine methyl ester (**43**).

For comparison, we carried out analytical LCMS of DEM30355/A (**28**). The base peak chromatogram of DEM30355/A (**28**) showed two peaks, one at 19.2 minutes (*m/z* signals of 403.1400 $[M+H]^+$, 425.1219 $[M+Na]^+$, 827.2530 $[2M+Na]^+$) and the second at 19.5 minutes (*m/z* signals of 403.1400 $[M+H]^+$, 425.1219 $[M+Na]^+$, 827.2530 $[2M+Na]^+$). These two peaks were assigned as the two known C-2 methyl epimers of DEM30355/A (**28**).

The base peak chromatogram of the reaction mixture of DEM30355/A (**28**) with L-cysteine hydrochloride (**41**) after 30 minutes showed a key peak at 15.5 minutes with *m/z* signals of 506.1513 $[M-H_2O+H]^+$, 524.1597 $[M+H]^+$, 1047.3108 $[2M+H]^+$, corresponding to the Michael addition product of DEM30355/A-cysteine (**52**).

Furthermore, the base peak chromatogram of the reaction mixture of DEM30355/A (**28**) with L-cysteine methyl ester hydrochloride (**43**) showed a key peak at 16.5 minutes with *m/z* signals of 520.1702, 538.1795 and 560.1612, corresponding to the $[M-H_2O+H]^+$, $[M+H]^+$ and $[2M+H]^+$ ions of the Michael addition product of DEM30355/A-cysteine methyl ester (**53**).

These experiments demonstrated rapid Michael addition of DEM30355/A (**28**) with both L-cysteine hydrochloride (**41**) and L-cysteine methyl ester (**43**). In both cases no significant changes were observed in the LCMS chromatograms of the reaction mixtures after 60, 90, 120, 150 and 180 minutes, suggesting the Michael addition reactions were completed in less than 30 minutes (Figure **4.14**).

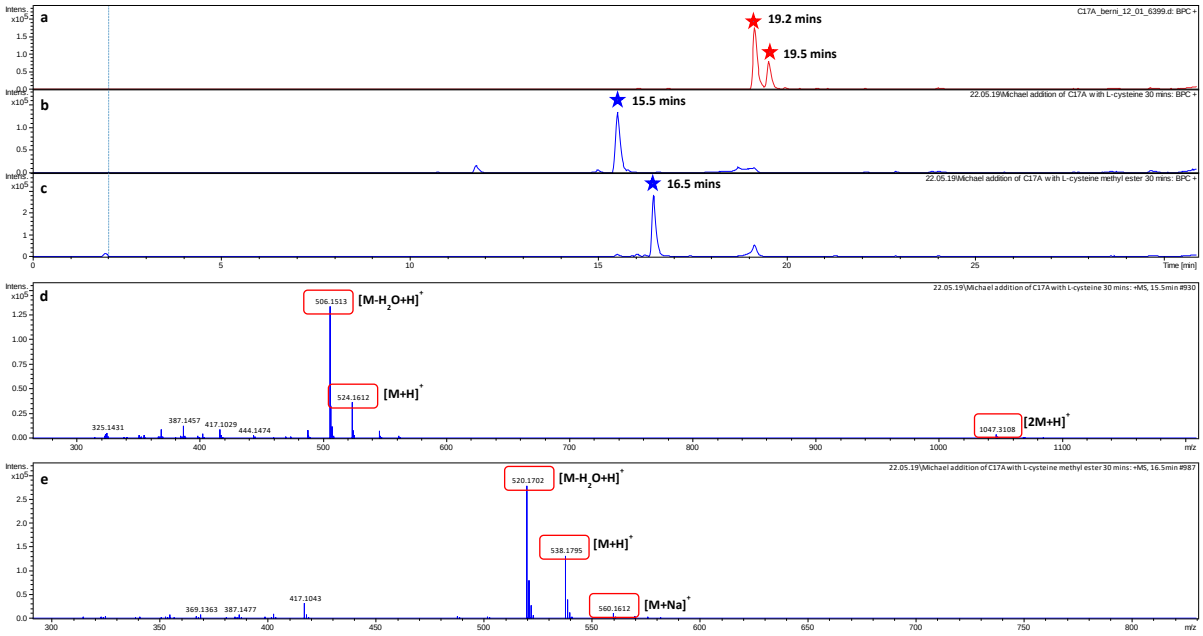

Figure 4.14: LCMS analysis of the Michael addition of DEM30355/A (**28**) with L-cysteine hydrochloride (**41**) and L-cysteine methyl ester hydrochloride (**43**). (**a**) base peak chromatogram (BPC) of DEM30355/A (**28**) for comparison (peak indicated with red stars); BPC of reaction mixture of DEM30355/A (**28**); (**b**) with L-cysteine hydrochloride (**41**)(Michael addition product indicated with a blue star); (**c**) with L-cysteine methyl ester hydrochloride (**43**) (Michael addition product indicated with a blue star); Mass spectrum of Michael addition product of: (**d**) DEM30355/A-cysteine (**52**) at 15.5 mins; (**e**) DEM 30355/A-cysteine methyl ester (**53**) at 16.5 mins.

4.3.2 Michael addition of DEM30355/A with LcrV (272-291)

Encouraged with successful Michael addition of DEM30355/A (**28**) with both L-cysteine (**41**) and L-cysteine methyl ester (**43**), next we examined the Michael addition of DEM30355/A (**28**) with LcrV (271-291) (**45**). We also predicted that the Michael addition of DEM30355/A (**28**) with DTT may occur alongside that with LcrV (272-291) (**45**) (Scheme **4.11**).

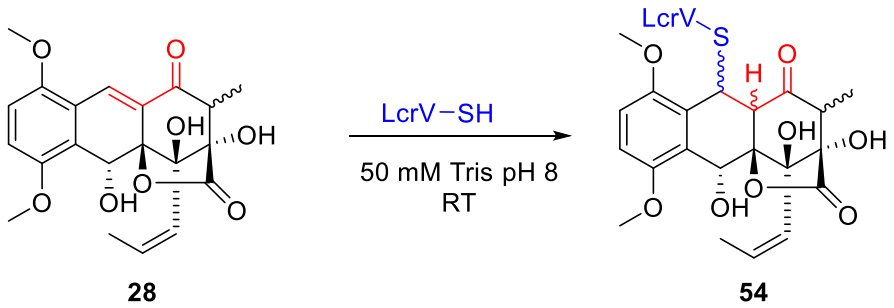

Scheme 4.11: Michael addition of DEM30355/A (**28**) with LcrV (271-291) (**45**).

Thus, following a similar previous method used in Michael addition of (-)-rishirilide A (**29**) with LcrV (271-291) (**45**), to 2.6 µL of water was added 4.4 µL of a 4.5 mM solution of LcrV (271-291) (**45**) in 20 mM DTT, 5 µL of a 200 mM solution of Tris buffer 200 mM (pH 8), and 8 µL of

a 25 mM solution of DEM30355/A (**28**) in DMSO, to give a 20 µL solution with final concentrations of 1 mM LcrV (271-291) (**45**) with 4.4 mM DTT, 50 mM Tris buffer and 10 mM DEM30355/A (**28**). The resulting mixture was mixed for 5 seconds (vortex) at room temperature. Aliquots (2 µL) of the reaction mixture were taken at 0, 15, 30, 45 and 60 minutes, diluted with 10 µL water and then analysed by LCMS.

The LCMS analysis was monitores at 210 nm as at this wavelength is recommended to analyse peptides. Control LCMS experiments showed the expected peak (15.0 mins) and mass spectra (*m/z* = 559.5788 $[LcrV+4H]^{4+}$, 745.7650 $[LcrV+3H]^{3+}$ and 1118.1314 $[LcrV+2H]^{2+}$) for LcrV (271-291) (**45**). However in the case of DEM30355/A (**28**), two peaks were observed in the LCMS chromatogram at 21.6 minutes (*m/z* = 425.1431 $[DEM30355/A+Na]^{+}$, 827.2901 $[(2xDEM30355/A)+Na]^{+}$ and 1229.4316 $[(3xDEM30355/A)+Na]^{+}$) and 22.1 minutes (*m/z* = 403.1597 $[DEM30355/A+H]^{+}$, 827.2901 $[(2xDEM30355)+Na]^{+}$ and 1229.4325 $[(3xDEM30355/A)+Na]^{+}$). We have assigned these to the presence of two C-2 epimers of DEM30355/A (**28**) present in our sample (Figure **4.15**).

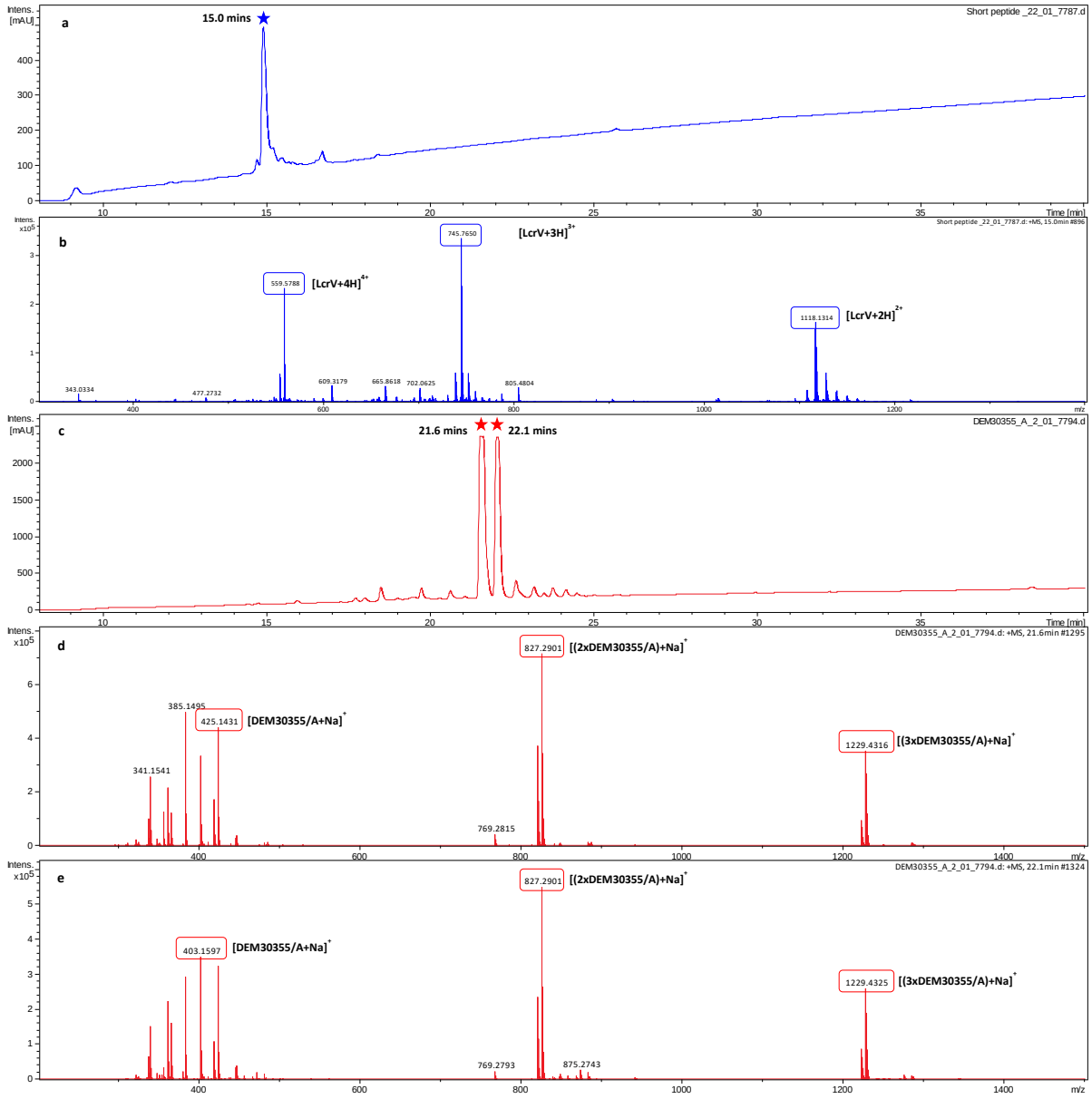

Figure 4.15: (**a**) LCMS chromatogram of LcrV (272-291) (**45**) (blue star); (**b**) Mass spectrum of LcrV (272-291) (**45**) at 15.0 mins; (**c**) LCMS chromatogram of DEM30355/A (**28**) (red stars); Mass spectra of DEM30355/A (**28**): (**d**) at 21.6 mins; (**e**) at 22.1 mins.

The LCMS chromatogram of the reaction mixture after 0 minutes showed six key peaks. A small peak was observed at 15.0 minutes (*m/z* = 559.5786 $[LcrV+4H]^{4+}$, 745.7648 $[LcrV+3H]^{3+}$, and 1118.1283 $[LcrV+2H]^{2+}$), corresponding to unreacted LcrV (272-291) (**45**) (Figure **4.16**).

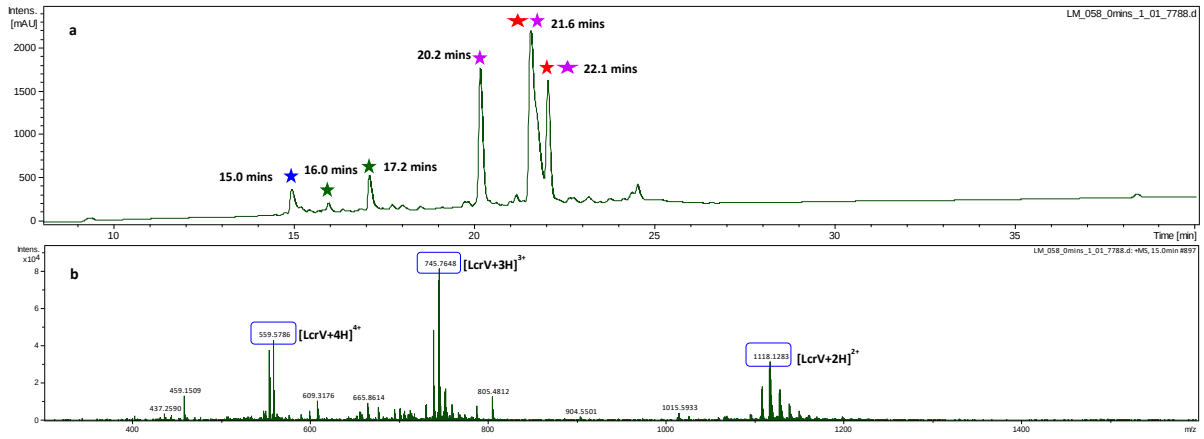

Figure 4.16: (**a**) LCMS chromatogram of the Michael addition reaction after 0 mins: unreacted LcrV (272-291) (**45**) (blue star), the Michael addition adducts of DEM30355/A and LcrV (272-291) (green stars), the Michael addition adduct of DEM30355/A (**28**) and DTT (purple stars), mixtures of unreacted DEM30355/A (**28**) (red stars); the Michael addition adducts 2:1 of DEM30355/A (**28**) and DTT (orange stars); (**b**) Mass spectrum of unreacted LcrV (272-291) (**45**) at 15.0 mins.

Furthermore, two peaks observed at 16.0 and 17.2 minutes (*m/z* = 879.8133 [DEM30355/A-LcrV+3H]$^{3+}$ and 1319.2005 [DEM30355/A-LcrV+2H]$^{2+}$) corresponded to the expected Michael addition adducts (**54**) of DEM30355/A and LcrV (272-291). As with (-)-rishirilide A (**29**), we rationalised the presence of two Michael addition adducts (**54a** and **54b**) to be due to the formation of two diastereomers in the reaction. It should be noted that further signals corresponding to unreacted LcrV (272-291) (**45**) were also observed in these spectra, likely due to an *in situ* fragmentation of the DEM30355/A-LcrV (272-291) Michael adduct (**54**) via a retro-Michael like reaction (Figure **4.17**).

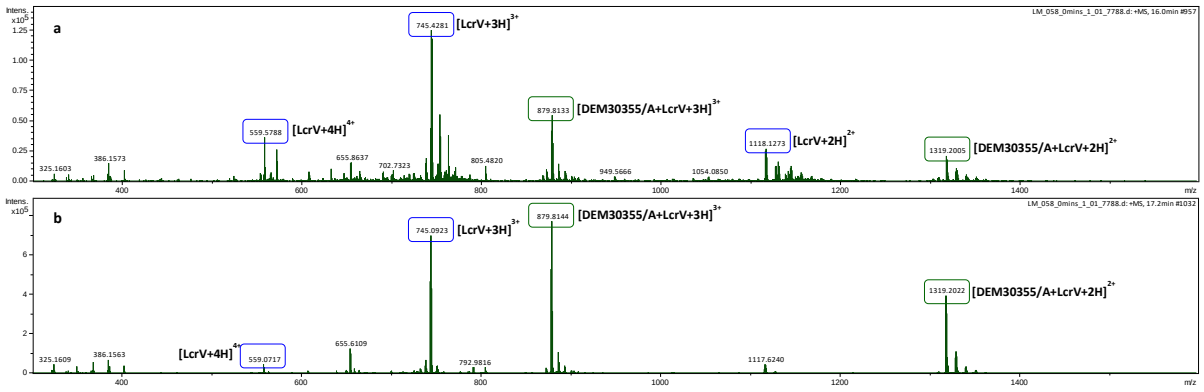

Figure 4.17: Mass spectrum of Michael addition products of DEM30355/A and LcrV (272-291) (**54**): (**a**) at 16.0; (**b**) at 17.2 mins.

A new peak observed at 20.2 minutes (*m/z* = 981.2090 [(2xDEM30355/A)+DTT+Na]$^{+}$) corresponded to a two to one Michael addition product of DEM30355/A and DTT (**55**). We

also assigned a further signal (*m/z* = 579.1638 [DEM30355/A-DTT+Na]$^+$) observed in the mass spectrum to a one to one Michael addition product of DEM30355/A (**28**) with DTT, again arising from an *in situ* retro-Michael fragmentation (Figure **4.18,** Scheme **4.12**).

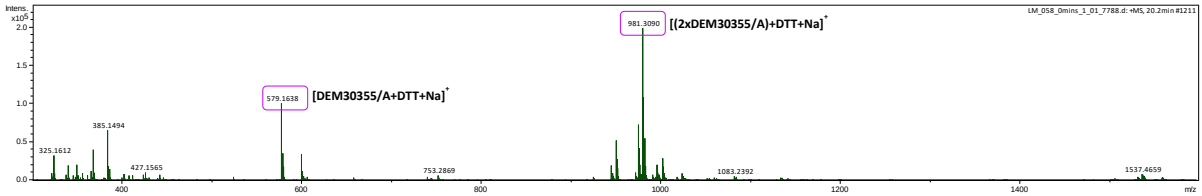

Figure 4.18: Mass spectrum of the Michael addition products (**55**) of DEM30355/A and DTT at 20.2 mins.

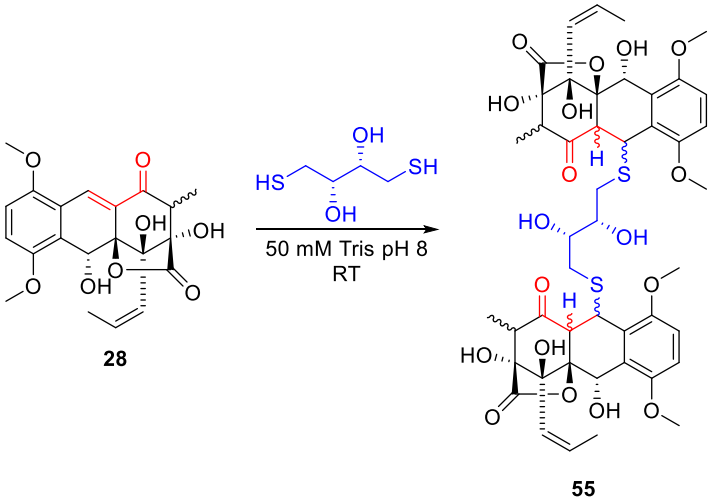

Scheme 4.12: Michael addition of DEM30355/A (**28**) with DTT.

The mass spectrum of the peak observed at 21.6 minutes showed the presence of two co-eluting molecules, unreacted DEM30355/A (**28**) and the 2:1 Michael addition adduct (**X**) of DEM30355/A and DTT. Thus the mass spectrum showed three ions corresponding to unreacted DEM30355/A (**28**) (*m/z* = 425.1451 [DEM30355/A+Na]$^+$, 827.2923 [(2xDEM30355/A)+Na]$^+$ and 1229.4350 [(3xDEM30355/A)+Na]$^+$), the observation of [2M+Na]$^+$ and [3M+Na]$^+$ ions being due to the relatively high concentration of DEM30355/A (**28**). Within the same peak ions could be observed that correspond to the 2:1 Michael addition adduct (**55**) of DEM30355/A and DTT (*m/z* = 981.3087 [(2xDEM30355/A)+DTT+Na]$^+$). Furthermore, a number of minor ions were observed corresponding to an *in situ* retro-Michael fragmentation product (*m/z* = 579.1619 [DEM30355/A+DTT+Na]$^+$) and a non-covalently bound dimer of the 2:1 Michael addition adduct of DEM30355/A with DTT (**55**) and

unreacted DEM30355/A (**28**) (*m/z* = 1383.4436 [(2xDEM30355/A)+DEM30355/A+DTT+Na]$^+$) (Figure **4.19**).

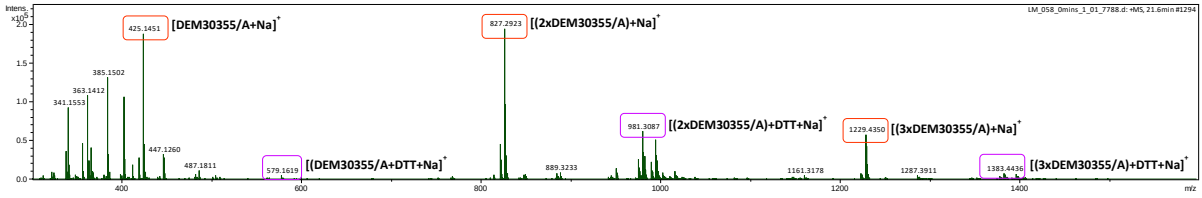

Figure 4.19: Mass spectrum of the Michael addition reaction of DEM30355/A (**28**) and DTT at 21.6 mins.

The mass spectrum of the peak observed at 22.1 minutes showed an additional diastereomeric, two to one Michael addition adduct (**55a** and **55b**) of DEM30355/A with DTT (*m/z* = 981.3113 [(2xDEM30355/A)+DTT+Na]$^+$). This peak also co-eluted with a trace of unreacted DEM30355/A (**28**) (*m/z* = 425.1445 [DEM30355/A+Na]$^+$, 827.2908 [(2xDEM30355/A)+Na]$^+$, 1229.4325 [(3xDEM30355/A)+Na]$^+$). Furthermore a non-covalently bound dimer of the 2:1 Michael addition adduct (**55**) of DEM30355/A with DTT could also be observed (*m/z* = 1383.4464 [(2xDEM30355/A)+DEM30355/A+DTT+Na]$^+$) (Figure **4.20**).

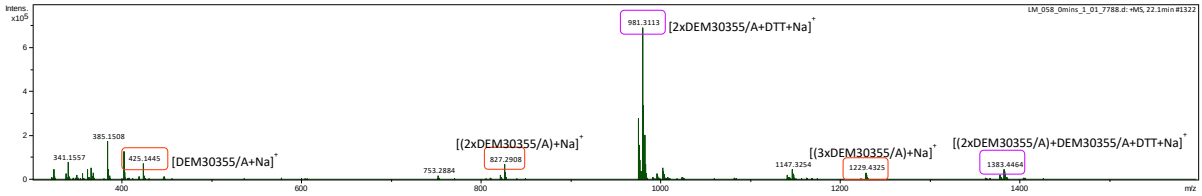

Figure 4.20: Mass spectrum of the Michael addition of DEM30355/A (**28**) and DTT at 22.1 mins.

The LCMS chromatograms of the reaction mixture after 15, 30, 45 and 60 minutes showed no significant changes compared to the 0 minutes time point. This suggests that the Michael addition of DEM30355/A (**28**) with LcrV (271-291) (**45**) (and DTT) occurred very quickly, prior to the sample analysis of our first time point.

In conclusion, we have successfully shown that DEM30355/A (**28**), which contains an α,β-unsaturated ketone and thus has a similar structure to (-)-rishirilide A (**29**), can act also as a Michael acceptor and undergoes Michael addition with thiol containing molecules, L-cysteine (**41**), L-cysteine methyl ester (**43**), LcrV (271-291) (**45**) and DTT.

4.4 Conclusion

The aim of this chapter was to examine whether (-)-rishirilide A (**29**) can act as a Michael acceptor in reactions with biologically relevant thiol containing molecules, as covalent binding of (-)-rishirilide A (**29**) to a thiol containing protein could result in irreversible inhibition.

We have successfully demonstrated that both (-)-rishirilide A (**29**) and the related natural product DEM30355A (**28**) can undergo rapid Michael additions with L-cysteine (**41**), L-cysteine methyl ester (**43**), a short peptide containing cysteine, LcrV (272-291) (**45**) and DTT. Interestingly the non-bioactive natural product (+)-rishirilide B (**30**), which does not contain an α,β-unsaturated ketone, does not act as a Michael acceptor under these conditions. This supports our postulate that the bioactivity of both (-)-rishirilide A (**29**) and DEM30355A (**28**) results from their Michael addition chemistry.

Encouraged by these results, we next decided to examine the synthesis of a number of chemical probes, based on (-)-rishirilide A (**29**), which could be used to aid in the identification of a possible target enzyme of (-)-rishirilide A (**29**).

Chapter 5. Chemical Probes for the Mode of Action Investigation of (-)-Rishirilide A

In the previous chapters, we have shown that the antibiotic mode of action (-)-rishirilide A (**29**) may be due to the depolarisation of the cell membrane in Gram-positive bacteria (*B. subtilis* 168CA). However, it is still unknown how treatment with (-)-rishirilide A (**29**) leads to membrane depolarisation. We have also shown that (-)-rishirilide A (**29**) is capable of acting as a Michael acceptor with thiol containing peptides, and thus could be an irreversible enzyme inhibitor. It is thus possible that (-)-rishirilide A (**29**) may inhibit key enzymes, through irreversible binding, which are responsible for the maintenance of the membrane potential, or that (-)-rishirilide A (**29**) may inhibit other vital enzymatic pathways leading to a subsequent loss of membrane potential. Therefore, in this chapter we will examine the synthesis of chemical probes which could be used to identify target enzymes of the natural product antibiotic (-)-rishirilide A (**29**).

To aid in target identification, we wished to make a series of chemical probes based on the (-)-rishirilide A (**29**) structure (e.g. containing a propargyl group). These probes would then be mixed with a cell free enzyme extract from a Gram-positive bacterium. Following irreversible binding (e.g. Michael addition) of the probe to a target enzyme we would use a biorthogonal reaction (e.g. click chemistry) to add a functional label (e.g. biotin) which could be used to isolate the target, allowing subsequent target identification by trypsin digest and MS^n analysis (Figure **5.1**).[70]

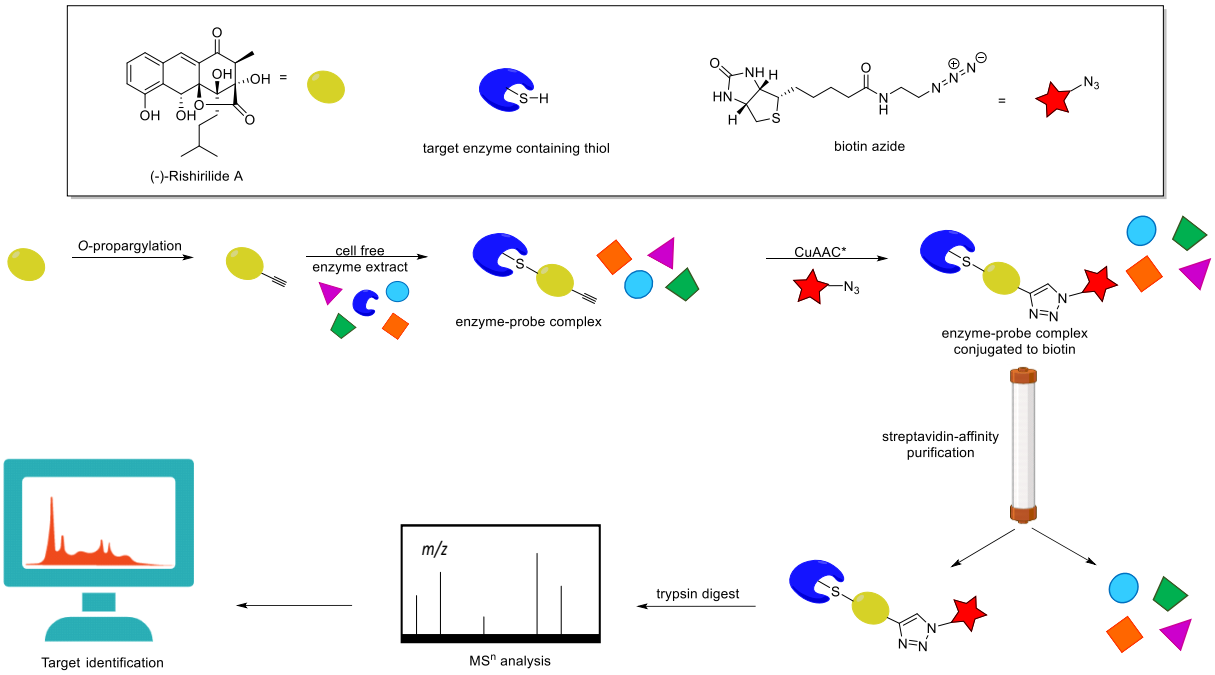

Figure 5.1: Proposed approach for target identification of (-)-rishirilide A (**29**). CuAAC*: Copper-catalysed Azide Alkyne Cycloaddition.

Therefore, our first aim for this chapter was to develop chemistry for the semi-synthetic modification of (-)-rishirilide A (**29**), in order to construct our desired chemical probes.

5.1 Phenolic *O*-alkylations of methyl 3-hydroxybenzoate

Due to the limited amount of (-)-rishirilide A (**29**) available, we decided to use a model compound to test the *O*-alkylation of (-)-rishirilide A (**29**) needed to incorporate the required alkyne functional group. Therefore, we selected 3-hydroxybenzoic acid (**56**) as our model compound since it contains a phenolic group similar to that of (-)-rishirilide A (**29**) (Figure **5.2**).

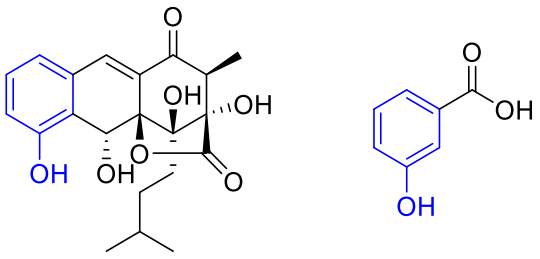

29 **56**

Figure 5.2: (-)-Rishirilide A (**29**) and 3-hydroxybenzoic acid (**56**), phenolic group highlighted in blue.

5.1.1 Synthesis of methyl 3-hydroxybenzoate

To protect the carboxylic group in 3-hydroxybenzoic acid (**56**), our first step was to undertake an acid catalysed Fischer esterification of 3-hydroxybenzoic acid (**56**).[71]

Firstly, we undertook a test reaction in which we reacted 3-hydroxybenzoic acid (**56**) with methanol in the presence of an acid catalyst (*p*-TSA) on a 36.4 mmol scale. Following silica gel column chromatography, the desired methyl 3-hydroxybenzoate (**57**) was isolated in 88% yield (Scheme **5.1**).

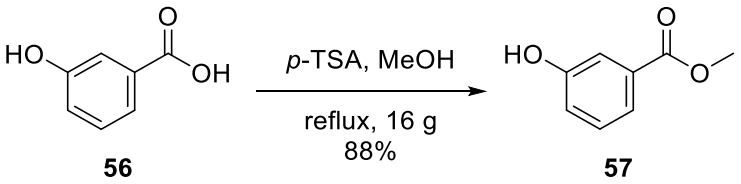

Scheme 5.1: Fischer esterification of 3-hydroxybenzoic acid (**56**).

The structure of methyl 3-hydroxybenzoate (**57**) was confirmed by analysis of the ^{1}H NMR spectra, which showed a new three proton singlet at 3.92 ppm corresponding to the formed methyl ester. In addition, single crystals of methyl 3-hydroxybenzoate (**57**) were grown from slow evaporation of an ethyl acetate solution and analysed by X-ray diffraction providing further structural confirmation (Figure **5.3**).

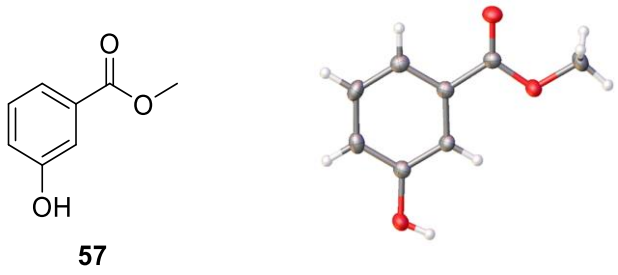

Figure 5.3: X-ray crystal structure of methyl 3-hydroxybenzoate (**57**).

In order to provide sufficient material for the next steps, we repeated the esterification of 3-hydroxybenzoic acid (**56**) on a 72 mmol scale. This scale up was successful resulting in 80% yield, corresponding to 8.8 g of material. Thus, with access to large quantities of methyl 3-hydroxybenzoate (**57**) we could proceed to examine the *O*-alkylation chemistry of the phenolic hydroxyl group.

5.2 *O*-Methylation of methyl 3-hydroxybenzoate

5.2.1 *O*-Methylation of methyl 3-hydroxybenzoate with $TMSCHN_2$

Diazomethane like reagents are known to be selective for acidic hydroxyl groups, and thus react preferentially with carboxylic acids and phenols to give methyl esters and methyl ethers respectively. Therefore, we wished to examine a diazomethane like reagent to allow selective alkylation of the phenolic group of methyl 3-hydroxybenzoate (**57**). However, diazomethane itself is known to be both explosive and highly toxic making its use difficult. Therefore, to examine the selective *O*-methylation of methyl 3-hydroxybenzoate (**57**), we decided to use $TMSCHN_2$ as it is known to be safer alternative to diazomethane.[72]

Thus, following a modified work of Barnes *et al.*, we initially reacted methyl 3-hydroxybenzoate (**57**) with 8 equivalents of $TMSCHN_2$ in MeOH-DCM (1:1) in a Schlenk flask at room temperature.[73] After 24 h, the reaction mixture was quenched with a solution of acetic acid-methanol (1:2) to remove any remaining $TMSCHN_2$. Following aqueous work-up, the reaction mixture was analysed by ^1H NMR. The desired methyl 3-methoxybenzoate (**58**) could be observed via the presence of a distinctive three proton singlet at 3.92 ppm corresponding the methyl ester. The percentage conversion of methyl 3-hydroxybenzoate (**57**) into methyl 3-methoxybenzoate (**58**) was obtained by comparing the ratio of the integrations of the two molecules in the ^1H NMR spectra (methyl 3-hydroxybenzoate (**57**) : methyl 3-methoxybenzoate (**58**) = 2.9:1.0) giving a conversion of 26% (Table **5.1**, Entry 1).

Thus, we have successful synthesised methyl 3-hydroxybenzoate (**57**), however the percentage conversion was low. Therefore, in order to improve the percentage conversion, we decided to examine repeating the *O*-methylation of methyl 3-hydroxybenzoate (**57**) with $TMSCHN_2$ but with extended reaction times.

Thus, we reacted methyl 3-hydroxybenzoate (**57**) with 8 equivalents of $TMSCHN_2$ as previously. After 2 days the reaction was quenched and worked up as before, unfortunately a similar percentage conversion (27%) to methyl 3-methoxybenzoate (**58**) was obtained (Table **5.1**, Entry 2). Based on this result, we postulated that the *O*-methylation might be improved through the addition of a weak base to increase the reactivity of the phenolic group, allowing us to also reduce the equivalencies of $TMSCHN_2$ employed.

Thus, following a modified method by Aoyama *et al.*, we reacted 0.033 mmol of methyl 3-hydroxybenzoate (**57**) with 1.5 equivalents of $TMSCHN_2$ in MeOH-MeCN (1:9) in the presence of 1 equivalent of DIPEA.[74] After 2 days, the reaction was quenched to remove excess $TMSCHN_2$ and following work-up, an improved conversion of 40% was obtained (Table **5.1**, Entry 3). In an attempt to further increase the yield of the *O*-methylation we decided to increase both the equivalents of $TMSCHN_2$ (3 eq.) and the reaction time, resulting in a much improved conversion (75-81%) (Table **5.1**, Entries 4-5).

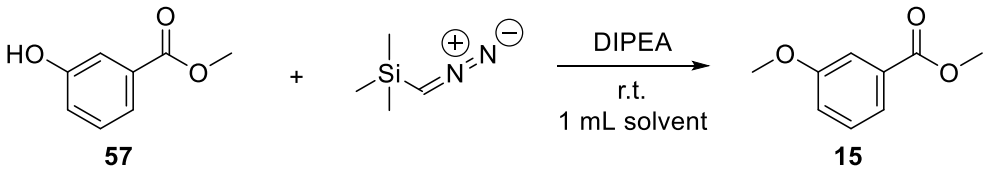

Entry	Moles of **57** (mmol)	eq. of $TMSCHN_2$	eq. of DIPEA	Solvent	Time	Conversion (%)[a]
1	0.025	8	0	MeOH-DCM (1:1)	1 d	26
2	0.025	8	0	MeOH-DCM (1:1)	2 d	27
3	0.033	1.5	1.0	MeOH-MeCN (1:9)	2 d	40
4	0.066	3.0	2.0	MeOH-MeCN (1:9)	3 d	75
5	0.066	3.0	2.0	MeOH-MeCN (1:9)	3 d	81

Table 5.1: *O*-Methylation of methyl 3-hydroxybenzoate (**57**) with $TMSCHN_2$. [a] % conversion was measured by ^1H NMR spectroscopy.

Although the *O*-methylation of methyl 3-hydroxybenzoate (**57**) with $TMSCHN_2$ gave us excellent conversions, $TMSCHN_2$ is known to be toxic and thus requires additional containment for safe handling. Thus, we wished to examine alternative approaches to this reaction using easier to handle reagents.

5.2.2 *O*-Methylation of methyl 3-hydroxybenzoate with MeI

Thus, to avoid the use of $TMSCHN_2$ we decided to look at the use of methyl iodide as an alternative *O*-methylating reagent for methyl 3-hydroxybenzoate (**57**).

Following a modified method of Boggu *et al.*, we first reacted methyl 3-hydroxybenzoate (**57**) (0.1 mmol) with 1 equivalent of methyl iodide in the presence of 1 equivalent of potassium carbonate in dry DMF at 60 ˚C in a Schlenk flask.[75] After 17 hours, the reaction was quenched with diethylamine to remove any remaining methyl iodide. After aqueous workup, the reaction mixture was analysed by ^{1}H-NMR spectrum giving a 14% conversion to methyl 3-methoxybenzoate (**58**) (Table **5.2**, Entry 1).

Based on this initial success, we next planned to improve the percentage conversion for the *O*-methylation reaction with methyl iodide. Thus, we repeated the *O*-methylation of methyl 3-hydroxybenzoate (**57**) with 3 equivalents of methyl iodide and an extended reaction time (24 h), resulting in a much-improved conversion of 61% (Table **5.2**, Entry 2).

Despite this improvement in conversion we were concerned that, despite the use of a sealed Schlenk flask, the high reaction temperature employed may have resulted in the loss of methyl iodide during the reaction (b.p. of MeI = 42 ˚C) preventing complete conversion. Therefore, we repeated the *O*-methylation of methyl 3-hydroxybenzoate (**57**) with 3 equivalents of methyl iodide but starting with an initial reaction temperature of 0 ˚C for 1 h, followed by heating to 50 ˚C. After 22 h the reaction mixture was quenched (Et_2NH) and worked up, resulting in a 44% conversion to methyl 3-methoxybenzoate (**58**) (Table **5.2**, Entry 3). Thus, we repeated the *O*-methylation of methyl 3-hydroxybenzoate (**57**) with methyl iodide again, under the same reaction conditions, but with an initial reaction temperature of 0 ˚C for 1 h, followed 22 h at room temperature (now below the b.p. of MeI).[76] Following standard workup this gave a much improved conversion to methyl 3-methoxybenzoate (**58**) of 77%, suggesting that even with the use of a sealed Schlenk flask some methyl iodide was lost from the reaction at high temperatures (Table **5.2**, Entry 4).

In an attempt to further improve the yield, next we examined an increase in the number of equivalents of methyl iodide and base. Thus, we reacted methyl 3-hydroxybenzoate (**57**) with 5 equivalents of methyl iodide with 2 equivalents of potassium carbonate under our previous conditions, resulting in a 83% conversion to methyl 3-methoxybenzoate (**58**) (Table **5.2**, Entry 5).

Finally, we wished to perform the *O*-methylation of methyl 3-hydroxybenzoate (**57**) on a much larger scale to allow for isolation of the product and to allow us to fully characterise the

product. Therefore, we scaled up the *O*-methylation methyl 3-hydroxybenzoate (**57**), from 0.1 mmol of methyl 3-hydroxybenzoate (**57**) to 0.66 mmol, with 5 equivalents of methyl iodide under our previously optimised reaction conditions. This large-scale reaction gave a 78% isolated yield, corresponding to 85 mg of methyl 3-methoxybenzoate (**58**), sufficient for characterisation (Table **5.2**, Entry 6).

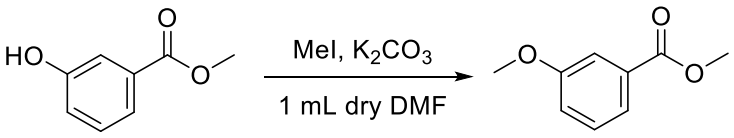

57 **58**

Entry	Moles of (**57**) mmol	eq. of CH_3I	eq. of K_2CO_3	Reaction condition	Conversion by ^1H NMR (%)
1	0.1	1.0	1.0	60 ˚C, 17 h	14
2	0.1	3.0	1.0	60 ˚C, 24 h	61
3	0.1	3.0	1.0	0 °C, 1 h then 50 °C, 22 h	44
4	0.1	3.0	1.0	0 °C, 1 h then r.t., 22 h	77
5	0.1	5.0	2.0	0 °C, 1 h then r.t., 22 h	83
6	0.66	5.0	2.0	0 °C, 1 h then r.t., 22 h	78[a]

Table 5.2: *O*-Methylation of methyl 3-hydroxybenzoate (**57**) with methyl iodide. [a]: isolated yield (%) following silica gel chromatography.

Following analysis of the NMR spectra, a new three proton singlet at 3.85 ppm was observed in the ^1H NMR and a new peak at 52.3 ppm was observed in the ^{13}C NMR corresponding to the new methyl ether. Furthermore, HMBC analysis showed a correlation between the C-3 atom and protons of the methyl ether, confirming that the new methyl ether was at the C-3 position (Figure **5.4**).

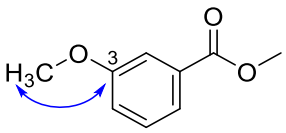

Figure 5.4: Key HMBC correlation in methyl 3-methoxybenzoate (**58**) (blue arrow).

After successfully conducting the *O*-alkylation of methyl 3-hydroxybenzoate (**57**) with methyl iodide, we planned to carry out further *O*-alkylations of methyl 3-hydroxybenzoate (**57**) with a range of different *O*-alkylating reagents. The selection of *O*-alkylating reagents was based on their ability to selectively react with the phenolic hydroxyl group in our compound of interest, (-)-rishirilide A (**29**), whilst also providing a future route to bio-orthogonal tagging of (-)-rishirilide A (**29**) itself. We envisaged that through the bio-orthogonal tagging of (-)-rishirilide A (**29**), we would be able to further probe the antibiotic mode of action of this molecule. Therefore, we decided to examine the benzylation, allylation and propargylation of our model compound methyl 3-hydroxybenzoate (**57**).

5.3 *O*-Benzylation of methyl 3-hydroxybenzoate with benzyl bromide.

Thus, the first reaction we chose to explore was the *O*-benzylation of methyl 3-hydroxybenzoate (**57**), for which we decided to use benzyl bromide under basic conditions. Following a modified method of Selva *et al.*, we reacted 0.1 mmol of methyl 3-hydroxybenzoate (**57**) with 1 equivalent of benzyl bromide in the presence of 1 equivalent of potassium carbonate in dry DMF at 60 °C.[77] After 4 h, TLC showed the loss of starting material and the formation of a new more lipophilic product. Following an aqueous workup a 67% conversion to methyl 3-(benzyloxy)benzoate (**59**) was observed by ^{1}H NMR, based on the integration of the benzylic protons (Table **5.3**, Entry 1). Next, we attempted to increase the percentage conversion for the *O*-benzylation of methyl 3-hydroxybenzoate (**57**) through increasing the equivalents of benzyl bromide. Thus reaction of methyl 3-hydroxybenzoate (**57**) with 3 eq. benzyl bromide under the previous conditions resulted, following an aqueous workup, in an excellent conversion to methyl 3-(benzyloxy)benzoate (**59**) of 99% (Table **5.3**, Entry 2).

As we wished to apply this *O*-benzylation to (-)-rishirilide A (**29**) in the future we wished to reduce the reaction temperature due to the more sensitive nature of the natural product. Therefore we repeated the *O*-benzylation of methyl 3-hydroxybenzoate (**57**) with 3 eq. benzyl bromide at room temperature, resulting in a 100% conversion by ^{1}H NMR to methyl 3-(benzyloxy)benzoate (**59**) after only 4 hours (Table **5.3**, Entry 3).

Finally, we repeated our optimised *O*-benzylation of methyl 3-hydroxybenzoate (**57**) on a 0.74 mmol scale to obtain sufficient product for full characterization. Following aqueous workup

and silica gel column chromatography, methyl 3-(benzyloxy)benzoate (**59**) was isolated in a 84% yield (Table **5.3**, Entry 4).

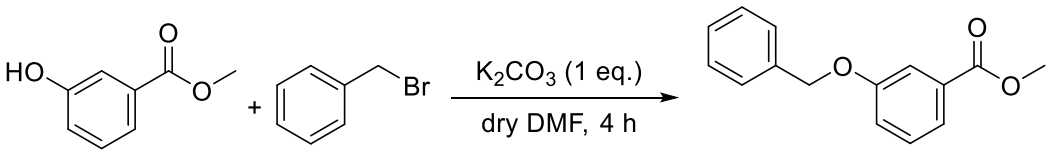

57 **59**

Entry	Mol of (**57**) (mmol)	Eq. of benzyl bromide	Temperature (˚C)	Conversion by ^{1}H NMR (%)
1	0.1	1.0	60	67
2	0.1	3.0	60	99
3	0.1	3.0	rt	100
4	0.74	3.0	rt	84[a]

Table 5.3: *O*-Benzylation of methyl 3-hydroxybenzoate (**57**) with benzyl bromide. [a]: isolated yield (%) from silica gel chromatography.

The structure of methyl 3-(benzyloxy)benzoate (**59**) was confirmed by ^{1}H NMR. The ^{1}H NMR spectra showing a new distinctive 2 proton singlet (5.11 ppm) and a 5 proton multiplet (7.31 – 7.48 ppm), corresponding to the benzylic and aromatic protons of the formed benzyl ether respectively. Furthermore, HMBC analysis showed correlation between benzylic protons and the carbons at C-2 and C-4 confirming the benzyl ether attachment at C-3 (Figure **5.5**).

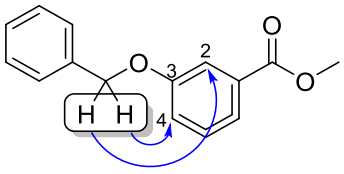

Figure 5.5: Key HMBC correlations in methyl 3-(benzyloxy)benzoate (**59**) (blue arrows).

To further support the structural assignment of methyl 3-(benzyloxy)benzoate (**59**) we then attempted to grow crystals of methyl 3-(benzyloxy)benzoate (**59**) for X-ray diffraction analysis. After one week, suitable single crystals of methyl 3-(benzyloxy)benzoate (**59**) were

formed from an slowly evaporating chloroform solution. Analysis of the crystal by X-ray diffraction, confirmed the structure of methyl 3-(benzyloxy)benzoate (**59**) (Figure **5.6**).

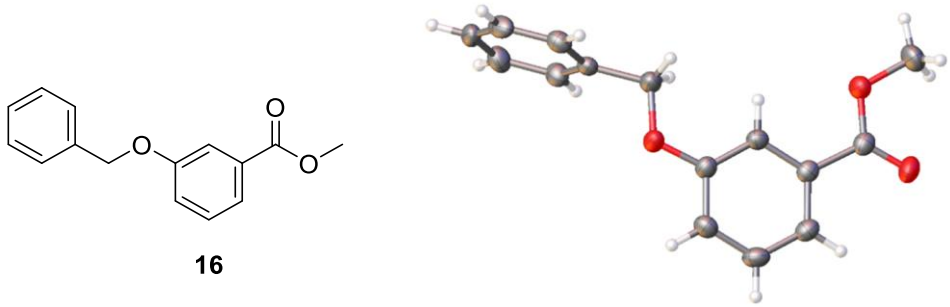

16

Figure 5.6: X-ray crystal structure of methyl 3-(benzyloxy)benzoate (**59**).

In conclusion, we have successfully developed a high yielding synthetic method for the *O*-benzylation of methyl 3-hydroxybenzoate (**57**) with benzyl bromide under mild conditions that we hope would be suitable for the possible future *O*-benzylation of (-)-rishirilide A (**29**).

5.4 *O*-Allylation of methyl 3-hydroxybenzoate with allyl bromide.

Following our successful *O*-benzylation of methyl 3-hydroxybenzoate (**57**) with benzyl bromide, next we planned to develop an *O*-allylation reaction of methyl 3-hydroxybenzoate (**57**) under mild reaction conditions.

Following a modified work of Harnoy *et al.*, we reacted 0.1 mmol of methyl 3-hydroxybenzoate (**57**) with 2 equivalents of allyl bromide in the presence of 3 equivalents of potassium carbonate in dry DMF, at 0 °C for 30 minutes followed by 60 °C for 4 h.[76] After aqueous workup, the reaction mixture was then analysed by ^{1}H NMR. Based on the integration of ^{1}H NMR signals corresponding to the protons of newly formed allylic methylene (4.58 ppm, dt, *J* = 5.3, 1.4 Hz, 2H), we could observe a 97% conversion to the desired methyl 3-(allyloxy)benzoate (**60**) (Table **5.4**, Entry 1).

Due to the high reaction temperatures in the previous alkylation reaction, we decided to re-examine the *O*-allylation conditions in an attempt to reduce the overall reaction temperature. Therefore, we repeated the *O*-allylation of methyl 3-hydroxybenzoate (**57**) with allyl bromide at room temperature. After aqueous workup, this room temperature *O*-allylation resulted in a similar percentage conversion (97%) to methyl 3-(allyloxy)benzoate (**60**) (Table **5.4**, Entry

2). With a mild and high yielding set of *O*-allylation conditions, we then aimed to scale-up this reaction to obtain sufficient isolated methyl 3-(allyloxy)benzoate (**60**) for complete characterization.

Therefore, we then repeated our optimised room temperature *O*-allylation of methyl 3-hydroxybenzoate (**57**) on a 0.67 mmol. Following aqueous workup and purification with silica gel column chromatography, methyl 3-(allyloxy)benzoate (**60**) (0.111 g, 0.576 mmol, 86%) was isolated as a colourless oil (Table **5.4**, Entry 3).

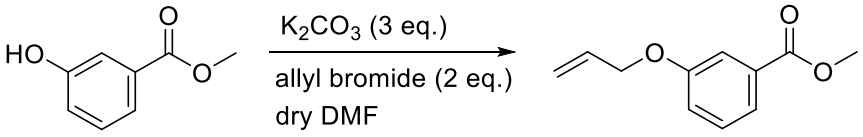

57 **60**

Entry	Mol of (**57**) (mmol)	Reaction condition	Conversion by ^{1}H NMR (%)
1	0.1	0 °C, 30 minutes then 60 °C, 4 h	97
2	0.1	0 °C, 30 minutes then r.t., 4h	97
3	0.67	0 °C, 30 minutes then r.t., 4 h	86[a]

Table 5.4: *O*-Allylation of methyl 3-hydroxybenzoate (**57**) with allyl bromide. [a]: isolated yield from silica gel column chromatography.

With gram quantities of methyl 3-(allyloxy)benzoate (**60**) available we were able to complete full structural characterization. The ^{1}H NMR spectra showed three new signals for the *O*-allyl ether at 4.58 ppm (dt, *J* = 5.3, 1.5 Hz, 2H) corresponding to the two allylic protons (H-9), 6.06 ppm (DTT, *J* = 17.2, 10.5, 5.3 Hz, 1H) corresponding to the alkene proton at H-10, and 5.30 ppm (dq, *J* = 10.5, 1,4 Hz, 1H) and 5.43 ppm (dq, *J* = 17.2, 1.6 Hz, 1H) corresponding the terminal alkene protons at H-11a and H-11b. The H-10 proton shows two large couplings to the terminal alkene protons H-11a and H-11b, a *cis*-coupling of 10.5 Hz to H-11a and a *trans*-coupling of 17.2 Hz to H-11b. The two terminal alkene protons H-11a and H-11b also show a small geminal ($^2J_{H\text{-}H}$) coupling with an average value of 1.5 Hz. Furthermore, HMBC analysis showed a correlation of the allylic protons at H-9 to carbon atom at C-3 confirming the attachment of the new allyl ether was at C-3 position (Figure **5.7**).

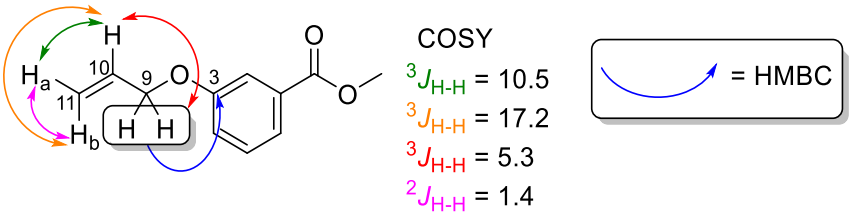

Atom	δ_H (ppm)
9	4.58
10	6.06
11a	5.30
11b	5.43

Figure 5.7: COSY and HMBC analysis of methyl 3-(allyloxy)benzoate (**60**), including coupling constants and assignments.

To conclude, we have successfully carried out the *O*-allylation of methyl 3-hydroxybenzoate (**57**) with allyl bromide under mild reaction conditions. Next, we planned to utilize a terminal alkyne as our next *O*-alkylating reagent. We chose a terminal alkyne *O*-alkylating reagent because terminal alkyne commonly used to provide suitable bio-orthogonal tagging. Thus, we expected the *O*-alkylation with terminal alkyne could be applied to (-)-rishirilide A (**29**).

5.5 *O*-Propargylation of methyl 3-hydroxybenzoate

Next, we decided to react our model compound, methyl 3-hydroxybenzoate (**57**), with propargyl bromide as the *O*-alkylating reagent, in order to introduce a terminal alkyne.

Following a modified method of Harnoy *et al.*, we initially reacted 0.1 mmol of methyl 3-hydroxybenzoate (**57**) with 3 equivalents of propargyl bromide in the presence of 3 equivalents of potassium carbonate in 1 mL of dry DMF at room temperature for 3 h.[71] Following aqueous workup, the reaction mixture was then analysed by ^{1}H NMR. The formation of methyl 3-(prop-2-yn-1-yloxy)benzoate (**61**) was confirmed by the observation of a new proton signal at 4.74 ppm corresponding to the propargyl methylene (d, *J* = 2.4 Hz, 2H). Comparison of the relative integrations for remaining methyl 3-hydroxybenzoate (**57**) and the newly formed methyl 3-(prop-2-yn-1-yloxy)benzoate (**61**) showed a conversion of 47% (Table **5.5**, Entry 1).

To improve the percentage yield of methyl 3-(prop-2-yn-1-yloxy)benzoate (**61**) we examined the *O*-propargylation reaction at higher concentration. Thus, we reacted twice the quantity (0.2 mmol) of methyl 3-hydroxybenzoate (**57**) with 0.6 mmol of propargyl bromide and 0.6 mmol of potassium carbonate for 3 hours, but in only 1 mL of DMF. This resulted in a

considerably faster reaction and thus a 95% conversion (by ^{1}H NMR) to the product methyl 3-(prop-2-yn-1-yloxy)benzoate (**61**) (Table **5.5**, Entry 2).

Finally, we scaled-up the *O*-propargylation of methyl 3-hydroxy benzoate (**57**), under the previous conditions, to obtain sufficient methyl 3-(prop-2-yn-1-yloxy)benzoate (**61**) for full structural characterisation and to allow subsequent testing of our planned click chemistry. Thus, we reacted methyl 3-hydroxybenzoate (**57**) on a 6.6 mmol scale under the previous high concentration reaction conditions. Following silica gel chromatography, our desired methyl 3-(prop-2-yn-1yloxy)benzoate (**61**) was isolated in 88% yield (Table **5.5**, Entry 3).

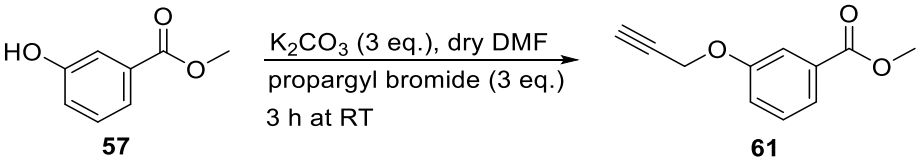

57 **61**

Entry	Mol of (**57**) (mmol)	Conversion by ^{1}H NMR (%)
1	0.1	47
2	0.2	95
3	6.6	88[a]

Table 5.5: *O*-Propargylation of methyl 3-hydroxybenzoate (**57**). [a] isolated yield from silica gel column chromatography.

To validate the structure of our propargyl ether (**61**), ^{1}H NMR analysis was carried out. The ^{1}H-NMR spectra showed a distinctive new proton triplet at 2.54 ppm, corresponding to a new terminal alkyne ether. Furthermore, an HMBC analysis showed a correlation of propargylic protons at H-9 to a carbon at C-3, confirming that the new terminal alkyne ether attachment was at atom C-3 position (Figure **5.8**).

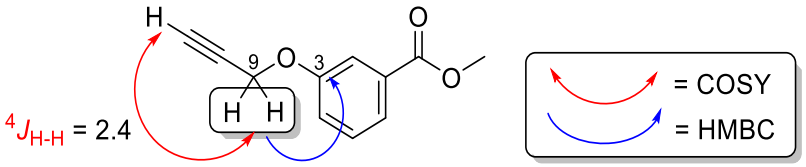

Figure 5.8: COSY and HMBC analysis of methyl 3-(prop-2-yn-1-yloxy)benzoate (**61**).

In addition, the analysis of infrared (IR) spectra of our *O*-propargylation product (**61**) showing a strong narrow band (at 3265 cm^{-1}) and a weak band (at 2125 cm^{-1}), confirmed the appearance of ≡C-H and -C≡C- stretching respectively.

For additional support of the structure of methyl 3-(prop-2-yn-1-yloxy)benzoate (**61**), we then planned to grow crystals of methyl 3-(prop-2-yn-1-yloxy)benzoate (**61**) in chloroform. Following a slowly evaporation of chloroform solution, single crystals of methyl 3-(prop-2-yn-1-yloxy)benzoate (**61**) were formed and then were analysed by X-ray diffraction. Analysis by X-ray diffraction confirmed that methyl 3-(prop-2-yn-1-yloxy)benzoate (**61**) had a monoclinic crystal system with $P2_1/c$ space group and Z = 4 (Figure **5.9**).

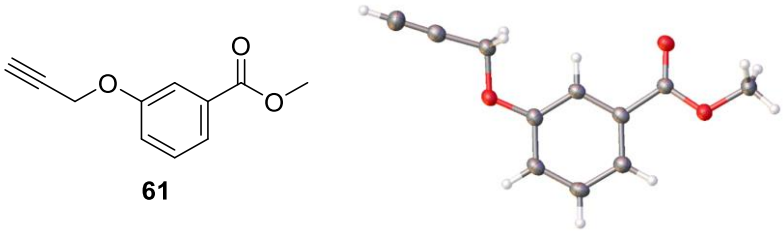

Figure 5.9: X-ray crystal structure of methyl 3-(prop-2-yn-1-yloxy)benzoate (**61**).

In conclusion, we have successfully reacted methyl 3-hydroxybenzoate (**57**) with propargyl bromide, making methyl 3-(prop-2-yn-1-yloxy)benzoate (**61**). Therefore, in the next step, we attempted to react methyl 3-(prop-2-yn-1-yloxy)benzoate (**61**) with an azide via CuAAc reaction

5.6 CuAAC of methyl 3-(prop-2-yn-1-yloxy)benzoate with an azide

With sufficient amount methyl 3-(prop-2-yn-1-yloxy)benzoate (**61**) in hand, next we decided to react the methyl 3-(prop-2-yn-1-yloxy)benzoate (**61**) with an available benzyl azide to represent a cleavable biotin probe (Scheme **5.2**).

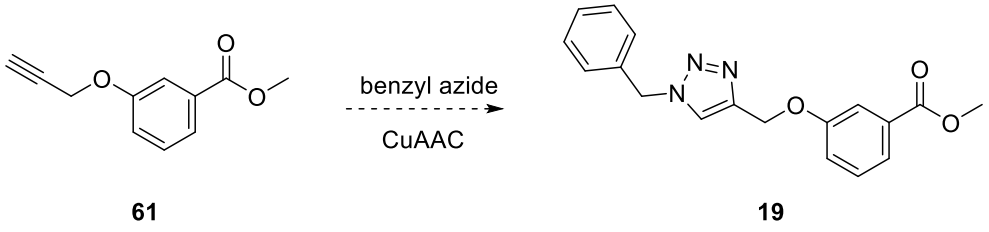

Scheme 5.2: CuAAC reaction of methyl 3-(prop-2-yn-1-yloxy)benzoate (**61**) with benzyl azide.

We initially reacted 0.45 mmol methyl 3-(prop-2-yn-1-yloxy)benzoate (**61**) with benzyl azide (1 eq.) in the presence of $CuSO_4.5H_2O$ (10 mol%) as a catalyst and sodium ascorbate (20 mol%) as *in situ* reductor in DMF:H_2O (1:1) at room temperature for 5 d.[79] Following aqueous workup, we then analysed the reaction mixture by ^{1}H NMR. Based on the integration of proton signal of the new proton of triazole ring, we observed only 1.7% conversion to the desired methyl 3-((1-benzyl-1*H*-1,2,3-triazol-4-yl)methoxy)benzoate (**62**) (Table **5.6**, Entry 1).

Due to the low percentage of conversion to methyl 3-((1-benzyl-1*H*-1,2,3-triazol-4-yl)methoxy)benzoate (**62**), we wished to improve our previous reaction by changing the reaction solvent. We then selected *t*-butanol and H_2O (1:1) as reaction solvent, which resulted in an unsatisfactory conversion of 5.7% (Table **5.6**, Entry 2). We then decided to use a halogenated solvent and increased the reaction temperature, which might improve the percentage conversion of methyl 3-(prop-2-yn-1-yloxy)benzoate (**61**) to CuAAC product (**19**).

Thus we decided to use a mixture of DCM:H_2O (1:1) as reaction solvent and repeated the CuAAC reaction of methyl 3-(prop-2-yn-1-yloxy)benzoate (**61**) at 50 °C. Based on the analysis of ^{1}H NMR spectrum, this attempt resulted in a 35% conversion to methyl 3-((1-benzyl-1*H*-1,2,3-triazol-4-yl)methoxy)benzoate (**62**) (Table **5.6**, Entry 3).

We have improved the CuAAC reaction for methyl 3-(prop-2-yn-1-yloxy)benzoate (**61**) from 5.7% to 35% conversion. However, we still wished to reduce the reaction time and use room temperature reaction so we could apply this reaction condition to further experiment using our natural product, (-)-rishirilide A (**29**).

Thus, we initially used 0.3 mmol methyl 3-(prop-2-yn-1-yloxy)benzoate (**61**) with benzyl azide (2 eq.) in 1,4-dioxane at room temperature.[80] The equivalent of $CuSO_4.5H_2O$ and sodium ascorbate were increased to two and four equivalents, respectively. Subsequently, we added one equivalent of triethylamine which used as ligands for copper(I) ions. After 2 days, a new spot on TLC plate observed and the reaction mixture was stopped. Following aqueous workup and ^{1}H NMR analysis, this reaction resulted in 24% conversion to methyl 3-((1-benzyl-1*H*-1,2,3-triazol-4-yl)methoxy)benzoate (**62**) (Table **5.6**, Entry 4). We were satisfied enough with this reaction result, yet we wished to improve the percentage conversion of this CuAAC reaction.

Therefore, we repeated previous CuAAC reaction of methyl 3-(prop-2-yn-1-yloxy)benzoate (**61**) with benzyl azide. To enhance our target product, we increased the equivalent of $CuSO_4.5H_2O$ (5 eq.), sodium ascorbate (10 eq.) and triethylamine (5 eq.). This attempt resulted in a much higher percentage conversion of 51% to methyl 3-((1-benzyl-1*H*-1,2,3-triazol-4-yl)methoxy)benzoate (**62**) and following silica gel chromatography, 6.8% yield of our desired product (**62**) was isolated (Tabel **5.6**, Entry 5). Until this step, we have pleasantly confirmed that we successfully underwent CuAAC reaction of methyl 3-(prop-2-yn-1-yloxy)benzoate (**61**) with benzyl azide. Nevertheless, we planned to use CuI as the source of copper (I) ion with the presence of $CuSO_4.5H_2O$ in further reaction.

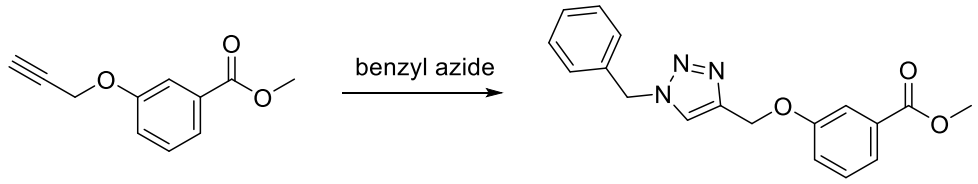

61 **62**

Entry	Mol of (**61**) (mmol)	Eq. of benzyl azide	Eq. of $CuSO_4.5H_2O$	Eq. of Na-asc.	Eq. of Et_3N	Solvents	Temp. (°C)	Time	Conversion by ^1H NMR (%)
1	0.45	1	0.1	0.2	-	DMF : H_2O	r.t.	5 d	1.7
2	0.45	1	0.1	0.2	-	*t*-BuOH:H_2O	r.t.	5 d	5.7
3	0.45	1	0.1	0.2	-	DCM:H_2O	50	5 d	35
4	0.3	2	2	4	1	1,4-dioxane	r.t.	2 d	24
5	0.3	2	5	10	5	1,4-dioxane	r.t.	2 d	6.8[a]

Table 5.6: CuAAC reaction of methyl 3-(prop-2-yn-1-yloxy)benzoate (**61**) with benzyl azide. [a] = isolated yield from silica gel column chromatography.

Encouraged with the conversion to methyl 3-((1-benzyl-1*H*-1,2,3-triazol-4-yl)methoxy) benzoate (**62**) in our previous CuAAC reaction, next we attempted to use copper(I) salt, CuI instead of $CuSO_4.5H_2O$ without sodium ascorbate.

Following similar previous reaction conditions, we repeated methyl 3-(prop-2-yn-1-yloxy)benzoate (**61**) (0.3 mmol) with benzyl azide in the presence of CuI (1 eq.) as a catalyst. Unfortunately, this reaction only resulted in a 19% conversion to our target molecule, methyl

3-((1-benzyl-1*H*-1,2,3-triazol-4-yl)methoxy)benzoate (**62**) (Tabel **5.7**, Entry 1). Having a disappointing result, we decided to increase the amount of sodium ascorbate and triethylamine.

Therefore, we repeated the previous CuAAC reaction of methyl 3-(prop-2-yn-1-yloxy)benzoate (**61**) with benzyl azide. However, in this reaction, we increased the amount of CuI (2 eq.), added sodium ascorbate (4 eq.) and triethylamine (1 eq.). This attempt resulted in an unsatisfactory conversion of 20% to produce methyl 3-((1-benzyl-1*H*-1,2,3-triazol-4-yl)methoxy)benzoate (**20**) (Table **5.7**, Entry 2). Following this, we wished to improve our reaction by increasing the amount of CuI, sodium ascorbate and triethylamine.

Thus, we repeated the CuAAC reaction using the same amount of methyl 3-(prop-2-yn-1-yloxy)benzoate (**61**) and benzyl azide in the previous reaction. Whereas we increased the amount of CuI (5 eq.), sodium ascorbate (10 eq.) and triethylamine (5 eq.). This attempt resulted in a satisfying conversion of 79% of methyl 3-(prop-2-yn-1-yloxy)benzoate (**61**) to methyl 3-((1-benzyl-1*H*-1,2,3-triazol-4-yl)methoxy)benzoate (**62**). Despite this good conversion, the purification of methyl 3-((1-benzyl-1*H*-1,2,3-triazol-4-yl)methoxy)benzoate (**62**) using silica gel column chromatography, monitored with TLC plate, resulted in a 4.8%. (Table **5.7**, Entry 3).

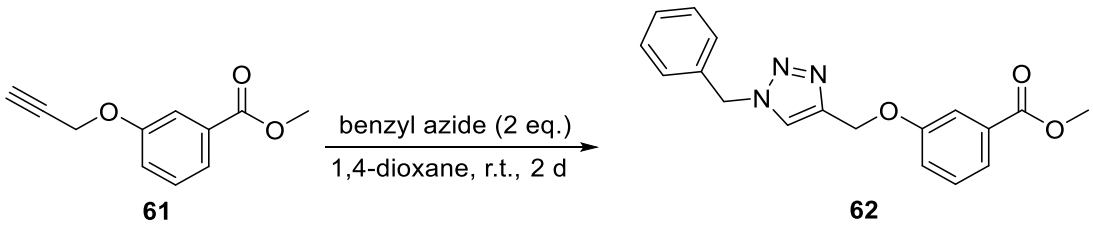

61 **62**

Entry	Eq. of Na-asc.	Eq. of CuI	Eq. of Et_3N	Conversion by ^1H NMR (%)
1	-	1	-	19
2	4	2	1	20
3	10	5	5	4.8[a]

Table 5.7: CuAAC reaction of methyl 3-(prop-2-yn-1-yloxy)benzoate (**61**) with benzyl azide. a: isolated yield from silica gel column chromatography.

To confirm the structure of methyl 3-((1-benzyl-1*H*-1,2,3-triazol-4-yl)methoxy)benzoate (**62**), we used ^{1}H NMR. The ^{1}H NMR spectrum, showed a singlet at 7.54 ppm and two proton singlets at 5.22 and 5.54 ppm, corresponding to a triazole proton and benzylic protons of methyl 3-((1-benzyl-1*H*-1,2,3-triazol-4-yl)methoxy)benzoate (**62**) respectively (Figure **5.10**).

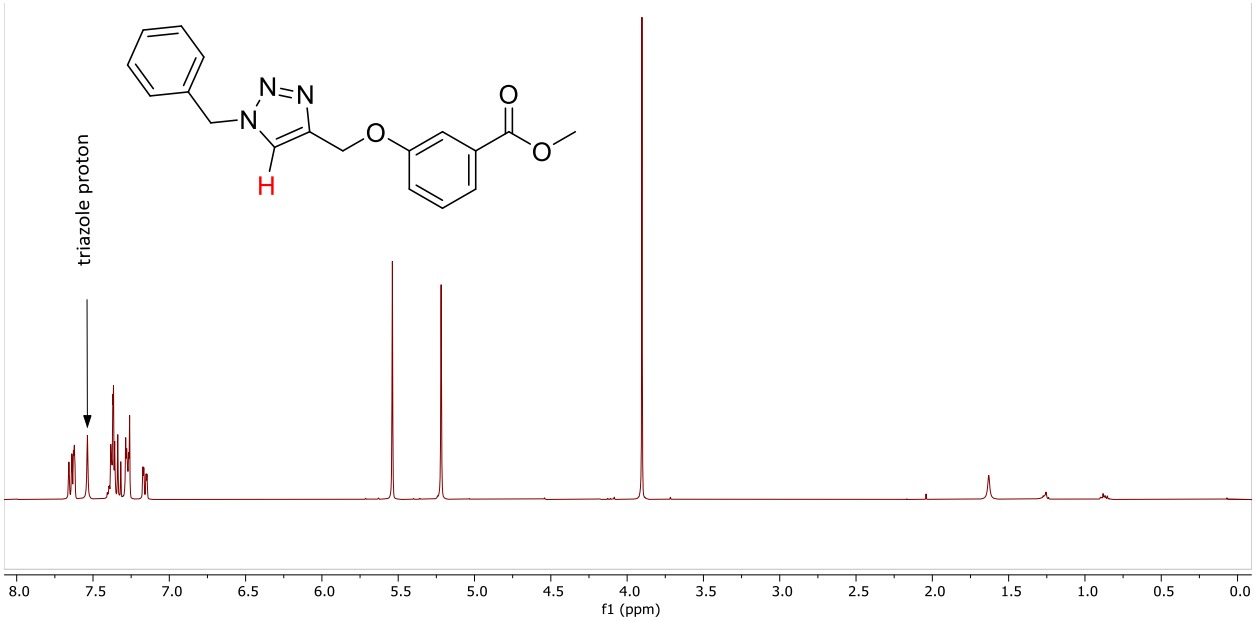

Figure 5.10: ^{1}H NMR spectrum of methyl 3-((1-benzyl-1*H*-1,2,3-triazol-4-yl)methoxy)benzoate (**62**).

Furthermore, to support the confirmation of this CuAAC result, we analysed the isolated methyl 3-((1-benzyl-1*H*-1,2,3-triazol-4-yl)methoxy)benzoate (**62**) with high resolution LCMS. The LCMS chromatogram showed a peak at 21 minutes which displayed key *m/z* signals of 324.1252, 346.1067 corresponding to the $[M+H]^+$ and $[M+Na]^+$ ions of methyl 3-((1-benzyl-1*H*-1,2,3-triazol-4-yl)methoxy)benzoate (**62**) (Figure **5.11**).

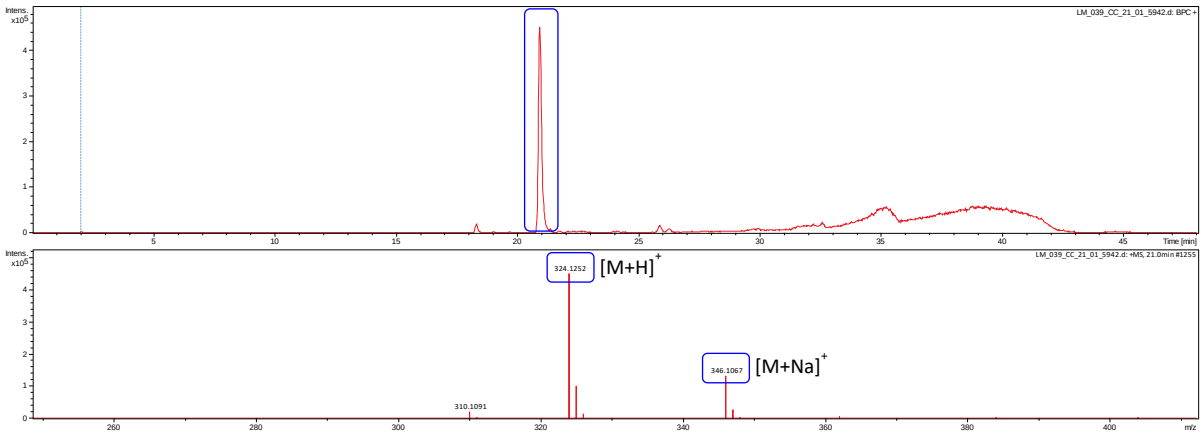

Figure 5.11: LCMS chromatogram of methyl 3-((1-benzyl-1*H*-1,2,3-triazol-4-yl)methoxy)benzoate (**62**) based on BPC.

In conclusion, we have successfully reacted methyl 3-(prop-2-yn-1-yloxy)benzoate (**61**) with benzyl azide, as a representative of cleavable probe, in the presence of $CuSO_4.5H_2O$, sodium ascorbate, triethylamine in 1,4-dioxane and resulted in 6.8% of the desired 1,2,3-triazole ring of CuAAC product, whilst the same CuAAC reaction with the presence of CuI, to replace the $CuSO_4.5H_2O$, resulted in 4.8%.

The CuAAC reaction of the model compound, methyl 3-(prop-2-yn-1-yloxy)benzoate (**61**), with a model azide, benzyl azide resulted in a very low yield. Therefore, we decided to optimize this CuAAC reaction in our future work and next, we will continue our mode of action investigation of (-)-rishirilide A (**29**) by undertaking *O*-alkylation using a propargyl.

5.7 *O*-Propargylation of natural product, (-)-rishirilide A

Encouraged by the positive result of *O*-alkylation of our model compound, methyl 3-(prop-2-un-1-yloxy)benzoate (**61**), herein we attempted to undertake *O*-alkylation of (-)-rishirilide A (**29**) with propargyl bromide (Scheme **5.3**).

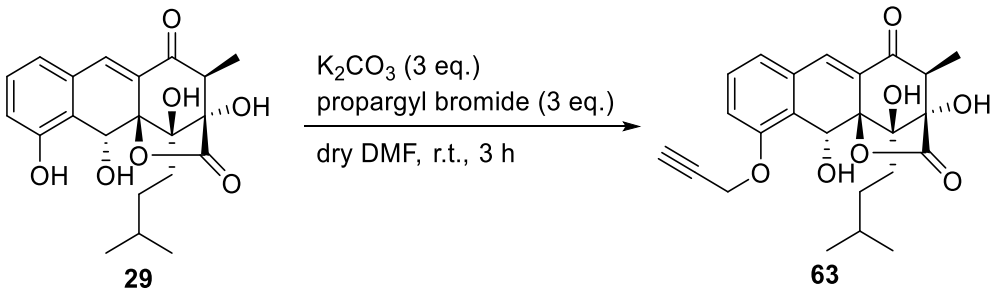

Scheme 5.3: *O*-Propargylation of (-)-rishirilide A (**29**) with propargyl bromide.

Following previous *O*-propargylation method on methyl 3-hydroxybenzoate (**57**) with propargyl bromide, here we reacted (-)-rishirilide A (**29**) (11.6 mM) and propargyl bromide (3 eq.) with the presence of potassium carbonate (3 eq.) in dry DMF. To monitor the reaction, a small aliquot (2 µL) was taken from the reaction mixture after 1, 2 and 3 hours and then analysed by LCMS.

To examine the presence of *O*-propargylation product, 5-(prop-2-un-1-yloxy) - (-)-rishirilide A (**63**), we used EIC chromatogram analysis. Therefore, we selected a range of molecular masses of 427.1651 – 427.1851, corresponding to $[M+H]^+$ ion of 5-(prop-2-un-1-yloxy) (-)-rishirilide A

(**63**). As a result, we observed a key peak at 26.8 minutes from the reaction mixture after 2 hours reaction with *m/z* signals of 427.1810, 449.1642, 465.1347 and 875.3271, corresponding to $[M+H]^+$, $[M+Na]^+$, $[M+K]^+$ and $[2M+Na]^+$ ions of the desired product (**63**) (Figure **5.12**).

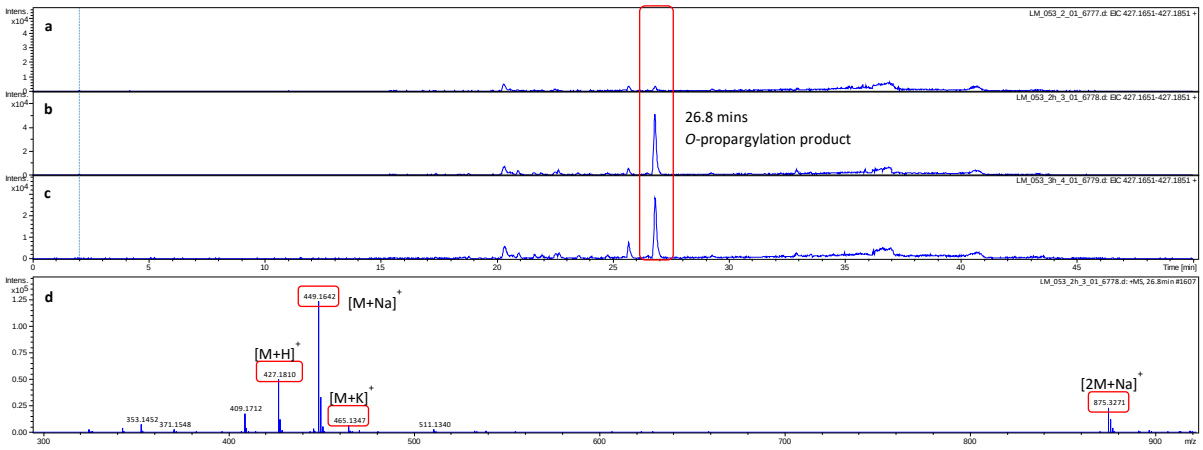

Figure 5.12: EIC chromatogram of *O*-propargylation of (-)-rishirilide A (**29**) with propargyl bromide. (**a**) after 1 h reaction; (**b**) after 2 h reaction; (**3**) after 3 h reaction; (**d**) Mass spectrum of reaction mixture after 2 h reaction.

In conclusion, we have successfully incorporated the required alkyne functional group of (-)-rishirilide A (**29**) via an *O*-propargylation with propargyl bromide. However, the subsequent CuAAC reaction of our test system between methyl 3-(prop-2-yn-1-yloxy)benzoate (**61**) and benzyl azide gave a low isolated yield of 6.8%. Therefore, in the future we wished to improve this CuAAC reaction of our test system and apply the improved CuAAC conditions to our proparagyl rishirilide A (**29**). Due to the time constraint of this project, we decided to investigate the target enzyme of (-)-rishirilide A (**29**) via an alternative route.

5.8 Conclusion

The aim of this chapter was to examine the synthesis of chemical probes which could be used to identify target enzymes of the natural product antibiotic (-)-rishirilide A (**29**).

We have successfully shown the incorporation of propargyl bromide into our model compound methyl 3-hydroxybenzoate (**57**), resulting in methyl 3-(prop-2-yn-1-yloxy)benzoate (**61**), as a demonstration of the propargylation chemistry required for chemical probe synthesis. The subsequent CuAAC reaction of methyl 3-(prop-2-yn-1-yloxy)benzoate (**61**) with benzyl azide has also been successfully demonstrated, however the

percent yield observed under our optimised reaction conditions remains low (6.8%). Therefore, in future work we will aim to improve the CuAAC reaction conditions to maximise the yield of the click chemistry products, as this would be a key step in the capture of any future (-)-rishirilide A (**29**) based chemical probe.

Our optimised *O*-propargylation reaction protocols were applied in the *O*-propargylation of our natural product, (-)-rishirilide A (**29**). The *O*-propargylation of (-)-rishirilide A (**29**) with propargyl bromide resulted in the successful incorporation of a propargyl group, as confirmed by LCMS. In the future the *O*-propargylation of (-)-rishirilide A (**29**) would need to be scaled up and further optimised to provide potential probe molecules to aid in MOA elucidation.

Chapter 6. Encapsulated Nanodroplet Crystallisation of Natural Products

In this chapter we will discuss our work on the crystallisation of natural products for single crystal X-ray diffraction analysis. We will investigate a new nanoscale high throughput crystallisation methodology (ENaCt) for the crystallisation and structural investigation of natural products, supporting our previous work on natural product discovery and isolation.

6.1 Introduction

As discussed in Chapter 1, natural products are very important due to their applications in medicine.[81,82] However, the discovery of new natural products is complicated by the difficulties associated with the structural analysis of an unknown molecule. Furthermore, natural products are often highly complex molecules and in the early stages of isolation of a new natural product, typically only a few milligrams are available for study. Because of their structural complexity and limited mass availability, subsequent structure elucidation (including relative and absolute stereochemistry) can be very difficult.[83]

The structure elucidation of a new natural product commonly employs a combination of analytical techniques including infrared spectroscopy (IR), UV/Visible spectroscopy, high-resolution mass spectrometry (HRMS), and nuclear magnetic resonance spectroscopy (NMR). However, these techniques each only provide partial information about the molecular structure of a molecule. HRMS provides accurate mass allowing the calculation of molecular formula, whilst IR spectroscopy allows identification of functional groups. In contrast, NMR is a powerful analytical technique in structural elucidation because it allows us to both observe multiple nuclei (^{1}H, ^{13}C, ^{14}N/^{15}N and ^{31}P), and provides information on their chemical environment (chemical shift) and neighbouring nuclei (e.g. coupling). Furthermore, the use of modern 2D techniques (COSY, NOESY, HMBC, HSQC etc.) allows us to build up the atomic connectivity in an unknown molecule. However, the interpretation of NMR spectra data can be challenging because of overlapping signals, areas of a molecule without sufficient NMR nuclei to allow 2D correlations to be obtained (e.g. sequential quaternary centres) and difficulties in assigning relative and absolute stereochemistry, resulting in the missassignment of numerous natural products in the literature.[84-87]

Single crystal X-ray diffraction (SCXRD) is however the most powerful analytical technique for the structural assignment of an unknown molecule. SCXRD allows us to see the 3D

arrangement and connectivity of all the atoms in a molecule, including the assignment of relative or even absolute stereochemistry, providing unambiguous structural assignment. Thus, in combination with NMR, SCXRD is an essential analytical technique to elucidate the molecular structure of new natural products.[88,89]

SCXRD can also assist in the correction of structurally missassigned natural products. For example, wentiquinone C, a compound derived from marine Brown alga-derived endophytic fungus *Aspergillus wentii* EN-48, was initially assigned as an oxidatively ring expanded anthraquinone derivative (**64**) using 1D and 2D NMR spectroscopy. Growth of single crystals of wentiquinone C and subsequent SCXRD analysis allowed revision of the structure to that of xanthone (**65**) (Figure **6.1**).[90,91]

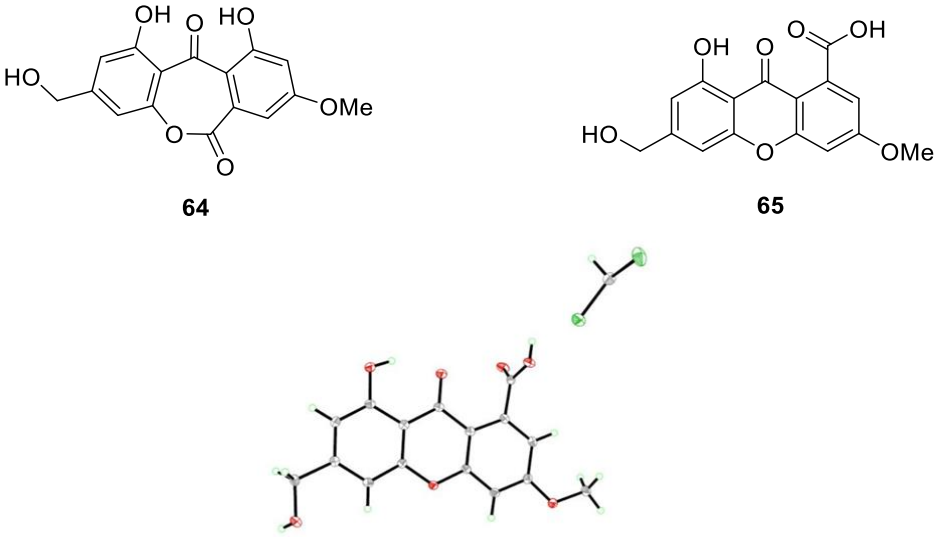

Figure 6.1: Structures proposed for wentiquinone C. (**65**) original structural proposition based on NMR data, (**65**) revised structure based on X-ray crystallography and X-ray crystal structure of wentiquinone C as a $CHCl_3$ solvate.

Although, SCXRD is an excellent technique to characterize structures of small organic molecules especially unknown natural products, growing single crystals for an unknown natural product which are suitable for SCXRD analysis is challenging in part due to the limited mass typically available (< 5 mg).[92-94]

In order to grow a single crystal of a natural product, many different crystallisation experiments (solvent, co-solvent, temperature, concertation etc.) have to be undertaken to find the optimal crystallisation conditions. Classic crystallisations (e.g. slow evaporation, slow cooling and vapour diffusion) require milligrams of material to carry out a single crystallisation

experiment, thus, to screen a range of crystallisation conditions, lots of material (10-100 mgs) is needed. In the case of natural product, obtaining 10-100 mgs of material in the early stage of isolation is often difficult and time consuming. Therefore, we need a new method capable of high-throughput parallel screening of crystallisation conditions which utilizes very small quantities of total material (< 5 mgs) but provides many crystallisation conditions (100-1000s experiments) to explore.

Our research group has recently developed an **E**ncapsulated **Na**nodroplets **Crystallisation** (ENaCt) method to grow single crystals of small organic molecules. ENaCt improves on classical crystallisations, as it allows us to use a few micrograms of material per crystallisation experiment and thus allows exploration of a wide spectrum of crystallisation conditions (primary solvents, secondary solvents, concentrations, etc.). ENaCt uses inert oils to encapsulate the analyte solutions, in order to control the rate of solvent, loss allowing miniaturisation of the crystallisation experiments. ENaCt is performed using an SPT Labtech mosquito® liquid-handling robot, allowing high throughput experimental set-up and facilitating parallel screening. However, the use of ENaCt to grow single crystals of natural products has not yet been explored in detail. Therefore, the aim of this chapter is to examine the use of ENaCt techniques for the crystallisation and subsequent structural analysis (SCXRD) of natural products.

6.2 Encapsulated Nanodroplet Crystallisation (ENaCt) for natural products

In this chapter, we wish to examine whether ENaCt can be used to grow single crystals from a number of different classes of natural products, using commercially available terpenoids (cannabidiol (CBD)), polyketides (rifamycin SV (**67**)) and semi-synthetic natural products (rifampicin (**21**)). Finally, we will apply ENaCt method to the growth of single crystals of our previously isolated natural products, (-)-rishirilide A and (+)-rishirilide B.

Thus, our first step was to compare classical crystallisation conditions to ENaCt for growth of single crystal for a number of natural products, in order to evaluate the ENaCt method against the current state-of-the-art. Therefore, to investigate the crystallisation of natural products using ENaCt, first we will have to identify suitable solvent(s) for small scale of classical crystallisations. Thus, the solubility of each natural product will be briefly assessed in a range of solvents, classical crystallisations will be undertaken followed by comparative ENaCt

crystallisations. Suitable single crystals will be identified by cross-polarised light microscopy and further analysed by X-ray diffraction (SCXRD).

6.3 Encapsulated Nanodroplet Crystallisation (ENaCt) of the terpene cannabidiol (CBD)

We chose cannabidiol (CBD) (**66**) as our first test molecule for ENaCt, as a representative example of a lipophilic terpenoid natural product. The terpenoid natural products are biosynthesised from isoprene (C_5) units linked in a head-to-tail manner,[95] and include the anticancer drug paclitaxel (Taxol®) and the antimalarial drug, artemisinin.[96] Another pharmacologically important terpenoid is CBD (**66**), a cannabinoid from the cannabis plant, *Cannabis sativa L.*. Recently CBD (**66**) has been investigated as a treatment for a number of conditions, and has been approved by the FDA for the treatment of Dravet syndrome and Lennox-Gastaut syndrome (Figure **6.2**).[97]

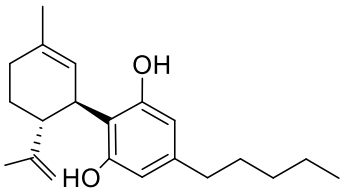

Figure 6.2: Cannabidiol (CBD) (**66**).

6.3.1 Classical crystallisation of cannabidiol (CBD)

Firstly, the purity of commercial CBD (**66**) was confirmed by both LCMS and NMR (^{1}H, ^{13}C, COSY, HSQC, HMBC). Following which we examined the crystallisation of CBD (**66**) under classical conditions. The single crystal X-ray structure of CBD (**66**) is known in the literature with three independent data sets available via the Cambridge Crystallographic Data Centre (CCDC) (CANDOM01[98], CANDOM10[99] and CANDOM11[100]) with crystals grown from both pentane[99] and *n*-heptane[100]. It should be noted that the most modern data set was collected using Cu Kβ wavelength radiation allowing the direct determination of absolute stereochemistry by anomalous dispersion.[100]

Therefore, we examined a number of classical crystallisation conditions for CBD (**66**) for later comparison to ENaCt. In an initial test of both solubility and crystallisation we placed a few crystals of CBD (**66**) into each well of two 9 well glass plates, added of a few drops of each test solvent and observed the samples under an optical microscope. CBD (**66**) dissolved well in

pentane, *n*-hexane, *n*-heptane, dichloromethane, chloroform, 1,2-dichloroethane, ethanol, 1-propanol, 2-propanol, 1-butanol, 1-hexanol, THF, 1,4-dioxane, toluene, chlorobenzene, DMF and DMSO, but proved insoluble in methanol. After approximately 30 minutes the wells were re-examined by cross-polarised light microscopy to search for crystalline material, following solvent concentration/evaporation. Pentane, *n*-hexane, dichloromethane and chloroform gave the best results, with large needle like crystals observed (Figure **6.3**).

Figure 6.3: CBD (**66**) crystals formed via evaporation from solvent (cross-polarised light microscope): (**1**) pentane; (**2**) *n*-hexane; (**3**) dichloromethane; (**4**) chloroform.

Following on from these results, we next carried out series of small-scale classical crystallisation experiments with CBD (**66**). Thus CBD (5 mg) (**66**) was placed in a straight sided glass sample tube, dissolved in 1 mL of a suitable solvent (pentane, *n*-hexane, *n*-heptane, dichloromethane and chloroform), covered and left to crystallise. Single crystals of CBD (**66**) were subsequently observed (1-2 weeks) from pentane, *n*-hexane, *n*-heptane and dichloromethane.

Full SCXRD analysis was performed on a crystal obtained from pentane by Dr Paul Waddell, to give an X-ray structure consistent with the literature (CANDOM01[98], CANDOM10[99] and CANDOM11[100]). X-ray analysis was also carried out on CBD (**66**) crystals obtained from *n*-hexane, *n*-heptane, and dichloromethane, showing that they had the same unit cell as those obtained previously (Figure **6.4**).

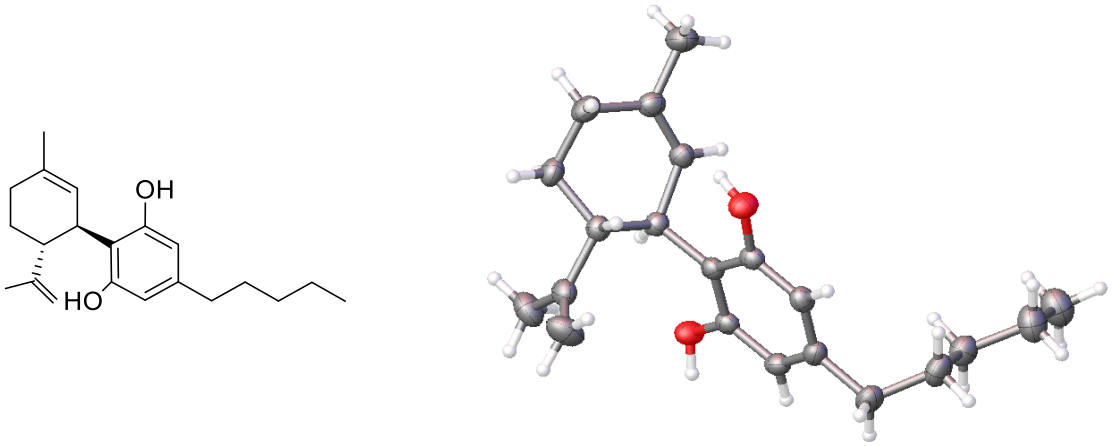

Figure 6.4: X-ray structure of CBD (**66**) obtained via classical crystallisation from pentane.

6.3.2 Encapsulated Nanodroplet Crystallisation (ENaCt) of CBD

Given the positive results from our classical crystallisation experiments, next we then examined the crystallisation of CBD (**66**) via ENaCt. ENaCt typically employs 50 nL of organic solvent per experiment, and thus the use of low boiling solvent is difficult due to their rapid evaporation, particularly during experimental set-up. Therefore, we decided to include a number of higher boiling point solvents in ENaCt, in comparison to our previous classical crystallisation experiments.

For our ENaCt experiments we first made-up stock solutions of CBD (**66**) in a range of solvents. Approximately, 50 mg of CBD (**66**) was dissolved in a minimum of 50 μL of solvent, with additional solvent added as required to dissolve the sample, resulting in a CBD (**66**) solutions in pentane [0.11 g/mL], *n*-hexane [0.084 g/mL], *n*-heptane [0.063 g/mL], chloroform [1.00 g/mL], 1,2-dichloroethane [1.00 g/mL], toluene [1.02 g/mL], fluorobenzene [1.00 g/mL], chlorobenzene [1.01 g/mL], and hexafluoro benzene [0.20 g/mL]. These concentrated stock solutions, labelled as high concentration (H), were also diluted by two fold, medium concentration (M), and four fold, low concentration (L), to make provide three different sample concentrations for our ENaCt experiments. Next, using a SPT LabTech mosquito® liquid-handling robot, 200 nL of each inert oil (PDMSO, FC-40, FY and mineral oil) were dispensed onto a Laminex™ 96-well glass plate, followed by injection of 50 nL of the appropriate CBD (**66**) solution into the oil. The 96-well glass plates were then sealed with a glass cover slip, stored in the dark at room temperature for up to 14 days (Scheme **6.1**).

Oils		50 nL of CBD stock solutions											
		no oils			with 200 nL oils								
		H	M	L	H			M			L		
		1	2	3	4	5	6	7	8	9	10	11	12
PDMSO	A												
	B												
FC-40	C												
	D												
FY	E												
	F												
Mineral oil	G												
	H												

Scheme 6.1: A typical arrangement of a 96-well glass plate containing inert oils and CBD (**66**) solutions. H = high concentration, M = medium concentration, L = low concentration.

The plates were checked for the presence of CBD (**66**) crystals by cross-polarised light microscopy at day 1, 7 and 14. Each experimental outcome was categorized as either: (1) in solution, (2) oiled-out, (3) non-crystalline or micro-crystalline solid, (4) small single crystals and (5) single crystals suitable for SCXRD (Figure **6.5**).

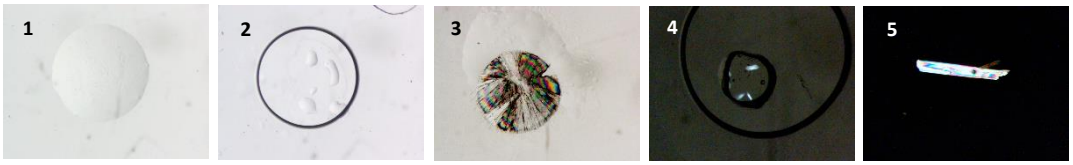

Figure 6.5: Examples of observation outcome of 96-well glass plate as: (**1**) solution; (**2**) oiled-out; (**3**) non-crystalline or micro-crystalline solid; (**4**) small single crystals; (**5**) single crystals under a cross-polarised light microscope.

From the 864 ENaCt experiments undertaken, 18 (2.1%) gave single crystals suitable for SCXRD (3 from chloroform, 4 from 1,2-dichloroethane, 6 from toluene, and 5 from fluorobenzene) after 14 days. 11 of 18 of the single crystals observed were formed from high concentration (H) solutions of CBD, whilst the majority 16 of 18 was formed from experiments containing mineral oil. Control experiments without the presence of inert oils gave no suitable single crystals (Figure **6.6**).

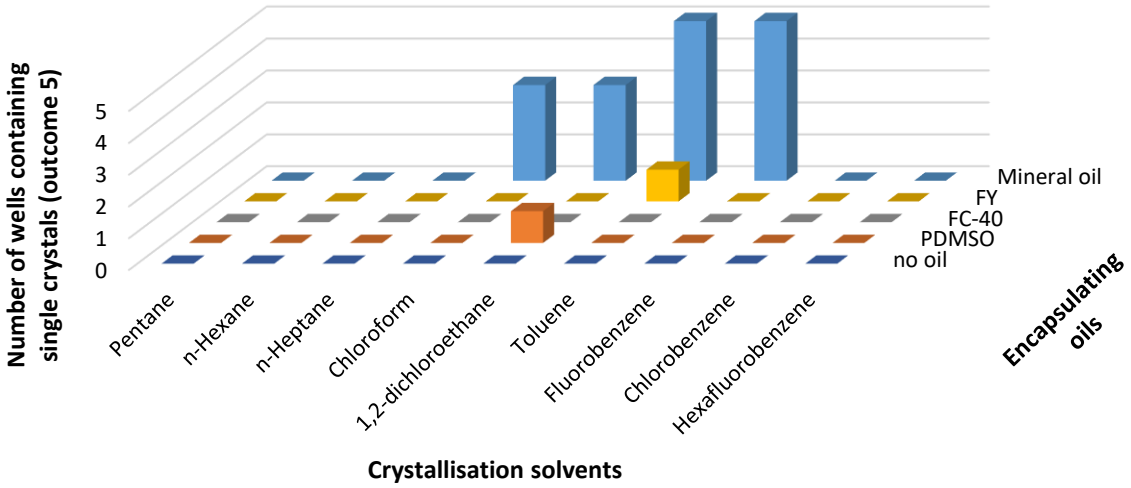

Figure 6.6: CBD (**66**) single crystals suitable for SCXRD (outcome 5) observed from different solvents and oils using ENaCt.

The majority of the single crystals of CBD grown via ENaCt showed a needle like morphology, similar to those grown under classical conditions. However, an unusual block like crystal habit for CBD was observed from 1,2-dichloroethane in mineral oil. Therefore, we examined five single crystals of CBD grown via ENaCt from chloroform (needle), 1,2-dichlorothethane (block), toluene (needle) and fluorobenzne (2x needles) using in-house X-ray analysis (Figure **6.7**).

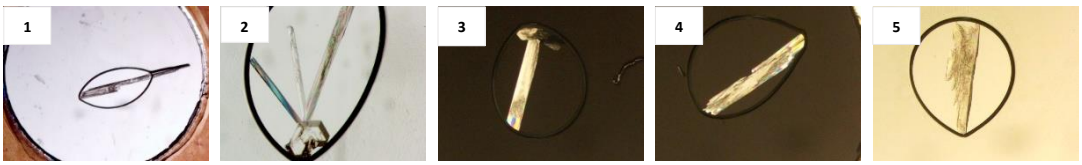

Figure 6.7: Single crystals of CBD (66) grown using ENaCt, with encapsulation by mineral oil, morphology in brackets. (**1**) in chloroform (needles); (**2**) in 1,2-dichloroethane (needles and blocks); (**3**) in toluene (needles); (**4**) in fluorobenzene (needles); (**5**) in fluorobenzene (needles).

X-ray analysis was undertaken by Dr Paul Waddell for all five of the single crystals selected, all of which gave unit cell data that matched the known crystal structure of CBD (**66**). This included the block like crystal obtained from 1,2-dichloroethane.

Finally, to demonstrate that CBD (**66**) single crystals grown via ENaCt were suitable for full structural analysis by X-ray diffraction, a complete X-ray crystal structure was determined for a CBD (**66**) crystal grown from toluene and mineral oil using Cu Kα radiation (λ = 1.54184 Å). This gave an excellent data set (R_1 = 0.0323) showing a monoclinic $P2_1$ space group with unit

cell dimensions of a = 10.43368(15) Å, b = 10.88596(18) Å, c = 16.7723(2) Å and angles of α = 90°, β = 95.4451(13)°, γ = 90°, which aligned well with the structural data available from the CCDC (CANDOM01[98], CANDOM10[99] and CANDOM11[100]). Furthermore, direct measurement of the absolute stereochemistry of CBD (**66**) was also possible, giving a Flack parameter of -0.11(8) (Figure **6.8**).

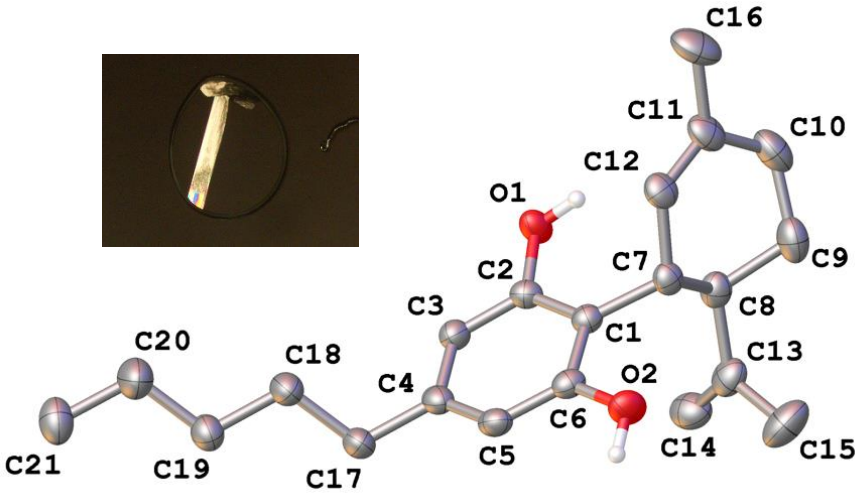

Figure 6.8: X-ray crystal structure of CBD (**66**) obtained from ENaCt (toluene, mineral oil).

6.3.3 Conclusion

Following our initial classical crystallisation, we have successfully grown single crystal of CBD (**66**) from hydrocarbon solvents (pentane, *n*-hexane, and *n*-heptane) which has been known in literature[98-100]. Interestingly, the CBD (**66**) crystal also can be grown from chlorinated solvent (1,2-dichloroethane), which was never known before.

We have also successfully grown single crystal of CBD (**66**) via ENaCt. Single crystals of CBD (**66**) were observed from chlorinated solvent (chloroform and 1,2-dichloroethane), aromatic solvent (toluene), and halogenated aromatic solvents (fluorobenzene), whilst no single crystals of CBD were observed from the hydrocarbon solvents that used previously in classical crystallisation. This could be caused by the low boiling point of the hydrocarbon solvents which evaporated quickly during the preparation of ENaCt. Next, we attempted to grow single crystals from polyketide natural product, rifamycin SV (**67**) using ENaCt method.

6.4 Encapsulated Nanodroplet Crystallisation (ENaCt) of the polyketide rifamycin

The next class of natural products that we wished to test in ENaCt was the polyketides. The polyketides are commonly occurring group of secondary metabolites, biosynthesised from acetyl-CoA, malonyl-CoA and methylmalonyl-CoA units linked together by ketosynthases and subsequently modified by a number of reductive and oxidative enzymes.[101] Large numbers of bioactive polyketides have been isolated from bacteria, leading to the discovery of several classes of clinically used antibiotics, including the tetracyclines (e.g. chlortetracycline (**6**)), the macrolides (e.g. erythromycin (**7**)) and the rifamycins (e.g. rifampicin **21**).[102-103] As discussed in Chapter 1, the rifamycins are an important class of natural product derived antibiotics, with particular application in the treatment of tuberculosis.[104] The parent natural product rifamycin SV (**67**), first isolated from *Amycolatopsis mediterranei*, is an important example of the rifamicins and is used as the starting point for the production of many semi-synthetic antibiotics.[105] Therefore we chose to examine the crystallisation of rifamycin SV (**67**) by ENaCt as a representative example of a complex polyketide. The single crystal X-ray structure of the sodium salt of rifamycin SV (**67**) has been previous solved as the ethanol solvate, reportedly grown from aqueous methanol (CCDC: BOBMOU[106] and BOBMOU10[107]) (Figure **6.9**).

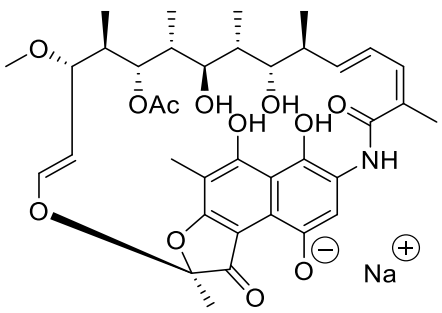

Figure 6.9: Sodium salt of rifamycin SV (**67**).

6.4.1 Encapsulated Nanodroplet Crystallisation (ENaCt) of sodium salt of rifamycin SV

Following an initial test of solubility using similar method as previously, we made-up stock solutions of sodium salt of rifamycin SV (**67**) in a range of solvents. The sodium salt of rifamycin SV (approx. 10 mg) (**67**) was dissolved in a minimum of 50 μL of solvent, with additional solvent added as required to dissolve the sample, resulting in solutions in methanol [57 mg/mL], ethanol [39 mg/mL], DMSO [34 mg/mL], DMF [45 mg/mL], 1-propanol [17 mg/mL], 1-butanol [11 mg/mL], 1-hexanol [8 mg/mL] and 2-propanol [6 mg/mL].

Next, using the SPT Labtech mosquito® liquid-handling robot, 200 nL of each inert oil (PDMSO, FC40, FY and mineral oil) were dispensed onto a Laminex™ 96-well glass plate, followed by injection of either 25, 50, or 100 nL of rifamycin SV sodium (**67**) solutions. Different volumes of analyte solution were added to the plates to examine the impact of volume on crystal growth and encapsulated droplet formation. Only high concentration solutions of rifamycin SV sodium (**67**) were used to maximise the rate of crystal growth. It should also be noted that on each Laminex™ 96-well glass plate two different solvents were examined. The resulting 96-well glass plates were then sealed and stored at room temperature and rifamycin SV (**67**) crystals was looked for using a cross-polarised light microscope at day 1, 7, and 14 (Scheme **6.2**).

			Rifamycin SV in solvent A (nL)						Rifamycin SV in solvent B (nL)					
			25	25	50	50	100	100	25	25	50	50	100	100
			1	2	3	4	5	6	7	8	9	10	11	12
200 nL of inert oils	PDMS	A												
		B												
	FC40	C												
		D												
	FY	E												
		F												
	Mineral oil	G												
		H												

Scheme 6.2: Arrangement of 96-well glass plate containing inert oils and rifamycin SV (67) stock solutions.

As before, the outcomes of the crystallisation experiments were categorised as either (1) in solution, (2) oiled-out, (3) non-crystalline or micro-crystalline, (4) small single crystals or (5) single crystals suitable for SCXRD.

After 14 days, 6 of the 384 ENaCt experiments undertaken (1.6%), gave single crystals suitable for SCXRD. All 6 of the successful crystallisation experiments used DMF as the solvent and FY as the oil, 4 from a 50 nL and 2 from a 100 nL solution of rifamycin SV sodium (**67**) (Figure **6.10**).

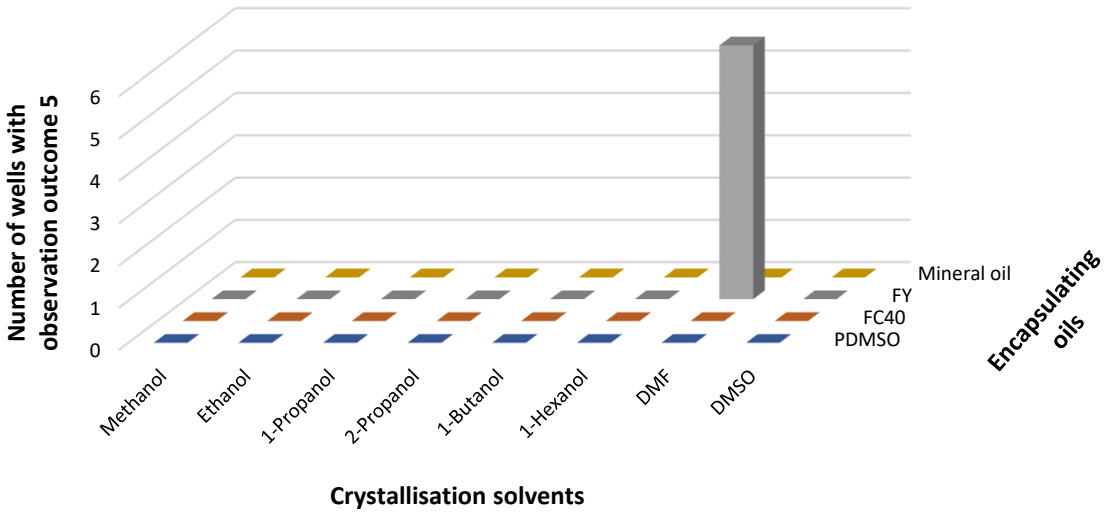

Figure 6.10: Rifamycin SV sodium (**67**) single crystals suitable for SCXRD (outcome 5) observed from different solvents and oils using ENaCt.

The optical microscopy showed that all 6 crystals of rifamycin SV sodium (**67**) obtained had grown as thin plates (Figure **6.11**). Following this, Dr Paul Waddell examined several of these crystals via in house X-ray diffraction. However, those examined gave poor X-ray diffraction, and structures could not be obtained. Therefore, to improve the quality of single crystals obtained we decided to re-examine the crystallisation of rifamycin SV (**67**).

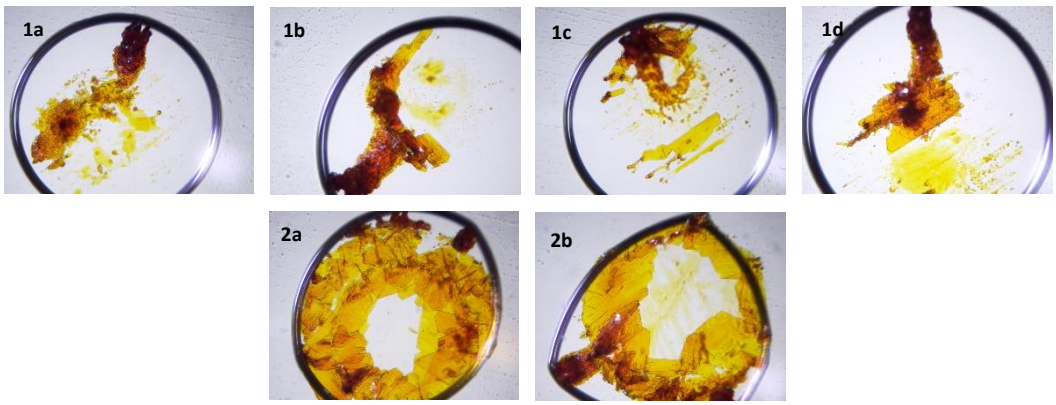

Figure 6.11: Rifamycin SV (**67**) single crystals observed from DMF in FY. (**1a-d**) 50 nL rifamycin SV solution and (**2a-b**) 100 nL rifamycin SV solution.

6.4.2 ENaCt crystallisation of sodium salt of rifamycin SV with the addition of secondary solvents

To improve the growth of single crystals, we decided to modify the ENaCt conditions by adding secondary solvents to allow fine tuning of the solubility of rifamycin SV sodium (**67**) in the crystallisation experiments. Therefore, we selected six secondary solvents with a wide range of properties (toluene, 1,4-dioxane, chlorobenzene, anisole, 1,2-dichloroethane and 2-butanone) to be included in our the next ENaCt experiment.

Thus, we used the SPT Labtech mosquito® liquid-handling robot to dispense 200 nL of each inert oil (PDMSO, FC40, FY, and mineral oil) onto a Laminex™ 96-well glass plate, followed by 50 nL of a rifamycin SV sodium (**67**) solution (methanol, ethanol, DMSO, DMF, 1-propanol, 1-butanol, 1-hexanol, and 2-propanol) and finally 25, 50, 75, or 100 nL of a secondary solvent (toluene, 1,4-dioxane, chlorobenzene, anisole, 1,2-dichloroethane and 2-butanone). The resulting glass plates were sealed, stored in the dark, at room temperature, and the appearance of rifamycin SV (**67**) crystals was checked for at 1, 7 and 14 days (Scheme **6.3**).

Plate number			50 nL of rifamycin SV solution											
			Secondary solvent A (nL)				Secondary solvent B (nL)				Secondary solvent C (nL)			
			25	50	75	100	25	50	75	100	25	50	75	100
			1	2	3	4	5	6	7	8	9	10	11	12
200 nL of inert oils	PDMS	A												
		B												
	FC40	C												
		D												
	FY	E												
		F												
	Mineral oil	G												
		H												

Scheme 6.3: A typical arrangement of a 96-well glass plate containing inert oils, rifamycin SV (**67**) solution and the addition of secondary solvents.

From the 1536 ENaCt experiment undertaken, 13 (0.85%) gave crystals of rifamycin SV sodium (**67**) suitable single for SCXRD. DMF was the most successful solvent from which to grow single crystals of rifamycin SV (**67**), with 10 crystals obtained from DMF in the presence of a secondary solvent. The most successful secondary solvent being chlorobenzene (5 crystals), followed by anisole (3) toluene (1) and 2-butanone (1). The other 3 single crystals of rifamycin

SV sodium (**67**) were obtained from 1-butanol with 2-butanone (2 crystals), and 1-propanol with 2-butanone (1) (Figure **6.12**).

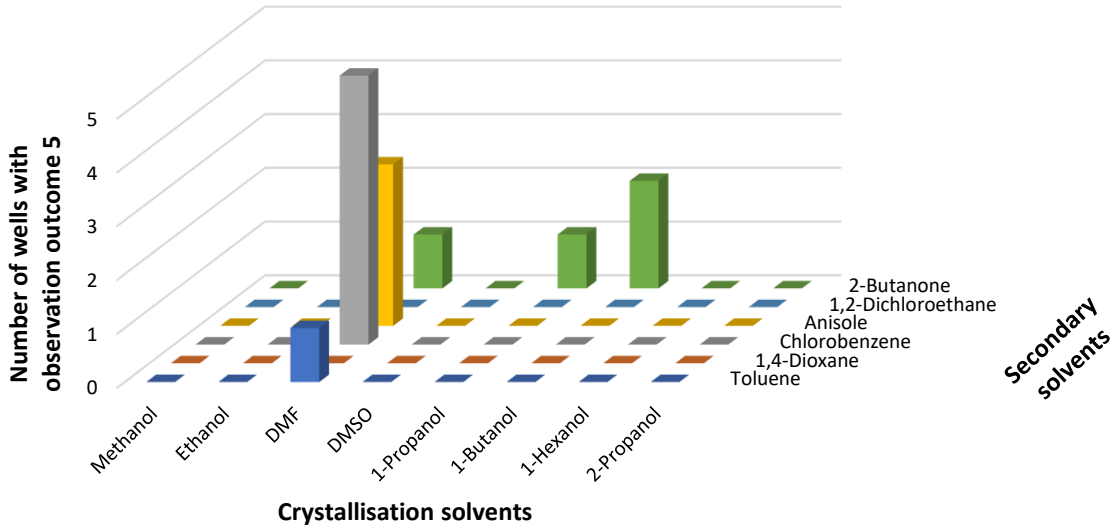

Figure 6.12: Rifamycin SV (**67**) single crystals suitable for SCXRD (outcome 5) observed from different solvents and secondary solvents using ENaCt.

FY was still the most successful oil used in these ENaCt experiments with secondary solvents, producing all 13 of the observed single crystals of rifamycin SV sodium (**67**) (Figure **6.13**).

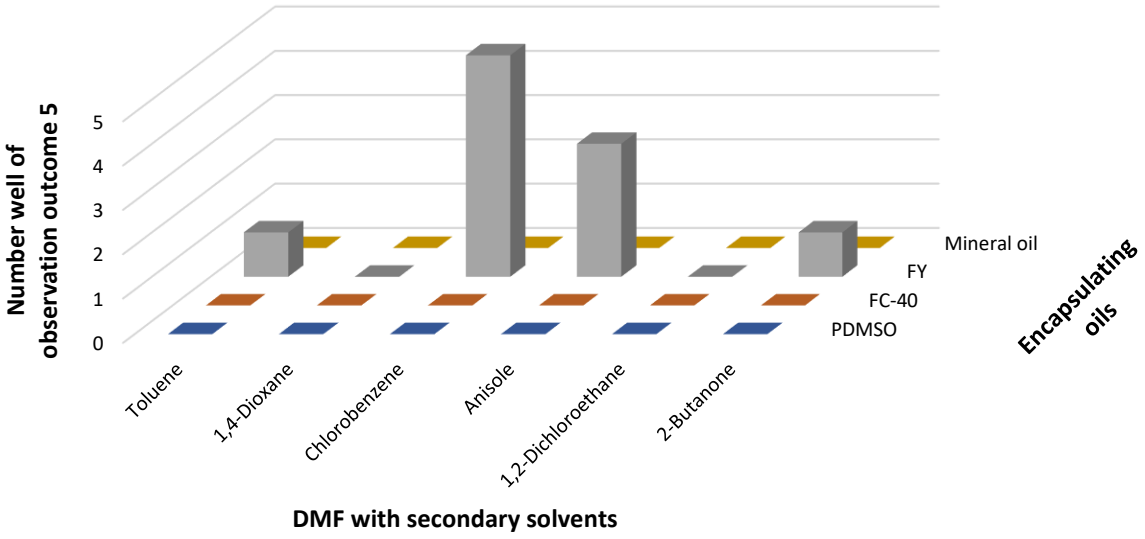

Figure 6.13: Number of single crystals with outcome 5 observed in rifamycin SV (**67**) in DMF with various secondary solvents encapsulated by four types of inert oils.

The optical microscopy showed that rifamycin SV sodium (**67**) had produced different crystal forms in different solvents, with plate/block morphology obtained from DMF/aromatics and

needle like crystals obtained from alcohol/butan-2-one solutions. Following this, Dr Paul Waddell examined all of the 13 crystals obtained for rifamycin SV sodium (**67**), for analysis by in-house X-ray diffraction. Unfortunately, the crystals were very fragile and broke during attempts to retrieve them from the plates. Three crystals (3, 6 and 11) were successfully mounted for X-ray analysis, however they showed poor diffraction and structural information could not be obtained (Figure **6.14**).

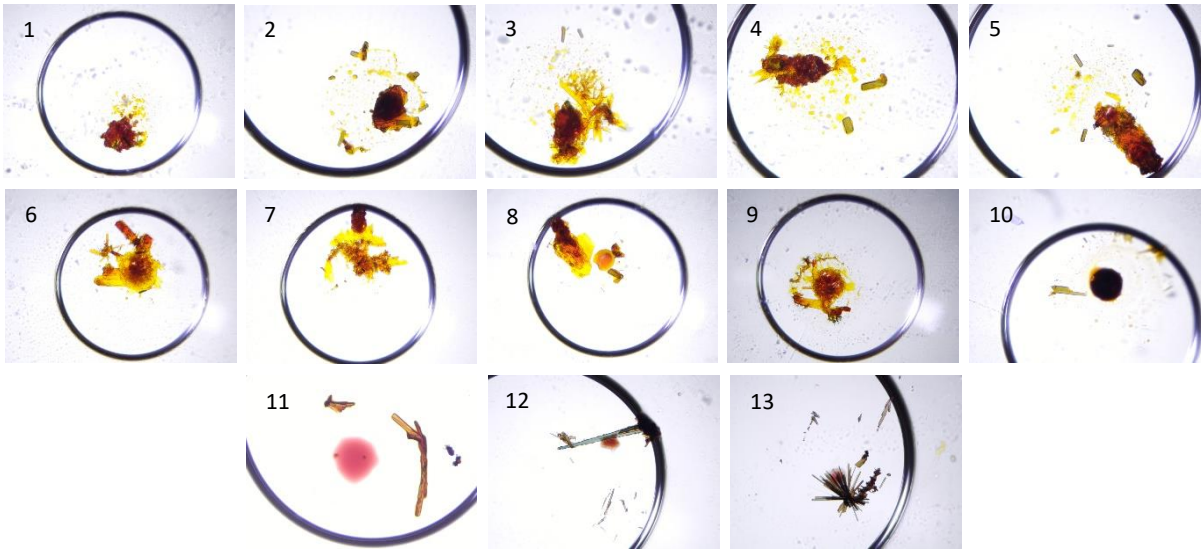

Figure 6.14: Rifamycin SV (**67**) single crystals observed by cross-polarised microscopy. DMF with chlorobenzene: (**1**) 25 nL; (**2**) 50 nL; (**3**) 50 nL; (**4**) 50 nL; (**5**) 75 nL. DMF with anisole: (**6**) 25 nL; (**7**) 50 nL; (**8**) 75 nL. (**9**) DMF with 50 nL toluene. (**10**) DMF with 75 nL 2-butanone. (**11**) 1-propanol with 50 nL 2-butanone. (**12**) 2-propanol with 75 nL 2-butanone. (**13**) 2-propanol with 100 nL 2-butanone.

6.4.3 Conclusion

In conclusion, we have successfully demonstrated that crystals of the sodium salt of rifamycin SV (**67**) can be grown using ENaCt, however the crystals obtained were not suitable for X-ray diffraction analysis. We examined two approaches, firstly using single solvents resulting in the best crystal growth from DMF/FY and secondly from a two solvent system in which DMF/aromatics/FY and alcohols/butan-2-one/FY proved most successful. In the future we aim to improve the growth of crystals of rifamycin SV sodium (**67**) via ENaCt, by slowing crystal growth by reducing the concentration of rifamycin SV sodium (**67**) and by further investigating DMF/aromatic and alcohol/butan-2-one solvent systems.

6.5 Encapsulated Nanodroplet Crystallisation (ENaCt) the semi-synthetic polyketide rifampicin

Encouraged with crystallisation results of rifamycin SV sodium (**67**) shown previously, herein we decided to examine crystallisation by ENaCt of a clinically important semi-synthetic derivative of rifamycin SV, namely the anti-TB medicine rifampicin (**21**). Rifampicin (**21**) is made by the semi-synthetic modification of rifamycin SV (**67**), by the introduction of a solubilising functional group at C-3 (Figure **6.15**).[108]

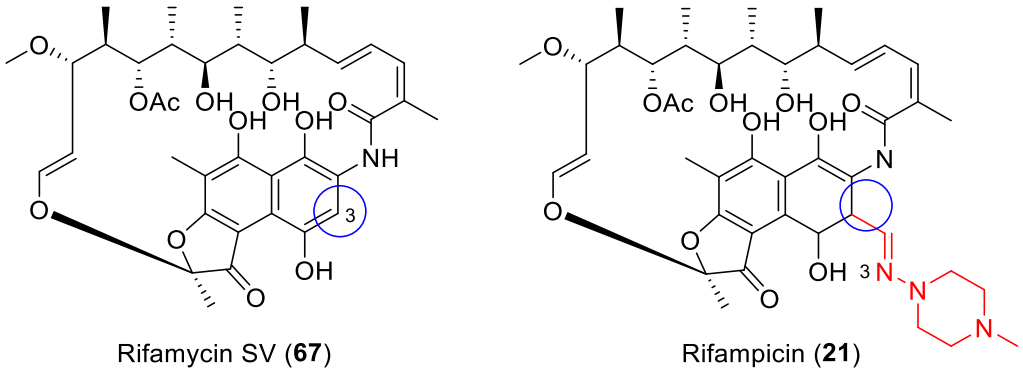

Figure 6.15: Rifamycin SV (**67**) and rifampicin (**21**), the different functional group at C-3 highlighted in red.

The single crystal X-ray structure of rifampicin (**21**) is known in the literature. The anhydrous form of rifampicin is known to have two polymorphs, the stable polymorph I (LOPZEX29[109]) and the metastable polymorph II (LOPZEX01[110]). In addition a large number of hydrates and solvates have been reported including: pentahydrate (HAXWUA[111], RIFAMP[112]), methanol solvate trihydrate (MAPHIW[113]), 1,1,1-trichloroethane solvate (MAPHES[113]), ethylene glycol solvate trihydrate (OWELOS and OWELUY[114]), 1-pentanol solvate hydrate (YELXUL[115]), 2-pentanol dichloromethane solvate hemihydrate (YELYAS[115]), 1-hexanol solvate monohydrate (YELYEW[115]), 2-propanol solvate monohydrate (YELYIA[115]), 3-pentanol solvate (YELYOG[115]), ethanol solvate hydrate (YELYUM[115]), acetone solvate hydrate (YELZAT[115]), 2-butanone solvate (YELZEX[115]), acetone solvate monohydrate (YELZIB[115]), 1-butanol solvate hemihydrate (YELZOH[115]), 1-propanol solvate monohydrate (YELZUN[115]), 2-butanol solvate hemihydrate (YEMBAW[115]), and dimethyl sulfoxide solvate hydrate (YEMCIF[115]).

Following similar initial test of solubility as previously, we prepared stock solutions of rifampicin (**21**) in six different solvents. The rifampicin (**21**) (approx. 10 mg) was dissolved in a minimum of 50 μL of solvent, with additional solvent added as required to dissolve the

sample, resulting solutions in toluene [14 mg/mL], 1,4-dioxane [37 mg/mL], chlorobenzene [105 mg/mL], THF [28 mg/mL], ethyl acetate [50 mg/mL], and 1,2-dichloroethane [11 mg/mL].

Next, using the SPT Labtech mosquito® liquid-handling robot, 200 nL of each inert oil (PDMSO, FC40, FY and mineral oil) were dispensed onto a Laminex™ 96-well glass plate, followed by addition of either 25, 50 or 100 nL of rifampicin (**21**) solutions. Different volumes of rifampicin (**21**) solution were added to plates to examine the impact of volume on the crystal growth and encapsulated droplet formation. It should be notes that on each Laminex™ 96-well glass plate two different solvents were examined. The resulting 96-well glass plates were then sealed and stored at room temperature and the rifampicin (**21**) crystals was checked using a cross-polarised microscope at day 1, 7 and 14 (Scheme **6.4**).

			Rifampicin in solvent A (nL)						Rifampicin in solvent B (nL)					
			25	25	50	50	100	100	25	25	50	50	100	100
			1	2	3	4	5	6	7	8	9	10	11	12
200 nL of inert oils	PDMS	A												
		B												
	FC40	C												
		D												
	FY	E												
		F												
	Mineral oil	G												
		H												

Scheme 6.4: A typical arrangement of a 96-well glass plate containing inert oils and rifampicin (**21**) solution.

As before, the outcomes of the crystallisation experiments were categorized as either (1) in solution, (2) oiled-out, (3) non-crystalline or micro-crystalline, (4) small single crystals or (5) single crystals suitable for SCXRD.

After 14 days, 2 of the 288 ENaCt experiment undertaken (0.69%), gave single crystals suitable for SCXRD. The 2 single crystals of rifampicin (**21**) were grown from 1,4-dioxane and FY, with a further 17 wells showing rifampicin (**21**) micro-crystals (Figure **6.16**).

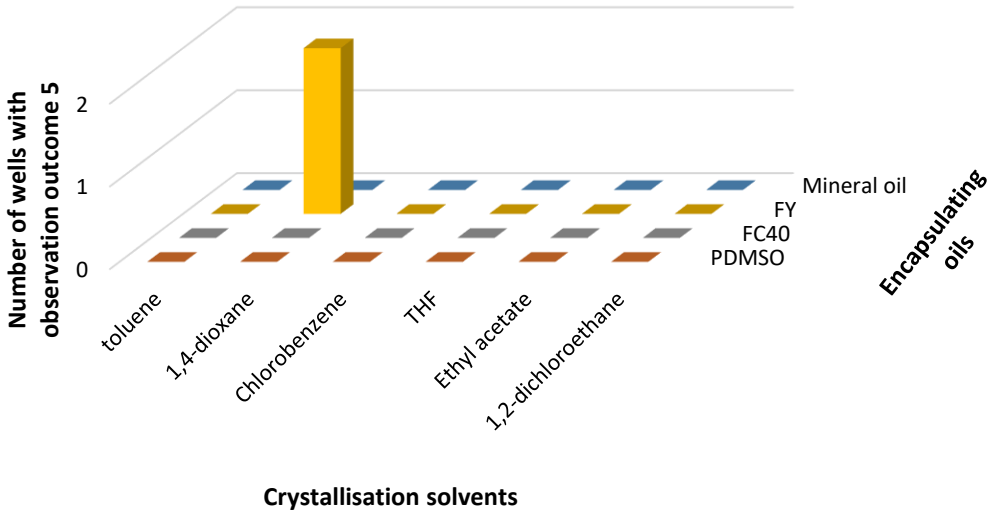

Figure 6.16: Number of single crystals with outcome 5 observed in rifampicin (**21**) encapsulated by four types of inert oils.

The optical microscopy showed that crystals of rifampicin (**21**) had grown in two morphologies, as either blocks (**1**) or plates (**2**). The plate like crystal (**2**) was then examined (Dr Michael Probert) using an in-house X-ray diffractometer (Figure **6.17**).

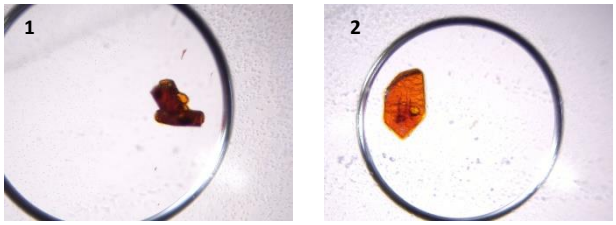

Figure 6.17: Rifampicin (**21**) single crystals observed from 1,4-dioxane with FY. (1) 50 nL 1,4-dioxane and (2) 100 nL 1,4-dioxane.

A complete X-ray crystal structure, using Cu Kα (λ = 1.54178 Å), was determined for the crystal grown from 1,4-dioxane and FY (**2**). This gave an excellent data set (Final R indexes = 0.0706) showing a orthorhombic P $2_12_12_1$ space group with unit cell dimensions of a = 20.2794(6) Å, b = 20.3110(5) Å, c = 27.8488(8) Å and angles of α = 90°, β = 90°, γ = 90°. Furthermore, direct measurement of the absolute stereochemistry was also possible, giving a moderate Flack parameter of 0.12(8).

Interestingly the X-ray crystal data showed that rifampicin had crystallised as a solvate with 1,4-dioxane, the crystal containing 2 molecules of rifampicin for every 3 molecules of 1,4-dioxane. Despite the extensive work undertaken in the search of rifampicin solvates,[111-115]

this rifampicin/1,4-dioxane solvate has not been previously reported. Interestingly, our rifampicin/1,4-dioxane solvate also appears to be a new type of rifampicin solvate as the structure does not map onto any of those knowb in the literature (Figure **6.18**).[115]

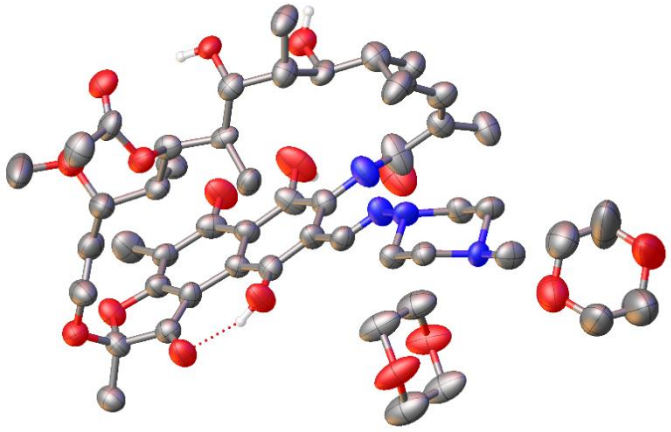

Figure 6.18: X-ray crystal structure of rifampicin 1,4-dioxane solvate.

In conclusion, we have successfully demonstrated that crystals of rifampicin (**21**) can be grown using ENaCt. We found that 1,4-dioxane/FY was the most successful solvent system from which to grow single crystals of rifampicin (**21**), resulting in the discovery of a new solvate. Encouraged with this successful result, we then attempted to apply the ENaCt method to our isolated natural product polyketides, (-)-rishirilide A and (+)-rishirilide B.

6.6 Encapsulated Nanodroplet Crystallisation (ENaCt) of the polyketides (-)-rishirilide A and (+)-rishirilide B

As discussed in Chapter 2 and 3, we have successfully isolated two natural product polyketides with antibiotic activity, (-)-rishirilide A (**29**) and (+)-rishirilide B (**30**) from *S. albus*::cos4. Although a crystal structure of (-)-rishirilide A (**29**) has been reported,[50] the absolute stereochemistry of (-)-rishirilide A (**29**) was not determined. Furthermore, although the structure and absolute stereochemistry of (+)-rishirilide B (**30**) has been determined through synthesis,[116] no crystal structure of (+)-rishirilide B (**30**) has been reported. Therefore, we wished to grow crystals of (-)-rishirilide A (**29**), in order to carry out a *de novo* absolute stereochemical determination, and (+)-rishirilide B (**30**) to provide the first crystal structure for this polyketide natural product.

Thus, we attempted to grow single crystals from both (-)-rishirilide A (**29**) and (+)-rishirilide B (**30**) using ENaCt. Similar to our previous ENaCt experiments, we prepared stock solutions of (-)-rishirilide A (**29**) in DMSO [9.8 mg/mL], whilst (+)-rishirilide B (**30**) was dissolved in 2 different solvents, DMF [16 mg/mL] and DMSO [12 mg/mL]. Using SPT Labtech mosquito® liquid-handling robot, 200 nL of each inert oil (PDMSO, FC40, FY and mineral oil) was dispensed onto a Laminex™ 96-well glass plates, followed by the addition of 50 nL of either (-)-rishirilide (A) (**29**) or (+)-rishirilide B (**30**) solution. It should be noted that also we examined the effects of oil encapsulation on the crystallisation of (-)-rishirilide (A) (**29**) and (+)-rishirilide B (**30**). Thus, in a typical 96-well glass plate columns 1 to 6 did not contain oils, whilst columns 7 to 12 contained 200 nL of each of the four test oils. The 96-well glass plates were then sealed and stored at room temperature, and the appearance of crystals was checked for after 1, 7, and 14 days (Scheme **6.5**).

Plate number		50 nL of (-)-rishirilide A or (+)-rishirilide B											
		without inert oils						with 200 nL inert oils addition					
		1	2	3	4	5	6	7	8	9	10	11	12
PDMS	A												
	B												
FC40	C												
	D												
FY	E												
	F												
Mineral oil	G												
	H												

Scheme 6.5: A typical arrangement of a 96-well glass plate containing either (-)-rishirilide A (**29**) or (+)-rishirilide B (**30**) solution and inert oils.

As before, the outcomes of the crystallisation experiments were categorized as either (1) in solution, (2) oiled-out, (3) non-crystalline or micro-crystalline, (4) small single crystals or (5) single crystals suitable for SCXRD.

After 14 days, none of the three 96-well glass plates for (-)-rishirilide A (**29**) in DMSO, (+)-rishirilide B (**30**) in DMSO and (+)-rishirilide B in DMF showed any crystals suitable for SCXRD (outcome 5). Most of the samples from both (-)-rishirilide A (**29**) and (+)-rishirilide B (**30**) had either remained in solution (outcome 1) or had oiled-out (outcome 2) (Table **6.1**).

	The number of wells with observation outcomes 1-5 of rishirilides, encapsulated with inert oil				
	Outcome 1	Outcome 2	Outcome 3	Outcome 4	Outcome 5
(-)-Rishirilide A	20	28	0	0	0
(+)-Rishirilide B	41	7	0	0	0
(+)-Rishirilide B	37	11	0	0	0

Table 6.1: Observation outcome (1-5) of single crystals growth of (-)-rishirilide A (**29**) and (+)-rishirilide B (**30**) under polarizing light microscope.

In conclusion, our initial attempts to grow single crystals of our isolated natural products, (-)-rishirilide A (**29**) and (+)-rishirilide B (**30**), using ENaCt have not proven successful. In the future we would wish to re-examine the use of ENaCt to crystallise both (-)-rishirilide A (**29**) and (+)-rishirilide B (**30**), however due to the limited quantities of (-)-rishirilide A (**29**) available, we decided to focus our attention on (+)-rishirilide B (**30**).

6.7 ENaCt crystallisation of (+)-rishirilide B with the addition of secondary solvents

Following on from our work on rifamcyin SV sodium, we decided to re-examine the crystallisation of (+)-rishirilide B (**30**) with the addition of secondary solvents.

Therefore, using an SPT Labtech mosquito® liquid-handling robot, 200 nL of each inert oil (PDMSO, FC40, FY and mineral oil) was dispensed onto a Laminex™ 96-well glass plate, followed by the addition of 50 nL of our stock solution of (+)-rishirilide B (**30**) in DMF [16 mg/mL]. Next 25, 50, 75 or 100 nL of a secondary solvent, toluene (aromatic), 1,4-dioxane (ether) and 1,2-dichloroethane (chlorinated), was then added. The 96-well glass plates were then sealed, stored at room temperature and appearance of crystals was looked for at day 1, 7 and 14 (Scheme **6.6**).

Plate number			50 nL of (+)-rishirilide B in DMF											
			Secondary solvent											
			25	25	25	50	50	50	75	75	75	100	100	100
			1	2	3	4	5	6	7	8	9	10	11	12
200 nL of inert oils	PDMS	A												
		B												
	FC40	C												
		D												
	FY	E												
		F												
	Mineral oil	G												
		H												

Scheme 6.6: A typical arrangement of a 96-well glass plate containing inert oils, (+)-rishirilide B (**30**) in DMF and the addition of a secondary solvent, toluene, 1,4-dioxane and 1,2-dichloroethane.

After 14 days, we checked all three of the 96 well plates containing (+)-rishirilide B (**30**) in DMF with secondary solvents for the presence of single crystals using cross-polarised light microscopy. Unfortunately, the majority of the ENaCt experiments were either still in solution (outcome 1) and had oiled-out (outcome 2) (Table **6.2**).

Secondary solvents	The number of observation outcomes 1-5 of (+)-rishirilide B in DMF				
	Outcome 1	Outcome 2	Outcome 3	Outcome 4	Outcome 5
Toluene	47	30	8	0	0
1,4-Dioxane	57	31	7	0	0
1,2-Dichloroethane	53	33	11	0	0

Table 6.2: Observation outcome (1-5) single crystals growth of (+)-rishirilide B (**30**) under crossed light microscope.

A few of the ENaCt experiments (26/288) showed very small crystals (outcome 3), but no crystals suitable for SCXRD were observed (Figure **6.19**).

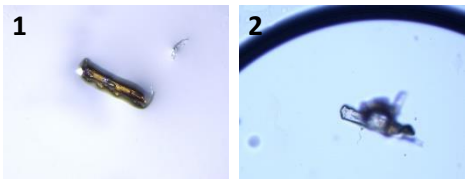

Figure 6.19: (+)-Rishirilide B (**30**) in DMF with the addition of secondary solvents: (**1** and **2**) in 1,2-dichloroethane.

In conclusion, we have attempted to grow single crystals of (+)-rishirilide B (**30**) in DMF with secondary solvents using ENaCt. Unfortunately, although some promising crystalline material

was observed, no single crystals suitable for SCXRD were obtained. Future work would look to refine our ENaCt with secondary solvent methods to grow crystals of (+)-rishirilide B (**30**).

6.8 Conclusion

The aim of this chapter was to investigate a new nanoscale high throughput crystallisation methodology (ENaCt) for the crystallisation and structural investigation of natural products by single crystal X-ray diffraction (SCXRD), to support our previous work in natural product discovery and isolation. In particular, we have looked at examples of terpenoids (CBD), polyketides (rifamycin SV sodium salt (**67**) and both (-)-rishirilide A and (+)-rishirilide B (**30**) and semi-synthetic polyketides (rifampicin (**21**)) in our crystallisation experiments.

In the case of the lipophilic terpenoids, we have shown that single crystals of CBD suitable for SCXRD could be grown using ENaCt. This work included showing that CBD could be crystallised via ENaCt from a number of novel solvent/oil systems including chlorinated (chloroform and 1,2-dichloroethane) or aromatic solvents (toluene and fluorobenzene) in combination with mineral oil.

For polyketides, our attempts to grow single crystals of (-)-rishirilide A (**29**) and (+)-rishirilide B (**30**) showed promise with some crystalline material observed, however further optimisation will be required to obtain crystals suitable for SCXRD. In the case of rifamycin SV sodium salt (**67**) we attempted two different approaches for ENaCt, firstly using single solvents and secondly using two solvent systems. Crystals were observed from both single solvent (DMF/FY) and two solvent (DMF/aromatics/FY and alcohols/butan-2-one/FY) experimental approaches, however single crystal X-ray diffraction data has yet to be obtained.

Finally, in the case of the semi-synthetic polyketide, rifampicin (**21**), single crystals were successfully grown from a single solvent/oil combination (1,4-dioxane/FY). SCXRD was also successful, giving high quality structural information and resulting in the discovery of a previously unknown 3:2 rifampicin:1,4-dioxane solvate.

Overall, we have successfully demonstrated that single crystals, suitable for SCXRD, of natural products and their derivatives can be grown using the ENaCt method, utilising only with small quantities material. We feel that the ENaCt approach could prove to be a valuable method for the structural analysis of sample limited natural products in the future.

Chapter 7. Conclusion and Future Work

7.1 Conclusion

The primary aim of this PhD project was to determine if (-)-rishirilide A (**29**) has antibiotic activity, based on its structural similarity to DEM30355/A (**28**). To achieve this, we examined several methods for the production and isolation of (-)-rishirilide A (**29**), via optimised bacterial fermentation. After demonstrating that (-)-rishirilide A (**29**) did indeed show antibiotic activity, we then examined the antibiotic mode of action this natural product. In addition, as a secondary aim we also examined the crystallisation of natural products, including both (-)-rishirilide A (**29**) and (+)-rishirilide B (**30**), using a new high-throughput nanoscale crystallisation to provide crystals for single crystal X-ray analysis.

Firstly, we examined the production of the (-)-rishirilide A (**29**) from the fermentation of the native bacteria *Streptomyces bottropensis* in liquid medium (GYM). However, only a small quantity of (+)-rishirilide B (**30**) was produced and no (-)-rishirilide A (**29**) could be observed. Thus, we next examined the engineered heterologous host *Streptomyces albus*::cos4 in the production of (-)-rishirilide A (**29**). Following extensive optimisation of both the fermentation and isolation methods, the fermentation of *S. albus*::cos4 (6 L, GYM) successfully produced both (-)-rishirilide A (25.3 mg) (**29**) and (+)-rishirilide B (55.9 mg) (**30**). This provided sufficient quantities to support full chemical characterisation (e.g. NMR) and further studies into the biology of both (-)-rishirilide A (**29**) and (+)-rishirilide B (**30**) (Figure **7.1**).

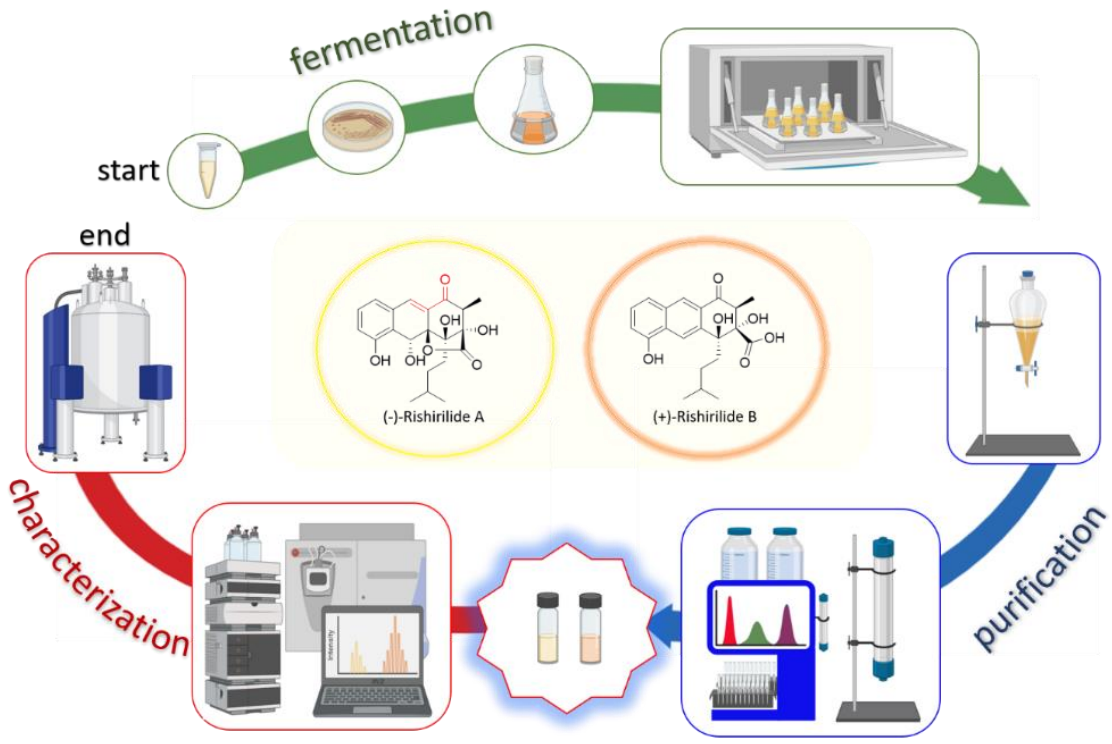

Figure 7.1: The production, isolation and characterisation of (-)-rishirilide A (**29**) and (+)-rishirilide B (**30**).

Our next step was to evaluated the antibiotic activity of both (-)-rishirilide A (**29**) and (+)-rishirilide B (**30**). (-)-Rishirilide A (**29**) showed antibiotic activity against Gram-positive bacteria (*S. aureus* RN4220, MIC = 1.56 μg/mL; *B. subtilis* 168CA, MIC = 3.125 μg/mL), whilst (+)-rishirilide B (**30**) was inactive. The further investigation into the mode of action of (-)-rishirilide A (**29**), using a $DiSC_3(5)$ (**36**) membrane potential assay in *B. subtilis* 168CA, suggested that bacterial cell death was associated with a loss of membrane potential (Figure **7.2**).

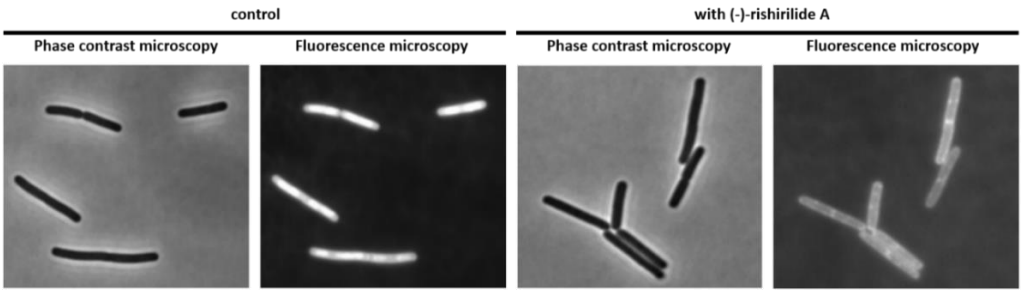

Figure 7.2: Phase contrast and fluorescence microscopy images of *B. subtilis* 168CA with $DiSC_3(5)$ (**36**) showing a loss in membrane potential; (**left**) control and (**right**) (-)-rishirilide A (**29**).

Further mode of action studies focussed on the presence of an α,β-unsaturated ketone moiety in (-)-rishirilide A (**29**), which could act as a Michael acceptor with biological

nucleophiles. We demonstrated that both (-)-rishirilide A (**29**) and the related natural product DEM30355/A (**28**) could undergo Michael addition reactions with thiols (L-cysteine (**41**), L-cysteine methyl ester (**43**) and the thiol containing short peptide LcrV (272-291) (**45**)) under biologically relevant conditions. Thus, we postulated that the mode of action of (-)-rishirilide A (**29**), and DEM30355/A (**28**), might involve the covalent modification of thiol containing target enzyme(s) (Figure **7.3**).

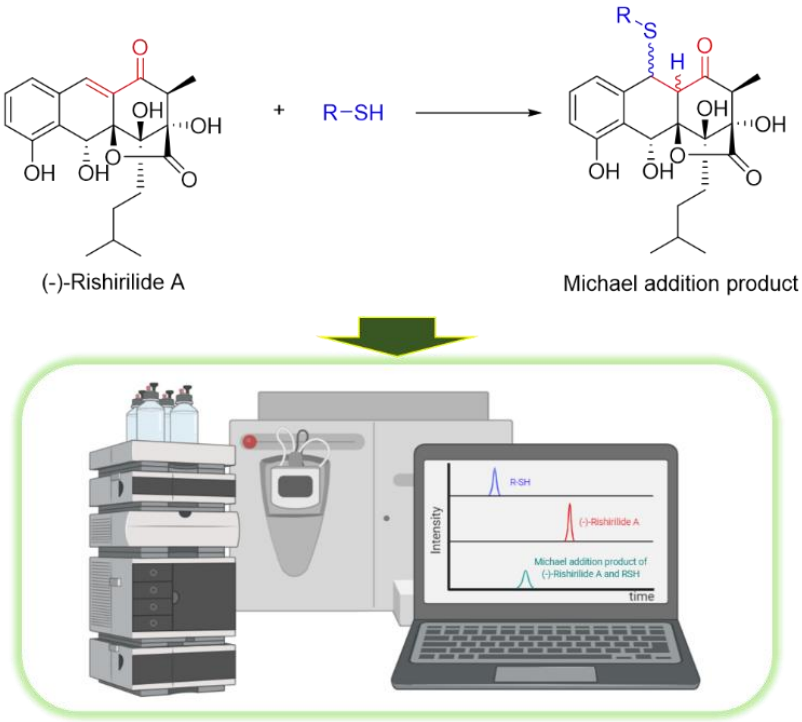

Figure 7.3: Michael addition reactions of (-)-rishirilide A (**29**) with thiol containing molecules and MS analysis.

Finally, we then attempted to chemically modify (-)-rishirilide A (**29**) to make chemical probes which could be used to identify target enzyme(s). Optimisation of the synthetic chemistry using a model compound (methyl 3-hydroxybenzoate (**57**)), showed that the phenolic moiety (present in (-)-rishirilide A (**29**)) could be *O*-alkylated to introduce a propargyl group followed by CuAAC ("Click") reaction with benzyl azide. Following which *O*-propargylation of (-)-rishirilide A was carried out, as confirmed by analytical LCMS. The next steps will be to examine *O*-propargyl (-)-rishirilide A in the identification of potential target enzymes (Figure **7.4**).

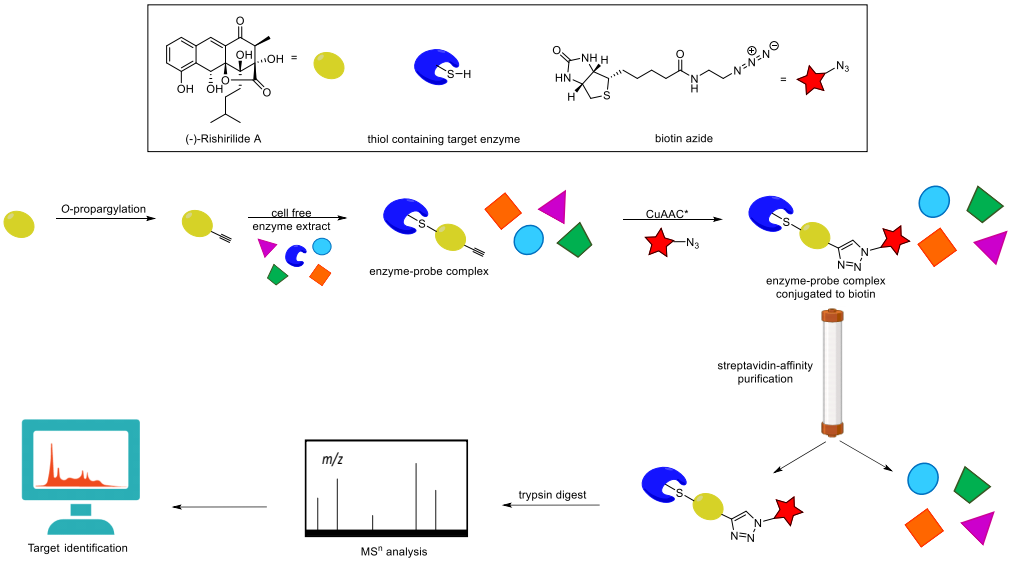

Figure 7.4: Proposed approach for target identification of (-)-rishirilide A (**29**). CuAAC*: Copper-catalysed Azide Alkyne Cycloaddition.

Our investigation of a new nanoscale high throughput crystallisation method (ENaCt) for the crystallisation and structural characterisation of natural products has resulted in a number of successful outcomes. In the case of the terpenoids, we have successfully grown single crystals of CBD (**66**) via ENaCt from a number of novel solvent/oil systems (e.g. aromatic solvents) with mineral oil. For the polyketides (-)-rishirilide A (**29**) and (+)-rishirilide B (**30**), we still need some further optimisation to be able to obtain crystals suitable for SCXRD, whilst for the rifamycin SV sodium salt (**67**), improvements (e.g. reducing the concentration to slow crystal growth) are required to obtain high quality single crystals. Finally, crystals of the semi-synthetic polyketide, rifampicin (**21**), suitable for SCXRD have been successfully obtained from 1,4-dioxane/FY, resulting in a new 3:2 rifampicin:1,4-dioxane solvate (Figure **7.5**).

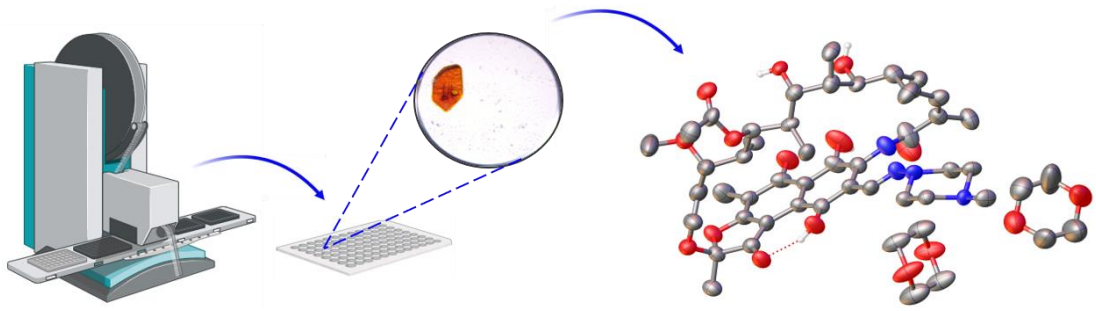

Figure 7.5: Crystallisation of the semi-synthetic polyketide rifampicin (**21**) via ENaCt, resulting in an X-ray crystal structure.

7.2 Future work

7.2.1 ENaCt crystallisation of (-)-rishirilide A and (+)-rishirilide B

In this work we have attempted to grow single crystals for SCXRD, via ENaCt, of both (-)-rishirilide A (**29**) and (+)-rishirilide B (**30**), as this would have allowed the assignment of absolute stereochemistry for (-)-rishirilide A (**29**) (currently unknown) as well as providing the first crystal structure of (+)-rishirilide B (**30**). Despite the success of ENaCt with other polyketides (e.g. rifampicin (**21**)) our attempts to grow suitable single crystals of suitable for SCXRD using ENaCt have so far proved unsuccessful. Thus, in the future we would like to carry out a more extensive investigation, via ENaCt, with a greater range of experimental conditions (e.g. reducing the concentration of sample solutions, and solvent systems). Since we are very sampled limited with (-)-rishirilide A (**29**) and (+)-rishirilide B (**30**), we would first look to optimise our ENaCt conditions using a related natural product polyketide, such as a commercially available tetracycline. Then we would apply our optimised conditions to our isolated natural products (-)-rishirilide A (**29**) and (+)-rishirilide B (**30**), hopefully allowing access to suitable crystals for SCXRD.

7.2.2 Antibiotic target validation of (-)-rishirilide A

During the course of this project, we have shown that (-)-rishirilide A (**29**) has interesting antibiotic activity, however we do not know its mode of action. We have also demonstrated that (-)-rishirilide A (**29**) can undergo Michael addition chemistry, and we have preliminary evidence supporting the *O*-propargylation of (-)-rishirilide A (**29**) as a method to synthesis a chemical probe. Thus, our next challenge will use *O*-propargylated (-)-rishirilide A (**63**) to help to identify the enzymatic target of (-)-rishirilide A (**29**) responsible for its antibiotic activity. To do this we would first show that *O*-propargyl-(-)-rishirilide A (**63**) has retained its antibiotic activity. Then we would react *O*-propargyl-(-)-rishirilide A (**63**) with a cell free extract of enzymes from a suitable bacteria (e.g. *B. subtilis*). We hope that *O*-propargyl-(-)-rishirilide A (**63**) will undergo a Michael addition with the target enzyme(s), forming a covalent adduct. Following which we would use a CuAAC reaction to attach a biotin label to the *O*-propargyl-(-)-rishirilide A-enzyme adduct to allow purification from the cell free enzymes extract. Subsequent trypsin digest and MS^n analysis would allow us to identify the target enzyme(s). Finally, we would wish to validate these target enzymes as responsible for the antibiotic

activity. This would involve both enzyme knocked-out models, to show that the enzyme target(s) is vital to bacterial survival, as well as expression of the target enzyme(s), crystallisation for X-ray/cryoEM structural analysis and finally "soak studies" to show that (-)-rishirilide A can bind to the target enzyme(s).

7.2.3 Chemical conversion of (-)-rishirilide A into (+)-rishirilide B

Finally, during the Michael addition reactions of (-)-rishirillide A (**29**) with the short peptide LcrV (272-291) (**45**) in the presence of DTT, we observed not only the predicted Michael addition adduct (**46**) of (-)-rishirilide A with LcrV (272-291), but also a new peak in the LCMS which corresponded to the formation of the related natural product (+)-rishirilide B (**30**).

Interestingly, Danishefsky *et al*. has previously proposed that (-)-rishirilide A (**29**) could be synthesised from (+)-rishirilide B (**30**) via an oxidative lactonisation reaction. However, he was unsuccessful in his attempts to carry out this chemistry in the laboratory.[110] We proposed that we may have observed the reverse reaction, in which DTT is acting as a reducing agent to convert (-)-rishirilide A (**29**) into (+)-rishirilide B (**30**).[111] Therefore, to prove this previous unobserved transformation, we would wish to re-examine the reaction of (-)-rishirilide A (**29**) with DTT on a sufficient scale to allow for the isolation and unambiguous characterisation of any (+)-rishirilide B (**30**) produced (Figure **7.6**).

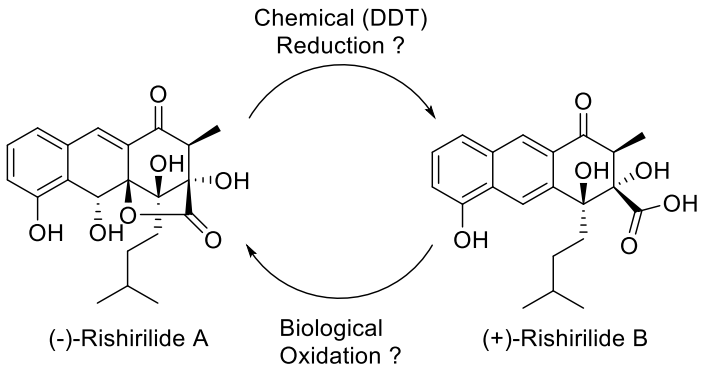

Figure 7.6: Proposed conversion between natural product polyketides, (-)-rishirilide A (**29**) and (+)-rishirilide B (**30**).

Chapter 8. Experimental

General experimental information: Microbiology

All procedures were done under sterile conditions.

8.1 Sources of *Streptomyces* strains

Streptomyces bottropensis and *Streptomyces albus*::cos4 were obtained from Prof. Andreas Bechthold, Freiburg University, Germany. These *Streptomyces* strains from Prof. Andreas Bechthold were stored in agar plates and for the storage, the grown spores on agar were harvested with the use of a sterile loop and transferred into a 20% glycerol solution in a 2 mL Eppendorf tube and stored at - 80 °C. For the revival of both *Streptomyces* strains, spores which are suspended in 20% glycerol solutions and stored at - 80 °C, are thawed and a loop-full of spores is collected, inoculated on solid suitable medium and then incubated for 2 to 7 days (depending on the strain) at 30 °C.

8.2 Liquid and solid growth media

Growth media were prepared in Duran glass bottles, using distilled water and the components listed below. Next, to the growth media was added 1 M $HCl_{(aq)}$ or 1 M $NaOH_{(aq)}$ to give desired pH of the growth media. To prepare solid growth media 20% agar-agar was added. Growth media were then sterilised in an Astell autoclave at 121 °C for 30 minutes. Liquid growth media were allowed to cool to room before use. Solid growth media were cooled to 50 °C in a water bath before pouring onto plates, after which they were allowed to cool to room temperature before use (Table **8.1**).

Growth Medium	Components per 1 L of medium	pH media
Nutrient broth (NB)	5 g peptone, 3 g yeast extract, 1 g glucose, and 6 g NaCl	pH 7.0
Nutrient agar (NA)	5 g peptone, 1.5 g yeast extract, 1.5 g beef extract and 5 g NaCl	pH 7.4
GYM	4 g yeast extract, 10 g maltose extract and 4 g glucose	pH 7.0
TSB	30 g tryptic soy broth	pH 7.2
SFM	20 g soy-bean flour and 20 g mannitol[a]	pH 7.0

a) tap water used in place of distilled water.

Table 8.1: A list of growth media and their composition.

8.3 Kirby-Bauer disc diffusion test

8.3.1 Test against Gram-positive and Gram-negative bacteria

Autoclaved NA and NB (1:1) were medium/agar used for antibiotic activity test. Typically for 100 mL NA and NB mixture, 100 µL of *E. coli*^{kanR} (Gram-negative) *or B. subtilis*^{eryR} (Gram-positive), 100 µL of antibiotic stock solution and 100 µL 5-bromo-4-chloro-3-indolyl-β-D-galactopyranoside (X-Gal) were added to the mixture of NA and NB. The diffusion agar mixture was then poured onto agar plates under sterile condition and allowed to settle before use.

Discs of sterile filter paper (5 mm in diameter) were labelled and spotted by 10 µL of samples, positive and negative controls and then allowed to dry. The spotted discs were mounted onto diffusion agar and incubated in Sanyo Ltd MIR-262 at 30 °C overnight. The zone of inhibition was recorded using a ruler (in mm) in the next day (Table **8.2**).

Representative of bacteria	Resistance	Positive control
E. coli^{kanR}(Gram-negative)	Kanamycin	Ampicillin
B. subtilis^{eryR}(Gram-positive)	Erythromycin	Bacitracin

Table 8.2: Bacteria used in antibiotic activity test against Gram-negative and Gram-positive bacteria.

8.3.2 Minimum inhibitory concentration (MIC) assay

For the minimum inhibitory concentration assay, we used two Gram-positive bacteria, *S. aureus* RN4220 and *B. subtilis* 168CA. The *S. aureus* RN4220 was derived from *S. aureus* NCT8325-4 using UV and chemical mutagenesis[119], whilst *B. subtilis* 168CA was isolated from Marburg strain which has been mutagenized by X-ray[120]. The MIC assay of (-)-rishirilide A and DEM30355/A against *S. aureus* RN4220 and *B. subtilis* 168CA was carried out by Dr B. Kepplinger.

8.3.3 Test against Gram-positive reporter strains

For assessing mode of action of samples, Kirby-Bauer disc diffusion assay was used. Autoclaved NA and NB (1:1) were the agar medium used for antibiotic activity test. Typically for 100 mL NA and NB mixture, 100 µL of *B. subtilis* reporter strains (*YvqI*^{eryR}, *YpuA*^{eryR}, *YvgS*^{eryR}, *YheH*^{eryR}, or *YjaX*^{eryR}), 100 µL of antibiotic stock solution and 100 µL of 5-bromo-4-chloro-3-indolyl-β-D-galactoside (X-Gal) were added to the mixture of NA and NB. The diffusion agar

mixture was then poured onto agar plates under sterile condition and allowed to settle before use.

Five reporter strains of *B. subtilis* which represent different mode of action were used to assess the mode of action of samples with the addition of X-Gal (Table **8.3**).

Bacillus reporter strain	Mode of action	Resistance	Positive control
YvqI^{erytR}	Lipid II (cell envelope)	Erythromycin	Bacitracin
YpuA^{erytR}	Cell wall synthesis	Erythromycin	Cefotaxime
YvgS^{erytR}	RNA synthesis	Erythromycin	Rifampicin
YheH^{erytR}	Protein synthesis	Erythromycin	Chloramphenicol
YjaX^{erytR}	Fatty acid synthesis	Erythromycin	Triclosan

Table 8.3: Reporter strains used in assessing mode of action of *B subtilis*.

8.3.4 Antibiotics

The stock concentration of antibiotics used for bioactivity screening are shown below (Table **8.4**).

Antibiotics	Concentrations(mg/L)	Solvents
Apramycin	50	H_2O
Chloramphenicol	25	70% ethanol in H_2O
Kanamycin	50	H_2O
Ampicillin	100	H_2O
Bacitracin	50	H_2O
Cefotaxime	25	H_2O
Erythromycin	3	70% ethanol in H_2O
Rifampicin	100	DMSO
Triclosan	5	70% ethanol in H_2O

Table 8.4: Antibiotic used in assessing antibiotic activity and their concentrations.

8.3.5 Solution for blue halo selection in bioassay

Solution of 5-bromo-4-chloro-3-indolyl-β-D-galactopyranoside (X-Gal) was prepared in DMF with the final concentration of 10 g/mL. The X-Gal solution was stored in 4 °C fridge.

8.4 Liquid fermentation of Streptomyces bottropensis and Streptomyces albus::cos4

8.4.1 Fermentation of *Streptomyces bottropensis* in liquid medium (GYM)

The production of (-)-rishilirilide A and (+)-rishirilide B from *S. bottropensis* was started by growing *S. bottropensis* on SFM agar. One eighth of the area of the agar plate containing *S. bottropensis* colonies were then taken by a sterile loop and placed into 50 mL TSB medium in a 250 mL baffled flask. The culture was incubated at 28 °C in Innova®40 enclosed orbital shaker (140 rpm) overnight. This culture was kept sequentially growing into 500 mL GYM medium in 2 L baffled flasks using a 10% inoculum. The fermentation broths were then incubated at 28 °C for 5 days. During the fermentation, approx. 1-2 mL of the fermentation broth was collected into a 2 Eppendorf vial which was then used to monitor the pH and to

test the antibiotic activity of *S. bottropensis* against *E. coli*^{kanR} and *B. subtilis*^{eryR} using a Kirby Bauer diffusion test.

8.4.2 Fermentation of *Streptomyces albus*::cos4 in liquid medium (GYM)

S. albus::cos4 was grown on SFM agar containing apramycin (50 μg/mL). One eighth of the area of the agar plate containing *S. albus*::cos4 colonies were taken and inoculated 50 mL TSB medium and incubated at 28 °C in Innova®40 enclosed orbital shaker (140 rpm) overnight. This culture was kept sequentially growing into 500 mL GYM medium in 2 L baffled flasks using a 10% inoculum and incubated at 28 °C overnight. Each 2 L baffled flask was used for 500 mL fermentation broth to allow enough aeration, thus if we carried out 1 L liquid fermentation, two 2 L baffled flasks were used, whilst to carry out 6 L fermentation, twelve 2 L baffled flasks were used. Then all the 2 L baffled flasks were incubated at 28 °C in a shaker incubator (140 rpm) for 5 days.

8.4.3 Large scale fermentation of *S. albus*::cos4 in liquid medium (GYM) using a 20 L bioreactor

S. albus::cos4 was grown on SFM agar containing apramycin (50 μg/mL). One eighth of the area of the agar plate containing *S. albus*::cos4 colonies were taken and inoculated 50 mL TSB medium and incubated at 28 °C in Innova®40 enclosed orbital shaker (140 rpm) overnight. This culture was kept sequentially growing into 800 mL GYM medium in 5 L baffled flasks using a 10% inoculum and incubated at 28 °C in a shaker incubator (140 rpm) overnight. Then the culture in 5 L baffled flask was transferred into 16 L GYM medium in a 20 L EZ-Control bioreactor. The temperature of bioreactor was set to30 °C with a stirrer of 250 rpm and the fermentation broth in the bioreactor was incubated for 5 days.

8.4.4 Extraction of the fermentation broth of *S. bottropensis* and *S. albus*::cos4

Fermentation broth of *S. bottropensis* or *S. albus*::cos4 was harvested at day 5 by adding resin Amberlite XAD-16N (20 g/L) and then incubated on a shaker overnight. The next day, the Amberlite XAD-16N was filtered from the fermentation broth using a sieve and then washed with distilled water (2 x 100-500 mL). The Amberlite XAD-16N was then soaked with methanol (250-2500 mL) overnight to let the Amberlite XAD-16N release secondary metabolites into methanol. Subsequently, the Amberlite XAD-16N was removed using filtration and the methanol solution was then concentrated under reduced pressure. To the methanol extract, was added water (100 – 1000 mL) and washed with petroleum ether (2 x 100-1000 mL) to remove lipids. The aqueous layer was acidified to pH 4 with 1 M $HCl_{(aq)}$ and extracted with

ethyl acetate (2 x 100-1000mL). The ethyl acetate extract was then concentrated under reduced pressure (Figure **8.1**).

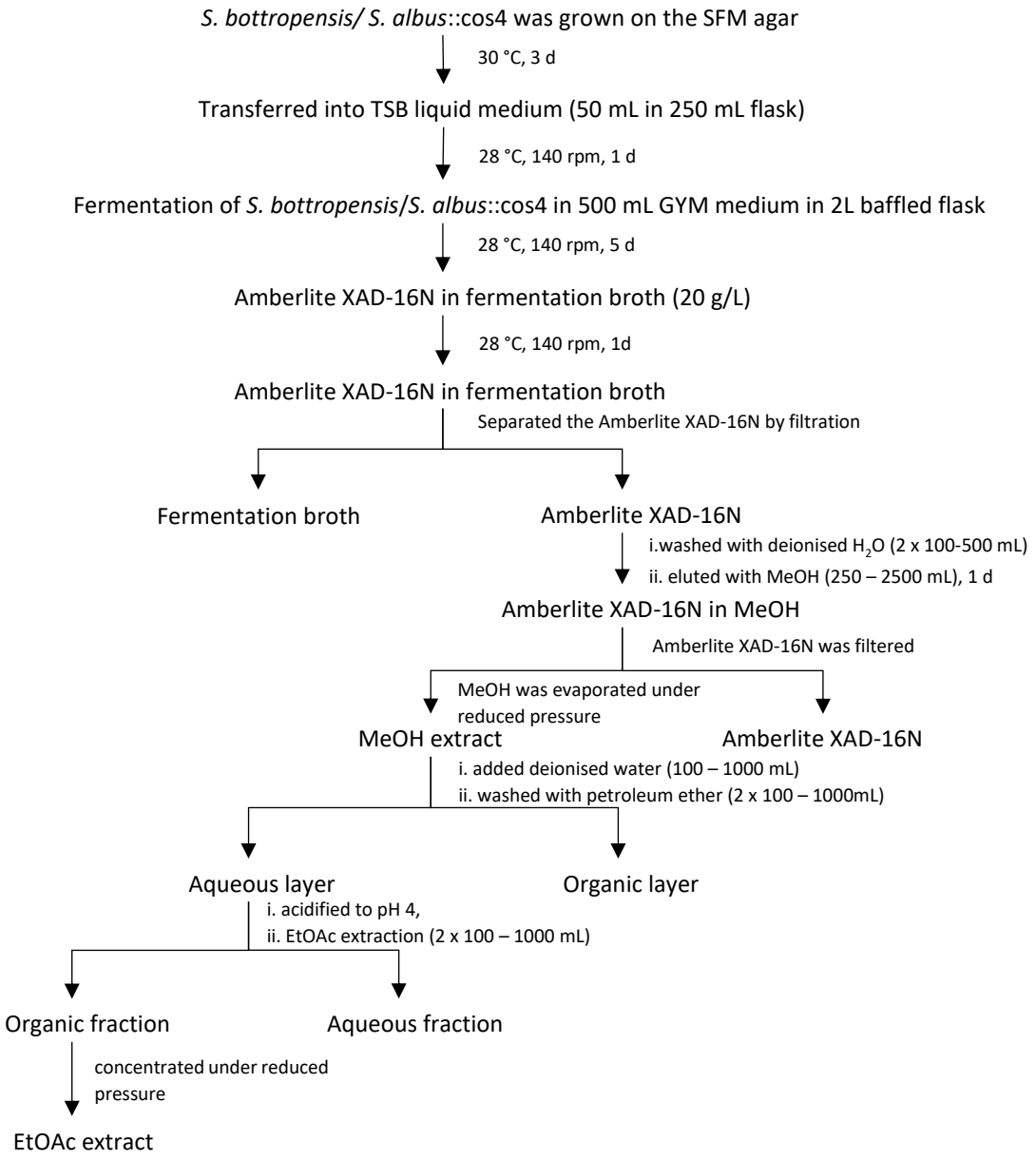

Figure 8.1: Flow diagram of liquid fermentation of *S. albus*::cos4 and liquid-liquid extraction.

8.5 Purification of (-)-rishirilide A and (+)-rishirilide B

8.5.1 Analytical High-Performance Liquid Chromatography (HPLC)

Analytical HPLC were performed on an Agilent 1260 infinity HPLC instrument equipped with an integrated diode array detector (DAD). Two of the following columns were used for all

HPLC analysis: Agilent Eclipse Plus C-18 column (4.6 x 150 mm, 3.5 µm) and Agilent Eclipse Plus C-18 column (4.6 x 250 mm, 5 µm) column. For analytical HPLC, gradient elution was performed from 20:80 to 95:5, acetonitrile (0.1% by v/v FA) and water (0.1% by v/v FA) over 35 minutes at a flowrate of 0.5 mL/min. Analytes were dissolved in 20:80, methanol : water to give a final concentration of 1 mg/mL and the resulting analyte solutionwas filtered with a 0.22 µm Millipore syringe filter. The volume of analyte used for analytical HPLC were between 20 to 50 µL. The UV/Vis absorbance was monitored at 254 nm and 320 nm (Table **8.5**).

Time (mins)	Solvent A (%)	Solvent B (%)
0	80	20
6	80	20
7	70	30
25	5	95
28	5	95
30	80	20
35	80	20

Flow rate 0.5 mL/min

Table 8.5: Gradient elution for analytical HPLC (Solvent A: water with 0.1% by v/v FA; Solvent B: acetonitrile with 0.1% by v/v FA).

8.5.2 Preparative High-Performance Liquid Chromatography (HPLC)

Preparative HPLC was performed on an Agilent 1260 infinity HPLC instrument equipped with an integrated diode array detector (DAD) and an Agilent Preparative C-18 column (10 x 250 mm, 5 µm). Gradient elution was performed from 20:80 to 95:5, acetonitrile (0.1% by v/v FA) and water (0.1% by v/v FA) over 35 minutes at a flowrate of 1 mL/min. Samples were dissolved in 20:80, methanol : water to give a final concentration up to 10 mg/mL, and the resulting sample mixture was filtered by 0.22 µm Millipore syringe filter. The injection volumes were between 500 and 800 µL. The UV/Vis absorbance was monitored at 254 and 320 nm.

8.5.3 Flash chromatography

Automated normal phase flash column chromatography was conducted with the use of both Biotage Isolera One and Biotage Isolera Large Scale (LS). SNAP KP-Sil or ULTRA (25 g, 50 g and

100 g) cartridges were used. To load a sample into the normal phase cartridge, the following two methods were carried out: (a) the sample was dissolved and directly injected into the cartridge and (b) sample was dry loaded onto the cartridge. To dry load, samples need to be absorbed into silica gel which can be done by dissolving the sample with suitable solvent. Then silica gel was added to absorb the resulting sample solution, followed by removing the solvent under reduced pressure to give dry silica containing sample (Table **8.6**).

	Solvent mixture		Length (Column Volume)
Equilibrium	A/B	0%	2.0
1	A/B	0% - 2%	2.0
2	A/B	2% - 10%	10.0
3	A/B	10% - 100%	10.0
4	A/B	100%	3.0
Flow rate 50 mL/min			

Table 8.6: Gradient elution for flash chromatography (Solvent A: methanol; Solvent B: dichloromethane).

8.5.4 Solid Phase Extraction (SPE)

Solid phase extraction (SPE) was performed using HyperSep C-18 extraction cartridge (100 mg bed weight and of silica C-18 with 3 mL column capacity). Prior to sample loading, cartridges were conditioned with methanol (3 x 3 mL), and then equilibrated with water (3 x 3 mL).

The ethyl acetate extract was dissolved with water. The resulting mixture was loaded onto the cartridge, washed 3-5 times with water and then eluted 2-3 times with methanol. The resulting methanol filtrate was evaporated under reduced pressure to give ethyl acetate/SPE extract.

8.5.5 Preparative Size Exclusion Chromatography (SEC)

Preparative size exclusion chromatography was carried out using glass columns (length 40 cm and 5 cm diameter) packed with Sephadex LH-20 gel in HPLC-grade methanol. Sample was dissolved with HPLC-grade methanol and loaded onto the gel using a glass syringe. With a

flowrate of 1 mL/min, fractions were collected into vials. Vials containing (-)-rishirilide A and (+)-rishirilide B were combined and concentrated under reduced pressure.

8.5.6 Liquid Chromatography Mass Spectrometry (LCMS)

LCMS analysis was performed on an Agilent 1260 Infinity HPLC system, equipped with an integrated diode array detector (DAD) and a C-18 Eclipse plus column (100 x 4.6 mm, 3.5 μm), coupled to a Bruker micrOTOF II mass spectrometer operating in positive electrospray ionization (ESI) mode. A typical gradient elution was performed using 20:80 to 95:5, acetonitrile (0.1% by v/v FA) and water (0.1% by v/v FA) over 35 minutes at a flow rate of 0.2 mL/min. Samples were dissolved in 20:80, methanol:water to give a final concentration up to 1 mg/mL, then filtered by 0.22 µm Millipore syringe filter. 2 µL of injection volume of sample was used for LCMS analysis.

General experiment information: Michael addition

To monitor Michael addition reaction, LCMS analysis was performed on an Agilent 1260 Infinity HPLC system, equipped with an integrated diode array detector (DAD) and a C-18 Eclipse plus column (100 x 4.6 mm, 3.5 μm), coupled to a Bruker micrOTOF II mass spectrometer operating in positive electrospray ionization (ESI) mode. A typical gradient elution was performed using 5:95 to 100:0, acetonitrile (0.1% by v/v FA) and water (0.1% by v/v FA) over 60 minutes at a flow rate of 0.2 mL/min. Samples were dissolved in 20:80, methanol:water. The sample volume used in Michael addition was 2 µL (Table **8.7**).

Time (mins)	Solvent A (%)	Solvent B (%)
0	95	5
2	95	5
30	0	100
35	0	100
40	95	5
50	95	5
Flow rate = 0.2 mL/min		

Table 8.7: Gradient elution for LCMS (Solvent A: water with 0.1% by v/v FA; Solvent B; acetonitrile with 0.1% by v/v FA).

8.6 Michael addition of (-)-rishirilide A

Stock solution of (-)-rishirilide A was prepared by dissolving (-)-rishirilide A (10 mg, 0.0257 mmol) with methanol (10 mL) to give 2.57 mM methanol stock solution of (-)-rishirilide A. The stock solution of L-cysteine was freshly prepared by dissolving L-cysteine hydrochloride (1.57 mg, 0.0100 mmol) with 1 mL of deionised water (1 mL) to give 0.01 M solution. In addition, the stock solution of L-cysteine methyl ester was freshly prepared by dissolving L-cysteine methyl ester hydrochloride (1.72 mg, 0.0100 mmol) with deionised water (1 mL) to give 0.01 M solution.

8.6.1 (-)-Rishirilide A – cysteine (42)

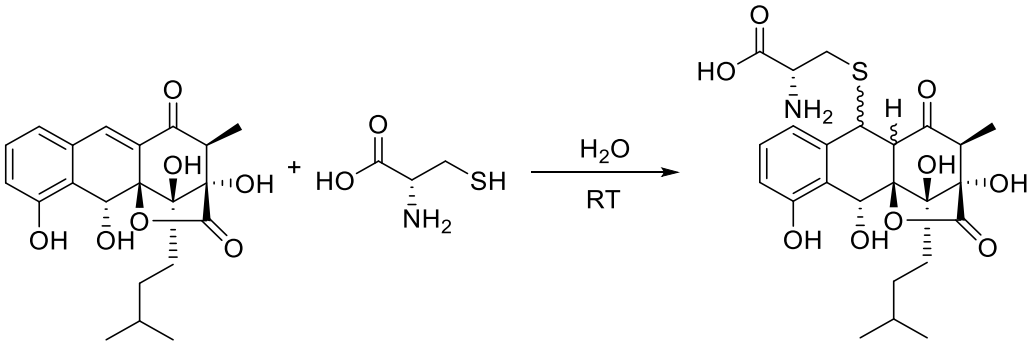

29 **41** **42**

To a 5 mL pear shaped round bottom flask (RBF), was added water (654 µL), of a 0.01 M solution of L-cysteine hydrochloride in water (96 µL, 0.960 µmol) and 2.57 mM solution of (-)-rishirilide A in methanol (250 µL, 0.640 µmol). The resulting mixture was stirred for 150 minutes at room temperature. At 30, 60, 90, 120 and 150 mins, a 50 µL aliquot of the reaction mixture was taken, diluted into 250 µL of water and analysed by LCMS to examine the presence of the Michael addition of (-)-rishirilide A-cysteine product (**42**).

8.6.2 (-)-Rishirilide A - cysteine methyl ester (44)

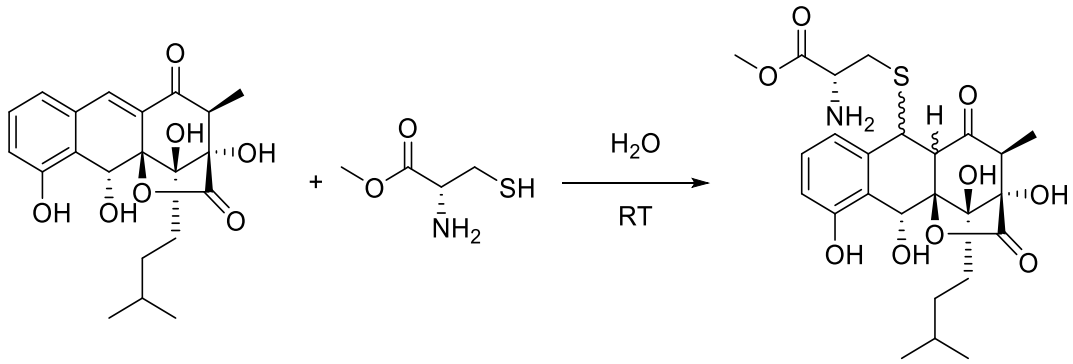

29 **43** **44**

To a 5 mL pear shaped RBF, was added water (654 µL), 0.01 M solution of L-cysteine methyl ester hydrochloride in water (96 µL, 0.960 µmol) and 2.57 mM solution of (-)-rishirilide A in methanol (250 µL, 0.640 µmol). The resulting mixture was stirred at room temperature for 180 mins. Subsequently, at 30, 60, 90, 120, 150 and 180 mins, a 50 µL aliquot of the reaction mixture was taken, diluted into 250 µL water to stop the reaction and analysed by LCMS to examine the presence of the Michael addition of (-)rishirilide A-cysteine methyl ester product (**44**).

8.6.3 (-)-Rishirilide A – LcrV (272-291) (46)

The concentration of the LcrV (272 – 291) was 4.5 mM in 20 mM dithiothreitol (DTT). (-)-Rishirilide A was prepared by dissolving (-)-Rishirilide A (8.9 mg, 0.023 mmol) in 1 mL DMSO to give final concentration of 23 mM. The buffer used in this experiment was buffer Tris pH 8 with concentration of 200 mM.

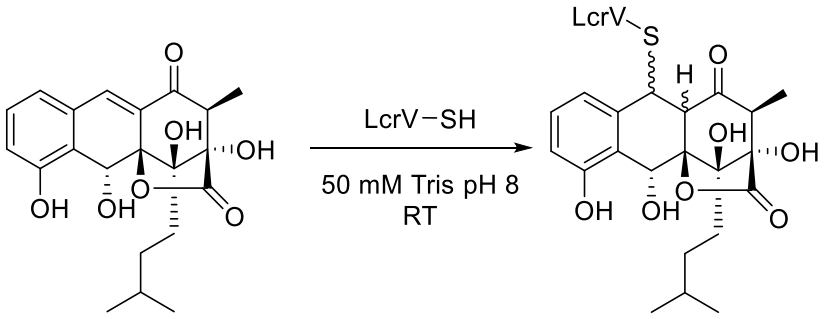

To a 0.2 mL Eppendorf tube, was added water (1.9 µL), 4.5 mM solution of LcrV (272 – 291) in 20 mM DTT (4.4 µL, 0.020 µmol), 200 mM solution of Tris buffer (pH 8 in water) (5 µL, 1.0 µmol) and 23 mM solution of (-)-rishirilide A (**1**) in methanol (8.7 µL, 0.20 µmol). The resulting mixture was mixed for 5 seconds at room temperature using vortex. After 0, 15, 30, 45 and 60 minutes, 2 µL aliquots were taken, diluted into 10 µL water and then analysed with LCMS to examine the presence of Michael addition (-)-rishirilide A- LcrV (272-291) product (**46**).

8.7 Michael addition of (+)-rishirilide B

Stock solution of (+)-rishirilide B was prepared by dissolving (+)-rishirilide B (10 mg, 0.027 mmol) with methanol (10 mL) to give 2.70 mM solution. The stock solution of L-cysteine was freshly prepared by dissolving L-cysteine hydrochloride (1.57 mg, 0.0100 mmol) with deionised water (1 mL) to give 0.01 M solution. In addition, the stock solution of L-cysteine methyl ester was freshly prepared by dissolving L-cysteine methyl ester hydrochloride (1.72 mg, 0.01 mmol) with deionised water (1 mL) to give 0.01 M solution.

8.7.1 (+)-Rishirilide B – cysteine (49)

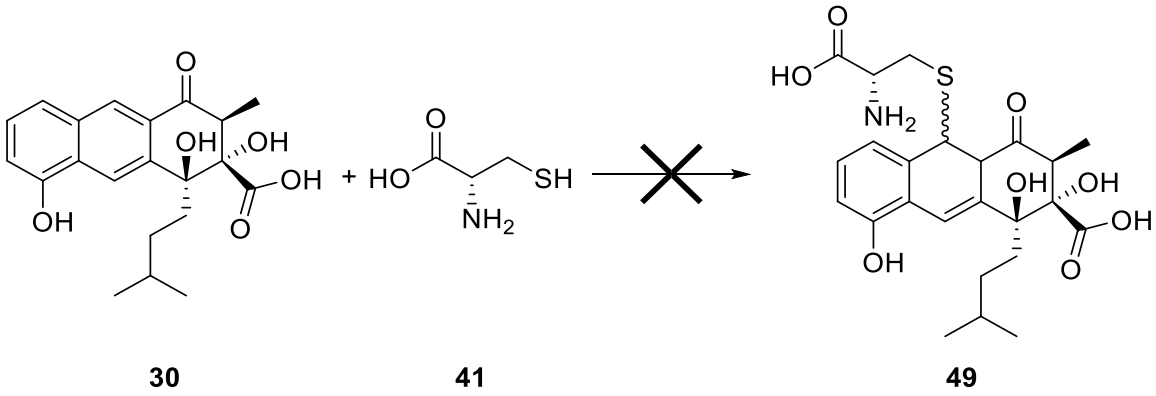

30 **41** **49**

To a 5 mL pear shaped RBF, was added water (649 µL), 0.01 M solution of L-cysteine hydrochloride in water (101 µL, 1.01 µmol) and 2.69 mM solution of (+)-Rishirilide B (**2**) in methanol (250 µL, 0.670 µmol). The resulting mixture was stirred for 180 minutes at room temperature. At 30, 60, 90, 120, 150 and 180 mins, a 50 µL aliquot of the reaction mixture was diluted into 250 µL of water, and then analysed using LCMS to examine the presence of the Michael addition of (+)-rishirilide B-cysteine product (**49**).

8.7.2 (+)-Rishirilide B – cysteine methyl ester (50)

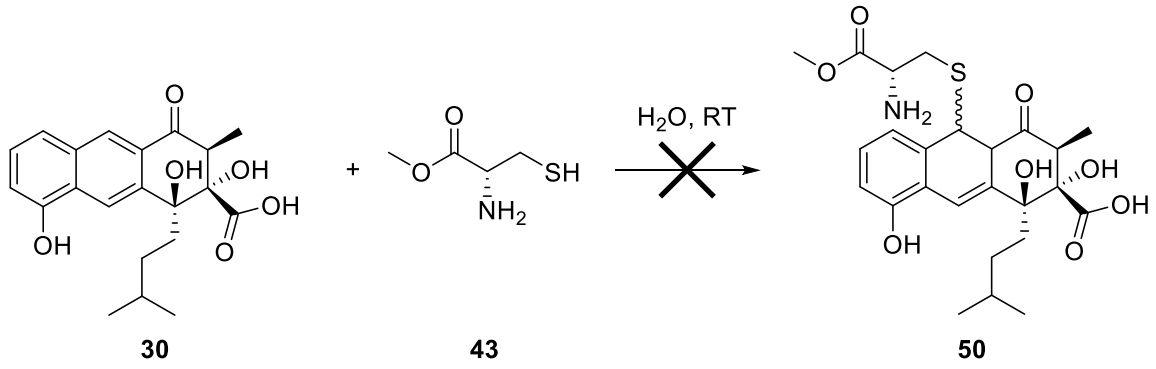

30 **43** **50**

To a 5 mL pear shaped RBF, was added water (649 µL), 0.01 M solution of L-cysteine methyl ester hydrochloride in water (101 µL, 1.01 µmol) and 2.69 mM solution of (+)-rishirilide B in methanol (250 µL, 0.670 µmol). The resulting mixture was reacted for 180 minutes at room temperature. At 30, 60, 90, 120, 150 and 180 mins, a 50 µL aliquot of the reaction mixture was taken, diluted into 250 µL of water, and subsequently analysed by LCMS to examine the presence of the Michael addition of (+)-rishirilide B-cysteine methyl ester product (**50**).

8.7.3 (+)-Rishirilide B - short peptide LcrV (272-291) (51)

For Michael addition with LcrV (272 – 291), (+)-Rishirilide B was prepared into 33.3 mM solution by dissolving (+)-Rishirilide B (12.4 mg, 0.033 mmol) with DMSO (1 mL). The concentration of LcrV (272 – 291) containing one cysteine was 4.5 mM and the buffer Tris pH 8 was 200 mM.

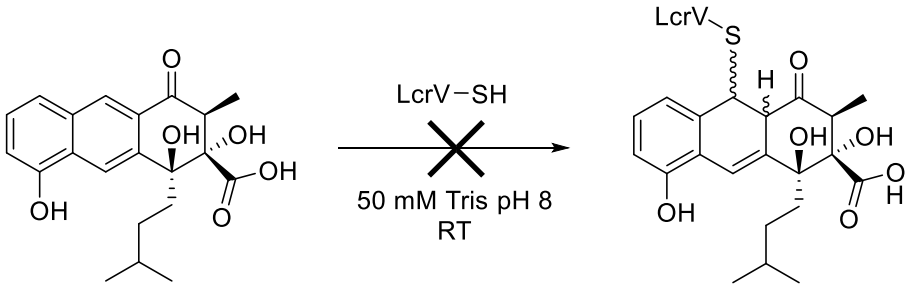

30 **51**

To a 0.2 mL Eppendorf tube, was added water (4.6 µL), 4.5 mM solution of LcrV (271-291) in 20 mM DTT (4.4 µL, 0.020 µmol), 200 mM Tris buffer (pH 8 in water) (5 µL, 1.0 µmol) and 33.3 mM solution of (+)-rishirilide B in methanol (6 µL, 0.20 µmol). The resulting mixture was mixed for 5 seconds (vortex) at room temperature. At 0, 30 and 60 minutes, 2 µL aliquots of the reaction mixture was taken, diluted into 10 µL of water, and then analysed by LCMS to examine the presence of Michael addition of (+)-rishirilide B-LcrV (272-291) product (**51**).

8.8 Michael addition of DEM30355/A

Stock solution of DEM30355/A was prepared by dissolving DEM30355/A (10 mg, 0.025 mmol) with DMSO (10 mL) to give 2.50 mM solution. The stock solution of L-cysteine was freshly prepared by dissolving L-cysteine hydrochloride (1.57 mg, 0.0100 mmol) with of deionised water (1 mL) to give 0.01 M solution. In addition, the stock solution of L-cysteine methyl ester was freshly prepared by dissolving L-cysteine methyl ester hydrochloride (1.72 mg, 0.0100 mmol) with of deionised water (1 mL) to give 0.01 M solution.

8.8.1 DEM30355/A – cysteine (52)

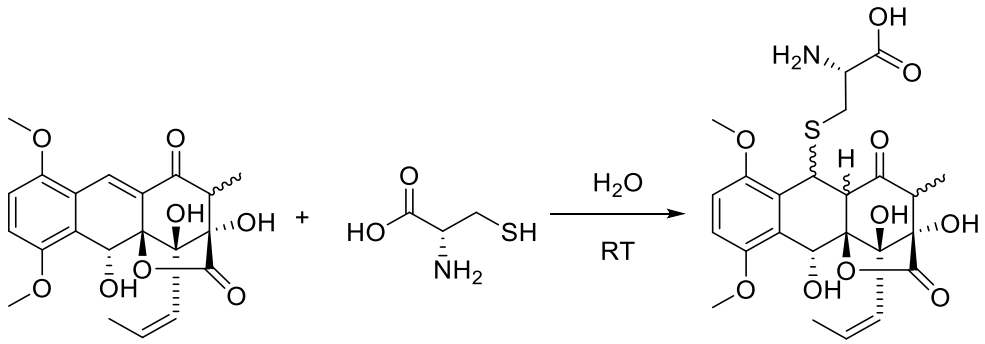

28 41 52

To a 5 mL pear shaped RBF, was added water (725 µL), 0.01 M solution of L-cysteine hydrochloride in water (75 µL, 0.75 µmol) and of a 2.50 mM solution of DEM30355/A in DMSO (200 µL, 0.50 µmol). The reaction mixture was stirred for 180 minutes at room temperature. After 30, 60, 90, 120, 150 and 180 mins, a 50 µL aliquot of the reaction mixture was diluted into 250 µL of water, and then analysed using LCMS to examine the presence of the Michael addition of DEM30355/A-cysteine product (**52**).

8.8.2 DEM30355/A - cysteine methyl ester (53)

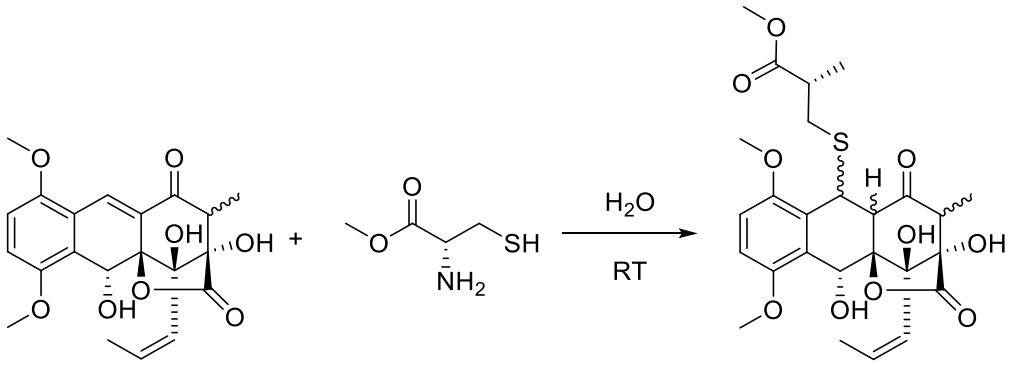

28 43 53

To a 5 mL pear shaped RBF, was added water (725 µL), 0.01 M solution of L-cysteine methyl ester hydrochloride in water (75 µL, 0.75 µmol) and 2.50 mM solution of DEM30355/A in DMSO (200 µL, 0.50 µmol). The reaction mixture was stirred for 180 mins at room temperature. After 30, 60, 90, 120, 150 and 150 mins, a 50 µL aliquot of the reaction mixture was diluted with 250 µL of water and subsequently analysed by LCMS to examine the presence of the Michael addition of DEM30355/A-cysteine methyl ester product (**53**).

8.8.3 DEM30355/A - short peptide LcrV (272-291) (54)

For Michael addition with LcrV (272 – 291), DEM30355/A was prepared into 25 mM solution by dissolving Dem30355/A (10 mg, 0.025 mmol) in 1 mL DMSO. The concentration of the LcrV (272 – 291) was 4.5 mM and the buffer Tris pH 8 was 200 mM.

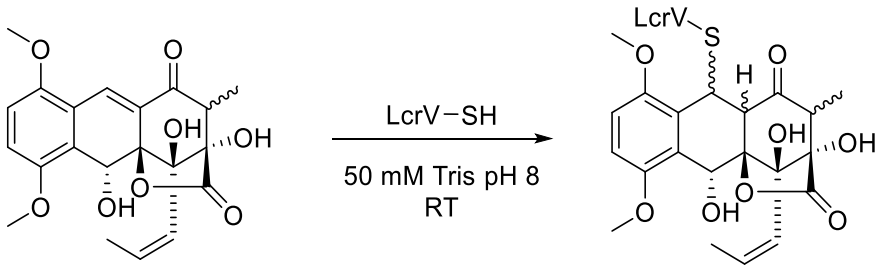

28 **54**

To a 0.2 mL Eppendorf tube, was added water (2.6 µL), 4.5 mM solution of LcrV (271-291) in 20 mM DTT (4.4 µL, 0.020 µmol), 200 mM solution of Tris buffer 200 mM (pH 8) (5 µL, 1.0 µmol) and 25 mM solution of DEM 30355/A in DMSO (8 µL, 0.20 µmol). The resulting mixture was mixed for 5 seconds (vortex) at room temperature. After 0, 15, 30, 45 and 60 minutes, a 2 µL aliquot of the reaction mixture was taken, diluted with 10 µL water and then analysed by LCMS to examine the presence of Michael addition of DEM 30355/A-LcrV (272-291) product (**54**).

Experimental procedures and structural characterization: The synthesis of chemical probes

Thin layer chromatography (TLC) was performed on silica gel 60 F254 plates and visualised using UV light 254 nm and 356 nm. Melting point were obtained using Stuart SMP3 melting point apparatus. ^{1}H and ^{13}C NMR spectra were recorded with a Bruker Avance III 300 MHz spectrometer, Jeol ECS-400 MHz or a Bruker Avance III HD 700 MHz spectrometer. Chemical shifts are quoted in δ (ppm) and coupling constants in hertz (Hz). Infrared (IR) spectra were obtained on a Varian 800 FT-IR Scimitar Series spectrometer. Liquid chromatography mass spectroscopy (LCMS) was carried out in Pinnacle Laboratory, Newcastle University.

Schlenk technique were performed for all chemical reactions involving air-sensitive reagents, under an atmosphere of nitrogen. Anhydrous solvents were distilled under an atmosphere of nitrogen and used directly. Manual flash column chromatography was carried out using Geduran silica gel 60 (40-63 μm).

8.9 Methyl 3-hydroxybenzoate (57)

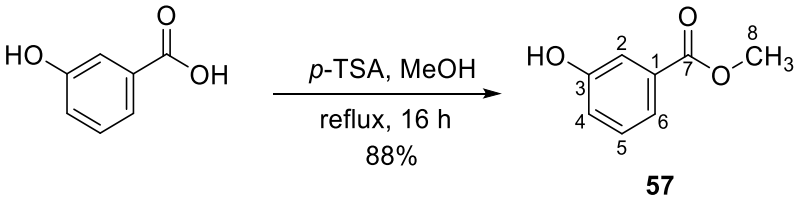

57

To a 250 mL RBF, was added 3-hydroxy benzoic acid (5.02 g, 36.4 mmol) and *p*-TSA (0.708 g, 3.72 mmol). Then the reaction vessel was attached to a reflux condenser and flushed under a nitrogen atmosphere for 30 minutes. Methanol (125 mL) was added to the reaction vessel and then the reaction mixture was refluxedfor 16 hours. The reaction mixture was cooled to room temperature and concentrated under reduced pressure. The crude reaction material was purified by silica gel column chromatography (4 : 1 petroleum ether : ethyl acetate) to give methyl 3-hydroxybenzoate (4.86 g, 32.0 mmol, 88%) as a white crystal solid.

R_f = 0.80 (petroleum ether : ethyl acetate 3 : 1; UV light). **Mp** = 69 – 70 °C [lit.69-71 °C]. **^{1}H NMR** (300 MHz, $CDCl_3$) δ 7.61 (ddd, *J* = 7.7, 1.5, 1.0 Hz, 1H, H-6), 7.54 (ddd, *J* = 2.7, 1.5, 0.4 Hz, 1H, H-2), 7.32 (ddd, *J* = 8.1, 7.7, 0.4 Hz, 1H, H-5), 7.06 (ddd, *J* = 8.1, 2.7, 1.0 Hz, 1H, H-4), 3.92 (s, 3H, H-8). **^{13}C NMR** (75 MHz, $CDCl_3$) δ 166.9 (C-7), 155.8 (C-3), 131.7 (C-1), 129.9 (C-5), 122.2 (C-6), 120.3 (C-4), 116.4 (C-2), 52.4 (C-8). **IR** (neat): ν_{max}/cm^{-1} 3325 (OH, br, s), 2930-2851 (CH, w), 1736 (CO, s).

Observed data (^{1}H NMR, ^{13}C NMR and IR) are consistent with that previously reported by Fu *et al*.[121]

8.10 Methyl 3-methoxybenzoate (TMSCN) (58)

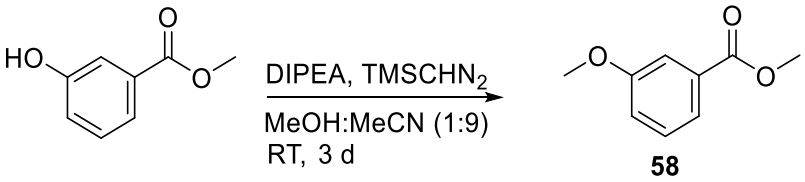

58

To a 5 mL pear-shaped flask, was added methyl 3-hydroxybenzoate (10.6 mg, 0.0660 mmol, 1 eq.), 1 mL of methanol-acetonitrile mixture (1:9), DIPEA (17.1 mg, 0.132 mmol, 2 eq.) and $TMSCHN_2$ (31.5 µL, 0.198 mmol, 3 eq.). The reaction mixture was stirred at room temperatureand monitored by TLC (ethyl acetate : petrol 1:4). After 3 d, reaction mixture was quenched with acetic acid (5 eq.) and the resulting reaction mixture stirred overnight, in air, at room temperature. The resulting reaction mixture was then transferred into 100 mL separating funnel, diluted in diethyl ether (10 mL) and washed with saturated $NaHCO_3$ (2 x 10 mL). The organic layer was then washedwashed with brine (10 mL) and dried over $MgSO_4$, filtered, and removed the solvent under reduced pressure to give 81% conversion based on the ^1H NMR integration.

8.11 Methyl 3-methoxybenzoate (MeI) (58)

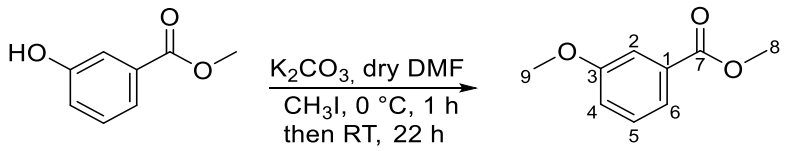

58

To a 25 mL Schlenk flask equipped with magnetic stirrer bar, was added methyl 3-hydroxy benzoate (0.101 g, 0.660 mmol, 1 eq.), K_2CO_3 (0.273 g, 1.980 mmol, 3 eq.) and dry DMF (6.6 mL) at room temperature. The resulting mixture was cooled to 0 ˚C in an ice bath and iodomethane (0.710 g, 5.0 mmol, 8 eq.) was added dropwise. After a complete addition, the reaction was stirred at 0˚C in an ice bath for 1 h. The ice bath was then removed, and the reaction was carried out at room temperature for 22 h. The reaction was then quenched by adding diethylamine (680 µL) and left for 30 minutes followed by transferring the resulting mixture into a 100 mL separating funnel and water (10 mL) was added followed by extraction using ethyl acetate (2 x 10 mL). The organic layer was collected, washed with brine (10 mL), dried over $MgSO_4$, filtered, and concentrated under reduced pressure to give methyl 3-methoxy benzoate 0.113 g as a light yellow oil. This was then purified via silica column chromatography (3 : 1 petroleum ether : ethyl acetate) to give methyl 3-hydroxybenzoate (0.085 g, 0.515 mmol, 78%) as a white powder.

R_f = 0.75 (petroleum ether : ethyl acetate 3 : 1, UV light). **^{1}H NMR** (300 MHz, $CDCl_3$) δ 7.63 (ddd, *J* = 7.6, 1.6, 1.1 Hz, 1H, H-6), 7.56 (ddd, *J* = 2.8, 1.5, 0.4 Hz, 1H, H-2), 7.34 (ddd, *J* = 8.1, 7.7, 0.4 Hz, 1H, H-5), 7.10 (ddd, *J* = 8.3, 2.7, 1.0 Hz, 1H, H-4), 3.91 (s, 3H, H-8), 3.85 (s, 3H, H-9). **^{13}C NMR** (75 MHz, $CDCl_3$) δ 167.1 (C-7), 159.7(C-3), 131.6 (C-1), 129.5 (C-2), 122.1 (C-6), 119.7 (C-4), 114.1 (C-5), 55.6 (C-9), 52.3 (C-8). **IR** (neat): ν_{max} cm^{-1} 2981 – 2838 (CH, m), 1717 (C=O, s). **LCMS** (ESI) calcd for $C_9H_{10}O_3Na$ $[M+Na]^+$: 189.0528, found 189.0538.

Observed data (^{1}H NMR and ^{13}C NMR) are consistent with that previously reported by O'Brien *et al*.[122]

8.12 Methyl 3-(benzyloxy)benzoate (59)

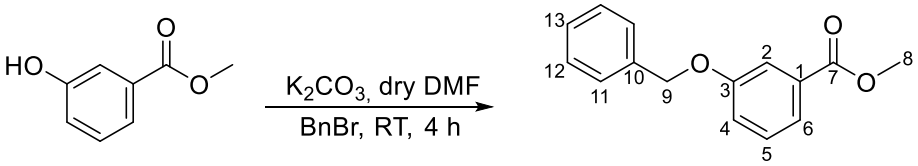

59

To a 25 mL Schlenk flask equipped with magnetic stirrer bar, was added methyl 3-hydroxybenzoate (0.113 g, 0.740 mmol, 1 eq.) and K_2CO_3 (0.307 g, 2.22 mmol, 3 eq.) at room temperature and under Nitrogen. Then dry DMF (7.4 mL) was added into the mixture, followed by benzyl bromide (0.296 g, 2.22 mmol, 3 eq.). The reaction mixture was stirred for 4 hours at room temperature. The resulting reaction mixture was then quenched with water (100 mL), transferred into a 250 mL separating funnel and extracted with ethyl acetate (2 x 100 mL). The organic layers were combined, washed with brine (200 mL), dried over MgSO4, filtered, and solvent was removed under reduced pressure to give a light-yellow liquid. This crude mixture was then purified via silica gel column chromatography (3 : 1 petroleum ether : ethyl acetate) to give methyl 3-hydroxybenzoate (7) (0.151 g, 0.620 mmol, 84%) as a white powder.

R_f = 0.80 (petroleum ether : ethyl acetate 3 : 1, UV light). **Mp** = 80 – 81°C. **^{1}H NMR** (300 MHz, $CDCl_3$) δ 7.68 – 7.64 (m, 2H, H-2 and H-6), 7.48 – 7.32 (m, 7H, H-5, H-11, H-12, and H-13), 5.11 (s, 2H, H-9), 3.92 (s, 3H, H-8). **^{13}C NMR** (75 MHz, $CDCl_3$) δ 167.0 (C-7), 158.9 (C-3), 136.7 (C-10), 131.6 (C-1), 129.6 (C-13), 128.8 (C-2),128.2 (C-12), 127.7 (C-11), 122.4 (C-5), 120.3 (C-4), 115.2 (C-6), 70.3 (C-9), 52.3 (C-8). **IR** (neat): ν_{max}/cm^{-1} 2884 – 2981 (CH, w), 1708 (CO, m). **LCMS** (ESI) calcd. for $C_{15}H_{14}O_3Na$ $[M+Na]^+$: 265.0841, found 265.0835.

Observed data (^{1}H NMR and ^{13}C NMR) are consistent with that previously reported by Kronenberger *et al*.[123]

8.13 Methyl 3-(allyloxy)benzoate (60)

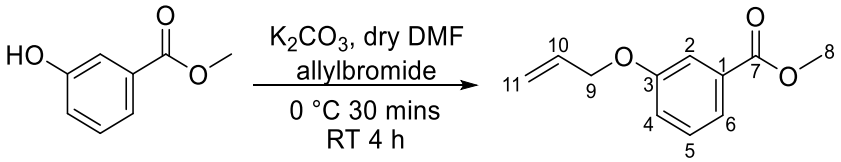

60

To a 25 mL Schlenk flask equipped with magnetic stirrer bar and under nitrogen, methyl 3-hydroxybenzoate (0.152 g, 0.670 mmol, 1 eq.) and K_2CO_3 (0.278 g, 2.01 mmol, 3 eq.) were added followed by the addition of dry DMF (6.7 mL) addition. The mixture was cooled to 0 ˚C in an ice bath and allyl bromide (0.162 g, 1.34 mmol, 2 eq.) was added dropwise. After complete addition, the reaction was stirred at 0 ˚C in an ice bath for 30 minutes. The ice bath was then removed, and the reaction was carried out at room temperature for 4 h. The reaction mixture was quenched by diethylamine (350 µL) and stirred for 30 minutes for 4 h. Then water (100 mL) was added to reaction mixture and transferred into a 250 mL separating funnel and extracted with diethyl ether (2 x 100 mL). The organic layers were combined, washed with brine, dried over $MgSO_4$ and csolvent was removed under reduced pressure to give a light yellow liquid. This was then purified via silica column chromatography (3 : 1 petroleum ether : ethyl acetate) and gave methyl 3-(allyoxy)benzoate (0.111 g, 0.576 mmol, 86%) as a colourless oil.

R_f = 0.55 (petroleum ether : ethyl acetate 3 : 1, UV light). **^{1}H NMR** (300 MHz, $CDCl_3$) *δ* 7.63 (ddd, *J* = 7.6, 1.5, 1.0 Hz, 1H, H-6), 7.57 (ddd, *J* = 2.7, 1.6, 0.4 Hz, 1H, H-2), 7.34 (ddd, *J* = 8.1, 7.7, 0.4 Hz, 1H, H-5), 7.12 (ddd, *J* = 8.3, 2.7, 1.1 Hz, 1H, H-4), 6.06 (DTT, *J* = 17.2, 10.5, 5.3 Hz, 1H, H-10), 5.43 (dq, *J* = 17.2, 1.6 Hz, 1H, H-11a), 5.30 (dq, *J* = 10.5, 1.4 Hz, 1H, H-11b), 4.58 (dt, *J* = 5.3, 1.5 Hz, 2H, H-9), 3.91 (s, 3H, H-8). **^{13}C NMR** (75 MHz, $CDCl_3$) *δ* 167.1 (C-7), 158.7 (C-3), 133.0 (C-10), 131.5 (C-1), 129.5 (C-5), 122.3 (C-6), 120.3 (C-4), 118.1 (C-11), 115.1 (C-2), 69.1 (C-9), 52.3 (C-8). **IR** (neat): ν_{max}/cm^{-1} 3081-2880 (CH, w), 1718 (CO, s). **LCMS** (ESI) calcd for $C_{11}H_{12}O_3Na$ $[M+Na]^+$: 192.0786, found 192.0790.

Observed data (^{1}H NMR, ^{13}C NMR, IR and LCMS) are consistent with that previously reported by Jones *et al*.[124]

8.14 Methyl 3-(prop-2-yn-1-yloxy)benzoate (61)

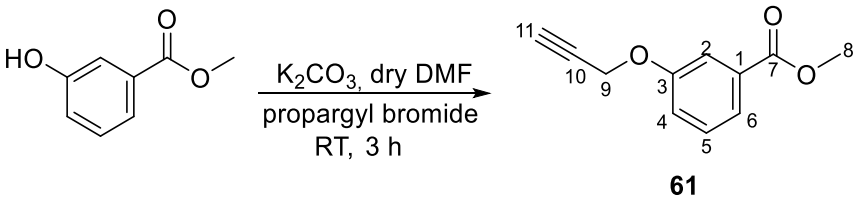

61

To a 50 mL Schlenk flask equipped with magnetic stirrer bar and under nitrogen atmosphere, methyl 3-hydroxybenzoate (1.00 g, 6.60 mmol, 1 eq.) and K_2CO_3 (2.74 g, 19.8 mmol, 3 eq.) were added. Then dry DMF (33 mL) was added followed by the addition propargyl bromide (0.572 mL, 19.8 mmol, 3 eq.). The resulting reaction mixture was stirred at room temperature for 3 hours. The reaction was then stopped by adding water (100 mL). The reaction mixture was transferred into a 250 mL separating funnel and extracted with diethyl ether (2 x 100 mL). The organic layers were combined, washed with brine (200 mL), dried over $MgSO_4$ and solvent was removed under reduced pressure to give a yellow liquid. This crude product was then purified via silica gel column chromatography (3 : 1 petroleum ether : ethyl acetate) to give methyl 3-(prop-3-yn-1-yloxy)benzoate (1.11 g, 5.818 mmol, 88%) as a clear oil.

R_f = 0.44 (petroleum ether : ethyl acetate 3: 1, UV light). **^{1}H NMR** (300 MHz, $CDCl_3$) δ 7.68 (ddd, *J* = 7.7, 1.5, 1.0 Hz, 1H, H-6), 7.63 (ddd, *J* = 2.7, 1.5, 0.4 Hz, 1H, H-2), 7.37 (ddd, *J* = 8.1, 7.6, 0.4 Hz, 1H, H-5), 7.18 (ddd, *J* = 8.3, 2.7, 1. Hz, 1H, H-4), 4.74 (d, *J* = 2.4 Hz, 1H, H-9), 3.91 (s, 3H, H-8), 2.54 (t, *J* = 2.4 Hz, 1H, H-11). **^{13}C NMR** (75 MHz, $CDCl_3$) δ 166.9 (C-7), 157.6 (C-3), 131.7 (C-1), 129.6 (C-5), 123.0 (C-6), 120.4 (C-4), 115.4 (C-3), 78.2 (C-10), 76.0 (C-11), 56.1 (C-9), 52.4 (C-8). **IR** (neat): ν_{max}/cm^{-1} 2885 – 2981 (CH, m), 2125 (C≡C, w), 1713 (CO, s).

Observed data (^{1}H NMR, ^{13}C NMR and IR) are consistent with that previously reported by Mandl *et al*.[125]

8.15 Methyl 3-((1-benzyl-1*H*-1,2,3-triazol-4-yl)methoxy)benzoate (62)

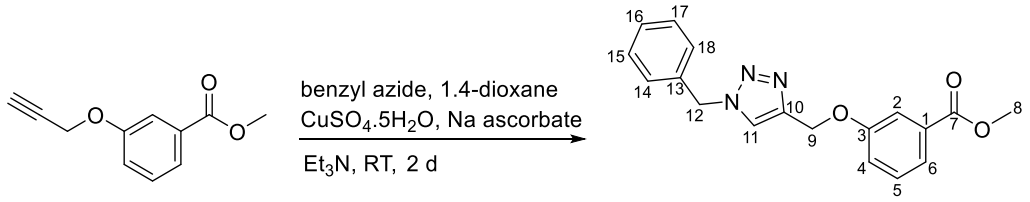

61 **62**

To a 50 mL Schlenk flask equipped with magnetic stirring bar, was added benzyl azide (80 µL, 0.640 mmol, 2 eq.), 1,4-dioxane (10 mL), methyl 3-(prop-2-yn-1-yloxy)benzoate (60.8 mg, 0.320 mmol, 1 eq.) in and followed by the addition of $CuSO_4.5H_2O$ (399.0 mg, 1.60 mmol, 5 eq.), sodium ascorbate (634.00 mg, 3.20 mmol, 10 eq.) and triethylamine (162 mg, 1.60 mmol, 5 eq.). The reaction mixture was stirred at room temperature for 2 d followed by the addition ofcold water (0°C) (50 mL) and then the resulting mixture was extracted with ethyl acetate (2 x 50 mL). The organic layers were combined, was washed with brine (100 mL), dried over $MgSO_4$, filtered and solvent was removed under reduced pressure. The crude material was purified by silica gel chromatography (1:1 hexane:ethyl acetate) to give methyl 3-((1-benzyl-1*H*-1,2,3-triazol-4-yl)methoxy)benzoate (7.0 mg, 0.022 mmol, 6.8%) as a white solid.

^{1}H NMR (400 MHz, $CDCl_3$) δ 7.68-7.60 (m, 3H), 7.54 (s, 1H), 7.43-7.24 (m, 6H), 7.20-7.12 (m, 2H), 5.54 (s, 2H), 5.22 (s, 2H), 3.90 (s, 3H). **LCMS** (ESI) calcd for $C_{18}H_{17}N_3O_3$: $[M+H]^+$: 324.1343, found 324.1252 and $[M+Na]^+$: 346.1162, found 346.1067.

Observed data (^{1}H NMR and LCMS) are consistent with that previously reported by Xiong *et al*.[126]

8.16 *O*-Propargylation of natural product (-)-rishirilide A

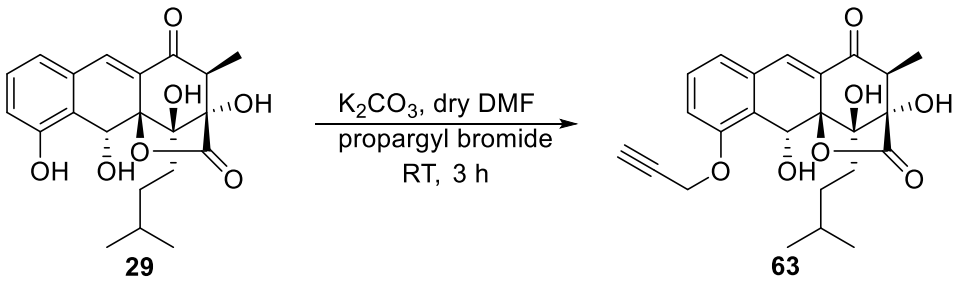

To a 5 mL Schlenk flask equipped with magnetic stirrer bar and under nitrogen, was added (-)-rishirilide A (2.00 mg, 5.15 µmol), K_2CO_3 (2.14 mg, 15.5 µmol) and dry DMF (200 µL). Then propargyl bromide (1.6 µL, 15.45 µmol) was slowly added and the resulting mixture was stirred at room temperature for 3 h. Before the reaction was stopped by adding water, 50 µL of the reaction mixture was taken out and centrifuged. The supernatant was analysed by LCMS to examine the presence of the desired product (**63**).

The observation of the O-propargylation product was carried out through extracted ion chromatogram (EIC) by inserting the *m/z* signal of 449.1471 – 449.1671 corresponding to $[M+H]^+$ ion of the desired product (**63**).

General experimental information: Encapsulated nanodroplet crystallisation (ENaCt)

8.17 Solubility test

To a 9-well spot plate, was placed a small quantity of analyte (a tip of a spatula) to each well and placed the 9-well spot plate under a polarising light microscope. The solubility of analyte is visually assessed when a drop of solvent is added into the analyte until all of the solids is dissolved.

8.18 Classical crystallisation of CBD

To a sample tube, 5 mg of CBD was weighed and dissolved with 0.5 – 1 mL of organic solvents (pentane, *n*-hexane, *n*-heptane, dichloromethane and chloroform) until the mixture dissolve completely and no solid remaining in the CBD solutions. All sample tube was then closed with a lid with two-three holes. Visual examination for the presence of CBD crystals is observed every couple day. The single crystals suitable for SCXRD was analysed by in-house X-ray diffractometer.

8.19 Encapsulated nanodroplet crystallisation of CBD

In a screw top vial, CBD was weighed and dissolved with a suitable solvent by adding a minimum of 50 µL, with additional solvent added as required to dissolve the sample. This resulted CBD solutions in pentane [0.11 g/mL], *n*-hexane [0.084 g/mL], *n*-heptane [0.063 g/mL], chloroform [1.00 g/mL], 1,2-dichloroethane [1.00 g/mL], toluene [1.02 g/mL], fluorobenzene [1.00 g/mL], chlorobenzene [1.01 g/mL], and hexafluoro benzene [0.20 g/mL]. These concentrated stock solutions, labelled as high concentration (H), were also diluted by two fold, medium concentration (M), and four fold, low concentration (L).

A SPT LabTech mosquito® liquid-handling robot, was used to dispense 200 nL of each inert oil (PDMSO, FC-40, FY and mineral oil) onto a Laminex™ 96-well glass plate, followed by injection of 50 nL of the appropriate CBD solution into the oil. The 96-well glass plates were then sealed with a glass cover slip, stored in the dark at room temperature for up to 14 days (Scheme **8.1**).

Oils		50 nL of CBD stock solutions											
		no oils			with 200 nL oils								
		H	M	L	H			M			L		
		1	2	3	4	5	6	7	8	9	10	11	12
PDMSO	A												
	B												
FC-40	C												
	D												
FY	E												
	F												
Mineral oil	G												
	H												

Scheme 8.1: A typical arrangement of a 96-well glass plate containing inert oils and CBD solutions. H = high concentration, M = medium concentration, L = low concentration.

8.20 Encapsulated nanodroplet crystallisation of the polyketide rifamycin SV sodium salt

The sodium salt of rifamycin SV (approx. 10 mg) was dissolved in a minimum of 50 μL of solvent, with additional solvent added as required to dissolve the sample, resulting in solutions in methanol [57 mg/mL], ethanol [39 mg/mL], DMSO [34 mg/mL], DMF [45 mg/mL], 1-propanol [17 mg/mL], 1-butanol [11 mg/mL], 1-hexanol [8 mg/mL] and 2-propanol [6 mg/mL]. A SPT Labtech mosquito® liquid-handling robot was used to dispense 200 nL of each inert oil (PDMSO, FC40, FY and mineral oil) onto a Laminex™ 96-well glass plate, followed by injection of either 25, 50, or 100 nL of rifamycin SV sodium solutions. Each Laminex™ 96-well glass plate had two different solvents.

The resulting 96-well glass plates were then sealed and stored at room temperature and rifamycin SV crystals was looked for using a cross-polarised light microscope at day 1, 7, and 14 (Scheme **8.2**).

			Rifamycin SV in solvent A (nL)						Rifamycin SV in solvent B (nL)					
			25	25	50	50	100	100	25	25	50	50	100	100
			1	2	3	4	5	6	7	8	9	10	11	12
200 nL of inert oils	PDMS	A												
		B												
	FC40	C												
		D												
	FY	E												
		F												
	Mineral oil	G												
		H												

Scheme 8.2: Arrangement of 96-well glass plate containing inert oils and rifamycin SV stock solutions.

8.21 Encapsulated nanodroplet crystallisation of rifamycin SV with the addition of secondary solvents

All the stock solutions of rifamycin SV sodium salt that used previously was employed in this ENaCt, with the addition of selected six secondary solvents (toluene, 1,4-dioxane, chlorobenzene, anisole, 1,2-dichloroethane and 2-butanone). The SPT Labtech mosquito® liquid-handling robot was used to dispense 200 nL of each inert oil (PDMSO, FC40, FY, and mineral oil) onto a Laminex™ 96-well glass plate, followed by 50 nL of a rifamycin SV sodium solution (methanol, ethanol, DMSO, DMF, 1-propanol, 1-butanol, 1-hexanol, and 2-propanol) with the addition of either 25, 50, 75, or 100 nL of a secondary solvent (toluene, 1,4-dioxane, chlorobenzene, anisole, 1,2-dichloroethane and 2-butanone). The resulting glass plates were sealed, stored in the dark, at room temperature, and the appearance of rifamycin SV crystals was checked for at 1, 7 and 14 days (Scheme **8.3**).

Plate number			50 nL of rifamycin SV solution											
			Secondary solvent A (nL)				Secondary solvent B (nL)				Secondary solvent C (nL)			
			25	50	75	100	25	50	75	100	25	50	75	100
			1	2	3	4	5	6	7	8	9	10	11	12
200 nL of inert oils	PDMS	A												
		B												
	FC40	C												
		D												
	FY	E												
		F												
	Mineral oil	G												
		H												

Scheme 8.3: A typical arrangement of a 96-well glass plate containing inert oils, rifamycin SV solution and the addition of secondary solvents.

8.22 Encapsulated nanodroplet crystallisation of the semi-synthetic polyketide rifampicin

The rifampicin (approx. 10 mg) was dissolved in a minimum of 50 μL of solvent, with additional solvent added as required to dissolve the sample, resulting solutions in toluene [14 mg/mL], 1,4-dioxane [37 mg/mL], chlorobenzene [105 mg/mL], THF [28 mg/mL], ethyl acetate [50 mg/mL], and 1,2-dichloroethane [11 mg/mL]. The SPT Labtech mosquito® liquid-handling robot was used to dispense 200 nL of each inert oil (PDMSO, FC40, FY and mineral oil) onto a Laminex™ 96-well glass plate, followed by addition of either 25, 50 or 100 nL of rifampicin

solutions. Each Laminex™ 96-well glass plate were added two different solvents (solvent A and B). The resulting 96-well glass plates were then sealed and stored at room temperature and the rifampicin crystals was checked using a cross-polarised microscope at day 1, 7 and 14 (Scheme **8.4**).

			Rifampicin in solvent A (nL)						Rifampicin in solvent B (nL)					
			25	25	50	50	100	100	25	25	50	50	100	100
			1	2	3	4	5	6	7	8	9	10	11	12
200 nL of inert oils	PDMS	A												
		B												
	FC40	C												
		D												
	FY	E												
		F												
	Mineral oil	G												
		H												

Scheme 8.4: A typical arrangement of a 96-well glass plate containing inert oils and rifampicin solution.

8.23 Encapsulated nanodroplet crystallisation of the polyketide (-)-rishirilide A and (+)-rishirilide B

The stock solutions of (-)-rishirilide A was prepared in DMSO [9.8 mg/mL], whilst (+)-rishirilide B was prepared in 2 different solvents, DMF [16 mg/mL] and DMSO [12 mg/mL]. Using a SPT Labtech mosquito® liquid-handling robot, 200 nL of each inert oil (PDMSO, FC40, FY and mineral oil) was dispensed only onto column 7 to 12 of a Laminex™ 96-well glass plate, whilst the addition of 50 nL of either (-)-rishirilide (A) or (+)-rishirilide B solutions were carried out onto each well. The 96-well glass plates were then sealed and stored at room temperature, and the appearance of crystals was checked for after 1, 7, and 14 days (Scheme **8.5**).

Plate number		50 nL of (-)-rishirilide A or (+)-rishirilide B											
		without inert oils						with 200 nL inert oils addition					
		1	2	3	4	5	6	7	8	9	10	11	12
PDMS	A												
	B												
FC40	C												
	D												
FY	E												
	F												
Mineral oil	G												
	H												

Scheme 8.5: A typical arrangement of a 96-well glass plate containing either (-)-rishirilide A or (+)-rishirilide B solution and inert oils.

8.24 Encapsulated nanodroplet crystallisation of (+)-rishirilide B with the addition of secondary solvents

In this ENaCt experiment, we used the previous stock solution of (+)-rishirilide B in DMF [16 mg/mL]. The secondary solvents that used in this ENaCt were toluene (aromatic), 1,4-dioxane (ether) and 1,2-dichloroethane (chlorinated). Using a SPT Labtech mosquito® liquid-handling robot 200 nL of each oil (PDMSO, FC40, FY and mineral oil) was dispensed onto a Laminex™ 96-well glass plate, followed by the addition of 50 nL of (+)-rishirilide B stock solution in DMF. Then either 25, 50, 75 or 100 nL of secondary solvent was added. The 96-well glass plates were then sealed, stored at room temperature and appearance of crystals was looked for at day 1, 7 and 14 (Scheme **8.6**).

Plate number			50 nL of (+)-rishirilide B in DMF											
			Secondary solvent											
			25	25	25	50	50	50	75	75	75	100	100	100
			1	2	3	4	5	6	7	8	9	10	11	12
200 nL of inert oils	PDMS	A												
		B												
	FC40	C												
		D												
	FY	E												
		F												
	Mineral oil	G												
		H												

Scheme 8.6: A typical arrangement of a 96-well glass plate containing inert oils, (+)-rishirilide B in DMF and the addition of a secondary solvent, toluene, 1,4-dioxane and 1,2-dichloroethane.

8.25 X-Ray Crystallography Data

X-Ray crystallography data of single crystals suitable for SCXRD were collected on a Xcalibur, Atlas, Gemini ultra-diffractometer equipped with a fine-focus sealed X-ray tube (λ CuKα = 1.54184 Å) and an Oxford Cryosystems Plus open-flow N_2 cooling device. The analysis of the X-ray diffraction data of all the following compounds were performed by Dr Paul Waddell and Dr Michael Probert.

References

1. Centers for Disease Control and Prevention, Morbidity and Mortality Weekly Report (MMWR), 1999, **48**, 1142-1164.
2. Alexander Fleming, *Br. J. Exp. Pathol.*, 1929, **10**, 226-236.
3. J. Clardy, M. Fischbach, and C. Currie, *Curr. Biol*., 2009, **19**, 437-441.
4. Nobelprize.org, https://www.nobelprize.org/uploads/2018/06/fleming-lecture.pdf, (accessed Oct 2020).
5. TB Section, Centre for Infectious Disease Surveillance and Control, Public Health Protection England, *Tuberculosis mortality and mortality rate from 1913-2013*, Public Health England, England and Wales; 2014.
6. B. R. da Cunha, L. P. Fonseca and C. R. C. Calado, *Antibiotics*, 2019, **8**, 1-21.
7. J. Willey, L. Sherwood, and C. Woolverton, *Antimicrobial chemotherapy,* Eds.; Colin Wheatley/Janice Roerig-Blong: New York, NY, USA, 2008; pp. 835–837.
8. G. D. Wrigh, *Can. J. Microbiol*., 2014, **60**, 147-154.
9. J. Bérdy, *J. Antibiot*., 2005, **58**, 1-26.
10. K. Gould, *J. Antimicrob. Chemother*., 2016, **71**, 572-575.
11. I. Chopra and M. Roberts, *Microbiol. Mol. Biol. Rev.*, 2001, **65**, 232-260.
12. D. Fernández-Villa, M. R. Aguilar and L. Rojo, *Int. J. Mol. Sci.*, 2019, **20**, 4996-5025.
13. B. Ekundayo and F. Bleichert, *PLoS Genet*., 2019, **15**, e1008320.
14. G Hartmann, W. Behr, K.-A. Beissner, K. Honikel and A. Sippel, *Angew. Chem., Int. Ed.*, 1968, **7**, 963-701.
15. S. K. Straus and R. E. W. Hancock, *Biochim. Biophys. Acta*, 2006, **1758**, 1215-1223.
16. J. M. Benarroch and M. Asally, *Trends in Microbiology*, 2020, **28**, 304-314.
17. J. A. Silverman, N. G. Perlmutler and H. M. Shapiro, *Antimicrobe. Agents Chemother*., 2003, **47**, 2538-2544.
18. T. Zhang, J. K. Muraih, B. MacCormick, J. Silverman and M. Palmer, *Biochim. Biophys. Acta*, 2014, **1838**, 2425-2430.
19. T. Dörr, P. J. Moynihan and C. Mayer, *Front. Microbiol*., 2019, **10**, 1-4.
20. T. J. Silhavy, D. Kahne and S. Walker, *CHS Perspect. Biol.*, 2010, **2**, a000414.
21. K. F. Kong, L. Schneper and K. Mathee, *APMIS: Acta Pathol., Microbiol. Immunol. Scand*., 2010, **118**, 1-36.

22. J. C. J. Barna and D. H. Williams, *Ann. Rev. Microbiol.,* 1984, **38**, 339-357
23. B. F. Erlanger and L. Goode, *Nature*, 1967, **213**, 183-184.
24. C. L. Ventola, *P T.*, 2015, **40** 277-283.
25. World Health Organization, Antimicrobial resistance, global report on surveillance, 2014.
26. Centers for Disease Control and Prevention, Antibiotic resistance threats in the United State, 2013, USA.
27. E. Christaki, M. Marcou and A. Tofarides, *J. Mol. Evol*., 2020, **88**, 26-40.
28. C. J. Graham, *J. Glob. Health Rep.*, 2017, **1**, e2017002.
29. *Global Tuberculosis Report,* World Health Organization (WHO), Switzerland, 2018.
30. Centers for Disease Control and Prevention, Antibiotic resistance threats in the United State, 2019, USA
31. D. J. Newman and G. M. Cragg, *J. Nat. Prod*., 2020, **83**, 770-803.
32. S. Y. Tan, Y. Tatsumura, *Singapore Med. J.*, 2015, **56**, 336-367.
33. S. A. Waksman, H. C. Reily and D. Johnstone, *J. Bacteriol*, 1946, **52**, 393-397.
34. J. Berdy. *J. Antibiot.,* 2012, **65***,* 385-395*.*
35. Y. Luo, R. E. Cobb, and H. Zhao, *Curr. Opin. Biotechnol.,* 2014, **30**, 230-237.
36. P. H. Rampelotto, *Life (Basel)*, 2013. **3**, 482-485.
37. S. Keller, G. Nicholson, C. Drahl, E. Sorensen, H. P. Fiedler, and R. D. Sussmuth, *J. Antibiot.*, 2007, **60**, 391-394.
38. M. Goodfellow, J. E. M. Stach, R. Brown, A. N. V. Bonda, A. L. Jones, J. Mexson, H. P. Fielder, T. D. Zucchi, and A. T. Bull, *Antonie van Leeuwenhoek*, 2012, **101**, 185-193.
39. *Uncultured Microorganisms*, S.S. Epstein, Springer, New York or Berlin, 2009, pp.182
40. L. L. Ling, T. Schneider, A. J. Peoples, A. L. Spoering, I. Engels, B. P. Conlon, A. Mueller, T. F. Schaberle, D. E. Hughes, S. Epstein, M. Jones, L. Lazarides, V. A. Steadman, D. R. Cohen, C. R. Felix, K. A. Fetterman, W. P. Millett, A. G. Nitti, A. M. Zullo, C. Chen, and K. Lewis, *Nature*, 2015, **517**, 455.
41. A. Parmar, A. Iyer, S. H. Prior, D. G. Llyod, E. T. L. Goh, C. S. Vincent, T. P. Pallag, C. Z. Bachrati, E. Breukink, A. Madder, R. Lakshminarayanan, E. J. Taylor and I. Singh, *Chem. Sci*., 2007, **8**, 8183-8192.
42. B. K. Okada and M. R. Seyedsayamdost, *FEMS Microbiol. Rev.*, 2017, **41**, 19-33.

43. N. Ichikawa, M. Sasagawa, M. Yamamoto, H. Komaki, Y. Yoshida, S. Yamazaki, and N. Fujita, *Nucleic Acids Res.*, 2013, **41**, D408-D414.
44. Y. M. Chiang, S. L. Chang, B. R. Oakley, and C.C.C. Wang, *Curr. Opin. Chem. Biol.*, 2011, **15**, 137-143.
45. P. A. Hoskisson and R. F. Seipke, *mbio. asm. org*., 2020, **11**, 1-5.
46. Y. Luo, R. E. Cobb, and H. Zhao*, Curr. Opin. Biotechnol.*, 2014, **30**, 230-237.
47. K. Blin, M. H. Medema, D. Kazempour, M. A. Fischbach, R. Breitling, E. Takano, and T. Weber, *Nucleic Acids Res.*, 2013, **41**, W204-W212.
48. K. A. Reynolds, H. Luhavaya, J. Lie, S. Dahesh, V. Nizet, K. Yamanaka and B. S. Moore, 2018, *J. Antibiot. (Tokyo)*, 2018, **7**, 333-338.
49. K. Yamanaka, K. A. Reynolds, R. D. Kersten, K. S. Ryan, D. J. Gonzales, V. Nizet, P. C. Dorrestein, and B. S. Moore, *Proc. Natl. Acad. Sci.,* 2014, **111**, 1957-1962.
50. B. Kepplinger, PhD thesis, Newcastle University, 2016.
51. H. Iwaki, Y. Nakayama, M. Takahashi, S. Uetsuki, M. Kido, and Y. Fukuyama, *J. Antibiot.*, 1984, **37**, 1091-1093.
52. X. Yan, Dissertation, University of Freiburg (Germany), 2012.
53. T. Mascher, S. L. Zimmer, T. A. Smith, and J. D. Helmann, *Antimicrob. Agents. Chemother.*, 2004, **48**, 2888-2898.
54. H. Zhang, w. Zhou, Y. Zhuang, X. Liang and T. Liu, *Genome Announc.*, 2013, **1**, e00019-13.
55. B. Plitzko, E.N. Kaweesa and S. Loesgen, *J. Biol. Chem.,* 2017, **292**, 21102-21116.
56. M. Arnold, PhD thesis, University of Gottingen (Germany), 2002.
57. X. Yan, K. Probst, A. Linnenbrink, M. Arnold, T. Paululat, A. Zeeck and A. Bechthold, *ChemBioChem.,* 2012, **13**, 224-230.
58. P. Schwarzer, J. Wunsch-Palasis, A. Bechthold, and T. Paululat, *Antibiotics (Basel)*, 2018, **7**, 20.
59. O. Tsypik, R. Makitrynskyy, B. Frensch, D. L. Zechel, T. Paululat, R. Teufel, and A. Bechthold, *J. Am. Chem. Soc*., 2020, **142**, 5913-5917.
60. L. D. Sabath, C. Garner, C. Wilcox and M. Finland, *Antimicrob. Agents Chemother*., 1976, **9**, 962-969.
61. A. Ziyat, M. Goodfellow, A. Nurgozhina, S. Sergazy and M. Nurgaziev, *J. Microbiol. Biotech. Food Sci.*, 2019, **8**, 1057-1065.

62. B. Hutter, C. Fischer, A. Jacobi, C. Schaab, and H. Loferer, *Antimicrob. Agents. Chemother.*, 2004, **48**, 2588-2594.
63. A. Urban, S. Eckermann, B. Fast, S. Metzger, M. Gehling, K. ZIegelbauer, H. Rübsamen-Waigmann, and C. Freiberg, *Appl. Environ. Microbiol*., 2007, **73**, 6436-6443.
64. J. M. Benarroch and M. Asally, *Trends. Microbiol.*, 2020, **28**, 304-314.
65. B. Kepplinger, S. Morton-Laing, K. H. Seistrup, E. C. L. Marrs, A. P. Hopkins, J. D. Perry, H. Strahl, M. J. Hall, J. Errington and N. E. E. Allenby, *ACS Chem. Biol*. 2018, **13**, 207-214.
66. J. D. Winkel, D. A. Gray, K. H. Seistrup, L. W. Hamoen and H. Strahl, *Front. Cell Dev. Biol.*, 2016, **4**, 1-10.
67. P. A. Jackson, J. C. Widen, D. A. Harki and K. M. Brummond, *J. Med. Chem.*, 2017, **60**, 839-885.
68. A. P. Anisimov, S. V. Dentovskaya, E. A. Panfertsev, T. E. Svetoch, P. Kh. Kopylov, B. W. Segelke, A. Zelma, M. V. Telepnev and V. L. Motin, *Infect. Genect. Evol.*, 2010, **10**, 137-145.
69. S. Ng and R. Derda, *Org. Biol. Chem.*, 2016, **14**, 5539-5545.
70. M. H. Wright and S. A. Sieber, *Nat. Prod. Rep*., 2016, **33**, 681-708.
71. E. Zhang, T. Xu, W. Wei, T. Huang, M. Yuan, W. Zeng, Y. Zou, *Synthesis*, 2014, **46**, 1167-1176.
72. T. J. van't Erve, R. H. Rautiainen, L. W. Robertson and G. Luthe, *Environmental International*, 2010, **36**, 835-842.
73. E. C. Barnes, P. Bezerra-Gomez, M. Nett and C. Hertweck, *J. Antibiot.*, 2015, **68**, 463-468.
74. T. Aoyama, S. Terasawa, K. Sudo and T. Shioiri, *Chem. Pharm. Bull.*, 1984, **32**, 3759-3760.
75. P. Boggu, E. Venkateswararao, M. Manickam, Y. Kim and S.H. Jung, *Arch. Pharm. Res.* 2017, **40**, 469-479.
76. U. S. Sørensen, E. Falch, T. B. Stenbøl, J. W. Jaroszewski, U. Madsen and P. Krogsgaard-Larsen, *Arch. Pharm. Pharm. Med. Chem*. 2001, **334**, 62-68.
77. M. Selva, C. A. Marques and P. Tundo, *J. Chem. Soc., Perkin Trans. 1*, 1995, **1**, 1889-1893.
78. A. J. Harnoy, G. Slor, E. Tirosh and R. J. Amir*, Org. Biol. Chem.*, 2016, **14**, 5813-5819.
79. P. Yadav, K. Lal, P. Rani, A. Kumar and A. Kumar, *Med. Chem. Res.*, 2017, **26**, 1469-1480.
80. D. M. Nguyen and D. H. Miles, *Synth. Commun*., 2011, **41**, 1759-1771.
81. D. A. Dias, S. Urban, U. Roessner, *Metabolites*, 2012, **2**, 303-336.

82. E. E. Carlson, *ACS Chem. Biol*., 2010, **5**, 639-653.
83. J. A. Beutler, *Curr. Protoc. Pharmacol*., 2009, **46**, 9.11.1-9.11.21.
84. G. Pescitelli, T. Kurtan, U. Florke and K. Krohn, *Chirality*, 2009, **21**, E181-E201.
85. H. Yoo, S. Nam, Y. Chin and M. Kim, *Arch.Pharmacal. Res*., 2016, **39**, 143-153.
86. K. V. Jayaseelan and C. Steinbeck, *BMC Bioinf*., 2014, **15**, 1-9.
87. T. J. Schmidt, W. Peters, F. R. Fronczek, N. H. Fischer*, J. Nat. Prod*., 1997, **60**, 783-787.
88. P. Muller, *Crystallogr. Rev*., 2009, **15**, 57-83.
89. J. Přichystal, K. A. Schug, K. Lemr, J. Novák and V. Havlíček, *Anal. Chem*., 2016, **88**, 10338-10346.
90. X. M. Li and B. G. Wang, *Mar. Drugs*, 2019, **17**, 1-8.
91. X. Li, X. M. Li, G. M Xu, C. S. Li, and B. G Wang, *Phytochem. Lett.*, 2014, **7**, 120-123.
92. A. R. M. Tyler, R. Ragbirsingh, C. J. McMonagle, P. G. Waddell, S. E. Heaps, J. W. Steed, P. Thaw, M. J. Hall and M. R. Probert, *Chem.*, 2020, **6**, 1755-1765.
93. C. G. Jones, M. W. Martynowycz, J. Hattne, T. J. Fulton, B. M. Stoltz, J. A. Rodriguez, H. M. Nelson, and T. Gonen, *ACS Cent Sci*., 2018, **4**, 1587-1592.
94. T. Gruene, J. T. C. Wennmacher, C. Zaubitzer, J. J. Holstein, J. Heidler, A. Fecteau-Lefebvre, S. D. Carlo, E. Muller, K. N. Goldie, I. Regeni, T. Li, G. Santiso-Qionones, G. Steinfeld, S. Handschin, E. van Genderen, J. A. van Bokhoven, G. H. Clever and R. Pantelic, *Angew. Chem. Int. Ed. Engl.*, 2008, **57**, 16313-16317.
95. J. R. Hanson, *Natural Products: The Secondary Metabolites*, RSC Publishing, United Kingdom, 2003.
96. G. Wang, W. Tang, R. R. Bidigare, in Natural Products: *Drug Discovery and Therapeutics Medicine*, ed. L. Zhang and A. L. Demain, Humana Press, New Jersey, 2005, Terpenoid as Therapeutic Drugs and Pharmaceutical Agents, pp. 197-227.
97. G. Lancini, *J. Antibiot.*, 2014, **67**, 609-611.
98. T. Ottersen, E. Rosenqvist, C. E. Turner, F. S. El-Feraly, *Acta Chem. Scand*., 1977, **31**, 807.
99. P. G. Jones, L. Falvello, O. Kennard, G. M. Sheldrick and R. Mechoulam, *Acta Crystallogr*., 1977, **B33**, 3211-3214.
100. T. Mayr, T. Grassl, N. Korber, V. Christoffel and M. Bodensteiner, *IUCrData*, 2017, **2**, x170276.
101. K. Tigdewell, B. R. Clark, W. H. Gerwick, *Compr. Nat. Prod. II*, 2010, 141-188.

102. World Health Organization, *WHO Model List of Essential Medicines (21st List, 2019)*, WHO, Geneva, 2019.
103. G. N. Stephanopoulos, A. A. Aristidou and J. Nielsen, *Metabolic engineering, Principles and Methodologies*, Academic Press, London, 1998, 203-283.
104. P. Sensi, *Rev. Infect. Dis.*, 1983, **5**, Suppl. 3, S402-406.
105. W. Zhao, Y. Zhong, H. Yuan et al., *Cell Res*., 2010, **20**, 1096-1108.
106. S. K. Arora, *Am. Crystallogr. Assoc. Series 2*, 1982, **10**, 41d.
107. S. K. Arora, *Mol. Pharmacol*., 1982, **23**, 133-140.
108. K. Pyta, A. Janas, M. Szukowska, P. Pecyna, M. Jaworska, M. Gajecka, F. Bartl, P. Przybylski, *Eur. J. Med. Chem*., 2019, **167**, 66-104.
109. A. L. Ibiapino, R. C. Seiceira, A. Pitaluga, A. C. Trindade, F. F. Ferreira, *Crys. Eng. Comm*., 2014, **16**, 8555-8562.
110. L. Pinho, P. Nogueira, Y. S de Oliveira, J. C. Fonseca, S. Costa, F. N. Raffin, J. Ellena and A. P. Ayala, *J. Mol. Struct*., 2018, **1155**, 260-266.
111. B. Wicher, K. Pyta, P. Przybyski, E. Tykarska and M. Gdaniec, *Acta Cryst*., 2012, **C68**, o260-266.
112. M. Gadret, M. Goursolle, J. M. Leger et J. C. Colleter, *Acta Cryst*., 1975, **B31**, 1454-1462.
113. K. Pyta, P. Przybylski, B, Wicher, M. Gdaniec and J. Stefanska, *Org. Biomol. Chem*., 2012, **10**, 2385-2388.
114. M. M. de Villers, M. R. Caira, J. Li, S. J. Strydom, S. A. Bourne and W. Liebenberg, *Mol. Pharmaceutics*, 2011, **8**, 877-888.
115. B. Wicher, K. Pyta, P. Przybylski and M. Gdaniec, *Cryst. Growth Des*., 2018, **18**, 742-754.
116. M. Odagi, K. Furukori, K. Takayama, K. Noguchi and K. Nagasawa, *Angew. Chem. Int. Ed.*, 2017, **36**, 1-5.
117. K. Yamamoto, M. F. Hentemann, J. G. Allen, and S. J. Danishefsky, *Chem. Eur. J.,* 2003, **9**, 3242-3252.
118. H. Jiang, C. M. S. Ahmed, A. Canchola, J. Y. Chena and Y-H. Lin, *Atmosphere*, 2019, **10,** 571.
119. D.R. Zeigler, Z. Prágai, S. Rodriguez, B. Chevreux, A. Muffler, T. Albert, R. Bai, M. Wyss, and J. B. Perkins, *J. Bacteriol*., 2008, **190**, 6983-6995.
120. B. N. Kreiswirth, S. Löfdahl, M. J. Betley, M. O'Reilly, P. M. Schlievert, M. S. Bergdoll, and R. P. Novick, *Nature*, 1983, **305**, 709-712.

121. M. Jiang, H. Yang, and H. Fu, *Org. Lett.*, 2016, **18**, 5248-5251.
122. U. Gross, P. Koos, M. O'Brien, A. Polyzos, and S. V. Ley, *Eur. J. Org. Chem*., 2014, 6418-6430.
123. T. Kronenberger, G. M. Ferreira, A. D. Ferreira de Souza, S. da Silva Santos, A. Poso, J. A. Ribeiro, M. T. Tavares, F. R. Pavan, G. H. G. Trossini, M. V. B. Diaz, R. Parise-Filho, *Bioorg. Med. Chem*., 2020, **28**, 115600, 1-10.
124. D. M. Gill, L. Male, and A. M. Jones, *Eur. J. Org. Chem*., 2019, 7568-7577.
125. F. A. Mandl, V. C. Kirsch, I. Ugur, E. Kunold, J. Vomacka, C. Fetzer, S. Schneider, K. Richter, T. M. Fuchs, I. Antes, and S. A. Sieber, *Angew. Chem. Int. Ed*., 2016, **55**, 14852-18857.
126. X. Xiong, H Chen, Z. Tang, and Y. Jiang, *RSC Adv*., 2014, **4**, 9830-9837.

Appendix

^{1}H NMR spectra of (-)-rishirilide A

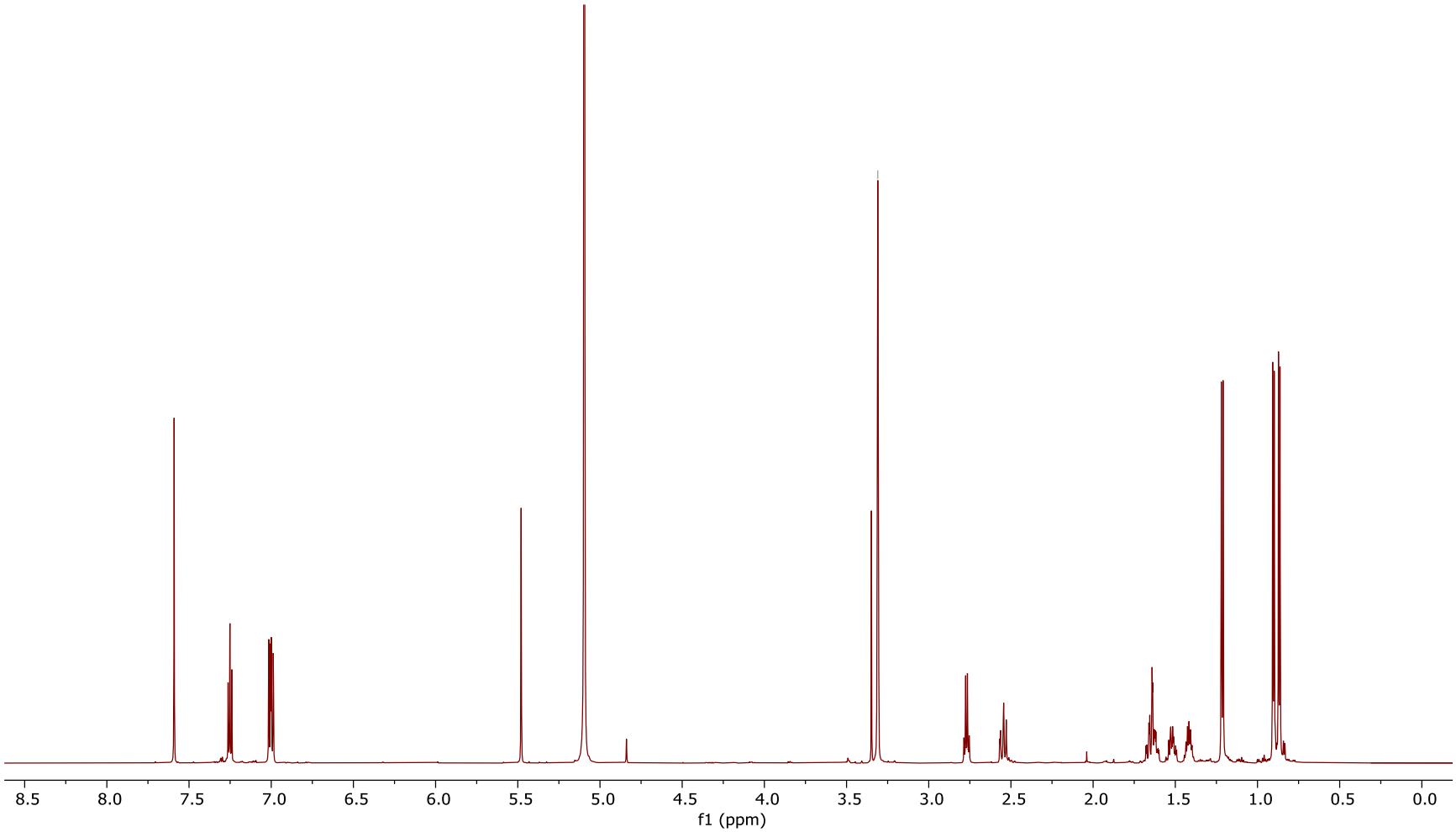

^{13}C NMR spectra of (-)-rishirilide A

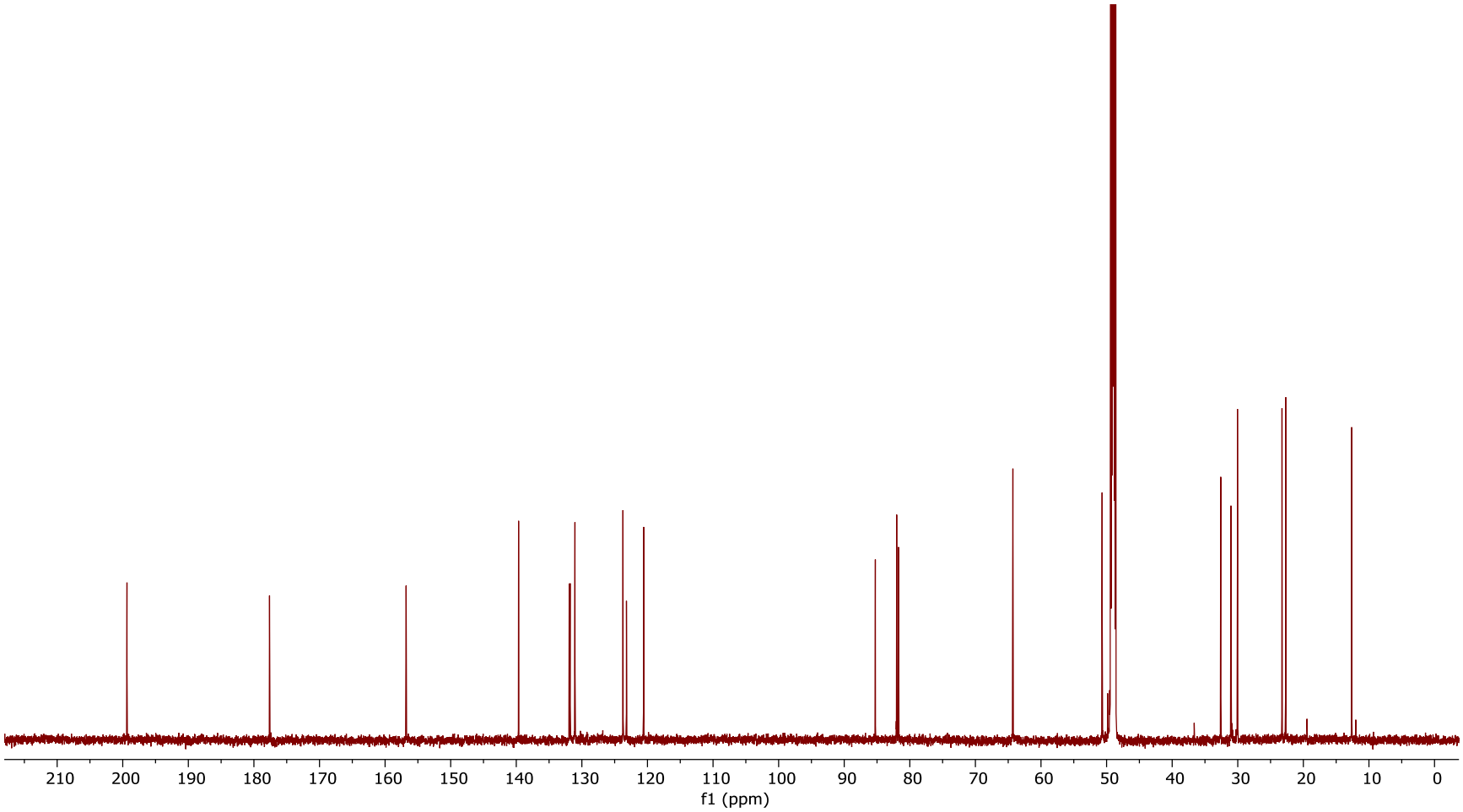

COSY spectra of (-)-rishirilide A

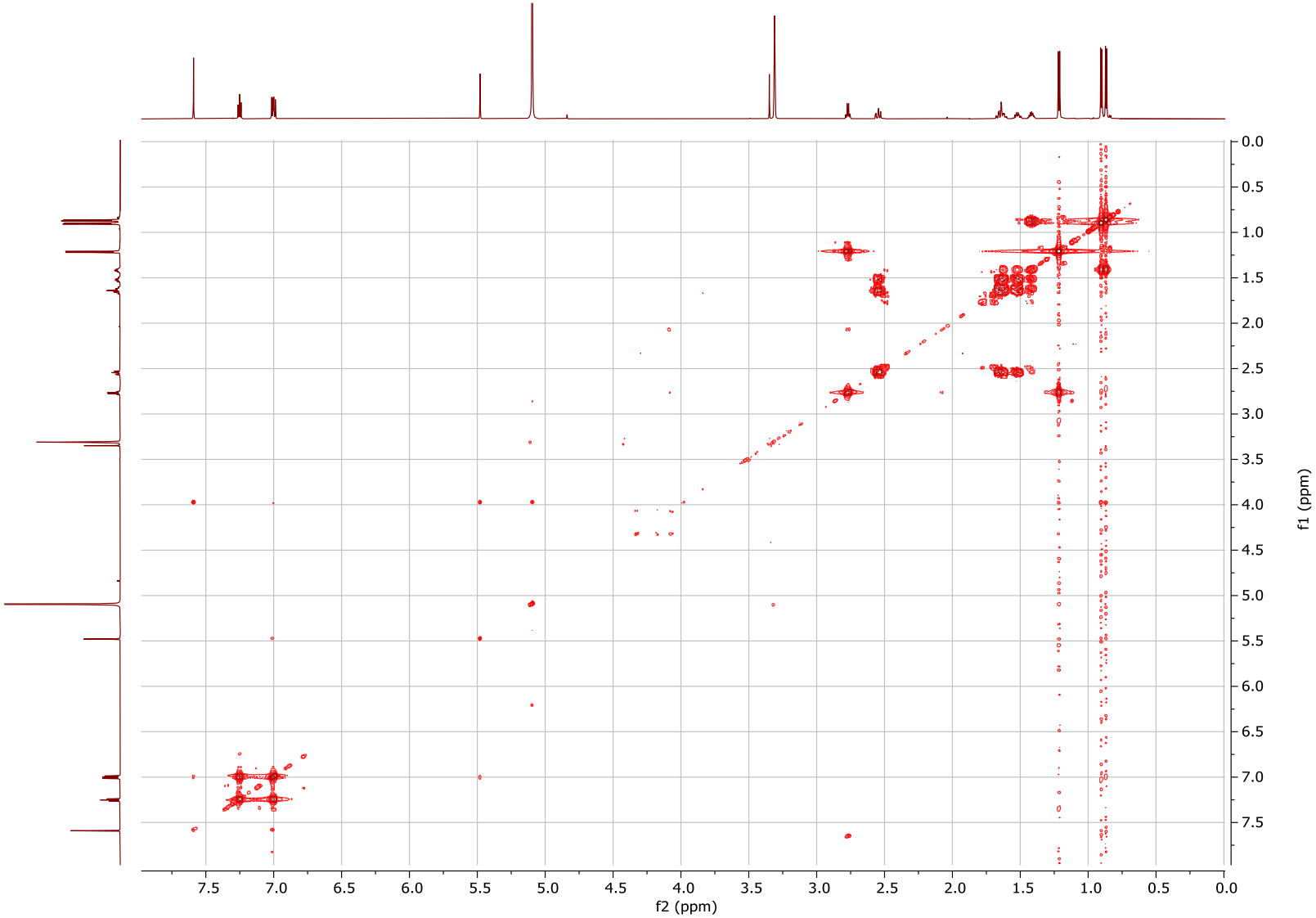

HSQC spectra of (-)-rishirilide A

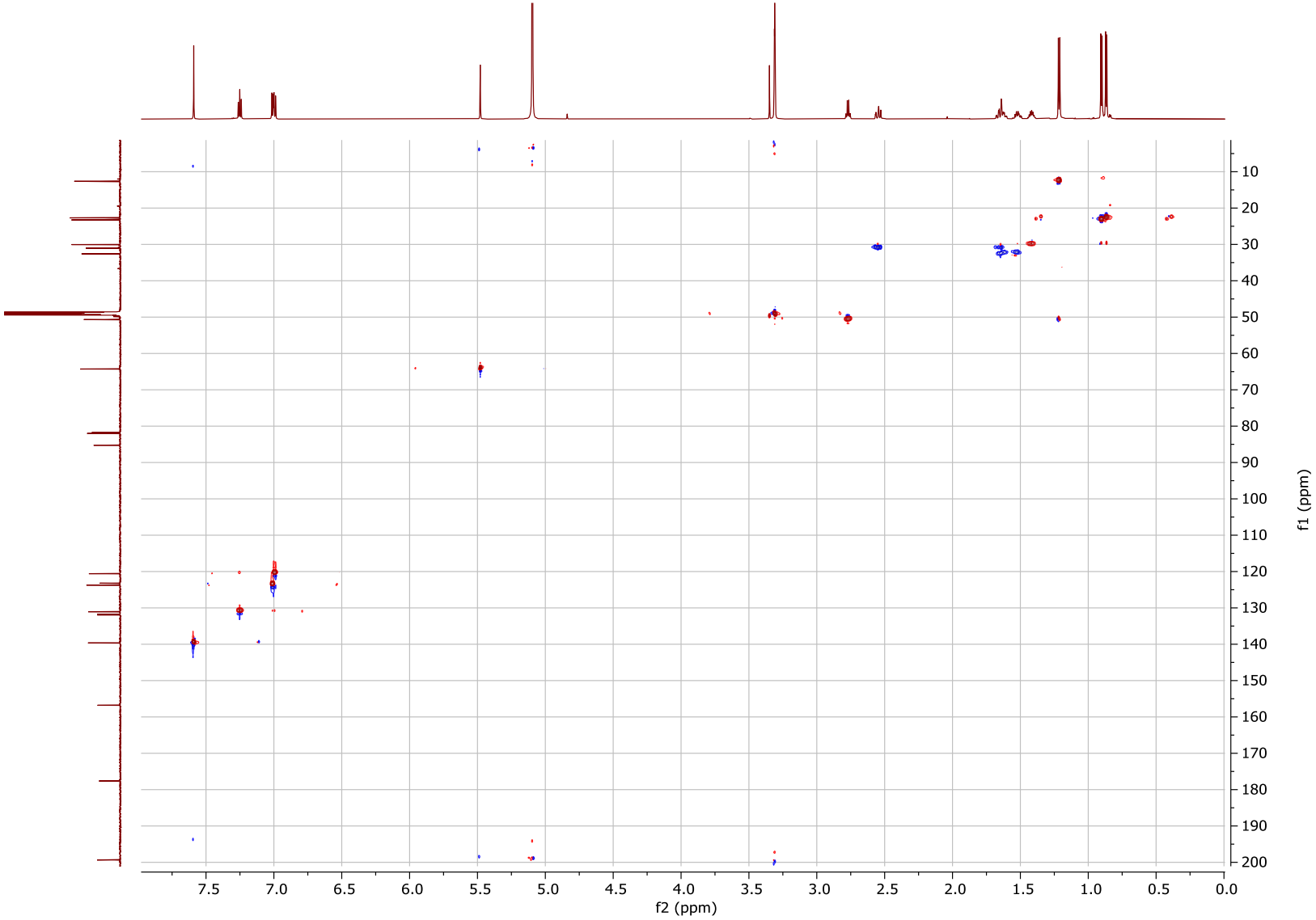

HMBC spectra of (-)-rishirilide A

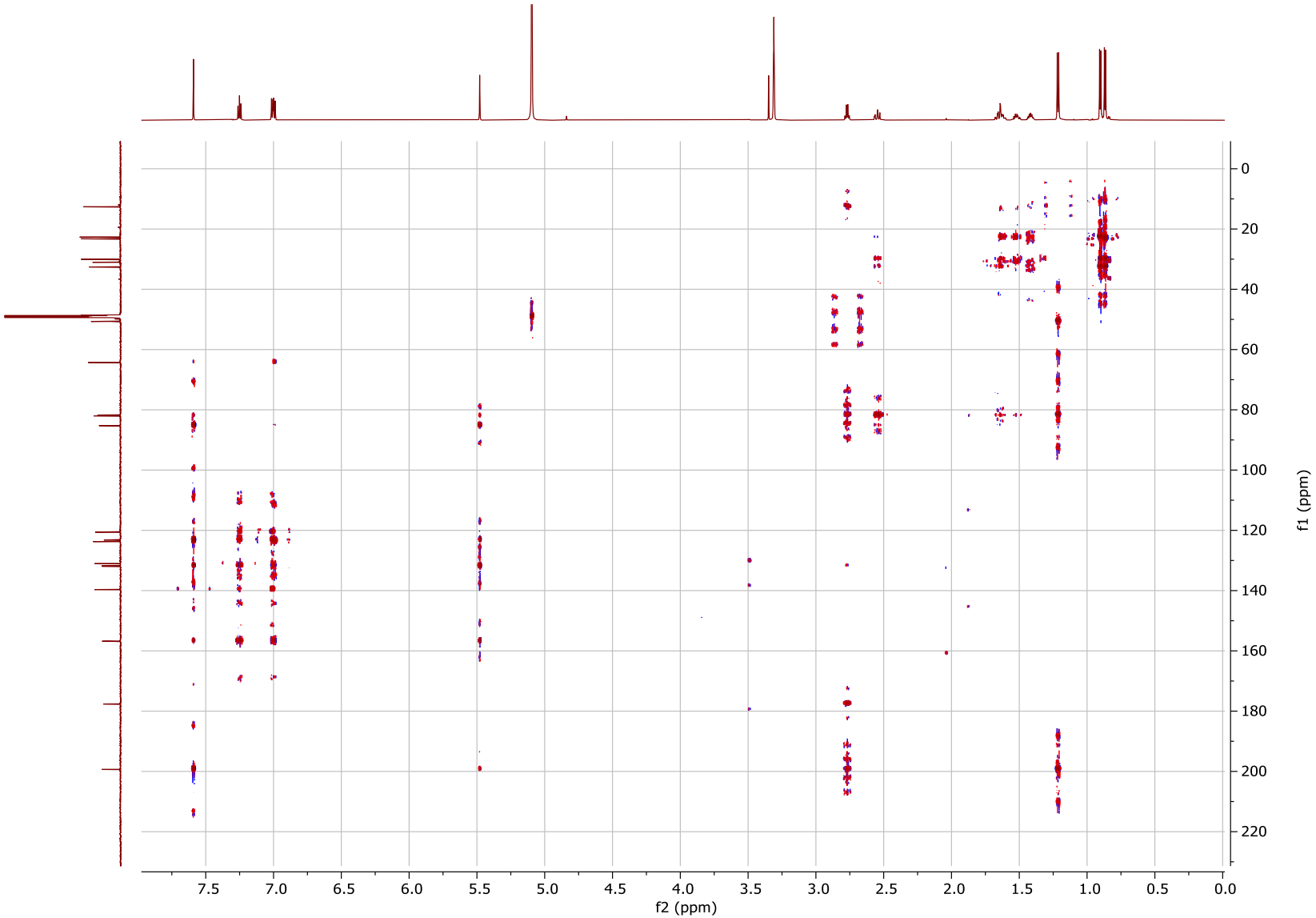

^{1}H NMR spectra of (+)-rishirilide B

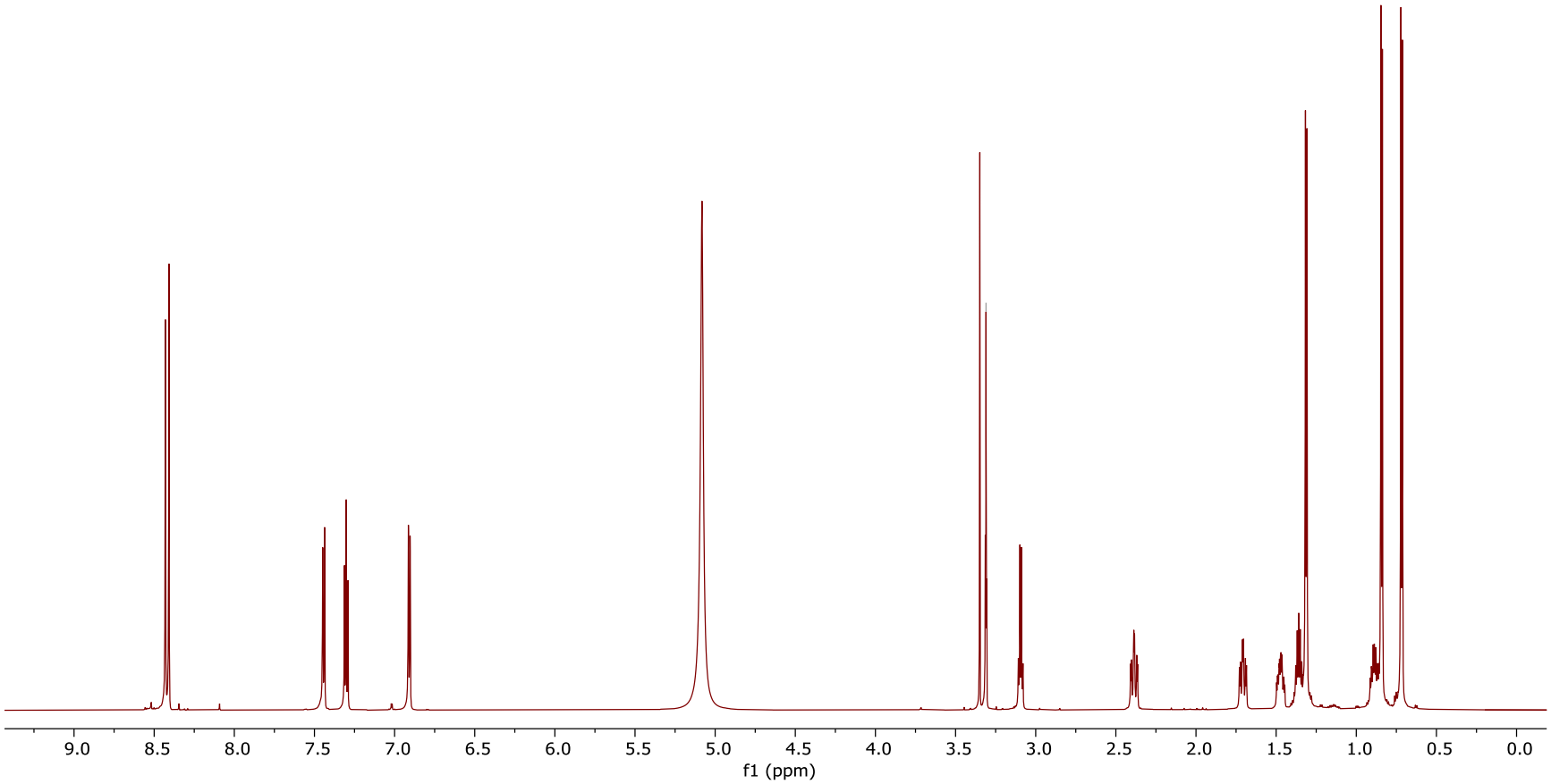

^{13}C NMR spectra of (+)-rishirilide B

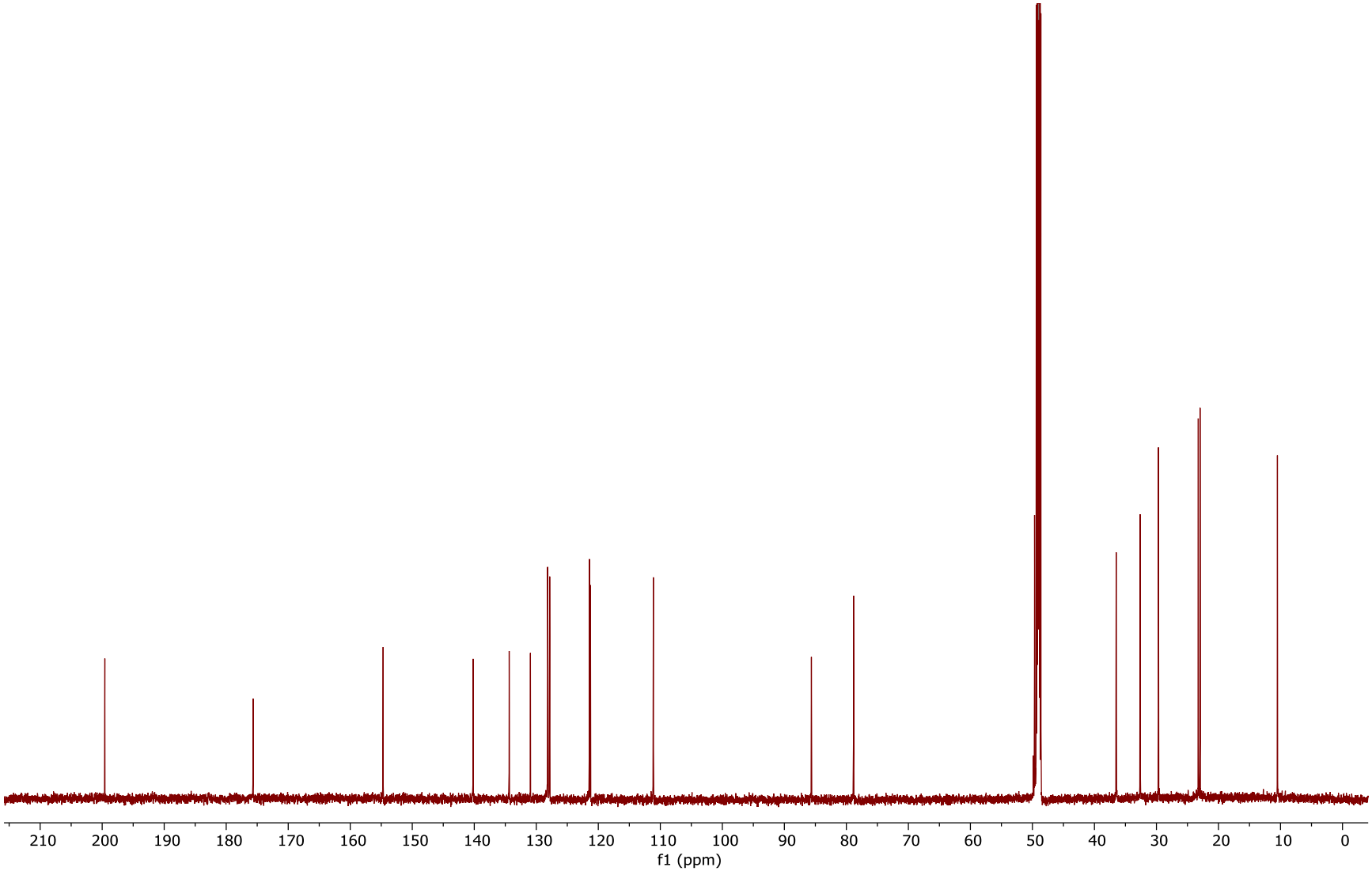

COSY spectra of (+)-rishirilide B

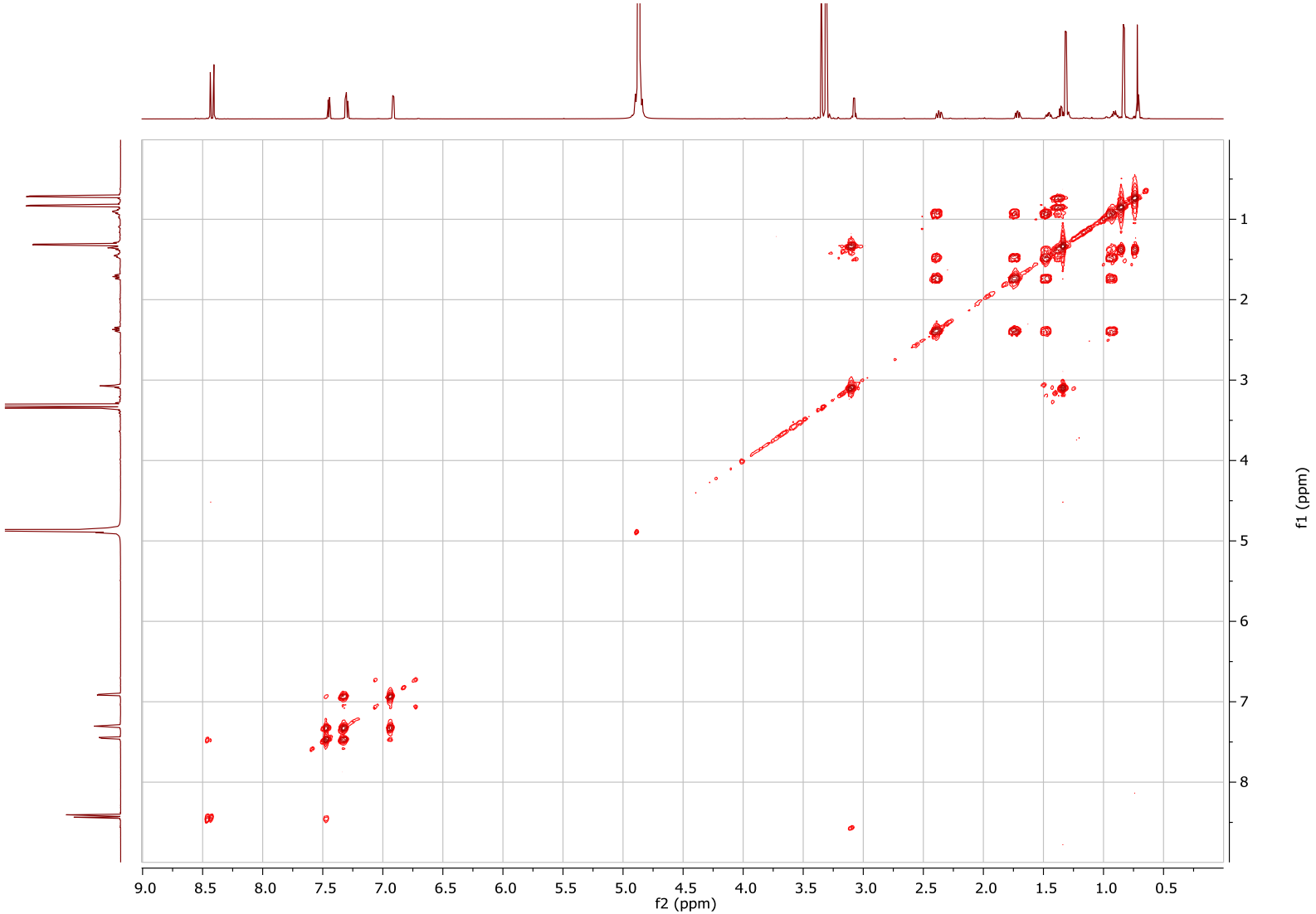

HSQC spectra of (+)-rishirilide B

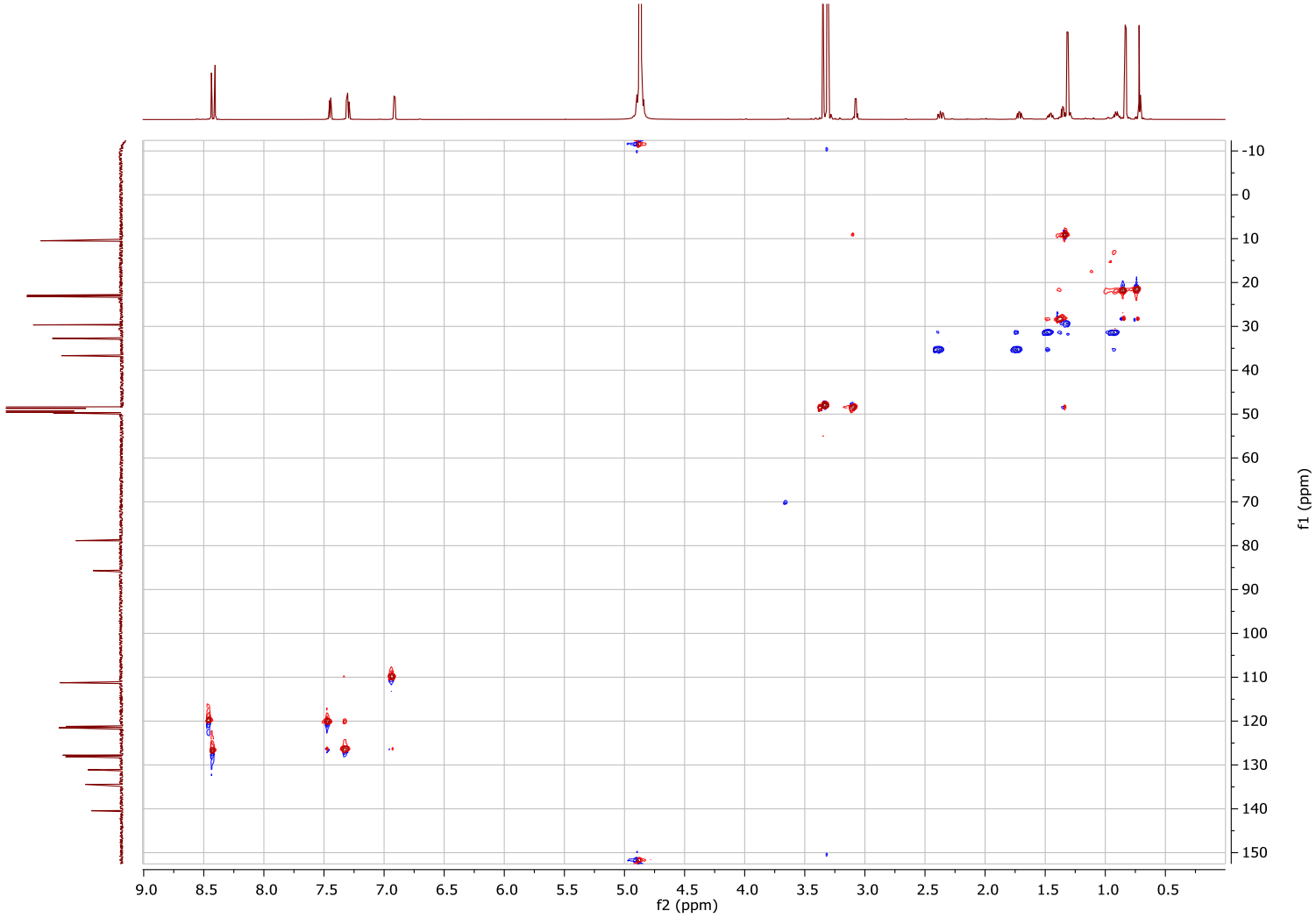

HMBC spectra of (+)-rishirilide B

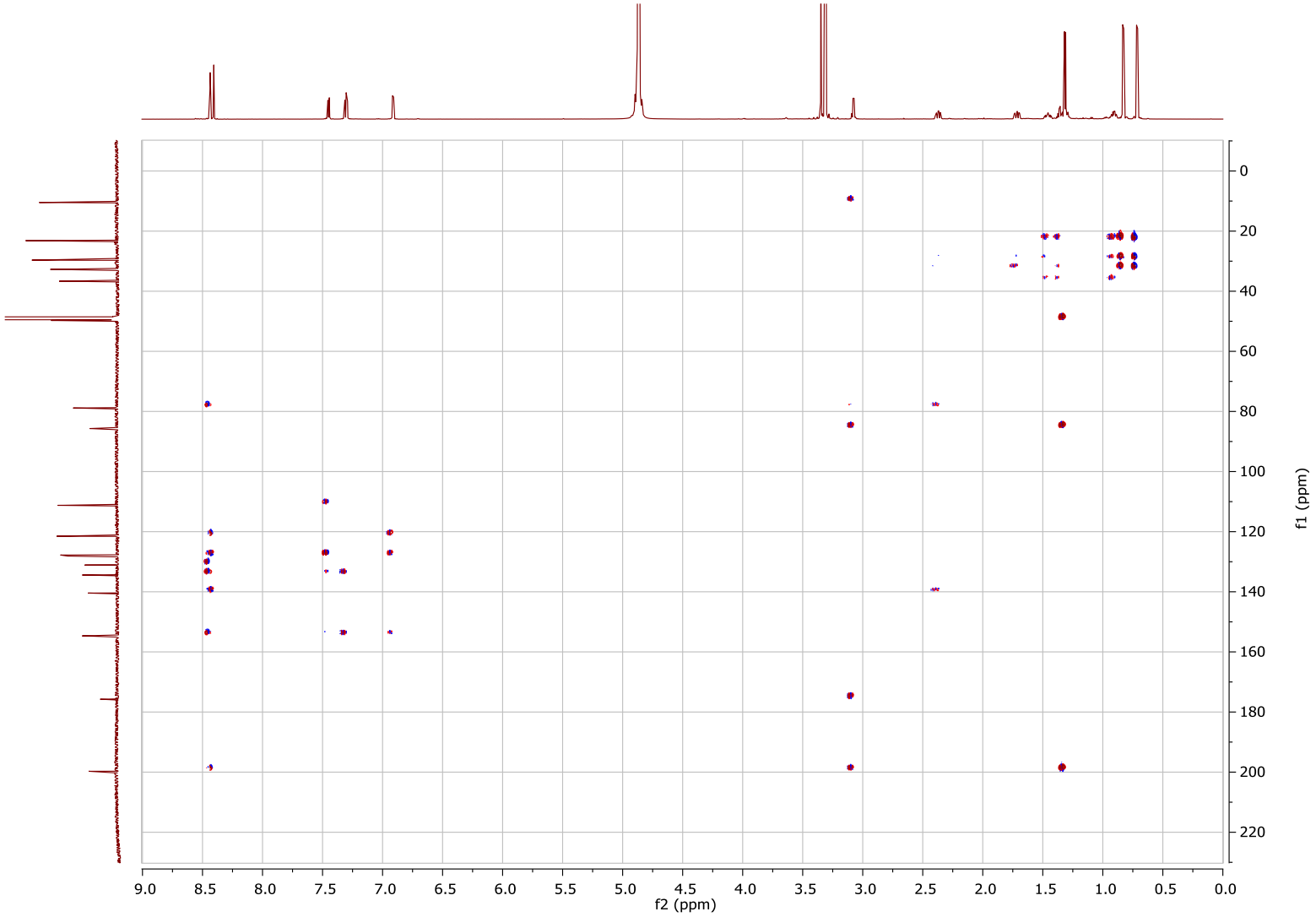

Methyl 3-hydroxybenzoate

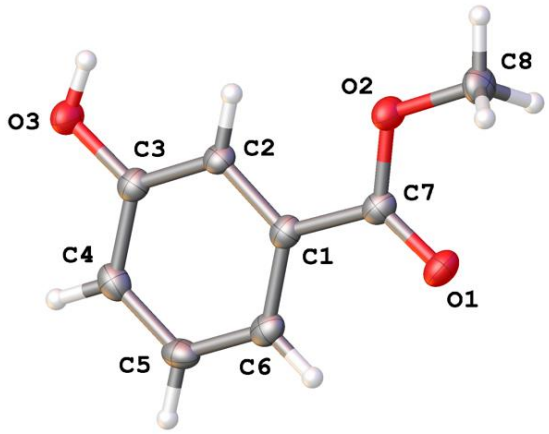

Identification code	mjh180059
Empirical formula	$C_8H_8O_3$
Formula weight	152.14
Temperature/K	100.0(2)
Crystal system	orthorhombic
Space group	$P2_12_12_1$
a/Å	4.0656(14)
b/Å	10.108(4)
c/Å	17.289(6)
α/°	90
β/°	90
γ/°	90
Volume/Å^3	710.5(4)
Z	4
ρ_{calc}g/cm^3	1.422
μ/mm^{-1}	0.103
F(000)	320.0
Crystal size/mm^3	0.203 × 0.042 × 0.009
Radiation	Synchrotron (λ = 0.6889)

2Θ range for data collection/°	4.524 to 53.202
Index ranges	$-5 \leq h \leq 5, -13 \leq k \leq 13, -22 \leq l \leq 22$
Reflections collected	7983
Independent reflections	1634 [R_{int} = 0.0582, R_{sigma} = 0.0375]
Data/restraints/parameters	1634/0/104
Goodness-of-fit on F^2	1.047
Final R indexes [I>=2σ (I)]	R_1 = 0.0343, wR_2 = 0.0848
Final R indexes [all data]	R_1 = 0.0383, wR_2 = 0.0871
Largest diff. peak/hole / e $Å^{-3}$	0.23/-0.12
Flack parameter	0.1(6)

Methyl 3-(benzyloxy)benzoate

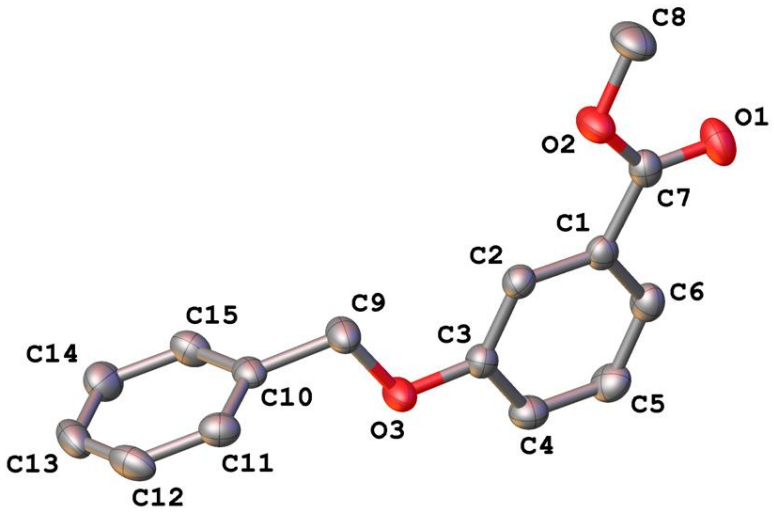

Identification code	mjh190011_fa
Empirical formula	$C_{15}H_{14}O_3$
Formula weight	242.26
Temperature/K	150.0(2)
Crystal system	triclinic
Space group	P-1
a/Å	8.2426(5)
b/Å	8.9479(7)
c/Å	9.5713(6)
α/°	63.837(7)
β/°	79.431(5)
γ/°	79.487(6)
Volume/Å^3	618.70(8)
Z	2
ρ_{calc}g/cm^3	1.300
μ/mm^{-1}	0.734
F(000)	256.0
Crystal size/mm^3	0.29 × 0.19 × 0.09

Radiation	CuKα (λ = 1.54184)
2Θ range for data collection/°	10.368 to 133.622
Index ranges	-9 ≤ h ≤ 7, -10 ≤ k ≤ 10, -11 ≤ l ≤ 11
Reflections collected	8762
Independent reflections	2185 [R_{int} = 0.0215, R_{sigma} = 0.0168]
Data/restraints/parameters	2185/0/165
Goodness-of-fit on F^2	1.038
Final R indexes [I>=2σ (I)]	R_1 = 0.0335, wR_2 = 0.0863
Final R indexes [all data]	R_1 = 0.0400, wR_2 = 0.0929
Largest diff. peak/hole / e $Å^{-3}$	0.19/-0.14

Methyl 3-(prop-2-yn-1-yloxy)benzoate

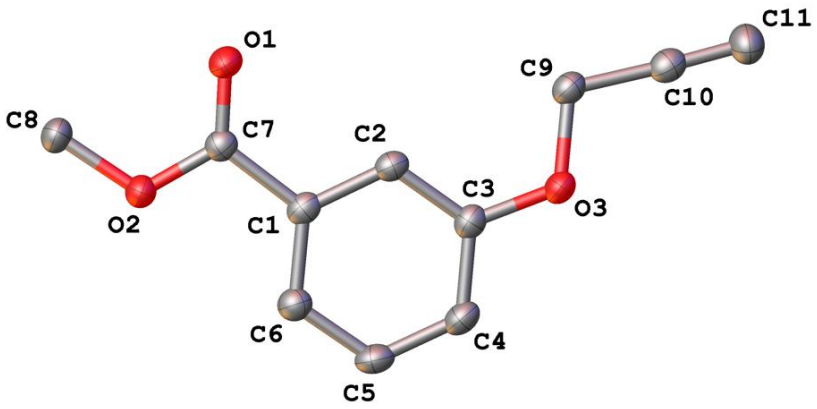

Identification code	mjh190013
Empirical formula	$C_{11}H_{10}O_3$
Formula weight	190.19
Temperature/K	150.0(2)
Crystal system	monoclinic
Space group	$P2_1/c$
a/Å	11.4311(3)
b/Å	5.88894(15)
c/Å	14.1771(4)
α/°	90
β/°	101.261(3)
γ/°	90
Volume/Å^3	935.99(4)
Z	4
ρ_{calc}g/cm^3	1.350
μ/mm^{-1}	0.815
F(000)	400.0
Crystal size/mm^3	0.33 × 0.17 × 0.12
Radiation	CuKα (λ = 1.54184)
2Θ range for data collection/°	7.886 to 133.544

Index ranges	$-13 \leq h \leq 13, -7 \leq k \leq 4, -16 \leq l \leq 16$
Reflections collected	6789
Independent reflections	1658 [$R_{int} = 0.0223$, $R_{sigma} = 0.0161$]
Data/restraints/parameters	1658/93/129
Goodness-of-fit on F^2	1.051
Final R indexes [I>=2σ (I)]	$R_1 = 0.0311$, $wR_2 = 0.0829$
Final R indexes [all data]	$R_1 = 0.0363$, $wR_2 = 0.0873$
Largest diff. peak/hole / e $Å^{-3}$	0.19/-0.17

(1'*R*,2'*R*)-5'-methyl-4-pentyl-2'-(prop-1-en-2-yl_-1',2',3',4'-tetrahydro-[1,1'-biphenyl]-2,6-diol/ (Cannabidiol)

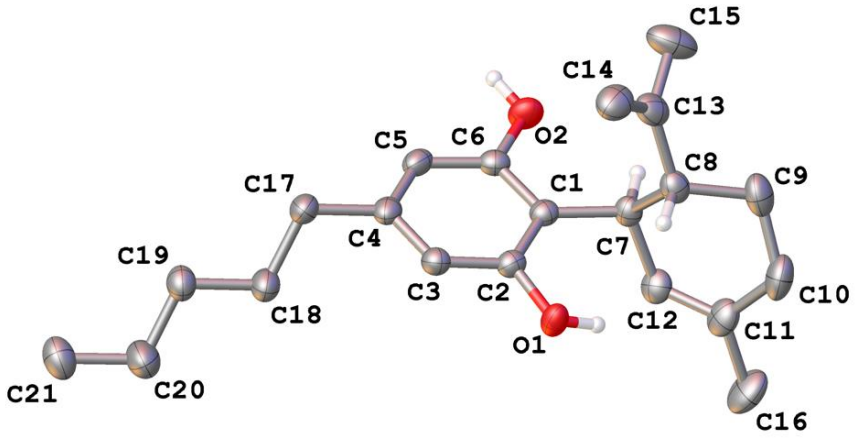

Identification code	mjh200017_fa
Empirical formula	$C_{21}H_{30}O_2$
Formula weight	314.45
Temperature/K	150.0(2)
Crystal system	monoclinic
Space group	$P2_1$
a/Å	10.43482(16)
b/Å	10.88547(17)
c/Å	16.7749(3)
α/°	90
β/°	95.4518(15)
γ/°	90
Volume/Å^3	1896.80(5)
Z	4
ρ_{calc}g/cm^3	1.101
μ/mm^{-1}	0.530
F(000)	688.0
Crystal size/mm^3	0.24 × 0.18 × 0.15

Radiation	CuKα (λ = 1.54184)
2Θ range for data collection/°	8.512 to 133.95
Index ranges	-12 ≤ h ≤ 9, -12 ≤ k ≤ 12, -19 ≤ l ≤ 19
Reflections collected	26857
Independent reflections	6671 [R_{int} = 0.0440, R_{sigma} = 0.0339]
Data/restraints/parameters	6671/1/434
Goodness-of-fit on F^2	1.080
Final R indexes [I>=2σ (I)]	R_1 = 0.0344, wR_2 = 0.0794
Final R indexes [all data]	R_1 = 0.0425, wR_2 = 0.0856
Largest diff. peak/hole / e $Å^{-3}$	0.16/-0.12
Flack parameter	-0.07(9)

(1'*R*,2'*R*)-5'-methyl-4-pentyl-2'-(prop-1-en-2-yl_-1',2',3',4'-tetrahydro-[1,1'-biphenyl]-2,6-diol/ (Cannabidiol)

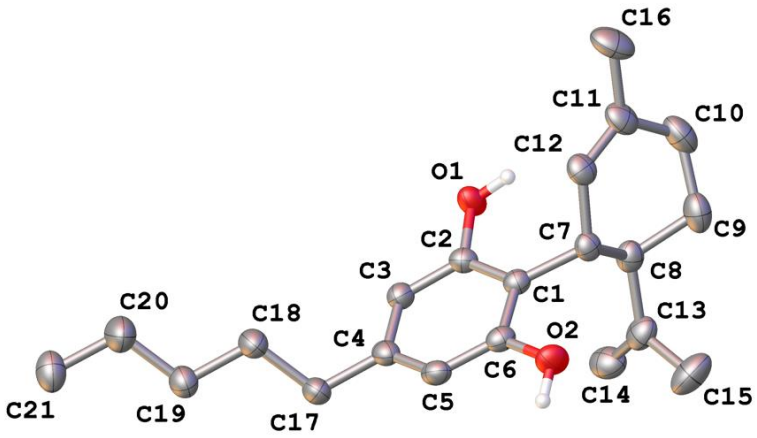

Identification code	mjh200020
Empirical formula	$C_{21}H_{30}O_2$
Formula weight	314.45
Temperature/K	150.0(2)
Crystal system	monoclinic
Space group	$P2_1$
a/Å	10.43368(15)
b/Å	10.88596(18)
c/Å	16.7723(2)
α/°	90
β/°	95.4451(13)
γ/°	90
Volume/Å^3	1896.41(5)
Z	4
ρ_{calc}g/cm^3	1.101
μ/mm^{-1}	0.531
F(000)	688.0
Crystal size/mm^3	0.35 × 0.17 × 0.12
Radiation	CuKα (λ = 1.54184)

2Θ range for data collection/°	8.514 to 133.752
Index ranges	-9 ≤ h ≤ 12, -12 ≤ k ≤ 12, -20 ≤ l ≤ 19
Reflections collected	26644
Independent reflections	6674 [R_{int} = 0.0371, R_{sigma} = 0.0283]
Data/restraints/parameters	6674/1/434
Goodness-of-fit on F^2	1.042
Final R indexes [I>=2σ (I)]	R_1 = 0.0323, wR_2 = 0.0786
Final R indexes [all data]	R_1 = 0.0369, wR_2 = 0.0823
Largest diff. peak/hole / e $Å^{-3}$	0.17/-0.12
Flack parameter	-0.11(8)

Rifampicin 1,4-dioxane solvate

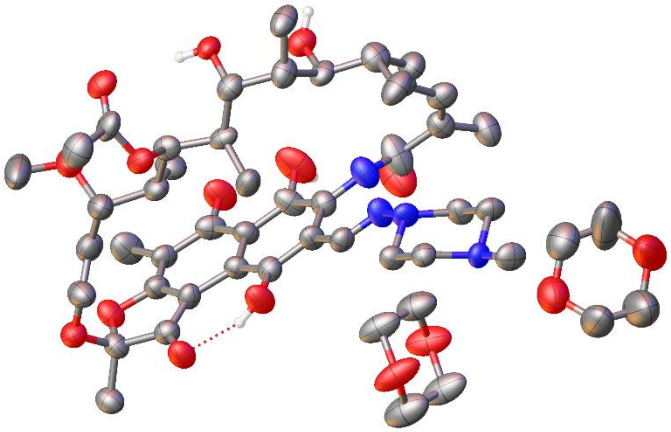

Identification code	mjh190062
Empirical formula	$C_{20}H_{20}N_5O_3$
Formula weight	378.41
Temperature/K	150
Crystal system	orthorhombic
Space group	$P2_12_12_1$
a/Å	20.2794(6)
b/Å	20.3110(5)
c/Å	27.8488(8)
α/°	90
β/°	90
γ/°	90
Volume/Å^3	11470.8(6)
Z	24
ρ_{calc}g/cm^3	1.315
μ/mm^{-1}	0.751
F(000)	4776.0
Crystal size/mm^3	0.11 × 0.09 × 0.07

Radiation	CuKα (λ = 1.54178)
2Θ range for data collection/°	5.386 to 100.868
Index ranges	-19 ≤ h ≤ 18, -20 ≤ k ≤ 20, -27 ≤ l ≤ 27
Reflections collected	141734
Independent reflections	11868 [R_{int} = 0.1268, R_{sigma} = 0.0479]
Data/restraints/parameters	11868/1050/1253
Goodness-of-fit on F^2	1.044
Final R indexes [I>=2σ (I)]	R_1 = 0.0706, wR_2 = 0.1939
Final R indexes [all data]	R_1 = 0.0989, wR_2 = 0.2193
Largest diff. peak/hole / e $Å^{-3}$	0.51/-0.28
Flack parameter	0.12(8)